The use of ^{10}Be surface exposure dating of erratic boulders in the reconstruction of the late Pleistocene glaciation history of mountainous regions, with examples from Nepal and Central Asia

Dissertation

zur Erlangung des Grades
Doktor der Naturwissenschaften
(Dr. rer. nat.)
der
Fakultät für Biologie, Chemie und Geowissenschaften
an der Universität Bayreuth

von

Dipl.-Geoökologe Uwe Abramowski
geb. am 10. 04. 1974 in Hamburg

Bayreuth, im August 2004

Die vorliegende Dissertation wurde erarbeitet in der Zeit zwischen dem 1. Januar 2001 und dem 1. August 2004 am Lehrstuhl für Bodenkunde und Bodengeographie der Universität Bayreuth, unter der Leitung von Prof. Dr. Wolfgang Zech. Gefördert wurde die Arbeit von der Deutschen Forschungsgemeinschaft (Az. ZE 151/1-3).

Eingereicht am:	18. August 2004
Wissenschaftliches Kolloquium am:	9. Februar 2005
1. Gutachter:	Prof. Dr. W. Zech
2. Gutachter:	Prof. Dr. L. Zöller
Prüfungsausschuss:	Prof. Dr. K. Bitzer (Vorsitz)
	Prof. Dr. W. Zech
	Prof. Dr. L. Zöller
	Prof. Dr. F. Seifert
	Prof. Dr. E. Beck

Kontakt / communications: uwe.abramowski@gmx.net

Verfügbar als PDF unter / available as PDF at: http://opus.ub.uni-bayreuth.de

TEBESEA.xls verfügbar unter / available at: http://opus.ub.uni-bayreuth.de

Vielfältig ist das Verhältnis des Geistes zum Wirklichen.
Einer stellt eine einzige, tief durchdachte Gleichung auf, schafft ein System von Begriffen,
dem die Wirklichkeit entsprechen soll, und unternimmt es nun, dafür zu sorgen,
dass die Wirklichkeit sich dem Begriff entsprechend verhalte.
Das tut sie aber niemals, die Gleichung sei so gescheit, wie sie sei.

GOLO MANN

There is something fascinating about science. One gets such wholesale returns of conjecture out of such a trifling investment of fact.

MARK TWAIN

Contents

I. Extended Summary

II. Cumulative Study

1. Introduction

2. An evaluation of existing calculation procedures in ^{10}Be surface exposure dating of erratic boulders, using TEBESEA, a newly-devised calculation program

List of Tables

List of Figures

List of Abbreviations

Standard mathematical functions, chemical formulae, directions, and trademarks have not been taken into this list.

°C	degree Celsius
A	Ampère(s)
a	annum, year(s)
a.s.l.	above sea level
a_{ij}	weighing factor in any of the virtual exponential depth functions of Schaller et al. (2002)
AK	Aksu Valley, Turkestan Range, Kyrgyzstan
AMS	accelerator mass spectrometry
ARGE	*Arbeitsgemeinschaft für vergleichende Hochgebirgsforschung*, German Work-group for Comparative Alpine Research
AT	Ailuitek Pass, central Pamir, Tajikistan
AV	Abramov glacier forefield, Alay Range, Kyrgyzstan
Az.	*Aktenzeichen*, grant number
B.P.	before present (1950)
BH	*Bhagirathi* glacial stage, Garhwal Himalaya, northern India
b_{ij}	attenuation length in any of the virtual exponential depth functions of Schaller et al. (2002)
BJ	*Borit Jheel* glacial stage, Karakoram, Pakistan
BK	Koefels landslide, Oetz Valley, Austria (*Bergsturz Koefels*)
BO	Gr. Bogchigir Valley, central Pamir, Tajikistan
BY	Yashilkul landslide, central Pamir, Tajikistan (*Bergsturz Yashilkul*)
c.	column
c/o	in care of
cal. ka B.P.	thousand calendar years before present
CH	Chhukung Valley, Khumbu Himal, Nepal
cm	centimeter(s)
DAAD	*Deutscher Akademischer Austausch-Dienst*, German Academic Exchange Service
DFG	*Deutsche Forschungsgemeinschaft*, German Research Foundation
e.g.	example given
EB	erratic boulder
E_{jk}	exponential term in the calculation procedure of ^{10}Be surface exposure ages, assuming a simple exponential depth profile of nuclide production
E_{jk}*	exponential term in the calculation procedure of ^{10}Be surface exposure ages, considering the refined depth profile of nuclide production of Heisinger et al. (2002)
ELA	equilibrium line altitude
eq.	equation
et al.	et alii, and others
ETH	*Eidgenössische Technische Hochschule*, Swiss Technical University
f	any correction factor in the calculation of ^{10}Be surface exposure ages

$f_{C,P}$	correction factor concerning the production rate of ^{10}Be
$f_{C,\Lambda}$	correction factor concerning the attenuation length of ^{10}Be production in rock
f_i	any of a number of correction factors considered
Fig.	figure
$f_M(t)$	correction factor for geomagnetic variation
$f_P(\varepsilon, t)$	correction factor for the eroding depth profile of ^{10}Be production by Heisinger et al. (2002), including the influence of the depth profile on thickness and surface cover correction
$f_P(\varepsilon, t)'$	correction factor for the eroding depth profile of ^{10}Be production by Heisinger et al. (2002), not including the influence of the depth profile on thickness and surface cover correction
f_{SC}	correction factor for shielding by surface cover, assuming a simple exponential depth profile of nuclide production
f_{SC}*	correction factor for shielding by surface cover, considering the refined depth profile of nuclide production of Heisinger et al. (2002)
f_{SDC}	correction factor for shielding by sediment cover
f_{SG}	correction factor for the influence of sample geometry
f_{SI}	correction factor for shielding by surface inclination
$f_{SI,P}$	correction factor for shielding by surface inclination concerning the production rate of ^{10}Be
$f_{SI,\Lambda}$	correction factor for shielding by surface inclination concerning the attenuation length of ^{10}Be production in the rock
f_{ST}	correction factor for shielding by surface topography
$f_{ST,P}$	correction factor for shielding by surface topography concerning the production rate of ^{10}Be
$f_{ST,\Lambda}$	correction factor for shielding by surface topography concerning the attenuation length of ^{10}Be production in the rock
f_{SVC}	correction factor for shielding by snow and vegetation cover
f_T	correction factor for sample thickness, assuming a simple exponential depth profile of nuclide production
f_T*	correction factor for sample thickness, considering the refined depth profile of nuclide production of Heisinger et al. (2002)
$f_U(t)$	correction factor for tectonic uplift
g	gram(s)
GAD	geocentric axial dipole
GeV	10^9 electron Volts
GH	*Ghulkin* glacial stage, Karakoram, Pakistan
GLPS	glacially polished surface(s)
GPS	global positioning system
GU	Gurumdy Valley, Southern Alichur Range, eastern Pamir, Tajikistan
H	horizontal geomagnetic field strength
h_0	altitude at the beginning of exposure
HHC	High Himalaya Crystalline
h_k	altitude during the k-th time interval of exposure

I	geomagnetic inclination
i.e.	it est, that is
ICAO	International Civil Aviation Organization
ICN	Institute for Cosmogenic Nuclides, Lawrence Livermore University, California, USA
ID	identification, label
k	index for time intervals of exposure
k'	index for the time interval of exposure into which the measured concentration of a sample is predicted
ka	kiloannum, thousand years
KD	Kanding area, eastern Tibet
KE	*Ketar* glacial stage, Garhwal Himalaya, India
KH	Khumbu Valley, Khumbu Himal, Nepal
KK	Koksu Valley, Alay Range, Kyrgyzstan
km	kilometer(s)
l	liter(s)
L_c	corrected geomagnetic latitude
L_{gm}	geomagnetic latitude
LGM	last glacial maximum
LI	Litang area, eastern Tibet
LIA	Little Ice Age
LJ	La Ji Mountains, eastern Tibet, China
LSB	landslide boulder
LT	Langtang Valley, Langtang Himal, Nepal
m	meter(s)
m	exponential factor in the sky angle dependency of cosmogenic rays
M	any dipole moment of the geomagnetic field
M_0	dipole moment of today's geomagnetic field
Ma	megaannum, millions of years
MASC	mean annual snow cover
max	maximum
M_{CB}	mass of ^{9}Be carrier added to the blank
M_{CS}	mass of ^{9}Be carrier added to the sample
mg	milligram(s)
MIS	marine isotope stage
MK	Macha Khola Valley, Gorkha Himal, Nepal
min	minimum
ml	milliliter(s)
mm	millimeter(s)
mod.	modification
M_S	mass of the sample
nA	10^{-12} Ampère(s)
N	concentration of ^{10}Be
n.d.	no data

n.r.	not reported
N_0	concentration of ^{10}Be at the beginning of exposure
N_A	Avogadro's number
N_B	concentration of ^{10}Be measured in the blank
N_c	corrected concentration of ^{10}Be
N_j	concentration of ^{10}Be produced by the mechanism *j*
N_{jk}	concentration of ^{10}Be produced by the mechanism *j* during the time interval *k*
N_k	concentration of ^{10}Be produced during the time interval *k*
N_{nc}	uncorrected concentration of ^{10}Be
NP	Nanga Parbat, western Himalaya, Pakistan
N_S	concentration of ^{10}Be measured in the sample
N_{tot}	total concentration of ^{10}Be
OED	*Oberflächenexpositionsdatierung*, surface exposure dating
OSL	optical stimulated luminescence
P	production rate of ^{10}Be
$p(t, t')$	mathematical propagator
p.a.	per analysi, for analysis
P_0	standard production rate of ^{10}Be
$P_{0,\,\mu-}$	standard production rate of ^{10}Be due to captures of negative muons
$P_{0,\,\mu f}$	standard production rate of ^{10}Be due to fast muon reactions
$P_{0,\,n}$	standard production rate of ^{10}Be due to neutron spallations
PC	pedocomplex
PE	polyethylene
pers. comm.	personal communication
pH	negative logarithm of the H^+ activity in a solution
$p_{i,\,\mu-}$	coefficient for the calculation of the correction factor $f_{SI,P}$ for production by capture of negative muons
$p_{i,\,\mu f}$	coefficient for the calculation of the correction factor $f_{SI,P}$ for production by fast muon reactions
$p_{i,\,n}$	coefficient for the calculation of the correction factor $f_{SI,P}$ for production by neutron spallation
ppm	parts per million
Q_1	first Quaternary stage in the Russian stratigraphy (early Pleistocene)
Q_2	second Quaternary stage in the Russian stratigraphy (middle Pleistocene)
Q_3	third Quaternary stage in the Russian stratigraphy (late Pleistocene)
Q_4	fourth Quaternary stage in the Russian stratigraphy (Holocene)
$q_{i,\,\mu-}$	coefficient for the calculation of the correction factor $f_{SI,A}$ for production by capture of negative muons
$q_{i,\,\mu f}$	coefficient for the calculation of the correction factor $f_{SI,A}$ for production by fast muon reactions
$q_{i,\,n}$	coefficient for the calculation of the correction factor $f_{SI,A}$ for production by neutron spallations
QS	Qilian Shan, northeastern Tibet, China
R	cutoff rigidity

R_B	measured ratio of $^{10}Be/^{9}Be$ in the blank
R_S	measured ratio of $^{10}Be/^{9}Be$ in the sample
rs.	rescaled
S	scaling factor
S'	value of the scaling factor
SED	surface exposure dating
SI	surface inclination = slope angle = dip
S_{jk}	scaling factor valid for the production fraction j during the time interval k
SLHL	sea level, high latitude
t	exposure time or age
t_0	beginning of exposure
Tab.	table
TEBESEA	program for the calculation of ten-beryllium surface exposure ages
TG	Tanggula Shan, central Tibet, China
TH	*Thyangboche* stage, Khumbu Himal, Nepal
THAR	toe-to-headwall altitude ratio
t_k	time of the of exposure
TK	Takhtakorum river area, north-central Pamir, Tajikistan
t_{k-1}	time of the interval before the k-th interval of exposure
TL	thermoluminescence
u	tectonic uplift rate
u_{Be}	mole-mass of beryllium
UK	Kol-Uchkol Valley, southeast-central Pamir, Tajikistan
UNEP	United Nations Environmental Program
unpubl.	unpublished
USA	United States of America
VADM	virtual axial dipole moment
vrs.	various
vs.	versus
YD	Younger Dryas chronozone
YK	Yashilkul area, south-central Pamir, Tajikistan
z	depth below the rock surface
z_0	depth of the rock surface
z_{BS}	depth of the base of the sample below the rock surface
z_C	thickness of any kind of cover
ZE	Zech
z_{SD}	thickness of sediment cover
z_{SV}	thickness of snow and vegetation cover
z_{TS}	depth of the top of the sample below the rock surface
Δt_k	length of time interval
Δz	thickness of the sample
$\Delta\varphi_i$	the i-th azimuth section
Λ	attenuation length
Λ_0	standard attenuation length

α	maximum slope angle of inclined surface
ε	erosion rate
$\gamma(\varphi_\alpha)$	slope angle of the inclined surface as a function of the azimuth angle respective to the direction of the maximum slope angle
φ_α	azimuth angle respective to the direction of the maximum slope angle
λ	decay constant
θ_i	horizon angle of the *i*-th azimuth section
θ_{pcl}	palaeocolatitude
ρ	rock density
™	trademark

The use of ^{10}Be surface exposure dating of erratic boulders in the reconstruction of the late Pleistocene glaciation history of mountainous regions, with examples from Nepal and Central Asia

[Der Einsatz der ^{10}Be-Oberflächenexpositionsdatierung erratischer Blöcke zur Rekonstruktion der spätpleistozänen Vergletscherungsgeschichte von Gebirgsräumen, mit Beispielen aus Nepal und Zentralasien]

Extended Summary

Abstract

^{10}Be surface exposure dating (SED) of erratic boulders is an innovative approach in Quaternary geochronology. It proves to be an excellent tool for the reconstruction of the glacial history of mountainous regions, which is an important part of climate change research. In the course of this work, I have 1) installed the analytical procedure to extract in-situ produced ^{10}Be from quartz-bearing rock surface samples in the laboratory of the Institute of Soil Science and Soil Geography at the University of Bayreuth; 2) developed and calibrated the program TEBESEA for quick calculation of ^{10}Be surface exposure ages with fully propagated errors, thereby evaluating the existing procedures; 3) deduced a new interpretation scheme for exposure age distributions from several stratigraphically related moraines in an area; 4) provided 37 new ^{10}Be exposure ages for the Nepal Himalaya, complementing earlier soil geographic studies in the Langtang Valley and the Macha Khola Valley; and finally 5) provided 108 new ^{10}Be exposure ages for the Pamir, and the Alay- and Turkestan Ranges, defining a new glacial chronology for Central Asia.

The analytical procedure used to extract ^{10}Be from quartz-bearing rocks and to prepare it for measurement closely followed the one established at the ETH Zurich, where all ^{10}Be measurements have been done. The accuracy of the analytical work in Bayreuth was confirmed by preparation of five calibration samples from the Koefels landslide, Oetz Valley, Austria.

The traditional scaling system of Lal (1991) as modified by Stone (2000) still proves to be the most suitable one to be used in ^{10}Be exposure age calculations. For this procedure, I have calibrated a total standard production rate at sea level, high latitude of 5.35 ± 0.15 atoms g^{-1} a^{-1}, using a contribution of capture of slow negative muons of 1.2%, and including all possible corrections. The altitude dependency of ^{10}Be production used in the scaling systems of Dunai (2001) and Desilets & Zreda (2003) is as yet not convincing, given the existing calibration data, but suggests that ages calculated for sites above 2000-3000 m in High Asia may be overestimates.

Detailed error propagation shows that the uncertainties of ^{10}Be surface exposure ages at present are dominated by the errors of the scaling factor, the erosion rate, and the tectonic uplift rate. As long as surface erosion and tectonic uplift rates cannot be constrained to within 10%, however, exposure ages older than 30-40 ka have uncertainties of ≥20% and can be no more than rough approximations.

For exposure age distributions from a set of stratigraphically related moraines, a new interpretation scheme is presented, which is able to detect ages older than the deposition age of the moraine (^{10}Be inheritance), and to interpret age clusters younger than the deposition age, which may be synchronous on several moraines (phases of regionally enhanced surface activity).

In the Nepal Himalaya, glacier advances in the Macha Khola Valley have occurred 70-100, 20-23, 11-12 and around 3 cal. ka B.P. Glacier advances in the Langtang Valley are dated to 14-15, 8-9 and ~3.5 cal. ka B.P. Late Pleistocene and Holocene glacial activity in the Nepal Himalaya seems to be controlled by the Indian monsoon rather than the westerly circulation. Only in the MIS 2, the westerly jetstream appears to have shifted as far south as to affect glaciation all over the Himalaya. During the Younger Dryas, the eastern limit of the influence of the westerly circulation on Himalaya glaciation may have been situated between the Manaslu and Langtang Himal.

Glacial advances in the Pamir and in the Alay and Turkestan Ranges have occurred >93->136, ~60-80, (40-55), ~27-25, ~22-20, ~18, ~15.5, ~14.3, and 10.5 cal. ka B.P. The most extensive late Pleistocene glaciation occurred during the MIS 5-3, and is characterized by ELA depressions of ~370-380 m in the eastern Pamir, as well as 600 m and >750 m, in the Alay and Turkestan Ranges, respectively. Late Pleistocene glacier advances in northwestern High Asia, were triggered by climatic cold phases rather than by monsoonal maxima. Climate in the region seems to have been mostly under the influence of the westerly circulation and the Siberian anticyclone. Asynchrony of Central Asian and western hemisphere glacier advances is due to increasing aridity in Central Asia in the course of the last glacial cycle. High altitude glaciers seem to have reached their maximum extent earlier (MIS 5-4) than low altitude glaciers (first half of MIS 3). Some indirect monsoonal influence in the eastern Pamir may be responsible for the existence of some of the lateglacial moraine stages in this area.

Zusammenfassung

Die ^{10}Be-Oberflächenexpositionsdatierung (OED) von Erratikern ist ein innovativer Ansatz in der quartären Geochronologie, der sich als ausgezeichnetes Mittel zur Rekonstruktion der Vergletscherungsgeschichte von Gebirgsräumen erweist, einem wichtigen Feld der Klimawandelforschung. In der vorliegenden Arbeit habe ich 1) die Analytik zur Extraktion von in-situ gebildetem ^{10}Be aus quarzhaltigen Proben von Gesteinsoberflächen in den Laboratorien des Lehrstuhls für Bodenkunde und Bodengeographie der Universität Bayreuth eingearbeitet, 2) das Programm TEBESEA erstellt und kalibriert, das die schnelle Berechnung von ^{10}Be-Expositionsaltern einschließlich ihrer vollständig fortgepflanzten Fehler ermöglicht, und dabei die derzeit verwendeten Berechnungsweisen evaluiert, 3) ein neues Schema entwickelt zur Interpretation von Expositions-Altersverteilungen von einer stratigraphischen Abfolge von Moränen, 4) mit 37 neuen ^{10}Be-Expositionsalter aus Zentral-Nepal die Ergebnisse früherer bodengeographischer Studien im Langtang-Tal und Macha-Khola-Tal bestätigt und ergänzt, und schließlich 5) mit 108 neuen Expositionsaltern aus dem Pamir sowie der Alay- und Turkestan-Kette eine neue Glazialchronologie für Zentralasien aufgestellt.
Der hier verwendete Analysengang zur Extraktion von ^{10}Be aus quarzhaltigen Gesteinsoberflächen und dessen Aufarbeitung lehnt sich eng an den an der ETH Zürich etablierten an. Die Qualität der analytischen Arbeiten in Bayreuth wurde bestätigt durch die Analyse von fünf Kalibrierproben vom Bergsturz Köfels (Ötztal).
Das traditionelle Skaliersystem von Lal (1991) in der Modifikation von Stone (2000) erweist sich als das derzeit angemessenste zur Berechnung von ^{10}Be-Expositionsaltern. Für dieses ergibt sich eine gesamte ^{10}Be-Standard-Produktionsrate in Meereshöhe und hoher Breite von 5,35 ± 0,15 Atomen g^{-1} a^{-1}, kalibriert mit einem Anteil aufgrund von Myoneneinfängen von 1,2% und unter Verwendung aller Korrekturen. Eine Höhenabhängigkeit der Produktion kosmischer Nuklide wie sie Dunai (2000) und Desilets & Zreda (2003) vorschlagen, ist bisher nicht überzeugend belegt, deutet aber möglicherweise eine derzeitige Überschätzung von Altern aus über 2000-3000 m Höhe an.
Die Fehler von ^{10}Be-Expositionsaltern werden derzeit bestimmt von den Fehlern des Skalierfaktors, der Erosionsrate und der tektonischen Hebungsrate. Solange Erosionsrate und tektonische Hebungsrate nicht innerhalb von 10% ihres Wertes festgelegt werden können, sind Expositionsalter >30-40 ka mit Fehlern von 20% und mehr behaftet und können lediglich als grobe Näherungen an das tatsächliche Alter aufgefasst werden.
Für Expositionsaltersverteilungen von einer stratigraphischen Abfolge von Moränen stelle ich ein neues Interpretationsschema vor, das gegenüber dem Alter der Moräne zu hohe Expositionsalter (Präexposition) erkennbar macht und die Interpretation von auf mehreren Moränen synchron auftretenden zu jungen Altershäufungen erlaubt (Phasen regional verstärkter Oberflächenaktivität).
Im Nepal-Himalaya habe ich Gletschervorstöße belegt im Macha-Khola-Tal um 70-100, 20-23, 11-12 und 3 cal. ka vor heute, sowie im Langtang-Tal um 14-15, 8-9 und ~3,5 cal. ka vor heute. Die spätpleistozäne und holozäne Gletscheraktivität im Nepal-Himalaya wird überwiegend vom Indischen Monsun gesteuert. Nur während des MIS 2 scheint sich der polare Jetstream weit genug nach Süden verlagert zu haben, um die Vergletscherung des gesamten Himalaya zu bestimmen. Während der Jüngeren Dryas lag die Einflussgrenze der Westwindzirkulation auf die Vergletscherung des Nepal-Himalaya möglicherweise zwischen dem Manaslu- und Langtang-Gebirge.
Gletschervorstöße im Pamir sowie in der Alay- und Turkestan-Kette sind aufgetreten um >93->136, ~60-80, (40-55), ~27-25, ~22-20, ~18, ~15,5, ~14,3 und 10.5 cal. ka vor heute. Die ausgedehnteste spätpleistozäne Vergletscherung fand in den MIS 5-3 statt. Sie war im Ostpamir durch eine Depression der Gleichgewichtslinie von 370-380 m gekennzeichnet; in der Turkestan- und Alay-Kette lagen die Depressionen um diese Zeit bei >750 m und 600 m. Gletschervorstöße im gesamten Nordwesten von Hochasien sind an klimatische Kaltphasen gebunden und korrelieren nicht mit Monsun-Maxima. Das spätpleistozäne Klima in der Region ist vor allem von der Westwindzirkulation und dem sibirischen Hochdruckgebiet bestimmt. Die Asynchronizität im Ausmaß der Pamirvergletscherung und der Kontinentalvergletscherung im Spätpleistozän ist zurückzuführen auf die im Laufe des letzten Glazialzyklus zunehmende Trockenheit in Zentralasien. Hochgelegene Pamirgletscher scheinen ihre maximale Ausdehnung früher (MIS 5-4) erreicht zu haben als tiefgelegene Gletscher (erste Hälfte des MIS 3). Indirekter Monsuneinfluss im Ostpamir ist möglicherweise mitverantwortlich für einige der spätglazialen Moränenstadien in diesem Gebiet.

1. Introduction

1.1 Rationale

Understanding Earth's climate is one of the most important and urgent tasks science is facing today. An accurate prediction of future climate shifts due to anthropogenic and natural impacts on atmospheric temperature and circulation is paramount for long-term planning of political and economic measures to secure and promote man's welfare in a changing environment. Physical circulation models, which could ultimately be able to simulate the non-linear effects of changes in climate forcing in a way precise enough for these purposes, integrally depend on palaeoclimate datasets to serve as either boundary conditions or evaluation benchmarks (Kohfeld & Harrison, 2000). One important palaeo-dataset for the evaluation of climate system models is the record of past mountain glaciations.

While studies in soil development in formerly glaciated mountain areas, e.g. considering horizon thickness, clay mineralogy, iron and aluminium chemistry, or feldspar weathering indices can be used to establish a relative chronology (Baeumler, 2001a), numerical ages can only be obtained using physical dating methods, e.g. radiocarbon dating, or luminescence dating (Bradley, 1999). The applicability of these methods in studies of glacial history, however, is limited.

Radiocarbon dating at present can provide reasonable ages only up to ~40 ka, and it is limited to preserved carbon-containing materials, which in arid regions may be few or absent. In addition, radiocarbon ages can provide no more than age limits for a great number of glacial deposits, because the radiocarbon age may not correspond to the glacial event, but reflect organisms dying long before, or long after it, respectively.

Luminescence dating requires fine-sandy to silty material well radiated during transport, but totally shielded from sunlight ever since deposition. Such material is not common in glacial deposits, and as the preservation of aeolian and fluvial sediments frequently is scarce in mountainous areas, chronologies obtained with luminescence dating are often fragmentary and leave room for different interpretations (e.g. Richards et al., 2000a, Kamp et al., 2003).

Surface exposure dating (SED) using the accumulation of in-situ cosmogenic nuclides (e.g. ^{3}He, ^{10}Be, ^{14}C, ^{26}Al, ^{21}Ne, ^{36}Cl) instead provides a way of dating rock surfaces directly, if

these have been freed from deep shielding (>3 m of rock cover) by a short-lived geologic event. Up to now, ^{10}Be surface exposure dating may be considered the most advanced and most widespread SED method. By employing ^{10}Be surface exposure dating in formerly glaciated catchments containing quartz rich rocks, complete glacial chronologies can be inferred without depending on the presence of buried organic material or the outcropping of suitable sediments for luminescence dating. Complete SED chronologies in turn can provide crucial information on palaeoclimate in the region, especially when combined with information derived from soil development investigations (Cerling & Craig, 1994, Fabel & Harbor, 1999, Gosse & Phillips, 2001).

This work is part of an effort to establish ^{10}Be surface exposure dating as an important new tool in the pedogeographical and palaeoecological research activities at the Institute of Soil Science and Soil Geography at the University of Bayreuth, in collaboration with the Paul Scherrer Institute at the ETH Zurich.

1.2 ^{10}Be surface exposure dating

In-situ cosmogenic ^{10}Be is continually produced within the upper one to three meters of the lithosphere by interaction of particles from the secondary cosmic radiation with the O and Si atoms of the quartz mineral lattice. The production rate of ^{10}Be in the mineral depends on the amount of cosmic radiation reaching the sample, which can be predicted by using empirical measurements of cosmic ray activity in the atmosphere, along with calibration measurements of ^{10}Be in rock surfaces with an independently known exposure age (Gosse & Phillips, 2001). In-situ produced ^{10}Be in quartz is locked in the mineral grid and therefore accumulates, its accumulation only limited by radioactive decay of the nuclide. The nuclide concentration N at a rock surface therefore is a function of its production rate P, the exposure time of the surface t, and its decay constant λ.

The standard physical model for ^{10}Be surface exposure dating is a flat, even, infinite rock surface z [g cm^{-2}] = 0, exposed to a full sky of cosmic radiation since a point in time t_0 [a] = 0 (Nishiizumi et al., 1993). The cosmogenic nuclide production rate at the surface is P [atoms g^{-1} a^{-1}], which below the surface decreases exponentially with the attenuation length Λ [g cm^{-2}] of the cosmic rays. No other way of production of ^{10}Be, e.g. by α-particles from U decay, is allowed in the model. Nuclides formed in the rock are completely retained and lost only by radioactive decay or surface erosion. Radioactive decay of the nuclide depends

on its concentration N [atoms g^{-1}] in the rock and its decay constant λ [a^{-1}]. In case of linear erosion with an erosion rate ε [g cm^{-2} a^{-1}], the resulting standard production equation used in ^{10}Be surface exposure dating is

$$N(t) = \frac{P}{\lambda + \frac{\varepsilon}{\Lambda}}\left(1 - \exp\left(-\left(\lambda + \frac{\varepsilon}{\Lambda}\right)t\right)\right), \tag{1}$$

or, resolved for t, the standard exposure age calculation equation,

$$t = -\frac{1}{\lambda + \frac{\varepsilon}{\Lambda}} \ln\left[1 - \left(\lambda + \frac{\varepsilon}{\Lambda}\right)\frac{N}{P}\right]. \tag{2}$$

Production in this model is simplified. The production rate P in fact has to be calculated separately for three production mechanisms (by neutrons, capture of slow negative muons, and reactions of fast muons) which are characterized by different values of Λ, and it has to be calculated as a product of the global standard production rate at sea level, high latitude, P_0, the local scaling factor S, and a set of correction factors f used to account for model weaknesses. These weaknesses are 1) the shielding of a part of the sky by topographic objects, 2) the shielding effect of surface inclination, 3) the shielding of the surface by overlying matter, like snow or vegetation, 4) the shielding effect of the finite thickness of the sample, 5) the neutron-scattering effects of the three-dimensional form of the sampled object, 6) the time-dependency of the production rate due to changes in the local magnetic field coordinates (dipole wobble) and strength (dipole moment), and 7) the time dependency of the production rate due to tectonic uplift or downlift of the sample surface.

Thus, despite the apparent simplicity of the production equation, a standard procedure for calculating ^{10}Be exposure ages still has not been agreed on. The differences are concerning 1) the scaling factors used to derive the local ^{10}Be production rate in quartz from the standardized ^{10}Be production rate in quartz at sea level in high latitude (SLHL), 2) the standardized production rate itself, 3) the complexity of treatment of the production by different production mechanisms, and 4) the set of correction factors used.

The interpretation of ^{10}Be exposure ages is also still problematic. Calculated exposure ages up to now are considered only within the uncertainties resulting from the errors of the measured concentrations. Rigorous error analysis is often put aside (Gosse & Phillips,

2001). Secondly, deriving a moraine age from surface exposure ages of a selection of erratic boulders has in some cases proven to be a more difficult task than thought at first. On the one hand, erratic boulders deposited on a moraine may contain ^{10}Be inherited from a previous period of exposure, leading to an overestimation of the moraine age; on the other hand, erratic boulders might have been broken free from a larger block, or might have been cleared from sediment cover long after deposition of the moraine, leading to an underestimation of the moraine age (Owen et al., 2003a, b). Several models have been proposed to derive a moraine age from a distribution of erratic boulder exposure ages (Zreda et al., 1994; Hallet & Putkonen, 1994; Shanahan & Zreda, 2000; Putkonen & Swanson, 2003), but all of them are based on linear moraine degradation, which can explain unimodal distributions of exposure ages only. However, bi- or even polymodal distributions are frequently observed (e.g. Owen et al., 2003a, b) and have to be interpreted.

In this work, I introduce TEBESEA (acronym for TEn BEryllium Surface Exposure Ages), a program I devised for the calculation of ^{10}Be surface exposure ages of erratic boulders with fully propagated errors, and I employ this program 1) to evaluate the current calculation procedures in the light of the standard in-situ cosmogenic ^{10}Be production rate calibration studies published up to now, 2) to compare them in the context of our dating studies in Nepal and Central Asia, and 3) to estimate the influence of the variable correction factors on exposure ages. Further, I discuss in detail both error propagation and interpretative model use in deriving moraine ages from ^{10}Be exposure ages of erratic boulders, in order to understand how moraine ages are best determined from erratic boulder exposure ages, and how exact those ages can safely be considered at present.

1.3 Palaeoglaciations of the Nepal Himalaya

Since the late 1990s, a lot of effort is spent in defining new glacial chronologies for the Nepal Himalaya using optically stimulated luminescence (OSL) and in-situ cosmogenic nuclide dating techniques (e.g. Richards et al., 2000b, Asahi et al., 2003, Finkel et al., 2003). These studies provide a new foundation for the discussion about past climatic conditions in the Himalaya as a whole, which is mainly about whether the past glaciations have been triggered during warm stages, in connection with an enhanced Indian monsoon, or during cold stages, in connection with a strengthening of the westerly circulation (Benn & Owen, 1998, Bush, 2000, Fort, 2000).

In this work, ^{10}Be surface exposure dating (SED) of erratic boulders is applied to confirm and complement the results of former soil geographic studies at two sites in the central Nepal Himalaya, the Macha Khola Valley (Zech et al., 2003), and the Langtang Valley (Baeumler et al., 1996, 1997, Baeumler, 2001a). Results are compared with other SED and OSL dating studies in order to evaluate, to which extent glacial advances in different regions of central Nepal have been synchronous.

1.4 Palaeoglaciations of the Pamir

A lot of effort is presently spent in defining numerical glacial chronologies all over High Asia, ranging from the mountain ranges of Central Asia in the northwest to the southeastern margin of the Tibetan plateau (e.g. Owen et al., 2002a, Owen et al., 2003c, Gillespie et al., 2003), a region that was extensively glaciated in the past and is considered a key locality for the understanding of the world's climate (Benn & Owen, 1998). However, there still is no consensus about the timing of glaciations in the different parts of the region and its implications for past climate change (Zheng et al., 2002, Ono et al., 2004, He et al., 2004).

In this study ^{10}Be SED is used to reconstruct the glacial history of the north-western part of High Asia, namely the Central Asian mountains between the Turkestan and Alay Ranges of south-western Kyrgyzstan, and the south-central Pamir plateau of eastern Tajikistan.

2. Materials & Methods

2.1 Sites & Samples

2.1.1 Nepal Himalaya

The central Nepal Himalaya (28°N, 83-86°E) is the highest mountain range of the world. In the west, it is dominated by the Dhaulagiri and Annapurna, in the east by the Khumbu and Khangchenjunga massifs, all culminating above 8000 m a.s.l. Climate in the region today is dominated by the Indian monsoon in summer and the westerly circulation in winter.

The Macha Khola is a first-order river originating at the southeastern end of the Manaslu massif east of the Annapurna massif. The present ELA in its valley is about 5100 m a.s.l. The detailed results of soil investigations in the Macha Khola Valley are presented by Zech

et al. (2003). Four different moraines were sampled, belonging to the most extensive late Pleistocene advance, as well as the proposedly last glacial maximum, lateglacial and neoglacial advances.

The Langtang Valley is an east-west-trending valley in the Langtang Himal, between the Manaslu and the Khumbu Himal. It has a mean annual precipitation of 1200 mm, a mean annual temperature of 2.7°C and an ELA of 5300 m (Miehe, 1990). The investigation of the glacial deposits in this valley has a long tradition (Heuberger et al., 1984, Ono, 1986, Shiraiwa & Watanabe, 1991, Baeumler et al. 1996, 1997). Three Lateglacial-to-Holocene moraines were sampled.

2.1.2 Central Asia

The Pamir (37-39°N, 71-75°E) is one of the highest mountain regions of the world with several peaks rising above 7000 m a.s.l. The western Pamir consists of rugged mountain chains with deeply incised valleys and large valley glaciers. The eastern Pamir, in contrast, is a high plateau of ~4000 m a.s.l., topped by more subdued and often heavily debris-covered mountain ranges, most of which at present are not or only scarcely glaciated. To the north, the Pamir block is tectonically converging on the east-west-trending Turkestan-Alay Range, both separated by the broad Alay Valley. Climate in the region today is dominated by the westerly circulation, bringing winter and spring rain to the western Pamir and leaving the eastern Pamir extremely arid in the rainshadow of the western chains (UNEP, 2002).

In this region, five areas were chosen for sampling, the Aksu Valley in the Turkestan Range, the Koksu Valley in the Alay Range, the Ailuitek Pass area in the north-central Pamir, the lake Yashilkul area in the south-central Pamir, and the Kol-Uchkol and Gurumdy Valleys in the southeast-central Pamir. In each case the moraines of the most extensive glaciation still recognizable, as well as a selection of younger Pleistocene moraines were sampled to reconstruct a new glacial chronology.

2.1.3 Sampling & Analysis

Chunks of up to 8 cm thickness have been loosened by hammer and chisel from the centre surfaces of the largest and tallest boulders positioned on the culminations of each sampled deposit. Boulders showing signs of spalling or recent dislocation were avoided. Position and altitude were read from a GPS and barometric altimeter combination. Topographic

shielding and surface inclination were noted using a compass and inclinometer. Samples were analyzed for ^{10}Be following the procedure of Kohl & Nishiizumi (1992) as modified by Ivy-Ochs (1996). ^{10}Be/^{9}Be was measured at the AMS facility of the Paul Scherrer Institute at the ETH Zurich and corrected to conform to ICN standards.

2.2 Calculation of exposure ages

The simple standard calculation equation of exposure ages (2) is no longer valid as soon as several production mechanisms of ^{10}Be with different parameters have to be considered, or if time-dependent correction factors apply. In this case a kind of iteration has to be used to solve the resulting set of equations (1) for the exposure age *t*. To do this, I have developed the program TEBESEA (acronym for TEn BEryllium Surface Exposure Ages).

2.2.1 TEBESEA

The program TEBESEA is devised as an MS-Excel™ file. For each sample, it requires the entry of 1) sample name, geographic latitude [°], geographic longitude [°], and altitude [m]; 2) the correction factors for topographic shielding, which can be calculated from compass-inclinometer data using a subroutine; 3) surface inclination and its azimuth [°]; 4) sample thickness [cm]; 5) snow or vegetation cover [g cm^{-2}] if any, and sediment cover [g cm^{-2}] if any; 6) the measured ^{10}Be concentration [atoms g^{-1}] with its error [atoms g^{-1}], which again can be calculated from measurement and laboratory data using a second subroutine; 7) the estimated or measured surface erosion rate [cm a^{-1}] with its uncertainty [cm a^{-1}]; 8) the estimated uplift rate [m a^{-1}], and 9) the rock density [g cm^{-3}] with its uncertainty [g cm^{-3}]. TEBESEA calculates the fully corrected exposure ages resulting from each of the presently used scaling systems (Stone, 2000, Heisinger et al., 2002b, Dunai, 2001, Schaller et al., 2002, Desilets & Zreda, 2003) with their fully propagated uncertainties.

Atmospheric depths are calculated from metrical altitudes using the physical standard atmosphere (Lide, 1999). For 0.5 to 10 ka, geomagnetic latitude is calculated from geographic latitude and the palaeo-pole positions of Ohno & Hamano (1992). From 11 cal. ka B.P. onwards geographic and geomagnetic latitudes are equated. To correct for changing dipole intensity, we used the Sint-200 record of Guyodo & Valet (1996), which was converted into absolute intensities by multiplying with $5.29 \cdot 10^{-22}$ Am² (Gosse & Phillips, 2001, their Fig. 7), supplemented for the Holocene by the VADM data of McElhinny & Senanayake (1982).

The decay constant λ for ^{10}Be is taken to be $(4.56 \pm 0.15) \cdot 10^{-7}$ a^{-1} (Holden, 1990). For quartz-rich rocks, a density ρ of 2.7 ± 0.1 g cm^{-3} is estimated. For the attenuation length Λ for neutron spallations in rock, a value of 155 ± 5 g cm^{-2} is adopted here (Gosse & Phillips, 2001). For slow negative muons, and fast muons, attenuation lengths of 1510 ± 10 g cm^{-2}, and 4320 ± 500 g cm^{-2}, respectively, are used (Heisinger et al., 2002a, b). Where the depth profile of Schaller et al. (2002) is used, the values for the attenuation lengths in rock are replaced by the *b*-values of their exponential functions (their Tab. A1.1). For the erosion rate ε of the sample surface, a maximum estimate of 5 ± 2 mm ka^{-1} for granitic rocks in a semiarid climate (Phillips et al., 1997; Owen et al., 2002b) is used as a reference. For uplift correction estimates, a model rate of 3 mm a^{-1} is used.

2.2.2 Calibration

For calibration of TEBESEA, the results of the best documented published calibration studies in water targets (Nishiizumi et al., 1996, Brown et al., 2000) and rocks (Bierman et al., 1996, Stone et al., 1998, Klein & Gosse, 2002, and Kubik & Ivy-Ochs, 2003) have been rescaled, applying all corrections possible given the available information. Erosion and tectonic uplift had to be neglected in all calibrations for lack of suitable data. The results from all scaling were compared and evaluated, and only the best ones were chosen for actual calibration for calculation of measured exposure ages.

3. Results & Discussion

3.1 Calibrations and comparison of scaling systems

The water target calibrations yield low translated production rates in quartz. Most likely, the reason for this is to be found in an inadequacy of the conversion factor to production rates in quartz as measured by Nishiizumi et al. (1996).

Apart from that, the scaling system of Lal (1991) in both modified forms is convincingly able to fit the measurements of Nishiizumi et al. (1996) alone or together with the measurements of Brown et al. (2000). Only the measurements of Brown et al. (2000) alone, including a single low-quality value, are best explained by the scaling systems of Desilets & Zreda (2003) and Dunai (2001). In this case however, the calibration yields an exceptionally low standard ^{10}Be production rate, most different from the mean standard production rates implied by the rock calibrations.

The calibrations in rock samples yield rates between 4.43 and 5.68 atoms g^{-1} a^{-1}. The calibration of Stone et al. (1998) results in a significantly lower production rate than the other three studies. If this study is excluded on the basis of possible influence of snow cover and tectonic uplift, the error of the mean is significantly reduced. The remaining three calibrations are again best brought into accord by the modified scaling systems of Lal (1991). Applying geomagnetic correction, the error of the mean is further reduced in all cases.

The difference in altitude scaling between the systems of Dunai (2000) and Desilets & Zreda (2003) on the one hand and the system of Lal (1991) on the other hand results in higher standard production rates from the low altitude calibration sites and lower standard production from the high altitude calibration sites using the former systems. Given the measured data, this leads to a larger span between the calibrated standard production rates in the systems with a variable atmospheric attenuation length. The present data therefore does not support the altitude scaling suggested by Dunai (2000) or Desilets & Zreda (2003), but confirms the earlier work by Lal (1991). Presently, the use of the scaling system of Lal (1991) as modified by Stone (2000), but with a negative muon capture contribution of 1.2% (Braucher et al., 2003), and including geomagnetic correction, yields the lowest uncertainties and must be considered the best option. For this system a standard production rate of 5.35 ± 0.15 atoms $g^{-1}a^{-1}$ is calibrated.

For all scaling systems in this comparison, the predicted ^{10}Be production is the same around 2000 m altitude at both sites. Above this altitude the newer scaling systems predict a higher, below they predict a lower production. The deviation between Lal's (1991) and the other two principal scaling systems passes 10% between altitudes of ~3000 and 4000 m a.s.l. and reaches up to 20-30% at 5000 m a.s.l; it is more pronounced at the higher latitude model site at 38°N, 74°E than at the lower latitude model site at 28°N, 85°E.

Comparing Dunai's (2001) and Desilets' and Zreda's (2003) scaling systems, the differences decrease with exposure time, and they are always lower than the assumed 10% uncertainty of the scaling factors themselves. The differences between the models result from their different calculation models for the local cutoff rigidity.

Up to now there is no convincing evidence for higher production rates in high altitudes as predicted by the more recent scaling systems. However, the database is still narrow. New high altitude calibrations are needed for clarification.

All middle and early late Pleistocene exposure ages are significantly increased by correcting for reasonable estimates of erosion and tectonic uplift, and they are significantly lowered by correction for geomagnetic variations and by the effects of the refined depth profile of ^{10}Be production measured by Heisinger et al. (2002a, b).

3.2 Interpretation of exposure ages

A general uncertainty of 11% is calculated to result from the present uncertainties of standard production rate, scaling factor, and measured concentration combined.

Rates of surface erosion and tectonic uplift as they are estimated at present increase the total uncertainty of exposure ages to great extent, the former more than the latter. Given these estimates, exposure ages of ~50 ka, ~100 ka, ~150 ka and ~200 ka have uncertainties of ~20%, ~30%, ~50%, and ~90%, respectively. If the erosion rate and the uplift rate are constrained to 5 ± 0.5 mm ka^{-1} and 3 ± 0.3 mm^{-1}, respectively, however, the uncertainty due to the uplift rate becomes insignificant, and the uncertainty due to the erosion rate becomes smaller than the uncertainty due to the scaling factor. In this case, the error of exposure ages would be ~20% for ages of ~100 ka and ~40% for ages of ~200 ka.

Exposure age distributions from single moraines frequently contain ages older than the deposition age due to inherited ^{10}Be in some of the boulders, and they frequently are not unimodal, but show two or more age clusters. In some cases, age clusters younger than the deposition age of a moraine are synchronous on different moraines in the same region, possibly indicating phases of enhanced, climate-driven surface activity. The interpretation of such a set of exposure age distributions is suggested to proceed along the following lines:

1) The oldest exposure age found on each moraine may be interpreted as a first approximation of the actual deposition age.
2) If comparison with other dated moraines of the same age or older shows that the oldest age is unreasonably high, inheritance is probable.
3) An oldest age equaled by others on stratigraphically related moraines can be considered close to the deposition age of the moraine with increased confidence.
4) If comparison with other dated moraines of the same age or younger shows that the oldest age on a moraine is unreasonably low, the deposition age of the moraine is

probably underestimated, i.e. all sampled boulders have likely been freed from cover or tilted during moraine degradation.

5) Ages too low to indicate deposition ages, if matched by ages on other moraines in the same area, or by other pedological, sedimentological or climatological proxies, may be interpreted to indicate phases of pronounced landform surface instability.

6) Spatial trends of moraine ages can give information on depositional or degradational chronologies of a moraine.

Sampling of a minimum of 3-5 boulders from each of a maximum number of different moraines, which should be stratigraphically related and should cover all encountered relative ages, may thus be necessary to draw any climatological conclusions from ^{10}Be SED.

3.3 Palaeoglaciations of the Nepal Himalaya

Boulders from the oldest moraine in the Macha Khola Valley yielded exposure ages between 34 and 97 ka, allowing for possible deposition of the moraine during the MIS 3 through 5, or even earlier. There is, however, a good agreement between these ages and those of the *Thyangboche* I stage in the Khumbu Himal (Finkel et al., 2003), pointing to deposition during the MIS 5.

The proposedly MIS 2 moraine dated in the Macha Khola Valley, MK5, yielded exposure ages between 11 and 26 ka. The three oldest ages allow for glacial advance between 19 and 26 cal. ka B.P., which is in excellent agreement with other data from the region (Richards et al., 2000b, Finkel et al., 2003, Schluetz & Zech, 2004). Along with the apparent absence of an MIS 4 advance, this might indicate, that in the late Pleistocene only during the late MIS 2, the influence of the westerly circulation on glaciation extended over the whole Himalayan system.

The lateglacial advance in the Macha Khola Valley is dated by our exposure ages to between 11.1 and 12.3 cal. ka B.P., covering the Younger Dryas event. Younger Dryas ages have not been found in the Khumbu Valley (Finkel et al., 2003), or in the Langtang Valley, but have been reported from the western Himalaya (Owen et al., 2001, 2002b). It may be that the influence of the westerly circulation during the time of the Younger Dryas just reached the Manaslu massif and did not extend farther to the east.

The neoglacial moraine in the Macha Khola Valley is dated to around 3 cal. ka B.P., confirming former radiocarbon dating (Zech et al., 2003).

The oldest moraine in the Langtang Valley yielded exposure ages of 11.6-14.7 ka. It is clearly correlative with the *Pheriche* II stage in the Khumbu area (Finkel et al., 2003).

An Holocene moraine, dated by Baeumler (2001a) to be older than 6 ka, is in fact 7.7-8.7 ka old. This deposit excellently correlates with the *Chhukung* stage in the Khumbu and Kanchenyunga Himal (Finkel et al., 2003, Asahi et al., 2000). This stage occurred during the Holocene maximum of monsoon strength (Leuschner & Sirocko, 2000) and is clearly indicative of monsoon influence on glaciation in the Himalaya.

Another Holocene moraine in the Langtang Valley has an exposure age of 3.3-3.5 ka, correlating with the *Thukhla* stage of the Khumbu area (Finkel et al., 2003) and the neoglacial advance in the Macha Khola Valley.

3.4 Palaeoglaciations of the Pamir

All moraines in the Aksu Valley, notwithstanding their different stratigraphical ages, yield similar distributions of erratic boulder exposure ages, which range from 9 to 25 ka. A radiocarbon age of 21,226 ± 146 a B.P. (~24 cal. ka B.P) from a buried A horizon on top of the youngest sampled moraine (W. Zech, unpubl.) shows, however, that this moraine is ~25 ka old, and that all older moraine surfaces in the valley must have experienced heavy degradation during the end of the last glacial. Comparison with the Koksu chronology suggests that the maximum late Pleistocene glacier advance with an ELA depression of >750 m probably occurred during MIS 4-3. Older moraine remnants may still be considered to be of middle Pleistocene age.

Exposure ages of 47-68 ka from the oldest moraine in the Koksu Valley with an ELA depression of ~600 m indicate deposition during the MIS 4 or early MIS 3. A proposed Younger Dryas moraine in 3440 m a.s.l. unambiguously yields exposure ages of ~10.5 ka. It apparently postdates the Younger Dryas event (YD, 11.5-12.9 cal. ka B.P.) by about 1500 years. Probably, the increasing moisture supply at the beginning of the Holocene had a larger effect on the advancing Abramov glacier than the temperature decrease during the YD.

At Ailuitek Pass, four of five exposure ages from the high lateral moraine left by the most extensive glacier advance recognizable lie between 61 and 83 ka, covering the late MIS 5 and the MIS 4. Three exposure ages from a younger, less extensive moraine at the Ailuitek lie between 14 and 20 ka, documenting the associated glacier advance to have occurred during the MIS 2.

At lake Yashilkul, the boulders from the oldest moraine, YK1, yield exposure ages ranging between 58 and 84 ka, covering the MIS 4 and late MIS 5. The age of the second moraine generation is problematic. Ages obtained from the outer wall of one moraine lobe scatter between 18 ka and 61 ka, while the ages of the recessional wall of a correlative lobe closely group around 18 ka. The ages on the probably correlative lateral moraines of both lobes in turn, scatter between 12 and 65 ka, clustering around 41, 30, 22, and 12 ka. While the ages below 40 ka on the lateral moraines can easily be explained by moraine degradation, the older ages from these moraines allow two ways of interpretation: Either the lateral moraines belong to the oldest moraine generation deposited during the MIS 5-4 and have been degraded in later times. In this case the younger lobes were deposited later, at some time before 18 cal. ka B.P., and the older ages are caused by inheritance. Or the lateral moraines have been deposited along with the younger lobes during the early MIS 3, 60-40 cal. ka B.P. At present, there is no way of deciding between the two hypotheses. Both stages are characterized by ELA depressions of ~370 m.

In the southern Alichur Range area, the oldest glacial deposit yield exposure ages of 66-86, and 93-136 ka. They were most probably left by a middle Pleistocene or even earlier advance. The maximum late Pleistocene glaciation in the Kol-Uchkol-Gurumdy area with an ELA depression of ~380 m is represented by exposure ages of 57-75 ka, covering the MIS 4. Younger deposits in both valleys with ELA depressions of 280-320 m yield similar exposure ages between 13 and 28 ka. Two stages, one around 27 cal. ka B.P., one around 22 cal. ka B.P. can be distinguished. Two more recessional stages occurred in the lateglacial period, around ~15.5 cal. ka B.P., and ~14.3 cal. ka B.P.

As the data show, late Pleistocene glaciation in the northwestern part of High Asia has been regionally synchronous, but globally asynchronous. The maximum late Pleistocene advance in this region most probably occurred during the MIS 4, 75-60 cal. ka B.P., or during the early MIS 3 (52-45 cal. ka B.P.). MIS 2 moraines are ubiquitous, but they are significantly smaller in extent than those of the earlier late Pleistocene advances.

Glaciation in western High Asia thus seems to be coupled to cold phases associated with insolation minima (Thompson et al., 1997, Berger & Loutre, 1991), but also to be clearly sensitive to moisture advection, which in the region has been successively decreasing over the course of the last glacial cycle. The reason for this aridification most likely is to be found in the growing strength of the Siberian Anticyclone, leading to a deflection of precipitation in winter and spring.

The maximum late Pleistocene advance has occurred earlier on high altitude plateaus than in lower altitude valleys, where it seems to have occurred during or lasted until the early MIS 3.

The ~15 cal. ka B.P. advance in the Southern Alichur Range may be an indicator of beginning monsoonal influence, as it is most pronounced in eastern Tibet (Owen et al., 2003a, b), but also occurred in the eastern Pamir and in the Indus Valley (Richards et al., 2000a).

4. Conclusions

The method of ^{10}Be surface exposure dating has been successfully established at the Institute of Soil Science and Soil Geography at the University of Bayreuth.

Age calculation in ^{10}Be surface exposure dating can now be rapidly done using the program TEBESEA. This allows quick comparison of results from different workgroups, which otherwise is difficult because of the various ways of calculation in use.

The traditional scaling system of Lal (1991), as modified by Stone (2000), still proves to be the one best able to bring existing calibration results into accord. Using current calibrations and a contribution of capture of slow negative muons of 1.2% (Braucher et al., 2003), the total standard production rate at sea level, high latitude, amounts to 5.35 ± 15 atoms g^{-1} a^{-1}.

The scaling systems of Dunai (2001) and Desilets & Zreda (2003) do not significantly differ from each other, but show differences in their way of accounting for past geomagnetic variations. Their refined altitude dependency of cosmogenic nuclide production is not convincing as yet given the existing calibration data. However, the notion that ages from high altitude sites may be much younger than calculated using the scaling system of Lal (1991) should be considered. New high altitude calibrations are needed for clarification.

The uncertainties of ^{10}Be surface exposure ages are presently dominated by the errors of the scaling factor, the erosion rate, and, in mountainous areas, the tectonic uplift rate. As long as surface erosion and tectonic uplift cannot be reasonably constrained to within 10%, exposure ages older than 30-40 ka are no more than rough estimates. In order to increase the precision of ^{10}Be exposure ages >40 ka, new methods are needed to put a better constraint on the surface erosion rates of any single exposed boulder.

In order to obtain a concise glaciation history of a mountainous region, ^{10}Be exposure ages from several moraines within a region have to be interpreted in the light of the local stratigraphical and climatological context. Sampling of a minimum of 3-5 boulders from each of a maximum number of different moraines, which should be stratigraphically related and should cover all encountered relative ages, may be necessary to draw any climatological conclusions from ^{10}Be SED.

^{10}Be surface exposure ages have excellently confirmed and complemented former soil geographic work in the Nepal Himalaya.

Late Pleistocene and Holocene glacier advances in the Macha Khola Valley have been dated at 70-100, 20-23, 11-12 and around 3 cal. ka B.P. In the Langtang Valley, lateglacial and Holocene glacier advances have been dated at 14-15, 8-9 and ~3.5 cal. ka B.P.

The new glacial chronology of the Nepal Himalaya shows that, except for the MIS 2, glacial activity in the region has been controlled by the Indian monsoon rather than the westerly circulation. During the coldest phase of the MIS 2, the westerly jetstream appears to have shifted as far south as to affect glaciation all over the Himalaya. During the Younger Dryas, the eastern limit of the influence of the westerly circulation on Himalaya glaciation may have been situated between the Manaslu and Langtang Himal.

The oldest erratic boulders dated in the Pamir have exposure ages of >93-136 ka. Most probably they have been deposited during the middle Pleistocene. Late Pleistocene glacial stages of successively reduced extent in the Pamir and the Alay Range have exposure ages of ~60-80 ka, (40-55 ka), ~27-25 ka, ~22-20 ka, ~18 ka, ~15.5 and ~14.3 ka, and 10.5 ka.

Late Pleistocene glaciation in the Pamir and all over northwestern High Asia was contemporaneous with climatic cold phases rather than monsoon maxima. Its extent was regionally synchronous but globally asynchronous, due to increasing aridity in Central Asia over the course of the last glacial cycle. In contrast to the Nepal Himalaya, climate in

this region seems to have been influenced mostly by the westerly circulation and the Siberian Anticyclone. Some indirect monsoonal influence in the eastern Pamir may be responsible for the existence of some late-glacial moraine stages in this area.

High altitude glaciers in Central Asia seem to have reached their maximum extent earlier (MIS 4) than low altitude glaciers (first half of MIS 3), possibly due to prolonged glacial aridity imparting with moisture advection into high altitudes, inducing glacial retreat, but prolonged cold during the same time imparting with glacier ablation in lower altitudes, inducing glacial advance.

5. References

ASAHI, K., TSUKAMOTO, S., AOKI, T., WATANABE, T. 2000. Late Quaternary glaciations in the Kangchenjunga Himal, eastern Nepal: based on absolute and relative dating. In: Abstract volume for the symposium on Quaternary glaciation in Monsoonal Asia, Academica Sinica, Chengdu, June 5-18, p. 1.

ASAHI, K., WATANABE, T., TSUKAMOTO, S. 2003. History of glaciations in the Nepal Himalayas and reconstruction of palaeoclimate since the last glacial. XVI INQUA Congress Programs with Abstracts, DRI, Reno, Nv., p. 156.

BAEUMLER, R. 2001a. Vergleichende bodenkundliche Untersuchungen in Hochasien und Kamtschatka. Relief Boden Palaeoklima 16, Gebrueder Borntraeger, Berlin, 125 p.

BAEUMLER, R. 2001b. Pedogenic studies in aeolian deposits in the high mountain area of eastern Nepal. Quaternary International 76/77, 93-102.

BAEUMLER, R., KEMP-OBERHETTINGER, M., ZECH, W., HEUBERGER, H., SIEBERT, A., MADHIKARMI, D. P., POUDEL, K. P. 1996. Soil weathering on glacial and glaciofluvial deposits in the Langtang Valley (central Nepal) and its relation to the glacial history. Zeitschrift fuer Geomorphologie N. F., Supplement-Band 103, 373-387.

BAEUMLER, R., MADHIKARMI, D. P., ZECH, W. 1997. Fine silt and clay mineralogical changes of a soil chronosequence in the Langtang Valley (central Nepal). Zeitschrift fuer Pflanzenernaehrung und Bodenkunde 160, 413-421.

BENN, D. I., OWEN, L. A. 1998. The role of Indian summer monsoon and the mid-latitude westerlies in Himalayan glaciations: review and speculative discussion. Journal of the Geological Society of London 155, 353-363.

BERGER, A. L., LOUTRE, M. F. 1991. Insolation values for the climate of the last 10 million years. Quaternary Science Reviews 10, 297-317.

BIERMAN, P., LARSEN, P., CLAPP, E., CLARK, D. 1996. Refining estimates of ^{10}Be and ^{26}Al production rates. Radiocarbon 38, 149.

BRADLEY, R. S. 1999. Palaeoclimatology, Second Edition. International Geophysics Series, vol. 64. Academic Press, London, 610 p.

BRAUCHER, R., BROWN, E. T., BOURLÈS, D. L., COLIN, F. 2003. In situ produced ^{10}Be measurements at great depths: implications for production rates by fast muons. Earth and Planetary Science Letters 211, 251-258.

BROWN, E. T., TRULL, T. W., JEAN-BAPTISTE, P., RAISBECK, G., BOURLÈS, D., YIOU, F., MARTY, B. 2000. Determination of cosmogenic production rates of ^{10}Be, ^{3}He, and ^{3}H in water. Nuclear Instruments and Methods in Physics Research B 172, 873-883.

BUSH, A. B. G. 2000. A positive climatic feedback mechanism for Himalayan glaciation. Quaternary International 65/66, 3-13.

CERLING, T. E., CRAIG, H. 1994. Geomorphology and in situ cosmogenic isotopes. Annual Review of Earth and Planetary Sciences 22, 273-317.

DESILETS, D., ZREDA, M. 2003. Spatial and temporal distribution of secondary cosmic-ray nucleon intensities and applications to in situ cosmogenic dating. Earth and Planetary Science Letters 206, 21-42.

DUNAI, T. J. 2000. Scaling factors for production rates of in situ produced cosmogenic nuclides: a critical reevaluation. Earth and Planetary Science Letters 176, 157-169.

DUNAI, T. J. 2001. Influence of secular variation of the geomagnetic field on production rates of in situ produced cosmogenic nuclides. Earth and Planetary Science Letters 193, 197-212.

FABEL, D., HARBOR, J. 1999. The use of in-situ produced cosmogenic radionuclides in glaciology and glacial geomorphology. Annals of Glaciology 28, 103-110.

FINKEL, R. C., OWEN, L. A., BARNARD, P. L., CAFFEE, M. W. 2003. Beryllium-10 dating of Mount Everest moraines indicates a strong monsoon influence and glacial synchroneity throughout the Himalaya. Geology 31, 561-564.

FORT, M. 2000. Glaciers and mass wasting processes: their influence on the shaping of the Kali Gandaki Valley (higher Himalaya of Nepal). Quaternary International 65/66, 101-119.

GILLESPIE, A., RUPPER, S., ROE, G. 2003. Climatic interpretation from mountain glaciations in Central Asia. XVI INQUA Congress Programs with Abstracts, DRI, Reno, Nv., p. 170.

GOSSE, J. C., PHILLIPS, F. M. 2001. Terrestrial in situ cosmogenic nuclides: theory and application. Quaternary Science Reviews 20, 1475-1560.

GUYODO, Y., VALET, J.-P. 1996. Relative variations in geomagnetic intensity from sedimentary records: the past 200.000 years. Earth and Planetary Science Letters 143, 23-26.

HALLET, B., PUTKONEN J. 1994. Surface dating of dynamic landforms: young boulders on aging moraines. Science 265, 937-940.

HE, Y., THEAKSTONE, W. H., ZHANG, Z., ZHANG, D., YAO, T., CHEN, T., SHEN, Y., PANG, H. 2004. Asynchronous Holocene climatic change across China. Quaternary Research 61, 52-63.

HEISINGER, B., LAL, D., JULL, A. J. T., KUBIK, P., IVY-OCHS, S., NEUMAIER, S., KNIE, K., LAZAREV, V., NOLTE, E. 2002a. Production of selected cosmogenic radionuclides by muons 1. Fast muons. Earth and Planetary Science Letters 200, 345-355.

HEISINGER, B., LAL, D., JULL, A. J. T., KUBIK, P., IVY-OCHS, S., KNIE, K., NOLTE, E. 2002b. Production of selected cosmogenic radionuclides by muons 2. Capture of negative muons. Earth and Planetary Science Letters 200, 357-369.

HEUBERGER, H, MASCH, E., PREUSS, E., SCHROECKER, A. 1984. Quaternary landslides and rock fusion in central Nepal and the Tyrolian Alps. Mountain Research and Development 4, 345-362.

HOLDEN, N. E. 1990. Total half-lives for selected nuclides. Pure and Applied Chemistry 62, 941-958.

IVY-OCHS, S. 1996. The dating of rock surface using in situ produced ^{10}Be, ^{26}Al and ^{36}Cl, with examples from Antarctica and the Swiss Alps. Diss. ETH No. 11763, Zuerich, 197 p.

KAMP, U. JR., HASERODT, K., SHRODER, J. F. JR. 2003. Quaternary landscape evolution in the eastern Hindu Kush, Pakistan. Geomorphology 57, 1-27.

KLEIN, J., GOSSE, J. C. 2002. Production rates of ^{10}Be and ^{26}Al in mid-latitudes and high altitudes. Goldschmidt Conference Abstracts 2002, A 403.

KOHFELD, K. E., HARRISON, S. P. 2000. How well can we simulate past climates? Evaluating the models using global palaeoenvironmental datasets. Quaternary Science Reviews 19, 321-346.

KOHL, C. P., NISHIIZUMI, K. 1992. Chemical isolation of quartz for measurement of in-situ produced cosmogenic nuclides. Geochimica et Cosmochimica Acta 56, 3583-3587.

KUBIK, P. W., IVY-OCHS, S. 2003. A re-evaluation of the 0-10 ka ^{10}Be production rate for exposure dating obtained from the Koefels (Austria) landslide. Nuclear Instruments and Methods in Physical Research B, in press.

LAL, D. 1991. Cosmic ray labelling of erosion surfaces: in situ nuclide production rates and erosion models. Earth and Planetary Science Letters 104, 424-439.

LEUSCHNER, D. C., SIROCKO, F. 2000. The low latitude monsoon climate during Dansgaard-Oeschger cycles and Heinrich events. Quaternary Science Reviews 19, 243-254.

LIDE, D. R. 1999. The physical standard atmosphere. In: CRC Handbook of Chemistry and Physics, 79th edition. CRC Press, Boca Raton, Florida, 14-16 – 14-22.

MCELHINNY, M. W., SENANAYAKE, W. E. 1982. Variations in the geomagnetic dipole 1: The past 50.000 years. Journal of Geomagnetism and Geoelectricity 34, 39-51.

MIEHE, G. 1990. Langtang Himal. Flora und Vegetation als Klimazeiger und -zeugen im Himalaya. Dissertationes Botanicae 158, 559 p.

NISHIIZUMI, K., KOHL, C. P., ARNOLD, J. R., KLEIN, J., FINK, D., MIDDLETON, R., LAL, D. 1993. Role of in situ cosmogenic nuclides ^{10}Be and ^{26}Al in the study of diverse geomorphic processes. Earth Surface Processes and Landforms 18, 407-425.

NISHIIZUMI, K., FINKEL, R. C., KLEIN, J., KOHL, C. P. 1996. Cosmogenic production of ^{7}Be and ^{10}Be in water targets. Journal of Geophysical Research 101, 22225-22232.

OHNO, M., HAMANO, Y. 1992. Geomagnetic poles over the past 10.000 years. Geophysical Research Letters 19, 1715-1718.

ONO, Y. 1986. Glacial fluctuations in the Langtang Valley, Nepal Himalaya. Goettinger Geographische Abhandlungen 81, 31-38.

ONO, Y., SHULMEISTER, J., LEHMKUHL, F., ASAHI, K., AOKI, T. 2004. Timings and causes of glacial advances across the PEP-II transect (East-Asia to Antarctica) during the last glaciation cycle. Quaternary International 118-119, 55-68.

OWEN, L. A., GUALTIERI, L., FINKEL, R. C., CAFFEE, M. W., BENN, D. I., SHARMA, M. C. 2001. Cosmogenic radionuclide dating of glacial landforms in the Lahul Himalaya, northern India: defining the timing of Late Quaternary glaciation. Journal of Quaternary Science 16, 555-563.

OWEN, L. A., FINKEL, R. C., CAFFEE, M. W. 2002a. A note on the extent of glaciation throughout the Himalayas during the Last Glacial Maximum. Quaternary Science Reviews 21, 147-157.

OWEN, L. A., FINKEL, R. C., CAFFEE, M. W., GUALTIERI, L. 2002b. Timing of multiple glaciations during the Late Quaternary in the Hunza Valley, Karakoram Mountains, northern Pakistan: defined by cosmogenic radionuclide dating of moraines. Geological Society of America Bulletin 28, 431-434.

OWEN, L. A., MA, H., DERBYSHIRE, E., SPENCER, J. Q., BARNARD, P. L., ZENG, Y. N., FINKEL, R. C., CAFFEE, M. W. 2003a. The timing and style of Late Quaternary glaciation in the La Ji Mountains, NE Tibet: evidence for restricted glaciation during the latter part of the Last Glacial. Zeitschrift fuer Geomorphologie N. F., Supplementband 130, 263-276.

OWEN, L. A., SPENCER, J. Q., MA, H., BARNARD, P. L., DERBYSHIRE, E., FINKEL, R. C., CAFFEE, M. W., ZENG, Y. N. 2003b. Timing of Late Quaternary glaciation along the southwestern slopes of the Qilian Shan, Tibet. Boreas 32, 281-446.

OWEN, L. A., BARNARD, P., BENN, D., CAFFEE, M. W., DERBYSHIRE, E., FINKEL, R., GUALTIERI, L., MA, H., SHARMA, M., SPENCER, J. 2003c. Late Quaternary glaciation in the Himalaya and Tibet. XVI INQUA Congress Programs with Abstracts, DRI, Reno, Nv., p. 155.

PHILLIPS, F. M., ZREDA, M. G., GOSSE, J. C., KLEIN, J., EVENSON, E. B., HALL, R. D., CHADWICK, O. A., SHARMA, P. 1997. Cosmogenic ^{36}Cl and ^{10}Be ages of Quaternary glacial and fluvial deposits of the Wind River Range, Wyoming. Geological Society of America Bulletin 109, 1453-1463.

PUTKONEN, J., SWANSON, T. 2003. Accuracy of cosmogenic ages for moraines. Quaternary Research 59, 255-261.

RICHARDS, B. W. M., OWEN, L. A., RHODES, E. J. 2000a. Timing of Late Quaternary glaciations in the Himalayas of northern Pakistan. Journal of Quaternary Science 15, 283-297.

RICHARDS, B. W. M., BENN, I. D., OWEN, L. A., RHODES, E. J., SPENCER, J. Q. 2000b. Timing of Late Quaternary glaciations south of Mount Everest in the Khumbu Himal, Nepal. Geological Society of America Bulletin 112, 1621-1632.

SCHALLER, M., BLANCKENBURG, F. V., VELDKAMP, A., TEBBENS, L. A., HOVIUS, N., KUBIK, P. W. 2002. A 30 000 yr record of erosion rates from cosmogenic 10Be in Middle European river terraces. Earth and Planetary Science Letters 204, 307-320.

SCHLUETZ, F., ZECH, W. 2004. Palynological investigations on vegetation and climate change in the Late Quaternary of Lake Rukche area, Gorkha Himal, central Nepal. Vegetation History and Archaeobotany 13, 81-90.

SHANAHAN, T. M., ZREDA, M. 2000. Chronology of Quaternary glaciations in East Africa. Earth and Planetary Science Letters 177, 23-42.

SHIRAIWA, T., WATANABE, T. 1991. Late Quaternary glacial fluctuations in the Langtang Valley, Nepal Himalaya, reconstructed by relative dating methods. Arctic and Alpine Research 23, 404-416.

STONE, J. O. H. 2000. Air pressure and cosmogenic isotope production. Journal of Geophysical Research 105 B10, 23753-23759.

STONE, J. O., BALLANTYNE, C. K., FIFIELD, L. K. 1998. Exposure dating and validation of periglacial weathering limits, northwest Scotland. Geology 26, 587-590.

THOMPSON, L. G., YAO, T., DAVIS, M. G., HENDERSON, K. A., MOSLEY-THOMPSON, E., LIN, P. N., BEER, J., SYNAL, H. A., COLE-DAI, J., BOLZAN, J. F. 1997. Tropical climate instability: the last glacial cycle from a Qinghai-Tibetan ice core. Science 276, 1821-1825.

UNEP 2002. Vital maps and graphics on climate change, Tajikistan. www.grida.no/enrin/htmls/tadjik/vitalgraphics/eng/html/climate.htm.

ZECH, W., GLASER, B., ABRAMOWSKI, U., DITTMAR, C., KUBIK, P. W. 2003. Reconstruction of the Late Quaternary Glaciation of the Macha Khola Valley (Gorkha Himal, Nepal) using relative and absolute (^{14}C, ^{10}Be, dendrochronology) dating techniques. Quaternary Science Reviews 22, 2253-2265.

ZHENG, B., XU, Q., SHEN, Y. 2002. The relationship between climate change and Quaternary glacial cycles on the Qinghai-Tibetan plateau: review and speculation. Quaternary International 97-98, 93-101.

ZREDA, M. G., PHILLIPS, F. M., ELMORE, D. 1994. Cosmogenic ^{36}Cl accumulation in unstable landforms, 2. Simulations and measurements on eroding moraines. Water Resources Research 30, 3127-3136.

The use of ^{10}Be surface exposure dating of erratic boulders in the reconstruction of the late Pleistocene glaciation history of mountainous regions, with examples from Nepal and Central Asia

Cumulative Study

1. Introduction

1.1 Rationale

This work is part of an effort to establish ^{10}Be surface exposure dating as an important new tool in the pedogeographical and palaeoecological research activities at the Institute of Soil Science and Soil Geography at the University of Bayreuth, in collaboration with the Paul Scherrer Institute at the ETH Zurich.

Studies in soil development in formerly glaciated areas require a way of dating the sequence of glacial deposits on which the soils have formed. While soil parameters themselves, e.g. horizon thickness, clay mineralogy, iron and aluminium chemistry, or feldspar weathering indices can be used to establish a relative chronology (Baeumler, 2001), numerical ages can only be obtained using physical dating methods, e.g. radiocarbon dating, or luminescence dating (Bradley, 1999). The applicability of these methods in studies of glacial history, however, is limited.

Radiocarbon dating at present can provide reasonable ages only up to ~40 ka, and it is limited to preserved carbon-containing materials (e.g. plant remains, buried A horizons), that in arid regions may be few or absent. But even if datable material is present, radiocarbon ages can provide no more than age limits for a great number of glacial deposits, because glacial activity is most often only indirectly coupled to the carbon cycle. An advancing glacier e.g. may bury a surface horizon, or a receding glacier may provide a trap for organic sediments. In both cases, the radiocarbon age may not correspond to the glacial event, but reflect organisms dying long before, or long after it, respectively. Only in the rare case of plant macrofossils preserved in a moraine, glacial activity and the radiocarbon event are directly coupled. Finally, radiocarbon ages are not equivalent to calendar ages because of long-term changes in the ^{14}C content of the atmosphere. Therefore, they have to be calibrated against other dating methods, a process that in some cases leads to ambiguous results (Stuiver & Reimer, 1993, Joeris & Weninger, 1998).

Luminescence dating requires fine sandy-silty material well radiated during transport, but totally shielded from sunlight ever since deposition. Such material is easily found in aeolian or fluvial, but is less common in glacial deposits. As the preservation of aeolian and fluvial sediments is frequently scarce in mountainous areas, and aeolian and fluvial activity

are not necessarily synchronous with glacial activity, chronologies obtained with luminescence dating are often fragmentary and leave room for different interpretations (e.g. Richards et al., 2000, Kamp et al., 2003). In optically stimulated luminescence (OSL) dating, several ways of age determination are possible that do not necessarily lead to the same results, and age limits of ~130 ka have to be expected (e.g. Frechen & Dodonov, 1998).

Surface exposure dating (SED) using the accumulation of in-situ cosmogenic nuclides (e.g. ^{3}He, ^{10}Be, ^{14}C, ^{26}Al, ^{21}Ne, ^{36}Cl) provides a way of dating rock surfaces directly, if these have been freed from deep shielding (>3 m of rock cover) by a short-lived geologic event. This method is thus ideally suited for glacial moraines containing large erratic boulders, or for glacially abraded bedrock, and it fills an important gap in geochronology, palaeoclimatology and palaeoecology (Schaefer, 2000). The different nuclide approaches have different requirements in detail and employ different analysis and measurement techniques (Gosse & Phillips, 2001), but the underlying principle is the same. Up to now, ^{10}Be surface exposure dating may be considered the most advanced and most widespread SED method. It requires exposed quartz-bearing rock surfaces, open HF digestion in the laboratory, and measurement of ^{10}Be/^{9}Be by accelerator mass spectrometry (AMS). By employing ^{10}Be surface exposure dating in formerly glaciated catchments containing quartz-rich rocks, complete glacial chronologies can be inferred without depending on the presence of buried organic material or the outcropping of suitable fine sediments for luminescence dating. Complete SED chronologies in turn can provide crucial information on palaeoclimate in the region, especially when combined with information derived from soil development investigations (Cerling & Craig, 1994, Fabel & Harbor, 1999, Gosse & Phillips 2001).

1.2 Introduction to ^{10}Be surface exposure dating

1.2.1 Historical development

Cosmogenic ^{10}Be on Earth, produced by reactions of cosmic neutrons and muons with terrestrial O and Si atoms, was first discovered in the 1950s in marine sediments by B. Peters in India and J. R. Arnold in the USA. However, its minute concentrations made measurements in most of its terrestrial archives impossible at that time (Lal, 2000).

This situation changed in the 1980s with the development of suitable mass spectrometres with an integrated electrostatic tandem accelerator (Klein et al., 1982, Elmore & Phillips,

1987), which lowered the detection limit for cosmogenic radionuclides by 4-5 orders of magnitude (Lal, 2000). The first measurements of in-situ cosmogenic ^{10}Be in terrestrial quartz were published by Nishiizumi et al. (1986). Nishiizumi et al. (1989) presented the first calibration of the terrestrial production rate of ^{10}Be, measured in glacially abraded rocks in the Sierra Nevada, which were already dated indirectly by basal radiocarbon ages from overlying peat bogs. They also provided a basic set of correction factors necessary to account for oversimplifications in the standard terrestrial production model they applied. Lal (1991) published the first consistent geographic scaling system for this calibrated production rate, along with the theoretical background of exposure age and erosion rate determinations, using, among other nuclides, in-situ cosmogenic ^{10}Be. Kohl & Nishiizumi (1992) finally set up the standard laboratory procedure for the extraction of ^{10}Be from quartz. With these studies, the foundation was laid for a fast expansion of ^{10}Be surface exposure dating in the 1990s, which is still in progress.

The last decade, along with the introduction of a multitude of applications of the technique in geomorphology and glaciology (for reviews, see Cerling & Craig, 1994, Fabel & Harbor, 1999, Gosse & Phillips, 2001), brought many improvements, 1) in the calibrated production rate, 2) in the distinction of production by neutron spallation and muon reactions, 3) in the calculation procedure including the scaling system, and 4) in the set of correction factors, as well as the interpretation of measured ^{10}Be surface exposure ages (for details, see sections 2 and 3). Today, ^{10}Be SED is gaining the status of an established physical dating method, already widely used in geochronology, geomorphology, palaeoglaciology and palaeoclimatology, but still open to improvement.

1.2.2 Methodic principles

In-situ cosmogenic ^{10}Be is continually produced within the upper one to three meters of the lithosphere by interaction of particles from the secondary cosmic radiation with the O and Si atoms of the quartz mineral lattice. The production rate of ^{10}Be in the mineral depends on the amount of cosmic radiation reaching the sample, which can be predicted by using empirical measurements of cosmic ray activity in the atmosphere, along with calibration measurements of ^{10}Be in rock surfaces with an independently known exposure age (Gosse & Phillips, 2001).

The cosmic radiation entering Earth's atmosphere, the so-called primary radiation, is composed of high-energy galactic cosmic rays – mostly protons with energies between 1 and

10^{10} GeV – and of low-energy solar cosmic rays. The latter reach the top of the lithosphere only in negligible amounts, and are therefore not important for in-situ production (Lal & Peters, 1967). The incoming primary cosmic proton flux, which is considered to be approximately constant, is modulated by the terrestrial magnetic field, which deflects all rays with energies lower than a certain threshold value, the so-called cutoff rigidity. The cutoff rigidity varies with the geomagnetic latitude and longitude, and with the strength of the geomagnetic field. It is highest near the equator, where the geomagnetic field lines run parallel to the surface, and lowest near the poles, where the geomagnetic field lines run normal to the surface (Gosse & Phillips, 2001). The ^{10}Be production rate at any site therefore firstly depends on its geomagnetic position, and the strength of the geomagnetic field, which can be described by its dipole moment in a first approximation.

Having entered the atmosphere, the primary cosmic radiation is transformed into secondary radiation in a cascade of nuclear reactions. This secondary cosmic radiation mainly consists of neutrons, pions and muons, accompanied by a shower of electrons and photons (Lal & Peters, 1967). The secondary neutron flux on its way down to the Earth's surface is further attenuated by successive collisions with atmospheric nuclei. ^{10}Be production at any surface therefore secondly depends on the amount of atmospheric nuclei encountered by the secondary radiation on its way there, i.e. on the altitude of the site and the structure of the atmosphere above it (Stone, 2000). The pathlength in the air, or in any other matter, required to attenuate the radiation flux by the factor of exp(-1) is called the attenuation length Λ, commonly given in the mass path unit, [g cm^{-2}]. All parameters in the metric unit, [cm], can be transformed into the mass path unit by multiplying with the density of the medium (i.e. [cm] times [g cm^{-3}] equals [g cm^{-2}]). For neutrons of the secondary cosmic radiation in the atmosphere, Λ amounts to approximately 150 ± 20 g cm^{-2}, and depends on the energy spectrum of the radiation. As near the equator only high-energy particles enter the atmosphere, Λ at low latitudes is slightly higher than at the poles. Beneath the solid surface, the attenuation length of secondary neutrons amounts to 150-160 g cm^{-2}, equivalent to about 55 cm of rock (Gosse & Phillips, 2001).

At sea level, 97-98% of the in-situ cosmogenic ^{10}Be in quartz are produced by spallation of fast neutrons (Stone 2000, Braucher et al., 2003). In high altitude, the percentage is even higher. Only in rocks >3 m below the surface, production by muon interactions becomes important as well (Heisinger et al., 1997). Production by muon interaction can be separated into production due to the capture of slow, negative muons (Heisinger et al., 2002b), and

into production due to fast muon reactions (Heisinger et al., 2002a). In its effects, production due to fast muons is similar to production due to neutron spallations. Therefore, it is considered a part of the neutron production fraction in the older studies, and has only recently been introduced into calculation procedures as a separate fraction (Schaller et al., 2002, Desilets & Zreda, 2003). Slow negative muons in the atmosphere have an attenuation length of 247 g cm^{-2} (Nishiizumi et al., 1989). This attenuation length increases with the energy of the muons (Heisinger et al., 2002b). There is no consensus yet as to what attenuation length applies for ^{10}Be production due to fast muons, values ranging from ~500 to ~5000 g cm^{-2} (Heisinger et al., 2002a, b, Schaller et al., 2002, Desilets & Zreda, 2003).

There is no ^{10}Be production pathway including epithermal or thermal neutron reactions, as is the case with e.g. cosmogenic ^{36}Cl (Gosse & Phillips, 2001). The depth profile of ^{10}Be production in rocks can therefore be considered a simple exponential in a first approximation. However, even for fast neutrons, a backscattering effect at the atmosphere-rock interface has been observed (Dep, 1995) and modelled (Masarik & Reedy, 1995). Schaller et al. (2002) therefore have fitted a more sophisticated depth function of ^{10}Be production, using data of Heisinger et al. (2002a, b), which features a plateau of ^{10}Be production in the upper 12 g cm^{-2} beneath the rock-atmosphere interface.

Most of the ^{10}Be present on Earth is no in-situ cosmogenic ^{10}Be, but meteoric, also called "garden variety" ^{10}Be, which is produced by spallation of atmospheric oxygen, and is transported into soils and sediments by wet precipitation (McHargue & Damon, 1991). Its concentration in rainwater or dust is several orders of magnitude higher than the concentration of in-situ produced ^{10}Be in quartz (Baumgartner et al., 1997). In the analytic procedure, quartz therefore has to be effectively cleaned of adsorbed meteoric ^{10}Be before HF digestion (Kohl & Nishiizumi, 1992), and any contamination of digested samples by dust has to be carefully avoided.

In-situ produced ^{10}Be in quartz is locked in the mineral grid and therefore accumulates, its accumulation only limited by radioactive decay of the nuclide. The nuclide concentration N at a rock surface therefore is a function of its production rate P, the exposure time of the surface t, and its decay constant λ.

1.2.3 Physical model formulation

To be described by a mathematical formula, ^{10}Be accumulation and decay in exposed rock surfaces have to be defined by a physical model, which has to be regarded as a simplification of reality. The standard model for ^{10}Be surface exposure dating is a flat, even, infinite rock surface z [g cm^{-2}] = 0, exposed to a full sky of cosmic radiation since a point in time t_0 [a] = 0 (Nishiizumi et al., 1993). The cosmogenic nuclide production rate at the surface is P [atoms g^{-1} a^{-1}], which below the surface decreases exponentially with the attenuation length Λ [g cm^{-2}] of the cosmic rays. No other way of production of ^{10}Be, e.g. by α-particles from U decay, is allowed in the model. Nuclides formed in the rock are completely retained and lost only by radioactive decay or surface erosion. Radioactive decay of the nuclide depends on its concentration N [atoms g^{-1}] in the rock and its decay constant λ [a^{-1}]. In case of linear erosion with an erosion rate ε [g cm^{-2} a^{-1}], the surface is given by eq. (1.1),

$$z = z_0 - \varepsilon t\,. \tag{1.1}$$

Given all this, the dynamic of the nuclide production and decay at any infinitely small depth interval z can be described by the differential equation (1.2),

$$\frac{dN}{dt} = -\lambda N + P\exp\left(-\frac{z}{\Lambda}\right) = -\lambda N + P\exp\left(-\frac{z_0 - \varepsilon t}{\Lambda}\right). \tag{1.2}$$

For a linear differential equation of the form shown in eq. (1.3),

$$\frac{dx}{dt} = A(t)x + B(t)\,, \tag{1.3}$$

the solution shown in eq. (1.4a, b) applies (propagator equation, Zeidler, 1996):

$$x(t) = p(t,t_0)x_0 + \int_{t_0}^{t} p(t,\tau)A(\tau)d\tau, \tag{1.4a}$$

$$p(t,\tau) = \exp\left(\int_{\tau}^{t} A(t')dt'\right). \tag{1.4b}$$

Comparison of eq. (1.4a, b) and eq. (1.2) leads to eq. (1.5),

$$N(t) = N_0\exp\left(-\lambda\int_{t_0}^{t} dt'\right) + \int_{t_0}^{t}\exp\left(-\lambda\int_{t'}^{t} dt'\right)P\exp\left(-\frac{z_0 - \varepsilon t'}{\Lambda}\right)dt', \tag{1.5}$$

where N_0 is the concentration at the beginning of the exposure time $t_0 = 0$. Integration yields eq. (1.6),

$$N(t) = N_0 \exp(-\lambda t) + P \cdot \frac{1}{\lambda + \frac{\varepsilon}{\Lambda}} \cdot \left(\exp\left(-\frac{z_0}{\Lambda} + \frac{\varepsilon t}{\Lambda} \right) - \exp\left(-\frac{z_0}{\Lambda} - \lambda t \right) \right). \tag{1.6}$$

Simplification of eq. (1.6) and introduction of eq. (1.1) then leads to eq. (1.7),

$$N(t) = N_0 \exp(-\lambda t) + \frac{P}{\lambda + \frac{\varepsilon}{\Lambda}} \cdot \exp\left(-\frac{z}{\Lambda} \right) \left(1 - \exp\left(-\left(\lambda + \frac{\varepsilon}{\Lambda} \right) t \right) \right). \tag{1.7}$$

The first term on the right side of eq. (1.7) describes the decay of ^{10}Be present in the rock at the beginning of the exposure period that ends with sampling. Generally, this term is considered to be zero, implying that no previous period of exposure of the rock has occurred before at least several half-lives of the nuclide. The first exponential factor of the second term in eq. (1.7) describes the depth dependency of nuclide production. As sampling usually is confined to the surface, this factor usually equals one. All this considered, eq. (1.7) yields the standard production equation used in ^{10}Be surface exposure dating,

$$N(t) = \frac{P}{\lambda + \frac{\varepsilon}{\Lambda}} \left(1 - \exp\left(-\left(\lambda + \frac{\varepsilon}{\Lambda} \right) t \right) \right), \tag{1.8}$$

or, resolved for t, the standard exposure age calculation equation,

$$t = -\frac{1}{\lambda + \frac{\varepsilon}{\Lambda}} \ln\left[1 - \left(\lambda + \frac{\varepsilon}{\Lambda} \right) \frac{N}{P} \right]. \tag{1.9}$$

It is important to note the assumptions implicit in these formulae:

1) There is only one pathway of cosmogenic production considered, characterized by its attenuation length Λ. Any other pathway to be considered, e.g. by muon reactions, has its own Λ and requires its own term on the right side of eq. (1.8). In case of several additive terms on the right side of eq. (1.8), however, the resolution of the equation for t as in eq. (1.9) is no longer possible, and eq. (1.8) has to be solved for t by a kind of iteration, which is described in section 2.

2) The depth profile of production is idealized by the simple exponential used in eq. (1.2). In case of a more complex profile, as e.g. given by Schaller et al. (2002), there are several 'virtual' production fractions with a different Λ for each pathway, increasing the number of necessary terms on the right side of equation (1.8) still further (section 2).

3) Radiogenic production of ^{10}Be is neglected. Indeed, Sharma & Middleton (1989) have shown that equilibrium concentrations of radiogenic ^{10}Be even in granites containing high concentrations of U are several orders of magnitude smaller than the usual cosmogenic concentrations.

4) No inherited ^{10}Be is assumed in the model. Dating glacial erratics or bedrock, this assumption is based on the intense glacial scouring of bedrock and has been confirmed by some studies on boulders of recent moraines (Zentmire, 1999, Davis et al., 1999, Shanahan & Zreda, 2000). However, warning voices have also been raised (Ivy-Ochs, 1996, Heisinger & Nolte, 2000), and recently, inherited ^{10}Be has been shown to be significant in bedrock polished by cold-based glaciers (Gosse & Willenbring, 2002, Fabel et al., 2002, Briner et al., 2003).

5) Production in this model is simplified. The production rate P in fact has to be calculated as a product of the global standard production rate at sea level, high latitude, P_0, the local scaling factor S, and a set of correction factors f used to account for model weaknesses. These weaknesses are 1) the shielding of a part of the sky by topographic objects, 2) the shielding effect of surface inclination, 3) the shielding of the surface by overlying matter, like snow or vegetation, 4) the shielding effect of the finite thickness of the sample, 5) the scattering effects of the three-dimensional form of the sampled object, 6) the time-dependency of the production rate due to changes in the local magnetic field coordinates (dipole wobble) and strength (dipole moment), and 7) the time dependency of the production rate due to tectonic uplift or downlift of the sample surface. All scaling and correction factors are treated in detail in section 2.

6) The erosion in this model is assumed to be a linear process, i.e. to procede by continuous loss of infinitely small particles. In reality, erosion is more of an episodic event (Bierman, 1994). However, as long as the thickness of the episodically loosened particles stays below ~5 cm, and the mean erosion rate is constant over a timescale of ~10 ka, the linear model has been shown to be a valid approximation of the real processes (Gillespie and Bierman, 1995, Small et al., 1997).

1.3 Practical aspects of ^{10}Be surface exposure dating

1.3.1 Sampling

Sampling is the most crucial step in surface exposure dating. Sampled surfaces must be unambiguously representative for the glacial events to be dated. In case of erratic boulders, those have to be chosen, which have been at the surface of the moraine ever since deposition, and which never have changed their position during this time. This is most probably the case with boulders situated on the crest of a moraine (Hallet & Putkonen, 1994). Boulders likely to have rolled down a slope, or to have rotated due to permafrost activity or the melt-out of buried ice are not suited for moraine age determinations (Schaefer et al., 2002, Balco et al., 2002). It is also important to exclude the possibility of boulders having once rolled or fallen onto the deposit from outcrops above, as well as to avoid complications due to possible complex histories of a deposit. Lateral moraines, for instance, may have received material from debris fans or tributary valleys upslope during the course of its formation, which may have a more complex exposure history than the material of the moraine proper (Iturrizaga, 2003).

In order to avoid model weaknesses, the flat centres of the largest available boulders in the most wind-exposed sites should be sampled (Gosse et al., 1995a, b). This strategy is likely to minimize 1) the influence of surface geometry, 2) shielding by surface inclination and snow cover, as well as 3) the effects of non-linear erosion. Edges and nooks, even if most easy to sample, have to be avoided (Masarik et al., 2000), as well as boulders with obvious signs of recent movement, blocky decay or desquamation of the surface. Signs of surface stability, like lichen crusts or desert varnish, are favourable, but do not exclude detachment of material prior to their formation, which may be a rather late feature (Dorn & Phillips, 1991).

Finally, the stratigraphical position of the sampled deposit has to be considered. Erratic boulders on frontal moraines are most likely to represent the maximum advance of a glacier, while lateral moraines or glacially polished bedrock up-valley may have fallen inactive at a significantly later time during glacial recession (Benn & Owen, 2002). The presence of an experienced local Quaternary geologist during sampling is therefore highly important when sampling for ^{10}Be SED (Ivy-Ochs, 1996).

1.3.2 Documentation

For accurate calculation of surface exposure ages, the following data have to be documented during sampling (uncertainty recommendations in brackets by Gosse & Phillips, 2001):

1. Tag, rock type.
2. Stratigraphic and geomorphologic position.
3. Geographic coordinates (± 0.01°) and altitude a.s.l. (± 3 m).
4. Shielding by topography. This may be done by separating the 360° azimuth into intervals with an approximately constant mean horizon angle, and to note each azimuth interval with its mean horizon angle.
5. Surface inclination (dip), including its azimuth.
6. Height of the boulder respective to the soil surface, and data on snow depths and densities, if available.
7. Actual and potential vegetation and / or sediment cover.
8. Characteristics of the sampled rock surface.
9. Mean sample thickness.

Photos or sketches of the sampled sites can help in the interpretation of problematical ages later.

1.3.3 Chemical analysis

The general method of chemical analysis for ^{10}Be in quartz has been worked out by Kohl & Nishiizumi (1992). In this work, their method is applied in the form developed by Ivy-Ochs (1996), introducing several small modifications. The following steps are performed for each sample:

1. Lichens, crusts, etc. adhering to the rock pieces of a sample are removed with a steel brush.
2. The rock pieces are grinded with a jaw crusher, until all grain diameters are <2 mm.
3. Dust from grinding is removed from the sample with the help of a 0.25 mm sieve.
4. The sieved grains are thoroughly rinsed with deionized water.

5. The sample is shaken in 5% HF (50 ml on 80 g of material in a 2 l PE flask) for 72 hours, in order to dissolve feldspars and mafic minerals, and to etch away meteoric ^{10}Be adsorbed on the surfaces of the quartz minerals. After each 72-hour shake, the remaining grains are thoroughly rinsed with deionized water. This step is repeated until all feldspars are dissolved.

6. The remaining grains are shaken in 65% HNO_3 for 72 hours in order to remove remnant organic material and to further etch the quartz surfaces. After the shake, the grains again are thoroughly rinsed with deionized water.

7. The dried grains are inspected under a binocular. Single non-quartz crystals, or quartz crystals carrying inclusions, are removed with a pair of pincers. If many grains still contain inclusions, the quartz is grinded into finer particles, until all of them are monomineralic. Ferromagnetic minerals can be removed with a handheld magnet.

8. Quartz and heavy minerals (including white mica) are separated in a 2.6-2.7 g cm^{-3} sodium polytungstate solution. The separated quartz is shaken overnight in 65% HNO_3, in order to remove contaminations from the polytungstate solution. Afterwards it is thoroughly rinsed with deionized water and dried.

9. The dried quartz is weighed into Teflon beakers, which have been thoroughly rinsed with deionized water and dried. As a spike, 0.45 ml of 1000-ppm ^{9}Be standard solution are added to each sample. One chemical blank is prepared onto 9 samples.

10. The quartz in the Teflon beaker is covered by 65% HNO_3, afterwards the beaker is filled up with 48% HF and set onto a hotplate (95°C) under the hood for dissolution. The beakers are refilled with 48% HF never to fall dry until all quartz is dissolved.

11. The completely dissolved sample on the hotplate is boiled down three times with 65% HNO_3, and afterwards is boiled down three times again with 32% HCl, in order to remove all fluorides and boron.

12. The completely boiled down sample is taken up in a few ml of 9 M HCl and transferred into a centrifuge tube. The sample is centrifuged and the solution decanted into a clean tube. The remaining insoluble salt is washed with a few ml of 9 M

HCl, centrifuged again, the solution added to that of the first step. This is repeated once. Still remaining insoluble salt is discarded.

13. The sample in 9 M HCl is eluted on an anion exchange column (50 ml exchange resin Biorad AG™ 1-X8), in order to remove dissolved iron. The column is prepared by elution with 50 ml each of 1 M HCl, deionized water, 1 M HCl, 4.5 M HCl, and 9 M HCl, respectively. After the sample has been added on the column, it is eluted into a Teflon beaker with 60 ml of 9 M HCl. The eluate is then boiled down on a hotplate, taken up in a few ml of 1 M HCl, and transferred into the tube again. After sample elution, the column is cleaned by elution with 6 times 50 ml of 1 M HCl.

14. The sample in 1 M HCl is eluted on a cation exchange column (50 ml exchange resin Biorad AG™ 50W-X8), in order to separate Be and Al. The column is prepared by elution with 50 ml each of 1 M HCl, deionized water, 1 M HCl, 2 M HCl, 4.5 M HCl, 9 M HCl, 4.5 M HCl, 2 M HCl, 1 M HCl. After the sample has been added on the column, 3 times 50 ml 1 M HCl are eluted and discarded, followed by 7 times 50 ml 1 M HCl, which contain the Be and are eluted into a Teflon beaker. Afterwards, 3 times 50 ml of 4.5 M HCl are eluted, containing the Al. Finally, the column is cleaned by elution of 6 times 1 M HCl. The Be fraction is boiled down on a hotplate, taken up in a few ml of 1 M HCl, and transferred into the tube again.

15. Be is precipitated in the tubes by adding a few drops of 25% NH_4OH, until a pH of 8-9 is reached. Afterwards the precipitate is centrifuged and the rest of the solution is decanted. If there is more precipitate in a sample than in the chemical blank, it is redissolved in a few ml of 1 M HCl, and steps 14-15 are repeated, until the precipitate is reduced to the amount present in the chemical blank.

16. The precipitate is thoroughly shaken in deionized water and recollected by centrifugation. The rest of the solution is discarded. This step is repeated twice.

17. The precipitate is transferred into boron-free quartz-glass crucibles and dried under an infrared lamp. Afterwards, the crucibles are closed with a quartz-glass lid and transferred into the oven. First, they are treated by 250°C for 2 hours, afterwards by 850°C for 2 hours again, in order to transform the precipitated $Be(OH)_2$ into BeO.

18. The cooled BeO is thoroughly pulverized, mixed with Cu powder, and pressed into a copper target for measurement.

After step 6, any contact of the sample with borosilicate glass has to be painstakingly avoided, and all added chemicals have to be boron-free because measurement is hampered by even minute concentrations of ^{10}B in the sample (Kubik, pers. comm.). The same is true for dust and water, which may contain significant amounts of ^{10}Be. Acids of the per-analysis (p.a.) grade may be used, but the deionized water, the ammonia and the quartz glass crucibles should be of purest quality. All beakers, taps and lids must be thoroughly cleaned and rinsed with deionized water before use.

1.3.4 Measurement

AMS measurement of the $^{10}Be/^{9}Be$ ratio in a sample is described by Finkel & Suter (1993). For this work, it has been done at the Paul Scherrer Institute at the Institute of Particle Physics of the ETH Zurich. Measured ratios were corrected to conform with ICN standards (Nishiizumi et al., 1989) in the AMS lab (Kubik, pers. comm.). Concentrations in quartz can subsequently be calculated following equation (1.10),

$$N_S = \frac{(R_S M_{CS} - R_B M_{CB}) N_A}{u_{Be} M_S}, \tag{1.10}$$

where N_S [atoms g^{-1}] is the ^{10}Be concentration in the quartz sample, R_S and R_B are the $^{10}Be/^{9}Be$ ratios measured in the sample and the associated chemical blank, respectively, M_{CS} and M_{CB} [g] are the masses of ^{9}Be carrier added to the sample and blank, respectively, M_S [g] is the mass of the quartz sample, u_{Be} = 9.021 g mol^{-1} is the mole mass of Be, and N_A = $6.022 \cdot 10^{23}$ atoms mol^{-1} is the Avogadro constant.

Errors of measurement are given in % of the mean and can be propagated applying Gauss law of error propagation on equation (1.10).

1.4 Tasks of this work

The tasks of this work have been:

1. to install the analytical procedure to extract in-situ produced ^{10}Be from rock surface samples as described in this section in the laboratory of the Institute of Soil Science and Soil Geography at the University of Bayreuth;
2. to review the current ways of calculation of ^{10}Be surface exposure, to develop a calculation program for quick determination of ages with fully propagated uncer-

tainties, and to compare the several existing scaling and correction procedures using this program (section 2);

3. to review the current ways of interpretation of exposure age distributions and to deduce a new interpretation scheme, relying on ages from several stratigraphically related moraines in an area (section 3);
4. to provide and interpret 37 new ^{10}Be exposure ages from the Nepal Himalaya, complementing earlier soil geographic studies in the Langtang Valley and the Macha Khola Valley (section 4);
5. to provide and interpret 108 new ^{10}Be exposure ages from the Pamir, and the Alay- and Turkestan Ranges, thereby defining a new glacial chronology for Central Asia (section 5).

The fulfilment of the tasks 2-5 is described in the sections 2-5, which will be published as separate papers.

1.5 References

BAEUMLER, R. 2001. Vergleichende bodenkundliche Untersuchungen in Hochasien und Kamtschatka. Relief Boden Palaeoklima 16, Gebrueder Borntraeger, Berlin, 125 p.

BALCO, G., STONE, J. O. H., PORTER, S. C., CAFFEE, M. W. 2002. Cosmogenic-nuclide ages for New England coastal moraines, Martha's Vineyard and Cape Cod, Massachusetts, USA. Quaternary Science Reviews 21, 2127-2135.

BAUMGARTNER, S., BEER, J., WAGNER, G., KUBIK, P., SUTER, M., RAISBECK, G. M., YIOU, F. 1997. ^{10}Be and dust. Nuclear Instruments and Methods 123, 296-301.

BENN, D. I., OWEN, L. A. 2002. Himalayan glacial sedimentary environments: a framework for reconstructing and dating the former extent of glaciers in high mountains. Quaternary International 97-98, 3-25.

BIERMAN, P. 1994. Using in situ produced cosmogenic isotopes to estimate rates of landscape evolution: A review from the geomorphic perspective. Journal of Geophysical Research 99, 13885-13896.

BRADLEY, R. S. 1999. Palaeoclimatology, Second Edition. International Geophysics Series, vol. 64. Academic Press, London, 610 p.

BRAUCHER, R., BROWN, E. T., BOURLÈS, D. L., COLIN, F. 2003. In situ produced ^{10}Be measurements at great depths: implications for production rates by fast muons. Earth and Planetary Science Letters 211, 251-258.

BRINER, J. P., MILLER, G. H., DAVIS, P. T., BIERMAN, P. R., CAFFEE, M. 2003. Last Glacial Maximum ice sheet dynamics in Arctic Canada inferred from young erratics perched on ancient tors. Quaternary Science Reviews 22, 437-444.

CERLING, T. E., CRAIG, H. 1994. Geomorphology and in situ cosmogenic isotopes. Annual Review of Earth and Planetary Sciences 22, 273-317.

DAVIS, P. T., BIERMAN, P. R., MARSELLA, K. A., CAFFEE, M. W., SOUTHON, J. R. 1999. Cosmogenic analysis of glacial terrains in the eastern Canadian Arctic: a test for inherited nuclides and the effectiveness of glacial erosion. Annals of Glaciology 28, 181-188.

DEP, W.H.L. 1995. Cosmogenic radionuclide production in terrestrial rocks: Accelerator mass spectrometry measurements and Monte Carlo simulations. Ph.D. thesis, Purdue University, West Lafayette, Indiana, 155 p.

DESILETS, D., ZREDA, M. 2003. Spatial and temporal distribution of secondary cosmic-ray nucleon intensities and applications to in situ cosmogenic dating. Earth and Planetary Science Letters 206, 21-42.

DORN, R. I., PHILLIPS, F. M. 1991. Surface exposure dating: review and critical evaluation. Physical Geography 12, 303-333.

ELMORE, D., PHILLIPS, F. M. 1987. Accelerator mass spectrometry for measurement of long-lived radioisotopes. Science 236, 543-550.

FABEL, D., HARBOR, J. 1999. The use of in-situ produced cosmogenic radionuclides in glaciology and glacial geomorphology. Annals of Glaciology 28, 103-110.

FABEL, D., STROEVEN, A. P., HARBOR, J., KLEMAN, J., ELMORE, D., FINK, D. 2002. Landscape preservation under Fennoscandian ice sheets determined from in situ produced ^{10}Be and ^{26}Al. Earth and Planetary Science Letters 201, 397-406.

FINKEL, R. C., SUTER, M. 1993. AMS in the earth sciences: technique and applications. Advances in Analytical Geochemistry 1, 1-114.

FRECHEN, M., DODONOV, A. E. 1998. Loess chronology of the Middle and Upper Pleistocene in Tajikistan. Geologische Rundschau 87, 2-20.

GILLESPIE, A. R., BIERMAN, P. R. 1995. Precision of terrestrial exposure ages and erosion rates estimated from analysis of cosmogenic isotopes produced in situ. Journal of Geophysical Research 100, 24637-24649.

GOSSE, J. C., PHILLIPS, F. M. 2001. Terrestrial in situ cosmogenic nuclides: theory and application. Quaternary Science Reviews 20, 1475-1560.

GOSSE, J. C., WILLENBRING, J. 2002. Glacier erosion factory: using ^{26}Al/^{10}Be, soils, and geomorphology to study relief development. Goldschmidt Conference Abstracts 2002, A 287.

GOSSE, J. C., EVENSON, E. B., KLEIN, J., LAWN, B., MIDDLETON, R. 1995a. Precise cosmogenic ^{10}Be measurements in North America: support for a global Younger Dryas cooling event. Geology 23, 877-880.

GOSSE, J. C., KLEIN, J., EVENSON, E. B., LAWN, B., MIDDLETON, R. 1995b. Beryllium-10 dating of the duration and retreat of the last Pinedale Glacial Sequence. Science 268, 1329-1333.

HALLET, B., PUTKONEN J. 1994. Surface dating of dynamic landforms: young boulders on aging moraines. Science 265, 937-940.

HEISINGER, B., NOLTE, E. 2000. Cosmogenic in situ production of radionuclides: Exposure ages and erosion rates. Nuclear Instruments and Methods in Physics Research B 172, 790-795.

HEISINGER, B., NIEDERMAYER, M., HARTMANN, J. F., KORSCHINEK, G., NOLTE E., MORTEANI, G., NEUMAIER, S., PETITJEAN, C., KUBIK, P., SYNAL, A., IVY-OCHS, S. 1997. In-situ production of radionuclides at great depths. Nuclear Instruments and Methods in Physics Research B 123, 341-346.

HEISINGER, B., LAL, D., JULL, A. J. T., KUBIK, P., IVY-OCHS, S., NEUMAIER, S., KNIE, K., LAZAREV, V., NOLTE, E. 2002a. Production of selected cosmogenic radionuclides by muons 1. Fast muons. Earth and Planetary Science Letters 200, 345-355.

HEISINGER, B., LAL, D., JULL, A. J. T., KUBIK, P., IVY-OCHS, S., KNIE, K., NOLTE, E. 2002b. Production of selected cosmogenic radionuclides by muons 2. Capture of negative muons. Earth and Planetary Science Letters 200, 357-369.

ITURRIZAGA, L. 2003. Distribution and genesis of lateroglacial valleys in the Karakoram Mountains (Pakistan). Zeitschrift fuer Geomorphologie N. F., Supplementband 130, 51-74.

IVY-OCHS, S. 1996. The dating of rock surface using in situ produced ^{10}Be, ^{26}Al and ^{36}Cl, with examples from Antarctica and the Swiss Alps. Diss. ETH No. 11763, Zuerich, 197 p.

JOERIS, O., WENINGER, B. 1998. Extension of the ^{14}C calibration curve to ca. 40,000 cal BC by synchronizing Greenland ^{18}O/^{16}O ice core records and north Atlantic foraminifera profiles: a comparison with U/Th coral data. Radiocarbon 40, 495-504.

KAMP, U. JR., HASERODT, K., SHRODER, J. F. JR. 2003. Quaternary landscape evolution in the eastern Hindu Kush, Pakistan. Geomorphology 57, 1-27.

KLEIN, J., MIDLLETON, R., TANG, H. 1982. Modification of an FN tandem for quantitative ^{10}Be measurement. Nuclear Instruments and Methods 193, 601-616.

KOHL, C. P., NISHIIZUMI, K. 1992. Chemical isolation of quartz for measurement of in-situ produced cosmogenic nuclides. Geochimica et Cosmochimica Acta 56, 3583-3587.

LAL, D. 1991. Cosmic ray labelling of erosion surfaces: in situ nuclide production rates and erosion models. Earth and Planetary Science Letters 104, 424-439.

LAL, D. 2000. Cosmogenic nuclide production rate systematics in terrestrial materials: Present knowledge, needs and future actions for improvement. Nuclear Instruments and Methods in Physics Research B 172, 772-781.

LAL, D., PETERS, B. 1967. Cosmic ray produced radioactivity on the Earth. In: Flugge, S.: Handbuch der Physik 4612, 551-612.

MASARIK, J., REEDY, R. C. 1995. Terrestrial cosmogenic-nuclide production systematics calculated from numerical simulations. Earth and Planetary Science Letters 136, 381-395.

MASARIK, J., KOLLAR, D., VANYA, S. 2000. Numerical simulation of in situ production of cosmogenic nuclides: effects of irradiation geometry. Nuclear Instruments and Methods in Physics Research B 172, 786-789.

MCHARGUE, L. R., DAMON, P. E. 1991. The global beryllium-10 cycle. Reviews of Geophysics 29, 141-158.

NISHIIZUMI, K., LAL, D., KLEIN, J., MIDDLETON, R., ARNOLD, J. R. 1986. Production of ^{10}Be and ^{26}Al by cosmic rays in situ and implications for erosion rates. Nature 319, 134-135.

NISHIIZUMI, K., WINTERER, E. L., KOHL, C. P., KLEIN, J., MIDDLETON, R., LAL, D., ARNOLD, J. R. 1989. Cosmic ray production rates of ^{10}Be and ^{26}Al in quartz from glacially polished rocks. Journal of Geophysical Research B 94, 17907-17915.

NISHIIZUMI, K., KOHL, C. P., ARNOLD, J. R., KLEIN, J., FINK, D., MIDDLETON, R., LAL, D. 1993. Role of in-situ cosmogenic nuclides ^{10}Be and ^{26}Al in the study of diverse geomorphic processes. Earth Surface Processes and Landforms 18, 407-425.

RICHARDS, B. W. M., OWEN, L. A., RHODES, E. J. 2000. Timing of Late Quaternary glaciations in the Himalayas of northern Pakistan. Journal of Quaternary Science 15, 283-297.

SCHAEFER, J. M. 2000. Reconstruction of landscape evolution and continental palaeoglaciations using in-situ cosmogenic nuclides: Examples from Antarctica and the Tibetan Plateau. Diss. ETH Nr. 13542, Zurich, 121 p.

SCHAEFER, J. M., TSCHUDI, S., ZHAO, Z., WU, X., IVY-OCHS, S., WIELER, R., BAUR, H., KUBIK, P. W., SCHLUECHTER, C. 2002. The limited influence of glaciations in Tibet on global climate over the past 170 000 yr. Earth and Planetary Science Letters 194, 287-297.

SCHALLER, M., BLANCKENBURG, F. v., VELDKAMP, A., TEBBENS, L. A., HOVIUS, N., KUBIK, P. W. 2002. A 30 000 yr record of erosion rates from cosmogenic 10Be in Middle European river terraces. Earth and Planetary Science Letters 204, 307-320.

SHANAHAN, T. M., ZREDA, M. 2000. Chronology of Quaternary glaciations in East Africa. Earth and Planetary Science Letters 177, 23-42.

SHARMA, P., MIDDLETON, R. 1989. Radiogenic production of ^{10}Be and ^{26}Al in uranium and thorium ores: Implications for studying terrestrial samples containing low levels of ^{10}Be and ^{26}Al. Geochimica et Cosmochimica Acta 53, 709-716.

SMALL, E. E., ANDERSON, R. S., REPKA, J. L., FINKEL, R. 1997. Erosion rates of alpine bedrock surfaces deduced from in situ ^{10}Be and ^{26}Al. Earth and Planetary Science Letters 150, 413-425.

STONE, J. O. H. 2000. Air pressure and cosmogenic isotope production. Journal of Geophysical Research 105 B10, 23753-23759.

STUIVER, M., REIMER, P. J. 1993. Extended ^{14}C database and revised CALIB 3.0 ^{14}C age calibration program. Radiocarbon 35, 215-230.

ZEIDLER, E. (ed.) 1996. Teubner Taschenbuch der Mathematik. B.G. Teubner, Stuttgart, 1298 p.

ZENTMIRE, K. N., GOSSE, J. C., BAKER, C., MCDONALD, E., WELLS, S. 1999. The problem of inheritance when dating alluvial fans and terraces with TCN: insights from the Matanuska glacier. GSA Abstracts and Programs 1999, p. 31.

2. An evaluation of existing calculation procedures in ^{10}Be surface exposure dating of erratic boulders, using TE-BESEA, a newly-devised calculation program

Uwe Abramowski & Wolfgang Zech

Institute of Soil Science and Soil Geography, University of Bayreuth, D-95440 Bayreuth, Germany

Abstract

Here we use TEBESEA, a program we devised for the calculation of ^{10}Be surface exposure ages of erratic boulders 1) to evaluate the current calculation procedures in the light of the standard *in situ*-cosmogenic ^{10}Be production rate calibration studies published up to now, 2) to compare them in the context of our dating studies in Central Asia and Nepal, and 3) to compare the influence of the variable correction factors on cosmogenic exposure ages. The traditional scaling system of Lal (1991), as modified by Stone (2000), still proves to be best able to bring published calibrations into accord. Variations in the scaling of muon production have only minor effects on calibration results. Low muon contributions as measured by Braucher et al. (2003) are in agreement with the calibrations as long as the scaling system of Lal (1991) in a modified form is used. The altitude dependency of cosmogenic nuclide production proposed by Dunai (2000) and Desilets & Zreda (2003) is as yet not convincing, given the existing calibration data. Given the best available data, we calibrate a total standard production rate at sea level, high latitude, of 5.35 ± 0.15 atoms g^{-1} a^{-1}, and a contribution of capture of slow negative muons of 1.2%. For rocks exposed at an altitude of more than 2000-3000 m a.s.l. in High Asia, the scaling systems of Dunai (2001a) and Desilets & Zreda (2003) yield exposure ages that are significantly lower than if calculated using the scaling system of Lal (1991), but that do not significantly differ from each other. Awaiting clarification, the fact that ages from high altitude sites may be much younger than calculated using the scaling system of Lal (1991) should be considered in high altitude studies. All middle and early late Pleistocene exposure ages are significantly increased by correcting for reasonable estimates of erosion and tectonic uplift, and they are significantly lowered by correction for geomagnetic variations and by the effects of the refined depth profile of ^{10}Be production measured by Heisinger et al. (2002a, b). The use of all corrections is recommended. A recalculation of Lal's (1991) system as a continuous function of cutoff rigidity and atmospheric depth, and a reasonable separation of fast muon production and production due to capture of slow negative muons in scaling would be desirable improvements, especially for use in lower latitudes.

2.1 Introduction

In the simplest case of a single exponential depth function of the nuclide production in rock, ^{10}Be exposure ages of linearly eroding, quartz-bearing rock surfaces can be calculated using eq. (2.1a-c),

$$t = -\frac{1}{\lambda + \frac{\varepsilon\rho}{f_{C,\Lambda}\Lambda_0}} \ln\left[1 - \left(\lambda + \frac{\varepsilon\rho}{f_{C,\Lambda}\Lambda_0}\right)\frac{N}{P_0 \cdot S \cdot f_{C,P}(\varepsilon,t)}\right], \tag{2.1a}$$

$$f_{C,\Lambda} = f_{ST,\Lambda} f_{SI,\Lambda}\,, \tag{2.1b}$$

$$f_{C,P} = f_{ST,P} f_{SI,P} f_{SG} f_{SC} f_T f_M(t) f_U(t) f_P(\varepsilon,t)\,, \tag{2.1c}$$

where t is the exposure age [a], λ is the decay constant of ^{10}Be [a^{-1}], ε is the physical erosion rate of the rock surface [cm a^{-1}], ρ is the rock density [g cm^{-3}], Λ_0 is the attenuation length for cosmic rays in rock [g cm^{-2}], N is the measured ^{10}Be concentration in quartz [atoms g^{-1}], P_0 is the standard ^{10}Be production rate at sea level in high latitude (SLHL) [atoms g^{-1} a^{-1}], S is the scaling factor accounting for local latitude and altitude, $f_{C,\Lambda}$, $f_{C,P}$ are correction factors concerning Λ_0 and P_0, respectively, $f_{ST,\Lambda}$, $f_{ST,P}$ are correction factors for shielding of the surface by topography, $f_{SI,\Lambda}$, $f_{SI,P}$ are correction factors for shielding by surface inclination, f_{SG} is a correction factor for the effects of the geometry of the surface, f_{SC} is a correction factor for shielding of the surface by any kind of cover, f_T is a correction factor for the effect of sample thickness, $f_M(t)$ is a correction factor for the effect of geomagnetic field variation, $f_U(t)$ is a correction factor for the effect of tectonic uplift, and $f_P(\varepsilon, t)$ is a correction factor for the effects of a depth profile of production other than simple exponential.

Even though there has been much progress in ^{10}Be surface exposure dating (SED) since the pioneer studies by Nishiizumi et al. (1989) and Lal (1991), a standard procedure for calculating ^{10}Be exposure ages still has not been agreed on. Several ways of calculating the parameters in eq. (2.1a-c) are presently in use. The differences are concerning 1) the scaling factors used to derive the local ^{10}Be production rate in quartz from the standardized ^{10}Be production rate in quartz at sea level in high latitude (SLHL), 2) the standardized production rate itself, 3) the complexity of treatment of the production by muons, and 4) the set of correction factors used.

In this paper, we introduce TEBESEA (acronym for TEn BEryllium Surface Exposure Ages), a calculation program we devised for ^{10}Be surface exposure ages of erratic boulders, and we employ this program 1) to evaluate the current calculation procedures in the light of the standard in-situ cosmogenic ^{10}Be production rate calibration studies published up to now, 2) to compare them in the context of our dating studies in Nepal and Central Asia (section 4, 5), and 3) to estimate the influence of the variable correction factors on exposure ages.

2.1.1 Scaling factors

In-situ cosmogenic ^{10}Be is produced in quartz by spallation of ^{16}O and ^{28}Si by fast neutrons and, to a lesser degree, by nuclear reactions of ^{16}O and ^{28}Si with muons. Muon reactions can be separated into captures of negative muons and reactions of fast muons (Heisinger et al., 2002a, b). Neutrons and muons reach the Earth's surface as part of the secondary cosmic radiation, of which local intensity is determined by 1) the geomagnetic field it has encountered, and 2) by the mass of atmosphere it has crossed on its way. The altitude and latitude dependencies of the nuclear reactions ("stars") produced by the secondary cosmic radiation have been empirically measured in cloud chambers. Different models have been fitted to these measurements to yield scaling factors *S*, which can be used to scale a standardized production rate P_0 to any location on the globe. Because at high latitude changes of the magnetic field have no significant influence on the production rate – the magnetic field lines near the poles running approximately normal to the surface – the standardized production rate, which is treated as a constant, has been agreed on to be the one present at sea level in >60° latitude (SLHL).

The first generally accepted scaling system for cosmogenic nuclide production, published by Lal (1991), consists of a set of polynoms with metrical altitude as the only free parameter, empirically fitted to measured "star" production in the atmosphere, which is assumed to be caused by neutron spallation only. A polynom is given for each ten-degree latitude step. For the scaling of total nuclide production, Lal (1991) assumes an additional contribution of 15.6% of P_0 at sea level due to the capture of slow negative muons, which can be scaled vertically as a separate fraction using an attenuation length of 247 g cm^{-2}.

Stone (2000) points out that the contribution of negative muon capture to ^{10}Be production at sea level has been overestimated by Lal (1991). He calculates a new value of 2.6% of the total production rate at SLHL, fitted to minimize the error of the mean of all calibration

studies for SLHL ^{10}Be production rates published until then. Stone (2000) also changes the free parameter of Lal's (1991) scaling system from altitude to atmospheric depth. This allows for the introduction of model atmospheres other than the standard atmosphere (Lide, 1999) if necessary.

Dunai (2000) in turn points out that the scaling system of Lal (1991) cannot account for effects of non-dipole components of the geomagnetic field, as it uses geomagnetic latitude instead of geomagnetic inclination as scaling parameter. Furthermore, he proposes that Lal's (1991) system does not account for an altitude dependency of the attenuation length of the secondary radiation in the atmosphere that some of the cloud chamber data suggest. He therefore devises a new scaling system, using a more extensive database of cosmic ray measurements, and choosing two parameters, geomagnetic inclination, and atmospheric depth as free parameters. In this way, he also overcomes the problem of interpolation between the ten-degree steps, for which Lal's parameters are given. Inclination can be calculated from geomagnetic latitude, or measured in a local geomagnetic record to account for non-dipole effects. Dunai (2001a) further improves his model by changing the first free parameter, geomagnetic inclination, into local cutoff rigidity. The local cutoff rigidity, being the energy threshold below which cosmic rays are deflected by the geomagnetic field, is the direct link between the field strength and cosmogenic nuclide production. Hence, this parameter allows non-dipole effects as well as temporal changes in the dipole and non dipole moments to be accounted for. Cutoff rigidities can be calculated using geomagnetic inclination and horizontal field strength as free parameters. The latter can be approximated using values for the geomagnetic virtual axial dipole moment (VADM). Like Lal (1991) and Stone (2000), Dunai (2000, 2001a) still assumes production due to muons in only one fraction, scaled with an atmospheric attenuation length of 247 g cm^{-2}. In contrast to Stone (2000), however, Dunai (2000) assumes the same latitude dependence for the negative muon capture and neutron spallation fractions.

Heisinger et al. (2002a, b) noted that, in the lithosphere, ^{10}Be production due to fast muons and ^{10}Be production due to slow negative muons have to be considered separately. By interpolation of the lithospheric muon flux to the rock-atmosphere interface, they derive standard production rates of ^{10}Be SLHL in quartz of 0.106 atoms g^{-1} a^{-1} due to the capture of slow negative muons, and of 0.093 atoms g^{-1} a^{-1} due to fast muon reactions. In the atmosphere, they consider production due to fast muons to be included in the "star" production, to which Lal's (1991) polynoms have been fitted. For slow negative muons, however, they

derive an atmospheric attenuation length of 1463 g cm^{-2}. This new attenuation length is based on measurements of the energy dependence of the atmospheric muon attenuation length (Boezio et al., 2000) and a mean momentum of the muon flux at SLHL of ~8 GeV/c, calculated from muon measurements underground (Heisinger et al., 2002a). Schaller et al. (2002) adopt the Heisinger et al. (2002b) values, but, unlike Heisinger et al. (2002b), they scale all three production fractions separately, using the attenuation length of 1463 g cm^{-2} to scale the production by fast muon reactions, the older attenuation length of 247 g cm^{-2} to scale the production due to the capture of slow negative muons, and the scaling system of Dunai (2000) to scale the nucleon component, ignoring the fact that Dunai (2000), like Lal (1991), does not discriminate the neutron and fast muon contributions to the nuclear disintegrations measured to derive the scaling factors.

Dunai's scaling system itself has been questioned for several reasons, giving rise to a scientific dispute (Desilets et al., 2001, Dunai, 2001b, Desilets & Zreda, 2001). Desilets and Zreda (2003) in consequence published their own scaling system, choosing atmospheric depth and local cutoff rigidity as free parameters as well, but using an even more extensive database and more complex fitting functions than Dunai (2000), and calculating the cutoff rigidity in a different way than Dunai (2001a). Desilets & Zreda (2003) scale production due to capture of slow negative muons and fast muon reactions separately, having corrected the nuclear disintegration measurements for their influence, and using varying atmospheric attenuation lengths of around 240 g cm^{-2} and around 550 g cm^{-2}, respectively.

Recently, Braucher et al. (2003) have measured ^{10}Be in a deep-reaching quartz vein in Brazil. They derive muon contributions to surface production of only (1.2 ± 0.6)% for captures of negative muons, and (0.65 ± 0.25)% for fast muon reactions, in contrast to the ~2% each given by Heisinger et al. (2002b), but in accord with other studies from deep tropical profiles (Brown et al., 1995b; Braucher et al., 1998).

2.1.2 Standard production rates

The standardized ^{10}Be production rate in quartz at SLHL, P_0, consisting of contributions by spallation and muon reactions, has been roughly estimated by numerical modelling (Masarik & Reedy, 1995), but up to now it can only be accurately determined empirically by measuring the nuclide concentration N in various surfaces with independently known exposure age t, and backscaling the resulting local production rate to SLHL.

Tab. 2.1: Overview of published ^{10}Be standard production rates SLHL.

Paper	P_0 [atoms g^{-1} a^{-1}]	Muon contribution SLHL [%]	Scaling system	Corrections applied	Site, samples and independent age	Possible shortcomings
Nishiizumi et al. (1989)	6.03	15.6	Lal (1991)	f_{ST}, f_T	Sierra Nevada, 10 GLPS, 11 ka	a, b, c, d, f
Brown et al. (1991)	6.4	15.6	Lal (1991)	f_T, ε	Antarctica, 9 EB, various ^{26}Al ages	a, b, c, e, f
Clark et al. (1995)	4.74	15.6	Lal (1991)	f_{ST}, f_T	rs. Nishiizumi et al. (1989), 14 ka	a, b, c, d, f
Clark et al. (1995)	4.76	15.6	Lal (1991)	f_{ST}, f_T	New Jersey, 15 EB, 21.5 ka	b, c, d, f
Masarik & Reedy (1995)	5.97	n. r.	physical model	-	-	g
Bierman et al. (1996)	5.17	15.6	Lal (1991)	f_{ST}, f_T	New Jersey, 16 EB 21.5 ka	b, c, d, f
Ivy-Ochs (1996)	5.7	15.6	Lal, (1991)	f_T	Antarctica, 5 EB, ^{10}Be equilibrium	b, e, f
Ivy-Ochs (1996)	5.6	15.6	Lal (1991)	f_{ST}, f_T	Swiss Alps, 1 EB, 12.4 ka	b, c, d, f
Nishiizumi et al. (1996)	5.21	15.6	Lal (1991)	-	Colorado, California, water targets	b, h
Nishiizumi et al. (1996)	5.80	15.6	Lal (1991)	f_{ST}, f_T	rs. Nishiizumi et al. (1989), 13 ka	a, b, c, d, f
Phillips et al. (1997)	5.4	15.6	Lal (1991)	f_{ST}, f_T	Wyoming, 10 EB, various ^{36}Cl ages	a, b, c, f
Kubik et al. (1998)	5.75	15.6	Lal (1991)	f_{ST}, f_{SC}, f_T	Tyrolian Alps, 5 LSB, 9.8 ka	b, c
Stone et al. (1998)	4.62	3	Lal (1991)	f_{ST}, f_T	Scotland, 3 GLPS, 11.5 ka	c, d, f
Stone (2000)	5.1	2.6	Lal (1991)	vrs.	rs. several studies	c, f
Heisinger & Nolte (2000)	6.47	8.8	n.r.	n.r.	n.r.	i
Schaller et al. (2001)	5.37	2.8	Lal (1991)	f_{ST}, f_{SC}, f_T	rs. Kubik et al. (1998)	c
Barrows et al. (2001)	5.02	n.r.	Lal (1991)	f_{ST}, f_T	rs. Stone et al. (1998)	c, i
Heisinger et al. (2002b)	5.51	3.6%	Lal (1991)	n.r.	rs. Nishiizumi et al. (1989, 1996)	a, c, d, f
Schaller et al. (2002)	5.53	3.6%	Dunai (2000)	f_{ST}, f_{SC}, f_T	rs. Kubik et al. (1998)	c
Hetzel et al. (2002)	5.42	n.r.	Dunai (2000)	f_{ST}, f_{SC}, f_T	rs. Kubik et al. (1998)	c
Klein & Gosse (2002)	5.33	2.6%	Lal (1991)	f_{ST}, f_{SC}, f_T	Wyoming, 10 EB, 11.6 ka	c, f
Klein & Gosse (2002)	4.71	2.6%	Dunai (2000)	f_{ST}, f_{SC}, f_T	Wyoming, 10 EB, 11.6 ka	c, f
Bierman & Caffee (2002)	5.2	2.6%	Lal (1991)	vrs.	rs. several studies	c, i
Kubik & Ivy-Ochs (2003)	5.44	3.6%	Lal (1991)	f_{ST}, f_{SC}, f_T	Tyrolian Alps, 4 LSB, 9.8 ka	c

GPS: glacially polished surfaces; EB: erratic boulders; LSB: landslide boulders; a: calibration dating uncertain; b: overestimated muon contribution; c: no correction for geomagnetic effects; d: no correction for snow cover; e: inadequate model atmosphere, f: thickness correction using a simple exponential profile; g: model insensitivity; h: erroneous translation factor; i: no explanation; rs. rescaled from, n.r.: not reported, vrs.: various

Several such calibration studies of the scaling systems have been published, using ^{14}C-dated glacially abraded rock surfaces (Nishiizumi et al., 1989; Stone et al., 1998), rock surfaces thought to be in equilibrium between production and decay (Brown et al., 1991; Ivy-Ochs, 1996), boulders from ^{14}C-dated moraines (Clark et al., 1995; Bierman et al., 1996; Ivy-Ochs, 1996; Klein & Gosse, 2002), boulders from ^{36}Cl-dated moraines (Phillips et al., 1997), or boulders from a ^{14}C-dated rockslides (Kubik et al., 1998). In a different approach, ^{10}Be production rates have been measured in artificially exposed water targets and translated into the respective ones for quartz using a constant ratio (Nishiizumi et al., 1996; Brown et al., 2000). As some of the independent dating has been questioned (Clark et al., 1995), and because there still is no convention as to the way of scaling and correcting, numerous recalculations of existing values have already been presented (Stone, 2000; Barrows et al., 2001; Schaller et al., 2001, 2002; Kubik & Ivy-Ochs, 2003; Hetzel et al., 2002; Klein & Gosse, 2002). Strictly speaking, each of these values is valid only for the exact way of calculation used in the respective calibration study and cannot be compared to the other values. The results of all mentioned calibration efforts, including the scaling procedures used and the possible shortcomings of each of the studies are listed in Tab. 2.1.

2.1.3 Correction factors

2.1.3.1 Geometrical correction factors

The calculation of the correction factors for the shielding effect of topography, $f_{ST,P}$ and $f_{ST,\Lambda}$, is explicitely treated by Dunne et al. (1999). The two factors are calculated following eq. (2.2) and (2.3):

$$f_{ST,P} = 1 - \frac{1}{360°} \sum_{i=1}^{n} \Delta\varphi_i \sin^{m+1} \theta_i \,, \tag{2.2}$$

$$f_{ST,\Lambda} = \frac{1 - \sum_{i=1}^{n} \frac{\Delta\varphi_i}{360°} \sin^{m+2} \theta_i}{1 - \sum_{i=1}^{n} \frac{\Delta\varphi_i}{360°} \sin^{m+1} \theta_i} \,, \tag{2.3}$$

with the azimuth circle divided into n parts $\Delta\varphi_i$, for which the mean angle between the horizon and the horizontal is θ_i, and the exponent m, which for the neutron component of the cosmic radiation is 2.3 (Nishiizumi et al., 1989), but possibly even 3.5 (Heidbreder et al., 1971), and around 2.1 for the muon components (Heisinger et al., 2002b).

In case of a non-horizontal surface, the surface inclination, described by the maximum slope angle α [°], has a shielding influence as well, on the one hand, because the upper part of the sloped surface shields a part of the incoming radiation, on the other hand because the normal of the depth penetration is altered from the vertical to the normal of the inclined surface. Both these effects have been calculated numerically by Dunne et al. (1999) for a single high-energy star production fraction. Distinguishing between a neutron spallation, a negative muon capture and a fast muon reaction production fraction with different values for m (2.3, 2.1, and 2.1, respectively) and Λ (155, 1510 and 4320 g cm^{-2}, respectively), and dividing the resulting correction factor into one correcting the production rate P, $f_{SI,P}$, and one correcting the attenuation length Λ, $f_{SI,\Lambda}$, a recalculation of the procedure presented by Dunne et al. (1999) yields values, which can be approximated by the polynoms in eq. (2.4):

$$\begin{aligned} f_{SI,P,j} &= p_{1j}\alpha + p_{2j}\alpha^2 + p_{3j}\alpha^3 + p_{4j}\alpha^4, \\ f_{SI,\Lambda,j} &= q_{0j} + q_{1j}\alpha + q_{2j}\alpha^2 + q_{3j}\alpha^3 + q_{4j}\alpha^4 + q_{5j}\alpha^5, \end{aligned} \tag{2.4}$$

where the index j stands for n, μ^- or μf. The coefficients p_{ij} and q_{ij} are given in Tab. 2.2.

The relations in eq. (2.4) are calculated to fit for $0° \leq \alpha \leq 90°$. However, for $\alpha > \sim 40°$, the approximation of the production depth function by a simple exponential with an attenuation length corrected by $f_{SI,\Lambda}$ will slightly underestimate the modelled correction in the upper ~ 100 g cm^{-2} of rock and slightly overestimate it below. If the sampled surface is inclined and eq. (2.4) are used, eq. (2.2) and (2.3) require a modification. In this case, θ_i is no longer measured from the horizontal, but from the prolongation of the inclined surface upwards to the actual horizon. The horizon angle of the prolonged inclined surface $\gamma(\varphi_\alpha)$ is given by eq. (2.5):

$$\begin{aligned} \gamma &= \arctan\left(\cos\varphi_\alpha \tan\alpha\right) \quad 270° < \varphi_\alpha < 90°, \\ \gamma &= 0 \qquad\qquad\qquad\qquad\quad 90° < \varphi_\alpha < 270°, \end{aligned} \tag{2.5}$$

where φ_α is the azimuth angle with the direction of the maximum slope angle α of the inclined surface. In the direction of α, $\varphi_\alpha \equiv 0$.

Masarik et al. (2000) as well as Masarik & Wieler (2003) suggest, that the size and form of a dated boulder can significantly influence the amount of ^{10}Be produced in its surface layer. As shown by their modelling, backscattering of a part of the incoming neutron flux at a sharply rounded or angled surface reduces the production by up to 10% in extreme cases.

Unfortunately, no practical procedure is presented to derive a correction factor from geometrical data documented in the field.

Tab. 2.2: Coefficients for the polynoms used for the calculation of the correction factors for surface inclination in eq. (2.4).

i	$p_{i,\,n}$	$q_{i,\,n}$	$p_{i,\,\mu-}$	$q_{i,\,\mu-}$	$p_{i,\,\mu f}$	$q_{i,\,\mu f}$
0	0	0	0	0	0	$2.0392 \cdot 10^{-2}$
1	$3.4808 \cdot 10^{-4}$	$5.8462 \cdot 10^{-4}$	$1.4513 \cdot 10^{-4}$	$1.7162 \cdot 10^{-3}$	$1.4513 \cdot 10^{-4}$	$-5.2767 \cdot 10^{-4}$
2	$-3.8138 \cdot 10^{-5}$	$2.1800 \cdot 10^{-4}$	$-1.7520 \cdot 10^{-5}$	$2.6690 \cdot 10^{-4}$	$-1.7520 \cdot 10^{-5}$	$6.6687 \cdot 10^{-4}$
3	$2.0203 \cdot 10^{-6}$	$-3.3705 \cdot 10^{-6}$	$1.6849 \cdot 10^{-6}$	$-4.2368 \cdot 10^{-6}$	$1.6849 \cdot 10^{-6}$	$-1.5447 \cdot 10^{-5}$
4	$-1.0609 \cdot 10^{-8}$	$2.6389 \cdot 10^{-8}$	$-9.1354 \cdot 10^{-9}$	$2.5539 \cdot 10^{-8}$	$-9.1354 \cdot 10^{-9}$	$1.4784 \cdot 10^{-7}$
5	0	$-9.1731 \cdot 10^{-11}$	0	$-5.1337 \cdot 10^{-11}$	0	$-5.2564 \cdot 10^{-10}$

2.1.3.2 Correction factors for surface cover and depth below the surface

The correction factors f_{SC} and f_T accounting for the effects of surface cover and sample thickness correction, respectively, can be derived in a first approximation assuming a single exponential decrease of production below the surface, as shown in eq. (2.6) and (2.7),

$$f_{SC} = \exp\left(-\frac{z_C}{f_{C,\Lambda}\Lambda_0}\right), \tag{2.6}$$

$$f_T = \frac{1}{\Delta z}\int_{z=0}^{z=0+\Delta z} \exp\left(-\frac{z'}{f_{C,\Lambda}\Lambda_0}\right) dz' = \frac{f_{C,\Lambda}\Lambda_0}{\Delta z}\left(1-\exp\left(-\frac{\Delta z}{f_{C,\Lambda}\Lambda_0}\right)\right) \tag{2.7}$$

where z_C = mean annual thickness of any cover [g cm^{-2}], z = depth below the surface [g cm^{-2}], and Δz = thickness of the sample [g cm^{-2}]. z in [g cm^{-2}] is calculated as the product of the metrical depth [cm] and the rock density [g cm^{-3}].

The relations shown by eq. (2.6) and (2.7), however, are only valid for materials with a low density (<1 g cm^{-3} may be assumed as a threshold). For high-density materials, model results by Masarik & Reedy (1995) have shown that ^{10}Be production stays approximately constant in the first 12 g cm^{-2} below the air-solid (or liquid) interface, due to neutron backscattering. This has been confirmed by measurements in rocks (Dep, 1995). At greater depth, the production profile is still not exactly exponential due to the increased relative influence of muon reactions (Heisinger et al., 2002a, b). Schaller et al. (2002) have presented

a depth function of ^{10}Be production that describes the measured depth profile of Heisinger et al. (2002a, b) to within 1%, and consists of several additive exponential functions.

As snow and vegetation on the average have low densities, their influence can be calculated according to eq. (2.6). For high density cover, e.g. loess or other sediment, and for thickness correction in rocks (and, probably, water targets), however, the more complex depth profile of production given by Schaller et al. (2002) should be applied, and eq. (2.6) and (2.7) should be changed into eq. (2.8) and (2.9), which have to be applied separately for each production fraction j (being as produced by neutron spallation, capture of slow negative muons, and fast muon reactions):

$$f_{SC,j}^{*} = \sum_{i=1}^{3} a_{ij} \exp\left(-\frac{z_C}{f_{ST,\Lambda,j} b_{ij}}\right), \tag{2.8}$$

$$f_{T,j}(\varepsilon,t)^{*} = \frac{1}{\Delta z} \cdot \frac{\sum_{i=1}^{3} a_{ij} f_{ST,\Lambda,j} b_{ij} \left(\exp\left(-\frac{z_{TS}}{f_{ST,\Lambda,j} b_{ij}}\right) - \exp\left(-\frac{z_{BS}}{f_{ST,\Lambda,j} b_{ij}}\right)\right)}{\sum_{i=1}^{3} a_{ij} \exp\left(-\frac{z_{TS}}{f_{ST,\Lambda,j} b_{ij}}\right)}, \tag{2.9}$$

where the depth of the sample top $z_{TS} = z_C + \varepsilon\rho t$, the depth of the sample base $z_{BS} = z_{TS} + \Delta z$, and the a_{ij} and b_{ij} are the depth function parameters given by Schaller et al. (2002, Tab. A1.1).

For clear distinction, correction for a snow and/or vegetation cover z_{SV} will be renamed $f_{SVC,j} = f_{SC,j}(z_{SV})$, and correction for a sediment cover z_{SD} will be renamed $f_{SDC,j} = f_{SC,j}^{*}(z_{SD})$, with $f_{SC} = f_{SVC} f_{SDC}$.

The shielding depth of vegetation cover has been shown to be small (Cerling & Craig, 1994). A tropical montane forest has a mean cover equivalent (depth times density) of 3 g cm^{-2} (Brown et al., 1995a). Snow cover, however is more difficult to estimate for longer periods of exposure, since past snow cover duration, heights and densities in most cases are unknown. For this reason, Lifton et al. (2001) consider this correction as non-admissible for samples older than the Holocene. It is generally agreed on, that, if high, wind-exposed surfaces are sampled, the error associated with snowfall can be minimized (Cerling & Craig, 1994). Such surfaces being chosen, f_{SC} is generally ignored in dating glacial erratics. Benson et al. (2004), however, have shown that this is likely to lead to serious underestimates of the exposure ages of some erratic boulders.

2.1.3.3 Correction for geomagnetic variations

The correction for variations in the geomagnetic field is twofold. On the one hand, there are the changing positions of the geomagnetic dipole that have to be accounted for, on the other hand there are the changes in dipole intensity. Dipole wobble can be modelled for the past 10 ka using the palaeo-pole positions of Ohno & Hamano (1992). For older exposures, the geocentrical axial dipole (GAD) hypothesis is generally accepted, which assumes that, on long-term average, the geomagnetic poles match the geographic poles. This hypothesis may only be valid for >20 ka, but since data are missing, it is also the best existing estimate for the period from 10 ka to 20 ka (Dunai, 2001a). Dipole intensity data are available in the form of so called virtual axial dipole moments (VADM). VADM data can be obtained from McElhinny & Senanayake (1984), or from the Sint-200 (Guyodo & Valet, 1996), or Sint-800 (Guyodo & Valet, 1999) records. Using the local cutoff rigidity as free parameter, the scaling models of Dunai (2001a) and Desilets & Zreda (2003) essentially integrate correction for geomagnetic field variations into the scaling procedure. A scaling factor can be calculated for each time interval, for which a VADM and a magnetic pole position are available. For the scaling system of Lal (1991), a similar scheme can be developed. One way of doing so is to vary the geomagnetic latitude as a function of the VADM, as described by Gosse and Phillips (2001). This, however, is only practicable for high- and mid-latitude sites, as for low latitude sites possible effective latitudes are severely restricted by the equator. Another way is to simulate the influence of the geomagnetic field in an empirical model and using the resulting factors to correct the scaling factor (Masarik et al., 2001). Because the magnitude of the correction of Masarik et al. (2001) is comparatively small and shows no altitude dependence, however, this correction has been argued to possibly result from a model insensitivity to changes in the dipole intensity and therefore to be inappropriate (Desilets & Zreda, 2003).

2.1.3.4 Correction for tectonic uplift

The influence of tectonic uplift on ^{10}Be production up to now has been considered only in a few studies (Brown et al., 1991; Gosse & Stone, 2001; Kober et al., 2002). Uplift can be integrated into the age calculations by varying the atmospheric depth in the scaling systems according to the altitude changes. As a first approximation, a linear uplift model may be used,

$$h_k = h_0 - ut_k , \tag{2.10}$$

where h_k [m] is the altitude in which the sample has been during the k-th time interval, t_k years ago, h_0 [m] is the altitude from which the sample has been taken, and u is the uplift rate [m a^{-1}].

In tectonically active mountain areas like the Himalayas and the Central Asian mountains, uplift rates are comparatively high and should be considered in SED. In our model calculations we use maximum values measured in the High Himalaya of ~3 mm a^{-1} (Leland et al., 1998, Jain et al., 2000). Similar values are reported from the Pamir (Dodonov, 2002).

2.1.3.5 Correction for a depth profile of production other than simple exponential

The introduction of the depth profile measured by Heisinger et al. (2002a, b) does not only change the calculation of the correction factors for sediment cover and sample thickness, but also influences the effects of erosion. An additional correction factor for P_0, $f_P(\varepsilon, t)'$, is therefore defined as the ratio between the production assuming the eroding depth function of Heisinger et al. (2002a, b) and the production assuming the eroding simple exponential depth function, which is implicit in eq. (2.1a). In case of no erosion, $f_P(\varepsilon, t)' = 1$, otherwise it depends on the amount of rock eroded, which is given by εt, and therefore on the erosion rate and the duration of exposure. For practical reasons, $f_P(\varepsilon, t)'$ can be changed to include the effects of profile correction on the correction factors for thickness and, if necessary, for sediment cover,

$$f_P(\varepsilon,t) = f_P(\varepsilon,t)'\frac{f_T^*}{f_T}\frac{f_{SC}^*}{f_{SC}}. \qquad (2.11)$$

The correction for profile correction can only be accurately calculated, if the local relative contributions of all production fractions are known. Thus, in all scaling systems, in which fast muon production is not scaled separately, it can only be approximated by using the neutron spallation and capture of negative muon profiles, ignoring the variations of the neutron spallation profile due to the inseparable fast muon contribution. This approximation, however, is valid as long as depths do not exceed ~800 g cm^{-2} (~2.5 m of rock).

2.2 Materials & Methods

2.2.1 Calculation procedure

2.2.1.1 General procedure

The simple calculation of exposure ages using eq. (2.1a-c) is no longer valid as soon as several production mechanisms of ^{10}Be have to be considered, for which different correction factors or parameters apply. In this case, the nuclide concentration N_{jk} resulting from the production by the production fraction j during the time interval $\Delta t_k = t_k - t_{k-1}$, is given by eq. (2.12),

$$N_{jk} = P_{j0} \cdot S_{jk} \cdot f_{ST,j} f_{SI,jk} f_{SC,j} f_{T,jk} \cdot E_{jk}\,, \tag{2.12}$$

where S_{jk} is the scaling factor for the fraction j taking into account the values for geomagnetic latitude, atmospheric depth and VADM valid during the time interval Δt_k; $f_{ST,j}$, $f_{SI,jk}$, $f_{SC,j}$, and $f_{T,jk}$, are the respective correction factors for shielding by topography, surface inclination, surface cover and sample thickness calculated for Δt_k using eq. (2.2), (2.4), (2.6) and/or (2.8), and (2.9), respectively; and E_{jk} is an exponential term, calculated for a simple exponential depth profile following eq. (2.13),

$$E_{jk} = \frac{\left[\exp\left(-t_{k-1}\left(\lambda + \frac{\varepsilon\rho}{f_{C,\Lambda,j}\Lambda_{0,j}}\right)\right) - \exp\left(-t_k\left(\lambda + \frac{\varepsilon\rho}{f_{C,\Lambda}\Lambda_{0,j}}\right)\right)\right]}{\left(\lambda + \frac{\varepsilon\rho}{f_{C,\Lambda,j}\Lambda_{0,j}}\right)}, \tag{2.13}$$

or, for the refined depth profile of Heisinger et al. (2002a, b), following eq. (2.14),

$$E_{jk}{}^{*} = \sum_{i=1}^{3} \frac{a_{ji}\left[\exp\left(-t_{k-1}\left(\lambda + \frac{\varepsilon\rho}{f_{C,\Lambda,j}b_{ji}}\right)\right) - \exp\left(-t_k\left(\lambda + \frac{\varepsilon\rho}{f_{C,\Lambda,j}b_{ji}}\right)\right)\right]}{\left(\lambda + \frac{\varepsilon\rho}{f_{C,\Lambda,j}b_{ji}}\right)}. \tag{2.14}$$

For calculation of exposure ages, the produced amounts of ^{10}Be by each fraction j, as predicted by the scaling model, are summed up for each time interval k. The amounts of ^{10}Be produced in each time interval are subsequently summed up, starting at $k = 1$ ($t_0 = 0$), and continuing up to that interval, indexed k', for which the sum of the produced amounts as predicted by the model $N(t_{k'})$ surpasses the measured amount N, while N still surpasses the

sum of the produced amounts as predicted by the model $N(t_{k'-1})$ for the previous interval, indexed k'-1. The exposure age is then found by linear interpolation between the corresponding ages $t_{k'-1}$ and $t_{k'}$. In mathematical terms, this procedure is given by eq. (2.15), where the N_{jk} are given by eq. (2.12):

$$
\begin{aligned}
&j = 1, 2, 3, \qquad k = 1, 2, 3, ..., \\
&t_0 = 0, \qquad \Delta t_k = t_k - t_{k-1}, \qquad t_{k'} = \sum_{k=1}^{k'} \Delta t_k, \\
&N_k = \sum_{j=1}^{3} N_{jk}, \qquad N(t_{k'}) = \sum_{k=1}^{k'} N_k, \\
&t = t_{k'-1} + \frac{N - N(t_{k'-1})}{N(t_{k'}) - N(t_{k'-1})}(t_{k'} - t_{k'-1}), \quad N(t_{k'-1}) < N < N(t_{k'});
\end{aligned}
\tag{2.15}
$$

The correction factors depending on time, $f_M(t)$, $f_U(t)$, and $f_P(\varepsilon, t)$, are determined after the $N(t_k)$ have been calculated for each time t_k, once including, once not including the correction in question. The relation shown in eq. (2.16) is then used to calculate mean factors for each t_k (or only for $t_{k'}$, which gives the factors relevant for a calculated exposure age):

$$
\frac{N_c(t_k)}{N_{nc}(t_k)} = \frac{\dfrac{P_0 \cdot S \cdot \prod_{i=1}^{n} f_i(t_k)}{\lambda + \dfrac{\varepsilon}{\Lambda}} \cdot \left(1 - \exp\left(-\left(\lambda + \dfrac{\varepsilon}{\Lambda}\right)t_k\right)\right)}{\dfrac{P_0 \cdot S \cdot \prod_{i=1}^{n-1} f_i(t_k)}{\lambda + \dfrac{\varepsilon}{\Lambda}} \cdot \left(1 - \exp\left(-\left(\lambda + \dfrac{\varepsilon}{\Lambda}\right)t_k\right)\right)} = f_n(t_k). \tag{2.16}
$$

The exposure age t, all $N_j(t)$ (the amounts of ^{10}Be produced by each single fraction during the exposure time t as predicted by the model) and all correction factors $f_{i(,j)}(t)$ known, a fully propagated uncertainty of t is calculated, for each production fraction applying Gauss' law of error propagation to the right side of eq. (2.1a), replacing N, P_0, S, Λ_0, $f_{C,P}$ *and* $f_{C,P}$ by the respective $N_j(t)$, $P_{0,j}$, S_j, $\Lambda_{0,j}$, $f_{C,j,\Lambda}$ *and* $f_{C,j,P}(t)$, and taking the mean of the resulting errors weighted by $N_j(t)\ N_{tot}(t)^{-1}$, $N_{tot}(t)$ being the sum of all $N_j(t)$. For each of the scaling and correction factors, a standard error of 10% was assumed (Lal, 1991). All other uncertainties are as measured or given in the literature. The uncertainties of the measured ^{10}Be concentrations are blank-corrected.

In all scaling procedures, atmospheric depths are calculated from metrical altitudes using the physical standard atmosphere (Lide, 1999, cited in Stone, 2000), which is within 0.2 ‰

of the ICAO atmosphere as cited by Dunai (2000). For 0.5 to 10 ka, geomagnetic latitude is calculated from geographic latitude and the palaeo-pole positions of Ohno & Hamano (1992) by subtracting the palaeo-colatitude from 90° (eq. 3.65 in Gosse & Phillips, 2001). From 11 ka onwards the GAD hypothesis is used and geographic and geomagnetic latitudes are equated. To correct for changing dipole intensity, we used the Sint-200 record of Guyodo & Valet (1996), which was converted into absolute intensities by multiplying with $5.29 \cdot 10^{-22}$ Am² (Gosse & Phillips, 2001, their Fig. 7, note that they give a different value in the text), supplemented for the Holocene by the VADM data of McElhinny & Senanayake (1982).

The decay constant λ for ^{10}Be is taken to be $(4.56 \pm 0.15) \cdot 10^{-7}$ a^{-1} (Holden, 1990). For quartz-rich rocks, a density ρ of 2.7 ± 0.1 g cm^{-3} is estimated. For the attenuation length $\Lambda_{0,n}$ for neutron spallations in rock, a value of 155 ± 5 g cm^{-2} is adopted here, as values between 150 and 160 g cm^{-2} have been reported in the literature (Gosse & Phillips, 2001). For slow negative muons, and fast muons, attenuation lengths of $\Lambda_{0,\mu-}$ = 1510 ± 10 g cm^{-2}, and $\Lambda_{0,\mu f}$ = 4320 ± 500 g cm^{-2}, respectively, are used (Heisinger et al., 2002a, b). In the depth profile of Schaller et al. (2002), the values for the attenuation lengths in rock are replaced by the *b*-values of their exponential functions (their Tab. A1.1), which can be interpreted as the attenuation lengths of virtual production fractions. For the erosion rate ε of the sample surface, a maximum estimate of 5 ± 2 mm ka^{-1} for granitic rocks in a semiarid climate has been given (Phillips et al., 1997; Owen et al., 2002) and is used as a reference in the comparisons. For uplift correction estimates, a model rate of 3 mm a^{-1} is used.

2.2.1.2 Calculation according to Lal (1991), modification 1

The scaling factors according to Lal (1991) are calculated using the formulation of Stone (2000), and taking atmospheric depths and VADM-corrected geomagnetic latitudes as free parameters. The scaling parameters are interpolated between the 10 degree latitude steps by fitting polynoms of the 5th or 6th grade between 20 and 50 degrees, and by linear interpolation between all other latitudes. VADM-corrected latitudes L_c are calculated from geomagnetic latitudes L_{gm} according to eq. (2.17),

$$\cos(L_c) = \left(\frac{M}{M_0}\right)^{\frac{1}{4}} \cos(L_{gm}), \tag{2.17}$$

where M is the averaged VADM for the time interval, and M_0 is today's VADM of $8.084 \cdot 10^{-22}$ Am². Production by fast muons is scaled together with production by neutron spallation. Production by capture of slow negative muons is scaled using an atmospheric attenuation length of 247 g cm^{-2}. Contributions of negative muon capture to the SLHL production rate of 2.6% (Stone et al., 2000), and 1.2% (Braucher et al., 2003) were tested. Correction for the effects of the depth profile of Schaller et al. (2002) was done using the neutron spallation and negative muon capture profiles only, as in this system there is no way of determining the relative production due to neutron spallation and fast muon reactions at any site above sea level.

2.2.1.3 Calculation according to Lal (1991), modification 2

The calculations are carried out as described in section 2.1.2, except for production due to negative muon capture, which is instead scaled using an atmospheric attenuation length of 1463 g cm^{-2}. SLHL ^{10}Be production rates due to negative muon capture of 0.106 atoms g^{-1} a^{-1} (Heisinger et al., 2002b), and 1.2% of the total SLHL production rate (Braucher et al., 2003), were tested.

2.2.1.4 Calculation according to Dunai (2001a)

For scaling according to Dunai (2001a), the geomagnetic inclination I is calculated from geomagnetic latitude L_{gm} by the GAD formula $\tan(I) = 2 \cdot \tan(L_{gm})$; the horizontal field strength H and the palaeo-colatitude θ_{pcl} are calculated according to Dunai's (2001a) eq. 16 and 17, respectively. The cutoff rigidity R is then given by Dunai's (2001a) eq. 2. Production due to fast muons is scaled together with production due to neutron spallation. Production due to capture of slow negative muons is scaled using an atmospheric attenuation length of 247 g cm^{-2}. Contributions of negative muon capture to the SLHL production rate of 2.6% (Stone, 2000), and 1.2% (Braucher et al., 2003) were tested. Correction for the effects of the depth profile of Schaller et al. (2002) was done for the neutron spallation and negative muon capture fractions only.

2.2.1.5 Calculation according to Dunai (2001a), modification

The calculations are carried out as described in section 2.1.3, except for the scaling of the production fractions due to muon reactions. Production by capture of slow negative muons and fast muon reactions are now scaled with attenuation lengths of 247 g cm^{-2}, and 1463 g cm^{-2}, respectively, as suggested by Schaller et al. (2002). With capture of negative muons,

SLHL production rates of 0.106 atoms g^{-1} a^{-1} (Heisinger et al., 2002b) and 1.2% of the total SLHL production rate (Braucher et al., 2003), with fast muon reactions SLHL production rates of 0.093 atoms g^{-1} a^{-1} Heisinger et al., 2002b), and 0.65% of the total SLHL production rate (Braucher et al., 2003) were tested. $P_{0,n}$ was calculated by subtracting the sum of $P_{0,\mu-}$ and $P_{0,\mu f}$ from the total calibrated production rate SLHL. As suggested by Dunai (2000), the same latitude dependency has been used for muon and neutron reactions.

2.2.1.6 Calculation according to Desilets & Zreda (2003)

For scaling according to Desilets & Zreda (2003), atmospheric depth, geomagnetic latitude and VADM in the form (M/M_0) are used as required in their eq. 10 and 19. In one approach, the production rates SLHL for fast and slow negative muon reactions given by Heisinger et al. (2002b) of 0.093 and 0.106 atoms g^{-1} a^{-1}, respectively, were used, even though they are not strictly valid for this scaling system due to the different attenuation lengths used. However, because Heisinger et al. (2002b) derive the SLHL production by slow negative muons unaffected by their atmospheric scaling, at least this value can be used with some confidence. In another approach, the production percentages given by Braucher et al. (2003) have been scaled to SLHL by the Desilets & Zreda (2003) model, giving 0.8% and 0.5% for negative muon capture and fast muon reactions at SLHL, respectively. This scaling was necessary, because in the Desilets & Zreda scaling model, muon and neutron reactions have different dependencies on latitude (i.e. cutoff rigidity) as well as on altitude.

2.2.1.7 TEBESEA

The program TEBESEA is devised as an MS-Excel™ file. For each sample, it requires the entry of sample name; geographic latitude [°], geographic longitude [°], and altitude [m]; the correction factors $f_{ST,P,n}$, $f_{ST,P,\mu}$, $f_{ST,\Lambda,n}$, and $f_{ST,\Lambda,\mu}$, which can be calculated from compass-inclinometer data using a subroutine; surface inclination SI and its azimuth [°]; sample thickness [cm], snow or vegetation cover [g cm^{-2}] if any; sediment cover [g cm^{-2}] if any; the measured ^{10}Be concentration N [atoms g^{-1}] with its error [atoms g^{-1}], which again can be calculated from measurement and laboratory data using a second subroutine; the estimated or measured surface erosion rate ε [cm a^{-1}] with its uncertainty [cm a^{-1}], the estimated uplift rate u [m a^{-1}], and the rock density ρ [g cm^{-3}] with its uncertainty [g cm^{-3}]. TEBESEA calculates the fully corrected exposure ages resulting from each of the five scaling systems described above with their fully propagated uncertainties.

2.2.2 Calibrations

For calibration of TEBESEA, the results of the four best documented calibration studies (Bierman et al., 1996, Stone et al., 1998, Klein & Gosse, 2002, and Kubik & Ivy-Ochs, 2003) have been rescaled, applying all corrections possible given the available information. Erosion and tectonic uplift had to be neglected in all calibrations for lack of suitable data. In case of the Koefels study, the results of three previously unpublished measurements (BK 1, 4 and 5) have been added (data shown in Tab. 2.3), whereas only the samples numbered K4, K5 and K101 of Kubik & Ivy-Ochs (2003) have been retained after the removal of outliers. For comparison, the calibrations using water targets (Nishiizumi et al., 1996, and Brown et al., 2000) have also been rescaled.

Tab. 2.3: Previously unpublished Koefels landslide calibration samples.

Sample ID	Altitude [m]	SI [°]	Thickness [cm]	$f_{ST,P,n}$	$f_{ST,P,\mu}$	$f_{ST,\Lambda,n}$	$f_{ST,\Lambda,\mu}$	N (^{10}Be) [atoms g^{-1}]
BK 1	1675	0	4	0.995	0.994	1.004	1.005	210700 ± 13700
BK 4	1671	20	2	0.991	0.988	1.007	1.008	198300 ± 9500
BK 5	1678	12	1	0.996	0.994	1.003	1.005	210800 ± 15200

2.3 Results & Discussion

2.3.1 Comparison of calibrations

The rescaled calibrations considered in our study are summarized in Tab. 2.4. With respect to the muon contributions tested, only those results are shown, with which the closest fits of the calibration data were obtained. For the scaling systems derived from Lal (1991), these proved to be the lower ones given by Braucher et al. (2003), which reduced the uncertainties by <1% of the means. For the other systems, the larger muon contributions given by Stone (2000) or Heisinger et al. (2002b) are significantly better able to bring the calibration results together, sometimes reducing the error by up to 4% of the respective mean.

The water target calibrations yield rather low translated production rates of below 4.5 atoms g^{-1} a^{-1} in quartz. The values above 5 atoms g^{-1} a^{-1} published by Nishiizumi et al. (1996) have been derived from the measured data by assuming a muon contribution larger by roughly one order of magnitude than the values now generally agreed on. Most likely,

the reason for the consistently low production rates in quartz calibrated from water targets is to be found in an inadequacy of the conversion factor to production rates in quartz as measured by Nishiizumi et al. (1996).

Tab. 2.4. Overview of selected calibration results for ^{10}Be production rate at SLHL.

Selected calibrated standard production rates SLHL of ^{10}Be in quartz [atoms g^{-1} a^{-1}]

	Lal (1991), modification 1	Lal (1991), modification 2	Dunai (2001a)	Dunai (2001a) modification	Desilets & Zreda (2003)
measured in water targets					
1) Echo Lake[a]	4.48 ± 0.24	4.49 ± 0.24	4.19 ± 0.23	4.27 ± 0.22	4.04 ± 0.21
2) Meyer Hall[a]	4.39 ± 0.72	4.39 ± 0.72	4.73 ± 0.78	4.74 ± 0.78	4.77 ± 0.79
3) Mont Blanc 1-4[b]	4.44 ± 0.31	4.43 ± 0.29	3.72 ± 0.30	3.81± 0.29	3.58 ± 0.29
4) Mont Blanc 5[b]	3.14	3.15	3.34	3.35	3.33
mean 1)-4)	*4.31 ± 0.54*	*4.32 ± 0.54*	*4.09 ± 0.63*	*4.15 ± 0.61*	*4.01 ± 0.67*
mean 1)-3)	***4.43 ± 0.40***	***4.44 ± 0.40***	***4.16 ± 0.61***	***4.23 ± 0.58***	***4.08 ± 0.67***
measured in rock samples, backscaled including correction for geomagnetic field variation					
1) An Telleach[c]	4.42 ± 0.27	4.43 ± 0.27	4.67 ± 0.28	4.70 ± 0.28	4.65 ± 0.28
2) New Jersey[d]	5.18 ± 0.16	5.19 ± 0.16	5.60 ± 0.17	5.62 ± 0.16	5.63 ± 0.16
3) Titcomb Lake[e]	5.39 ± 0.09	5.41 ± 0.09	5.04 ± 0.09	5.11 ± 0.08	4.81 ± 0.08
4) Koefels[f]	5.48 ± 0.20	5.49 ± 0.21	5.64 ± 0.21	5.68 ± 0.21	5.51 ± 0.20
mean 1)-4)	*5.12 ± 0.48*	*5.13 ± 0.48*	*5.24 ± 0.47*	*5.28 ± 0.46*	*5.15 ± 0.49*
mean 2)-4)	***5.35 ± 0.15***	***5.36 ± 0.16***	***5.43 ± 0.33***	***5.47 ± 0.31***	***5.32 ± 0.44***
measured in rock samples, backscaled without correction for geomagnetic field variation					
1) An Telleach[c]	4.41 ± 0.27	4.42 ± 0.26	4.65 ± 0.28	4.68 ± 0.27	4.61 ± 0.27
2) New Jersey[d]	5.13 ± 0.15	5.14 ± 0.15	5.52 ± 0.16	5.54 ± 0.16	5.55 ± 0.16
3) Titcomb Lake[e]	5.03 ± 0.09	5.05 ± 0.09	4.63 ± 0.08	4.70 ± 0.08	4.47 ± 0.07
4) Koefels[f]	5.43 ± 0.20	5.44 ± 0.20	5.58 ± 0.21	5.63 ± 0.21	5.45 ± 0.20
mean 1)-4)	*5.00 ± 0.43*	*5.01 ± 0.43*	*5.10 ± 0.53*	*5.14 ± 0.52*	*5.02 ± 0.56*
mean 2)-4)	*5.20 ± 0.21*	*5.21 ± 0.21*	*5.24 ± 0.53*	*5.29 ± 0.51*	*5.15 ± 0.60*

a: Nishiizumi et al., 1996; b: Brown et al., 2000; c: Stone et al., 1998; d: Bierman et al., 1996; e: Klein & Gosse, 2002; f: Kubik et al., 1998, Kubik & Ivy-Ochs, 2003, unpublished data added.

Apart from this problem, the scaling system of Lal (1991) in both modified forms is convincingly able to fit the measurements of Nishiizumi et al. (1996) alone (within an error of 11% of the mean as compared to 13% or even 15% of the mean as obtained with the scaling systems of Dunai, 2001a, and Desilets & Zreda, 2003, respectively), or together with the measurements of Brown et al., 2000 (within an error of 13% of the mean as compared to 15% and 17% of the mean obtained with the scaling systems of Dunai, 2001a, and Desilets & Zreda, 2003, respectively). If a single low altitude, low concentration measurement of Brown et al. (2000) is left out which is of an admittedly lesser quality than the other double, high concentration measurements at the Mont Blanc, the scaling fit is further improved (resulting in an error within 9% of the mean in case of the scaling system

of Lal, 1991, as compared to errors of 14-15% and 16% of the mean obtained by using the scaling systems of Dunai, 2001a, and Desilets & Zreda, 2003, respectively). Only the measurements of Brown et al. (2000) alone, including the single low concentration sample, are best explained by the scaling systems of Desilets & Zreda and Dunai (within errors of 8% and 9% of the mean, respectively, as compared to 15% of the mean obtained using the scaling system of Lal, 1991). In this case however, the calibration yields an exceptionally low standard ^{10}Be production rate, most different from the mean standard production rates implied by the rock calibrations.

The calibrations in rock samples yield rates between 4.43 and 5.68 atoms g^{-1} a^{-1}, depending on the site considered, on whether or not a correction for geomagnetic variations is included, and on the scaling system used. The calibration of Stone et al. (1998) results in a significantly lower production rate than the other three studies. If this study is excluded, the error of the mean is significantly reduced in all cases. Stone et al. (1998) sampled rather flat bedrock, which may have been covered by significant amounts of snow or even by soil or regolith in the past. The area of sampling, which has been covered by an ice sheet during the last glacial maximum (LGM), may also have been subject to considerable isostatic uplift. Both cover and uplift would have acted to reduce the apparent production rate. The calibration study of Stone et al. (1998) may therefore be reasonably left out of consideration. Barrows et al. (2001) reported, that a correction of Stone's et al. (1998) calculations would lead to a production rate of 5.02 ± 0.27 atoms g^{-1} a^{-1}, which would be in significantly better agreement with the other three calibration studies considered. As, however, Barrows et al. (2001) do not specify this correction, it could not be reconstructed for this study.

The remaining three calibrations are again best brought into accord by the modified scaling systems of Lal (1991), whether geomagnetic correction is applied or not. Without geomagnetic correction, the resulting mean standard production rate obtained using Lal's (1991) system has an error of 4%, as compared to 11% and 13% errors of the mean obtained using the systems of Dunai (2001a) and Desilets & Zreda (2003), respectively. Applying geomagnetic correction, the error of the mean is consistently reduced, from 4% to 3% in the scaling systems based on Lal (1991), from 11% to 6% in the scaling systems based on Dunai (2001a) and from 13% to 9% in the scaling system of Desilets & Zreda (2003). The larger reduction in the scaling systems of Dunai and Desilets & Zreda is mainly due to the increase of the standard production rate resulting from the highest situated calibration stu-

dy of Klein & Gosse (2002). At this key calibration site in ~3240 m altitude and far-western mid-latitude, the lowering of the resulting standard production rate caused by the use of the altitudinal scaling of Dunai (2000) or Desilets & Zreda (2003) instead of the altitude scaling of Lal (1991) is counteracted by a strong effect of geomagnetic variation. This effect in turn is larger in the system of Dunai (2001a) than in the system of Desilets & Zreda (2003), explaining the larger reduction of the error of the calibrated mean in the former system.

Generally, the difference in altitude scaling between the systems of Dunai (2000) and Desilets & Zreda (2003) on the one hand and the system of Lal (1991) on the other hand results in higher standard production rates from the low altitude calibration sites and lower standard production from the high altitude calibration sites if the former systems are used (see below). Given the measured data, however, this leads to a larger span between the calibrated standard production rates in the systems with a variable atmospheric attenuation length than in the system with a constant attenuation length. This larger span can only be narrowed by applying larger geomagnetic corrections to the high altitude sites, or by generally assuming larger muon contributions. At least for the latter, there is no evidence, considering the results of Braucher et al. (2003). The present dataset therefore does not support the changes in altitude scaling suggested by Dunai (2000) and Desilets & Zreda (2003), but confirms the earlier work by Lal (1991). Graham et al. (2000) and Lifton et al. (2002) have announced further altitude transect studies to test the validity of the different approaches which may change this conclusion. However, up to now, the use of the scaling system of Lal (1991) as modified by Stone (2000), but with a negative muon capture contribution of 1.2% and including geomagnetic correction, must be considered the best option.

The mean calibrated standard production rate itself is the same within errors for all scaling systems. Without geomagnetic correction it lies between 5.15 ± 0.60 atoms g^{-1} a^{-1} (Desilets & Zreda, 2003) and 5.29 ± 0.51 atoms g^{-1} a^{-1} (Dunai, 2001a, modification 1), including geomagnetic correction it lies between 5.32 ± 0.44 and 5.47 ± 0.31 atoms g^{-1} a^{-1} (the same, respectively). The value we recommend is 5.35 ± 0.15 (Lal, 1991, modification 1).

2.3.2 Comparison of the scaling systems at two High Asian model sites

Differences between the modifications of the systems of Lal (1991) and Dunai (2001a) among themselves have been shown to be negligible (see above). Comparisons of the three principal scaling systems for our two model sites, using the calibration described above to

assign the most appropriate standard production rate to each scaling system, are depicted in Fig. 2.1.

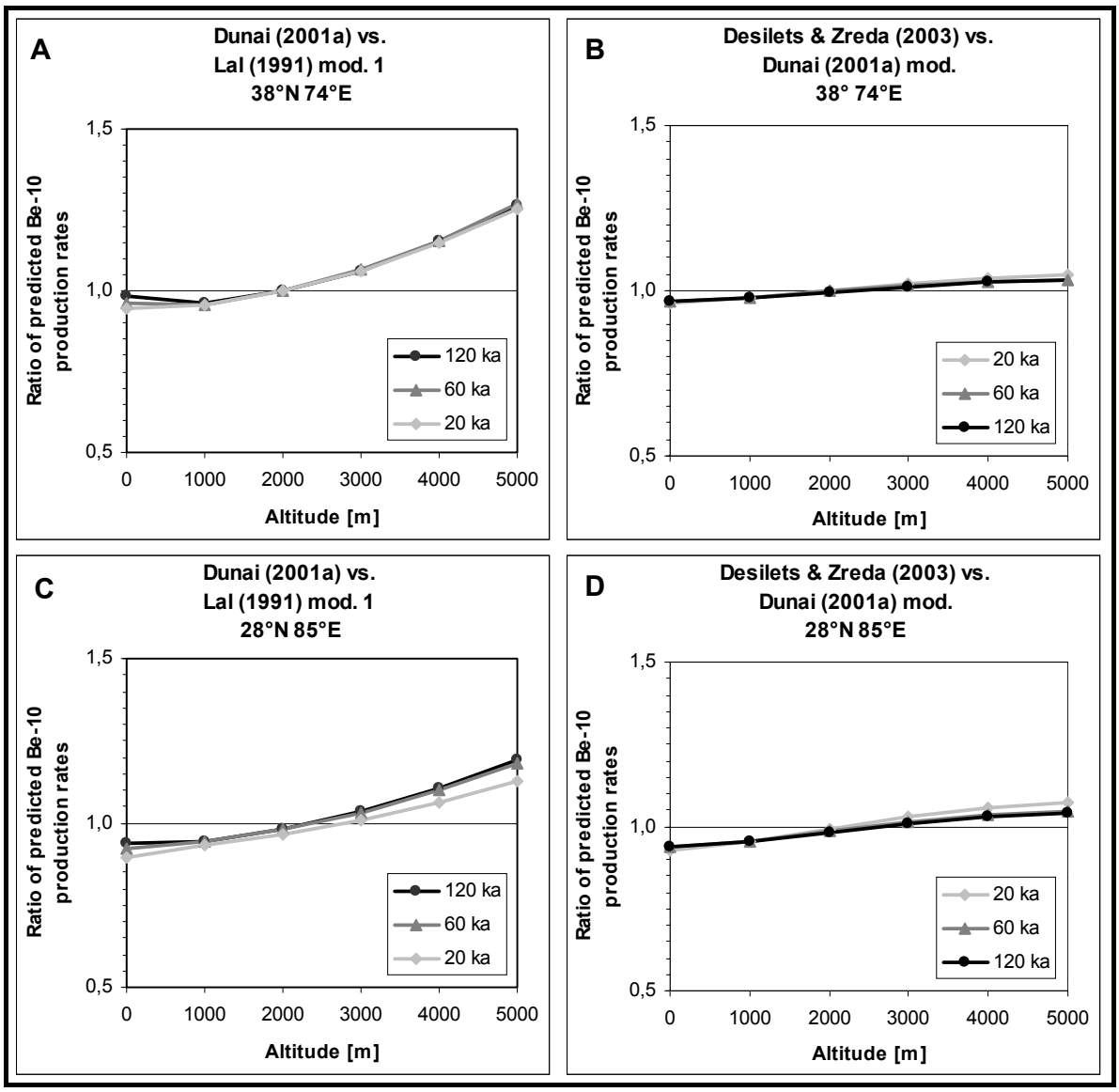

Fig. 2.1: Ratios of mean ^{10}Be production rates for exposure times of 20, 60 and 120 ka predicted with different scaling systems as a function of altitude for model sites in the A, B) Pamir (38°N 74°E) and C, D) central Nepal (28°N 85°E). See text for explanation.

The predicted production in all systems is the same around 2000 m altitude at both sites. Above this altitude the newer scaling systems predict a higher, below, they predict a lower production of in-situ ^{10}Be. The deviation between Lal's (1991) and the other two principal scaling systems passes 10% between altitudes of ~3000 and 4000 m a.s.l. and reaches up to 20-30% at 5000 m a.s.l; it is more pronounced at the higher latitude model site at 38°N, 74°E than at the lower latitude model site at 28°N, 85°E, where the altitude of similar production is also lower. The differences are caused mainly by the lower, altitude-dependent

values of about 130 g cm^{-2} for the atmospheric attenuation length of the secondary neutrons used by Desilets & Zreda (2003) as well as Dunai (2001a), as compared with the constant value of 150 g cm^{-2} used by Lal (1991). For mid-latitudes and altitudes of 3000 m and above, the more recently published scaling systems and the one by Lal (1991) therefore cannot be considered equivalent, as has been done by some authors (e.g. Lifton et al., 2001).

Comparing Dunai's (2001a) and Desilets' and Zreda's (2003) scaling systems, the differences decrease with exposure time, and they are always lower than the assumed 10% uncertainty of the scaling factors themselves, especially at the 38°N latitude site. The reduction of the differences with time and latitude shows that they mainly result from the different corrections for dipole wobble, which become less important after exposures much longer than the Holocene and which is generally less at higher latitudes. The disagreement between Dunai (2000, 2001a, b) and Desilets and co-workers (Desilets et al. 2001, Desilets & Zreda, 2001, 2003) therefore seems to be pointless to a certain extent. Larger differences between the models only result from their different calculation models for the local cutoff rigidity.

As calibration (see above) has shown, up to now there is no convincing evidence for higher production rates in high altitudes as predicted by the more recent scaling systems. But even if it is rather doubtful, whether younger exposure ages at high altitude sites obtained using the scaling of Dunai (2001a) or Desilets & Zreda (2003) are closer to the real ages than older ages obtained by using the scaling of Lal (1991): the notion that exposure ages in such sites may be as much younger should be taken into account in the interpretation of any such data, until the approach of the aforementioned authors has consistently been proven wrong. New high altitude calibrations are definitely needed for clarification. Younger Dryas ages obtained by Tschudi et al. (2003) for a moraine in ~4250 m altitude in Tibet using the scaling system of Lal (1991), together with the clear Younger Dryas signal in Chinese loess lend further credit to Lal's scaling system. However, as long as the moraine itself is not independently dated, its exposure ages cannot be taken for granted.

2.3.3 Comparison of the influence of correction factors

2.3.3.1 Correction for sample geometry

The correction for surface topography is independent from scaling and is generally small. Only for sites in deeply incised valleys with horizon angles of more than 30° from the hori-

zontal for more than half of the azimuth circle it may exceed 5% of P_n or Λ_n. The correction for surface inclination concerning P_n exceeds 10% for inclinations > 48°. For inclinations up to 20° it stays within 1%. Surface inclination correction concerning Λ_n is larger, exceeding 5% for inclinations of > 6° and 10% for inclinations > 24°. The corrections for the muon parameters are larger than the ones for the neutron fraction, but as muon contributions remain within 5% of the total, these corrections have a much smaller influence on the exposure ages than the corrections for the neutron fraction.

Until a practical model will be developed to account for correction for boulder form and size, we consider the boulder-geometry correction too imprecise to be estimated with any confidence yet. It is therefore neglected in our calculations, which is reasonably as long as flat centre surfaces of large boulders or glacially polished surfaces are sampled. For smaller boulders or uneven surfaces, the exposure ages will be underestimated.

2.3.3.2 Corrections for snow and vegetation cover

Corrections for snow and vegetation cover, calculated assuming a simple exponential depth profile of production (no neutron scattering due to low density) are independent of scaling as well. For a reduction of nuclide production of 5%, a cover of ~7 g cm^{-2} would be needed. If snow density is estimated at 0.25 g cm^{-2} (Benson et al., 2004), this would imply a snow cover of >1 m for >3 months every year. However, a reduction of up to 4% (resulting from ~1 m of snow cover for three months of the year) should be considered in mountains with a seasonal climate that is not extremely arid. The correction factors f_{SVC} concerning neutron spallations and muon reactions for cover density-lengths of up to 25 g cm^{-2} is shown in Fig. 2.2A. Correction for both muon fractions is similar and not much larger than 1 % over the shown range.

2.3.3.3 Corrections influenced by a production depth profile other than simple exponential

The corrections for high-density sediment cover, sample thickness and erosion, depending on the depth profile of ^{10}Be production, are shown in Fig. 2.2A-D. Correction of neutron spallations for sediment cover (Fig. 2.2A) is within 1% of the production rate for up to 12 g cm^{-2} of sediment (equivalent to 5 - 7 cm), and within 5% of the production rate for up to ~18 g cm^{-2} (8 - 11 cm). However, if sediment is present on top of the sample, its thickness correction is also increased (Fig. 2.2B). As with snow and vegetation cover, the sediment

cover correction factors for captures of slow negative muons and fast muon reactions are equal over the shown range and not much larger than 1%.

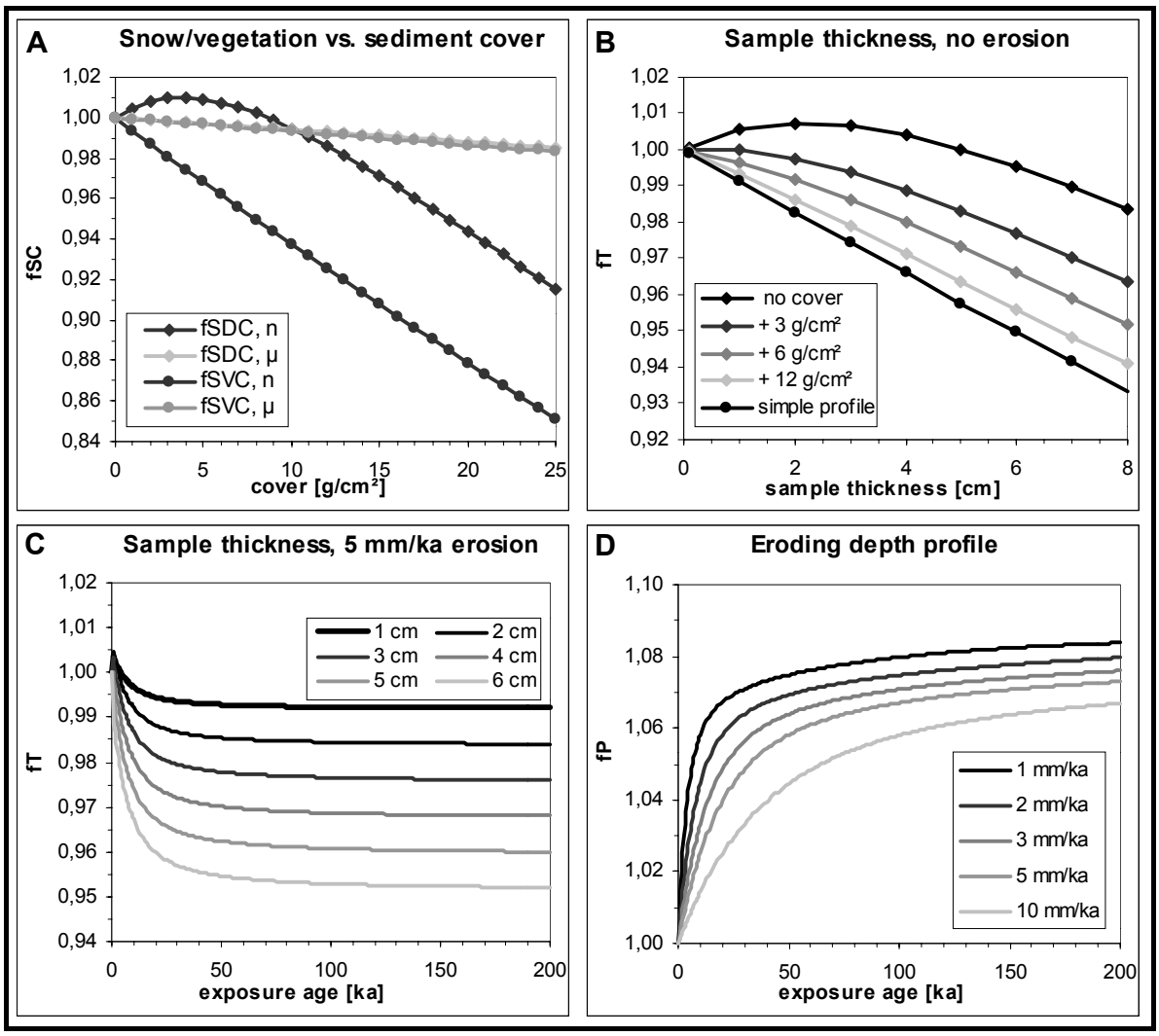

Fig. 2.2. Correction factors associated with the depth profile of Heisinger et al. (2002a, b). A) Correction for surface cover by low-density (snow/vegetation, f_{SVC}) and high-density (sediment, f_{SDC}) cover, shown for the neutron spallation and the muon reactions as a function of cover mass depth. B) Correction of neutron spallations for sample thickness, f_T, in case of no surface erosion as a function of sample thickness and cover mass depth. Correction using a simple exponential depth profile without cover is also shown. C) Correction of neutron spallations for sample thickness, f_T, in case of 5 mm ka^{-1} surface erosion as a function of sample thickness and exposure age. D) Correction of neutron spallation for the eroding depth profile of Heisinger et al. (2002b) as a function of exposure age for different erosion rates.

Correction for sample thickness apart from sample thickness itself depends on sediment cover and erosion rate. Fig. 2.2B shows the correction factors f_T for neutron spallations for different sample thickness and sediment cover mass depth in case of no erosion. Only for a thickness of more than 5 cm or with a sediment cover depth of more than 6 g cm^{-2} the correction exceeds 2%. This is several percentages less than if correction would follow a

simple exponential decrease of production with depth. Corrections of the muon reactions (not shown) are not significant over the shown range of conditions. As neutron backscattering does not increase total production, but only changes its distribution, it is therefore important to know, which form of thickness correction has been applied in any calibration effort, as only calculations applying the same form of correction may use the resulting calibrated standard production rate. In case of erosion (Fig. 2.2C), the zone of neutron backscattering in the upper 12 g cm² of material is moving steadily downwards, so that thickness correction increases with exposure age until an equilibrium value is reached, which depends on the sample thickness and lies between 0.6% for 1 cm thickness and 4.6% for 6 cm thickness. The exposure age, beyond that this value is reached decreases with the erosion rate. With an erosion rate of 5 mm ka^{-1} it is about 50 ka.

The correction of neutron spallations for the eroding depth profile (Fig. 2.2D) is lowering the exposure ages respective to the ones calculated with the same erosion rates, but assuming a simple exponential depth profile. The profile correction of production due to neutron spallations is increasing with the exposure age up to a maximum value dependent on the erosion rate. Assuming an erosion rate of 1 mm ka^{-1}, the correction reaches 5% of P_n after ~60 ka and up to 7% of P_n after 200 ka. Assuming an erosion rate of 5 mm ka^{-1} it reaches 5% of P_n after ~15 ka and up to 8% of P_n after 200 ka. Assuming an erosion rate of 10 mm ka^{-1} the correction even exceeds 8% after 200 ka of exposure. The production rate by slow muon capture (not shown) is slightly decreased by correction, but only within 1% of $P_{\mu-}$. The production rate by fast muon reactions (also not shown) is increased by up to 3% of $P_{\mu f}$ assuming an erosion rate of 5 mm ka^{-1}, and by up to 5% of $P_{\mu f}$ assuming an erosion rate of 10 mm ka^{-1}. Maximum ages for erratic boulders calculated using an assumed surface erosion rate without correction for the measured depth profile are therefore likely to be overestimates by up to 8%.

2.3.3.4 Correction for geomagnetic variations

The correction factors for geomagnetic variations, $f_M(t)$, are different for each site and each general scaling system. For the lower latitude site at 28°N, the $f_M(t)$ for each system are shown for the last 200 ka and altitudes from zero to 5000 m a.s.l. in Fig. 2.3. For the higher latitude model site at 38°N, the functions (not shown) are broadly similar, but the absolute values reach only roughly half the respective ones at 28°N, due to the decrease in cutoff rigidity with latitude. The lower the cutoff rigidity, the smaller the fraction of incoming rays that is deflected. This can be modified by changes in the geomagnetic field. Unlike

stated in Masarik et al. (2001), the factor $f_M(t)$ is generally a function of altitude in the calculations used here.

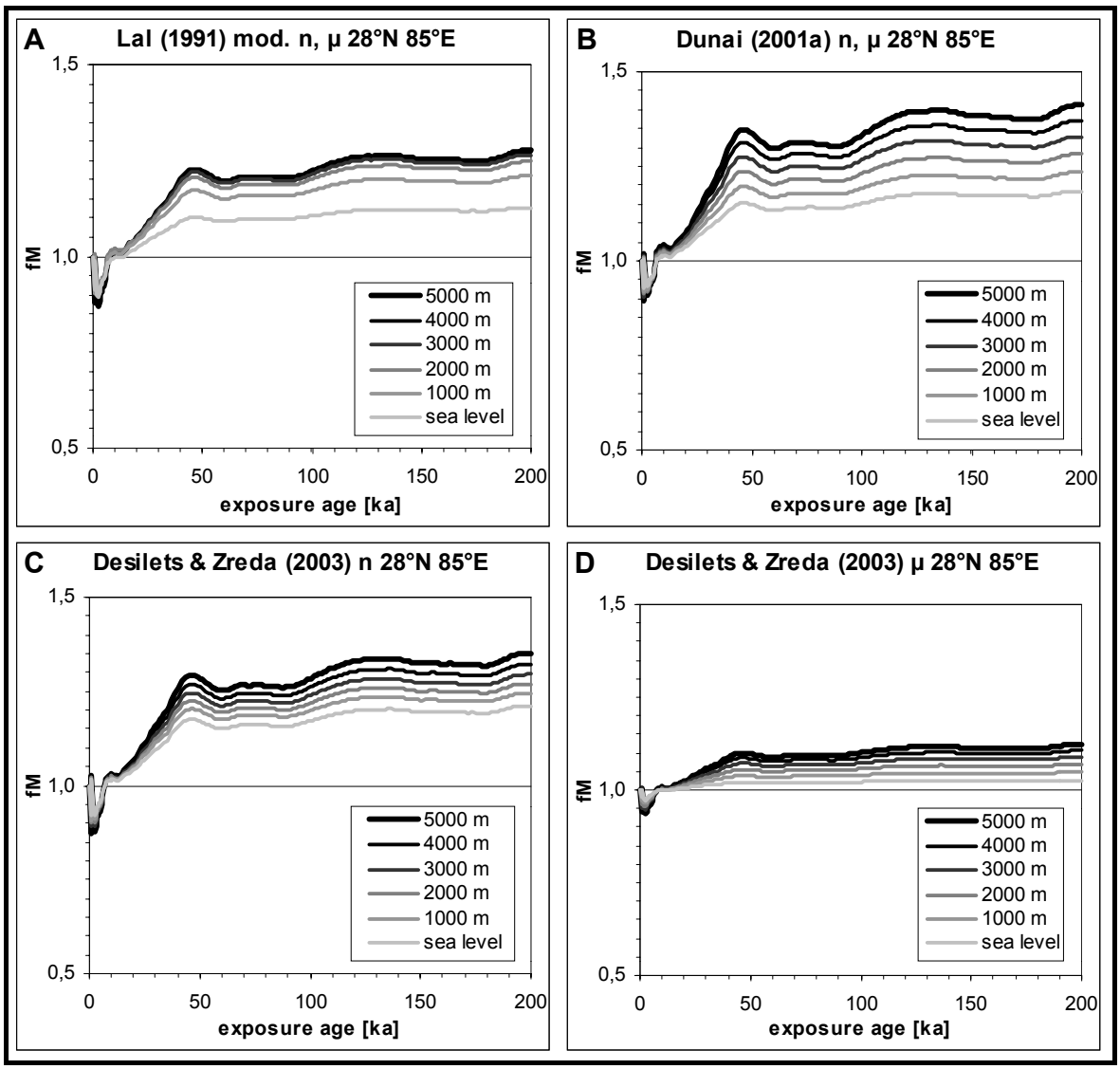

Fig. 2.3. Correction factors $f_M(t)$ for variations in the geomagnetic field at 28°N 85°E for neutron spallations (n) and muon reactions (μ), calculated as a function of exposure age and altitude for use within the scaling systems of A) Lal (1991) modified, B) Dunai (2001a) and C, D) Desilets & Zreda (2003).

In the calculation scheme adopted for the modified scaling systems of Lal (1991), in contrast to the other schemes, $f_M(t)$ does not increase linearly with altitude, but the function reaches a saturation level between 3000 and 4000 m a.s.l. The reason is that in this model, the VADM influences altitude scaling only indirectly via latitude scaling. In Dunai's (2001a) and Desilets' and Zreda's (2003) model, latitudinal and altitudinal scaling both directly depend on the VADM. The values of $f_M(t)$ are significantly higher in the system of Dunai (2001a) than in the system of Desilets and Zreda (2003). In Desilets' and Zreda's

(2003) system, due to the different cutoff rigidity dependency of neutron spallation used as compared with muon reactions, there are also differences in the geomagnetic correction factors for neutrons and muons, the latter being much smaller than the former. In Dunai's (2001a) system, the cutoff rigidity dependency of neutron and muon reactions are assumed to be the same, so that the correction factors for geomagnetic variations are equal as well. In the modified scaling systems of Lal (1991), there are only insignificant differences in the f_M values for neutron spallation reactions and muon reactions, as both are given roughly the same latitude dependency.

Geomagnetic correction at the model site at 28° latitude in all systems exceeds 20% of P for altitudes of > 2000 m and ages > 30 ka. At the model site at 38° latitude it still exceeds 10% for the same altitudes and ages. At 28° latitude, it amounts to up to 10% of P even in the Holocene. Corrections of this order are too large to be neglected, even if they are associated with a pronounced uncertainty (Gosse & Phillips, 2001). As all geomagnetic corrections considered here lead to a better fit of the calibration studies in the respective scaling system (see above), they are at least creditable in this form, which is in favour of Desilets' & Zreda's (2003) doubts concerning the correction factors proposed by Masarik et al. (2001). Hence, these geomagnetic corrections should be applied in all dating studies. The somewhat clumsy empirical correction scheme developed for Lal's (1991) scaling system yields no seriously different results than the more sophisticated models of Dunai (2001a) and Desilets & Zreda (2003). However, it may be worth a reformulation in a more analytical way similar to those used in the latter.

2.3.3.5 Correction for tectonic uplift

The correction factor for tectonic uplift, $f_U(t)$, depends on altitude scaling and is therefore different for each site, each scaling system, and each production fraction. In Fig. 2.4, it is shown for the 38°N 74°E site and an uplift rate of 3 mm a^{-1}. For the 28°N 85°E site, the corrections (not shown) are similar, but insignificantly smaller. The uplift correction increases with exposure age but decreases with final altitude.

The differences in tectonic uplift correction between the scaling systems are small. For the scaling systems of Dunai (2001a) and Desilets and Zreda (2003), the $f_U(t)$ values are essentially the same. Using the scaling system of Lal (1991), however, a more pronounced altitude dependency results from the different altitudinal scaling; the corrections for higher final altitudes being smaller than the respective corrections in the other systems.

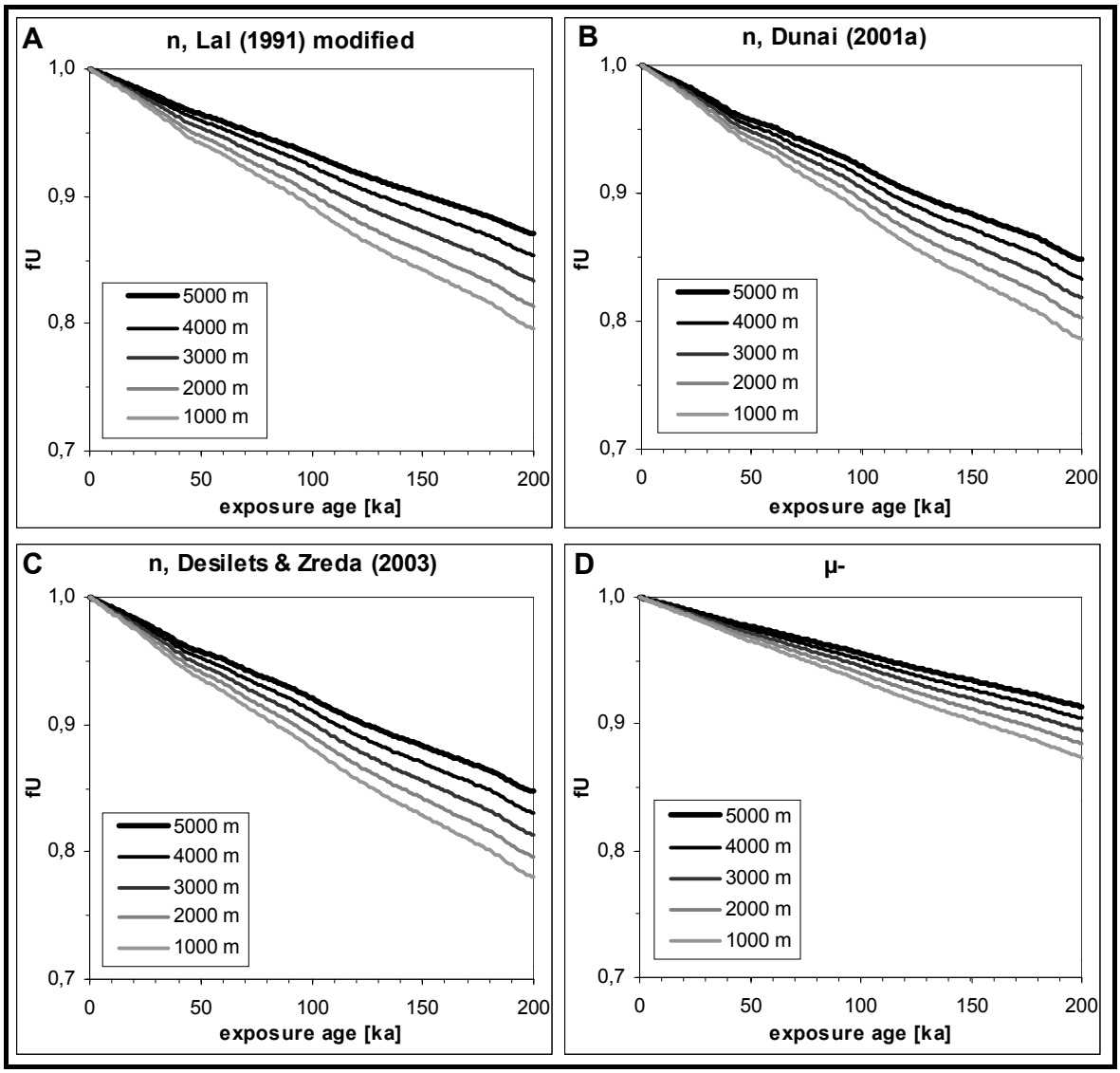

Fig. 2.4. Correction factors $f_U(t)$ for 3 mm a^{-1} tectonic uplift as functions of exposure age and altitude at 38°N 74°E, calculated for the neutron spallation production fraction in the scaling systems of A) Lal (1991) modified, B) Dunai (2001a), and C) Desilets & Zreda (2003), as well as D) for the capture of negative muon fraction as scaled with an atmospheric attenuation length of 247 g cm^{-2}.

In 1000 m altitude, uplift correction for production due to neutron spallation assuming a moderate uplift rate of 3 mm a^{-1} reaches 10% of the production rate after ~80 ka of exposure. In 4000 m altitude the same is reached after about ~ 110 ka. For capture of slow negative muons with an atmospheric attenuation length of 247 g cm^{-2}, the correction still reaches 5% of P after the same time. For high-energy muon reactions with an atmospheric attenuation length of >1000 g cm^{-2}, the correction becomes negligible. Given these values, uplift correction should always be included when dating middle and early late Pleistocene exposures in moderate or even low altitudes of actively upthrust regions, even if the uncertainty of the uplift rate is high. Otherwise, calculated exposure ages will be under-

estimated. Since extensive middle Pleistocene or early late Pleistocene glaciations might have led to some isostatic lowering of the crust, the adjustment after melting of these ice masses should rather add to the long-term tectonic uplift, so that high uplift rates are rather likely in such settings (Kaufmann & Lambeck, 1997).

2.4 Conclusions

The traditional scaling system of Lal (1991), as modified by Stone (2000), still proves to be the one best able to bring existing calibrations into accord, if problematical studies excluded. Low muon contributions as measured by Braucher et al. (2003) are in accord with calibrations relying on the neutron scaling of Lal (1991), but not with the neutron scaling of the other systems. Generally, however, variations in the scaling of muon production have only minor effects on calibration results.

At least for mid-to-high latitude areas, we still recommend the use of the scaling system of Lal (1991) as modified by Stone (2000), but using a standard production rate at sea level, high latitude, of 5.35 ± 15 atoms g^{-1} a^{-1} and a contribution of capture of slow negative muons of 1.2% rather than the respective parameters given by Stone (2000).

The ages resulting from the use of the scaling systems of Dunai (2001a) and Desilets & Zreda (2003) do not significantly differ from each other. Small differences result from their disagreeing ways of accounting for past geomagnetic variations. The different altitude dependency of cosmogenic nuclide production proposed by these authors is not convincing yet given the existing calibration data. The use of these scaling systems, however, yields significantly lower exposure ages than the use of the scaling system of Lal (1991) in rocks that have been exposed at altitudes of more than 2000 - 3000 m a.s.l. at our High Asian model sites. The notion that ages from high altitude sites may be much younger than calculated using the scaling system of Lal (1991) should be considered, even if it is doubtful at present. New high altitude calibrations are definitely needed for clarification.

All middle and early late Pleistocene exposure ages are significantly increased by correcting for reasonable estimates of erosion and tectonic uplift, and they are significantly lowered by correction for geomagnetic variations and by the effects of the refined depth profile of ^{10}Be production measured by Heisinger et al. (2002a, b). Principally, the use of all possible corrections is recommended, including correction for surface inclination and tectonic uplift.

A recalculation of Lal's (1991) system as a continuous function of cutoff rigidity and atmospheric depth, including a reasonable separation of fast muon production and production due to capture of slow negative muons in scaling would be desirable improvements, especially for use in lower latitudes.

2.5 Acknowledgements

This work was made possible by the German Research Foundation (DFG), grant ZE 154-51. We thank Dr. Peter W. Kubik for his cooperation in measuring $^{10}Be/^{9}Be$ in our samples at the AMS facility of the Paul Scherrer Institute at the ETH Zurich, and Prof. Dr. Hanns Kerschner, University of Innsbruck, for his help during resampling of the Koefels landslide.

2.6 References

BARROWS, T. T., STONE, J. O., FIFIELD, L. K., CRESSWELL, R. G. 2001. Late Pleistocene glaciation of the Kosciuszko massif, Snowy Mountains, Australia. Quaternary Research 55, 179-189.

BENSON, L., MADOLE, R., PHILLIPS, W., LANDIS, G., THOMAS, T., KUBIK, P. 2004. The importance of snow and sediment shielding on cosmogenic ages of north-central Colorado Pinedale and Pre-Pinedale moraines. Quaternary Science Reviews 23, 193-206.

BIERMAN, P. R., CAFFEE, M. 2002. Cosmogenic exposure and erosion history of Australian bedrock landforms. Geological Society of America Bulletin 114, 787-803.

BIERMAN, P., LARSEN, P., CLAPP, E., CLARK, D. 1996. Refining estimates of ^{10}Be and ^{26}Al production rates. Radiocarbon 38, 149.

BOEZIO, M., CARLSON, P., FRANCKE, T., WEBER, N., SUFFERT, M., HOF, M., MENN, W., SIMON, M., STEPHENS, S. A., BELLOTTI, R., CAFAGNA, F., CIRCELLA, M., DE MARZO, C., FINETTI, N., PAPINI, P., PICCARDI, S., SPILLANTINI, P., RICCI, M., CASOLINI, M., DE PASCALE, P., MORSELLI, A., PICOZZA, P., SPARVOLI, R., BARBIELLINI, G., SCHIAVON, P., VACCHI, A., ZAMPA, N., GRIMANI, C., MITCHELL, J. W., ORMES, J. F., STREITMATTER, R. E., BRAVAR, U., GOLDEN, R. L., STOCHAJ, S. J. 2000. Measurement of the flux of atmospheric muons with the CAPRICE94 apparatus. Physical Review D 62, 032007-1 – 032007-15.

BRAUCHER, R., BOURLÈS, D. L., COLIN, F., BROWN, B., BOULANGÉ, B. 1998. Brazilian laterite dynamics using in-situ produced ^{10}Be. Earth and Planetary Science Letters 163, 197-205.

BRAUCHER, R., BROWN, E. T., BOURLÈS, D. L., COLIN, F. 2003. In situ produced ^{10}Be measurements at great depths: implications for production rates by fast muons. Earth and Planetary Science Letters 211, 251-258.

BROWN, E. T., EDMOND, J. M., RAISBECK, G. M., YIOU, F., KURZ, M. D., BROOK, E. J. 1991. Examination of surface exposure ages of Antarctic moraines using in situ produced ^{10}Be and ^{26}Al. Geochimica et Cosmochimica Acta 55, 2269-2283.

BROWN, E. T., STALLARD, R. F., LARSEN, M. C., RAISBECK, G. M., YIOU, F. 1995a. Denudation rates determined from the accumulation of in situ-produced ^{10}Be in the Luquillo experimental Forest, Puerto Rico. Earth and Planetary Science Letters 129, 193-202.

BROWN, E. T., BOURLES, D. L., COLIN, F., RAISBECK, G. M. 1995b. Evidence for muon-induced production of ^{10}Be in near-surface rocks from the Congo. Geophysical Research Letters 22, 703-706.

BROWN, E. T., TRULL, T. W., JEAN-BAPTISTE, P., RAISBECK, G., BOURLÈS, D., YIOU, F., MARTY, B. 2000. Determination of cosmogenic production rates of ^{10}Be, ^{3}He, and ^{3}H in water. Nuclear Instruments and Methods in Physics Research B 172, 873-883.

CERLING, T. E., CRAIG, H. 1994. Geomorphology and in situ cosmogenic isotopes. Annual Review of Earth and Planetary Sciences 22, 273-317.

CLARK, D. H., BIERMAN, P. R., LARSEN, P. 1995. Improving in situ cosmogenic chronometers. Quaternary Research 44, 366-376.

DEP, W. H. L. 1995. Cosmogenic radionuclide production in terrestrial rocks: Accelerator mass spectrometry measurements and Monte Carlo simulations. Ph.D. Thesis, Purdue University, West Lafayette, IN. 155 pp.

DESILETS, D., ZREDA, M. 2001. On scaling cosmogenic nuclide production rates for altitude and latitude using cosmic-ray measurements. Earth and Planetary Science Letters 193, 213-225.

DESILETS, D., ZREDA, M. 2003. Spatial and temporal distribution of secondary cosmic-ray nucleon intensities and applications to in situ cosmogenic dating. Earth and Planetary Science Letters 206, 21-42.

DESILETS, D., ZREDA, M., LIFTON, N. A. 2001. Comment on 'Scaling factors for production rates of in situ produced cosmogenic nuclides: a critical reevaluation' by Tibor J. Dunai. Earth and Planetary Science Letters 188, 283-287.

DODONOV, A. E. 2002. The Quaternary of Middle Asia. Transactions of the Russian Academy of Sciences, Geological Institute 546, 250 pp. (in Russian).

DUNAI, T. J. 2000. Scaling factors for production rates of in situ produced cosmogenic nuclides: a critical reevaluation. Earth and Planetary Science Letters 176, 157-169.

DUNAI, T. J. 2001a. Influence of secular variation of the geomagnetic field on production rates of in situ produced cosmogenic nuclides. Earth and Planetary Science Letters 193, 197-212.

DUNAI, T. J. 2001b. Reply to comment on 'Scaling factors for production rates of in situ produced cosmogenic nuclides: a critical reevaluation' by Darin Desilets, Marek Zreda and Nathaniel Lifton. Earth and Planetary Science Letters 188, 289-298.

DUNNE, A., ELMORE, D., MUZIKAR, P. 1999. Scaling factors for the rates of production of cosmogenic nuclides for geometric shielding and attenuation at depth on sloped surfaces. Geomorphology 27, 3-11.

GOSSE, J. C., PHILLIPS, F. M. 2001. Terrestrial in situ cosmogenic nuclides: theory and application. Quaternary Science Reviews 20, 1475-1560.

GOSSE, J. C., STONE, J. O. 2001. Terrestrial cosmogenic nuclide methods passing milestones towards palaeo-altimetry. EOS Transactions of the American Geophysical Union 82, 82-89.

GRAHAM, I. J., BARRY, B. J., DITCHBURN, R. G., WHITEHEAD, N. E. 2000. Validation of cosmogenic nuclide production rate scaling factors through direct measurement. Nuclear Instruments and Methods in Physics Research B 172, 802-806.

GUYODO, Y., VALET, J.-P. 1996. Relative variations in geomagnetic intensity from sedimentary records: the past 200.000 years. Earth and Planetary Science Letters 143, 23-26.

GUYODO, Y., VALET, J.-P. 1999. Global changes in intensity of the Earth's magnetic field during the past 800 ka. Nature 399, 249-252.

HEIDBREDER, E., PINKAU, K., REPPIN, C., SCHOENFELDER, V. 1971. Measurement of the distribution in energy and angle of high-energy neutrons in the lower atmosphere. Journal of Geophysical Research 76, 2905-2916.

HEISINGER, B., NOLTE, E. 2000. Cosmogenic in situ production of radionuclides: exposure ages and erosion rates. Nuclear Instruments and Methods in Physics Research B 172, 790-795.

HEISINGER, B., LAL, D., JULL, A. J. T., KUBIK, P., IVY-OCHS, S., NEUMAIER, S., KNIE, K., LAZAREV, V., NOLTE, E. 2002a. Production of selected cosmogenic radionuclides by muons 1. Fast muons. Earth and Planetary Science Letters 200, 345-355.

HEISINGER, B., LAL, D., JULL, A. J. T., KUBIK, P., IVY-OCHS, S., KNIE, K., NOLTE, E. 2002b. Production of selected cosmogenic radionuclides by muons 2. Capture of negative muons. Earth and Planetary Science Letters 200, 357-369.

HETZEL, R., NIEDERMANN, S., IVY-OCHS, S., KUBIK, P. W., TAO, M., GAO, B. 2002. ^{21}Ne versus ^{10}Be and ^{26}Al exposure ages of fluvial terraces: the influence of crustal Ne in quartz. Earth and Planetary Science Letters 201, 575-591.

HOLDEN, N. E. 1990. Total half-lives for selected nuclides. Pure and Applied Chemistry 62, 941-958.

IVY-OCHS, S. 1996. The dating of rock surface using in situ produced ^{10}Be, ^{26}Al and ^{36}Cl, with examples from Antarctica and the Swiss Alps. Diss. ETH No. 11763, Zurich 197 p.

JAIN, A. K., KUMAR, D., SINGH, S., KUMAR, A., LAL, N. 2000. Timing, quantification and tectonic modelling of Pliocene-Quaternary movements in the NW Himalaya: evidence from fission track dating. Earth and Planetary Science Letters 179, 437-451.

KAUFMANN, G., LAMBECK, K. 1997. Implications of late Pleistocene glaciation of the Tibetan Plateau for present-day uplift rates and gravity anomalies. Quaternary Research 48, 267-279.

KLEIN, J., GOSSE, J. C. 2002. Production rates of ^{10}Be and ^{26}Al in mid-latitudes and high altitudes. Goldschmidt Conference Abstracts 2002, A 403.

KOBER, F., SCHLUNEGGER, F., IVY-OCHS, S., WIELER, R. 2002. The dependency of cosmogenic nuclides to climate and surface uplift in transient landscapes. Goldschmidt Conference Abstracts 2002, A 408.

KUBIK, P. W., IVY-OCHS, S. 2003. A re-evaluation of the 0-10 ka ^{10}Be production rate for exposure dating obtained from the Koefels (Austria) landslide. Nuclear Instruments and Methods in Physical Research B, in press.

KUBIK, P. W., IVY-OCHS, S., MASARIK, J., FRANK, M., SCHLUECHTER, C. 1998. ^{10}Be and ^{26}Al production rates deduced from an instantaneous event within the dendro-calibration curve, the landslide of Koefels, Oetz Valley, Austria. Earth and Planetary Science Letters 161, 231-241.

LAL, D. 1991. Cosmic ray labelling of erosion surfaces: in situ nuclide production rates and erosion models. Earth and Planetary Science Letters 104, 424-439.

LELAND, J., REID, M. R., BURBANK, D. W., FINKEL, R., CAFFEE, M. 1998. Incision and differential bedrock uplift along the Indus River near Nanga Parbat, Pakistan Himalaya, from ^{10}Be and ^{26}Al exposure age dating of bedrock straths. Earth and Planetary Science Letters 154, 93-107.

LIDE, D. R. 1999. The physical standard atmosphere. In: CRC Handbook of Chemistry and Physics, 79th edition. CRC Press, Boca Raton, Florida, 14-16 – 14-22.

LIFTON, N. A., JULL, A. J. T., QUADE, J. 2001. A new extraction technique and production rate estimate for in situ cosmogenic ^{14}C in quartz. Geochimica et Cosmochimica Acta 65, 1953-1969.

LIFTON, N. A., PIGATI, J., JULL, A. J. T., QUADE, J. 2002. Altitudinal variation of in situ cosmogenic ^{14}C production rates: preliminary results from the southwestern U.S. Goldschmidt Conference Abstracts 2002, A 457.

MASARIK, J., REEDY, R. C. 1995. Terrestrial cosmogenic-nuclide production systematics calculated from numerical simulations. Earth and Planetary Science Letters 136, 381-395.

MASARIK, J., WIELER, R. 2003. Production rates of cosmogenic nuclides in boulders. Earth and Planetary Science Letters 216, 201-208.

MASARIK, J., KOLLAR, D., VANYA, S. 2000. Numerical simulation of in situ production of cosmogenic nuclides: effects of irradiation geometry. Nuclear Instruments and Methods in Physics Research B 172, 786-789.

MASARIK, J., FRANK, M., SCHAEFER, J. M., WIELER, R. 2001. Correction of in situ cosmogenic nuclide production rates for geomagnetic field intensity variations during the past 800,000 years. Geochimica et Cosmochimica Acta 65, 2995-3003.

MCELHINNY, M. W., SENANAYAKE, W. E. 1982. Variations in the geomagnetic dipole 1: The past 50.000 years. Journal of Geomagnetism and Geoelectricity 34, 39-51.

NISHIIZUMI, K., WINTERER, E. L., KOHL, C. P., KLEIN, J., MIDDLETON, R., LAL, D., ARNOLD, J. R. 1989. Cosmic ray production rates of ^{10}Be and ^{26}Al in quartz from glacially polished rocks. Journal of Geophysical Research B 94, 17907-17915.

NISHIIZUMI, K., FINKEL, R. C., KLEIN, J., KOHL, C. P. 1996. Cosmogenic production of ^{7}Be and ^{10}Be in water targets. Journal of Geophysical Research 101, 22225-22232.

OHNO, M., HAMANO, Y. 1992. Geomagnetic poles over the past 10.000 years Geophysical Research Letters 19, 1715-1718.

OWEN, L. A., FINKEL, R.C., CAFFEE, M. W., GUALTIERI, L. 2002. Timing of multiple glaciations during the Late Quaternary in the Hunza Valley, Karakoram Mountains, northern Pakistan: defined by cosmogenic radionuclide dating of moraines. Geological Society of America Bulletin 114, 593-604.

PHILLIPS, F. M., ZREDA, M. G., GOSSE, J. C., KLEIN, J., EVENSON, E. B., HALL, R. D., CHADWICK, O. A., SHARMA, P. 1997. Cosmogenic ^{36}Cl and ^{10}Be ages of Quaternary glacial and fluvial deposits of the Wind River Range, Wyoming. Geological Society of America Bulletin 109, 1453-1463.

SCHALLER, M., VON BLANCKENBURG, F., HOVIUS, N., KUBIK, P. W. 2001. Large-scale erosion rates from in situ-produced cosmogenic nuclides in European river sediments. Earth and Planetary Science Letters 188, 441-458.

SCHALLER, M., VON BLANCKENBURG, F., VELDKAMP, A., TEBBENS, L. A., HOVIUS, N., KUBIK, P. W. 2002. A 30 000 yr record of erosion rates from cosmogenic ^{10}Be in Middle European river terraces. Earth and Planetary Science Letters 204, 307-320.

STONE, J. O. H. 2000. Air pressure and cosmogenic isotope production. Journal of Geophysical Research 105 B10, 23753-23759.

STONE, J. O., BALLANTYNE, C. K., FIFIELD, L. K. 1998. Exposure dating and validation of periglacial weathering limits, northwest Scotland. Geology 26, 587-590.

TSCHUDI, S., SCHAEFER, J. M., ZHAO, Z., WU, X., IVY-OCHS, S., KUBIK, P., SCHLUECHTER, C. 2003. Glacial advances in Tibet during the Younger Dryas? Evidence from cosmogenic ^{10}Be, ^{26}Al, and ^{21}Ne. Journal of Asian Earth Sciences 22, 301-306.

3. The interpretation of ^{10}Be surface exposure ages of erratic boulders in reconstructions of the regional glaciation history of High Asia

Uwe Abramowski & Wolfgang Zech

Institute of Soil Science and Soil Geography, University of Bayreuth, D-95440 Bayreuth, Germany

Abstract

In this paper, we discuss both the propagated uncertainties of ^{10}Be surface exposure ages and the use of moraine degradation models in ^{10}Be surface exposure dating of moraines, with special emphasis on studies in High Asia. The uncertainties of ^{10}Be surface exposure ages at present are dominated by the uncertainties of the scaling factor, the erosion rate, and the tectonic uplift rate. For High Asia, a surface erosion rate for granitic boulders of 3 ± 2 mm ka^{-1} seems to be a reasonable maximum estimate. As long as surface erosion and tectonic uplift rates cannot be constrained to within at least 10%, exposure ages older than 30-40 ka have uncertainties of ≥20% and can be considered no more than rough approximations. Not in accord with current models of linear moraine degradation, exposure age distributions from single moraines frequently contain ages older than the deposition age due to inherited ^{10}Be in some of the boulders, and they frequently are not unimodal, but show two or more age clusters. In some cases, age clusters younger than the deposition age of a moraine are synchronous on different moraines in the same region, possibly indicating phases of enhanced, climate-driven surface activity. In order to obtain a concise glaciation history of a mountainous region, ^{10}Be exposure ages from several moraines within a region have to be interpreted in the light of the local stratigraphical and climatological context. Sampling of a minimum of 3-5 boulders from each of a maximum number of different moraines, which should be stratigraphically related and which should cover all encountered relative ages, may be necessary to draw any climatological conclusions from SED. A scheme for interpretation of the resulting boulder age distributions is presented.

3.1 Introduction

Precision and accuracy of moraine ages derived from ^{10}Be surface exposure ages of erratic boulders are generally considered to be high. Such ages have been used to define short-term glacial events (e.g. Gosse et al., 1995a, b), or even to correlate glacial advances with narrow climatic events found in continuous proxy archives, like Heinrich events (e.g. Owen et al., 2002).

In most of those studies, however, exposure ages are considered only within the uncertainties resulting from the errors of the measured concentrations, which can be reduced to 3% or even less by presently employed AMS techniques (Kubik, pers. comm.). Rigorous error analysis is often put aside, given that many of the individual errors attached to the calculation scheme are not precisely known and can only be estimated (Gosse & Phillips, 2001).

Secondly, deriving a moraine age from surface exposure ages of a selection of erratic boulders situated on its crest has in some cases proven to be a more difficult task than thought at first. On the one hand, erratic boulders deposited on a moraine may contain ^{10}Be inherited from a previous period of exposure, either on a former moraine, or on the rock slope above the glacier, both leading to an overestimation of the moraine age. On the other hand, erratic boulders might have been broken free from a larger block, or might have been cleared from sediment cover long after deposition of the moraine, both leading to an underestimation of the moraine age (Brook et al., 1993, Hallet & Putkonen, 1994, Owen et al., 2003a, b). Therefore, some kind of model has to be used to derive a moraine age from a distribution of erratic boulder exposure ages. Several such models have already been proposed (see below), but all of them are based on linear moraine degradation, which can explain unimodal distributions of exposure ages only. However, bi- or even polymodal distributions are frequently observed (e.g. Phillips et al., 1997, Marsella et al., 2001) and have to be interpreted.

In this paper, we discuss in detail both error propagation and interpretative model use in deriving moraine ages from ^{10}Be exposure ages of erratic boulders, in order to understand how moraine ages can best be determined from erratic boulder exposure ages, and how precise those ages can safely be considered at present.

3.1.1 Uncertainties of cosmogenic exposure ages

Gosse & Phillips (2001) calculate a total, fully propagated error of the SED method of about 13%, but argue that the true error is likely to be smaller. The largest uncertainty adding to the 13% is the error of the factor used to scale the production rate of ^{10}Be from the calibration sites to the sampling site, which has been estimated to be about 10% (Lal, 1991). Recently, there have been efforts to establish new scaling systems with smaller uncertainties (Dunai, 2000, 2001; Desilets & Zreda, 2003). At present, however, these new scaling systems are no more successful than Lal's (1991) system in bringing published calibrations into accord (section 2), so that the proposed reduction in uncertainty remains questionable.

However, in calculating their propagated estimate of 13%, Gosse & Phillips (2001) have left out three important sources of uncertainty, being the erosion rate of the rock surface, which has a large influence on exposure ages (Gillespie & Bierman, 1995), the correction factor for tectonic uplift, which is important in tectonically active mountain areas (section 2), and the correction factor for snow cover. The reason for this neglect is that surface erosion, tectonic uplift, and snow cover are considered to be leading to systematical errors in the first place, because they are most often ignored in age calculations. If they are not ignored, however, their respective uncertainties are of a stochastic nature and have to be propagated as well, adding to the total uncertainty of the exposure age.

The erosion rate of a sample surface most often can only be estimated within a large interval. Some authors use the amount of relief between some part of the rock (e.g. a quartz vein) and the matrix to constrain its magnitude (e.g. Ivy-Ochs et al., 1999, Balco et al., 2002); however, as long as the higher parts of the surface do not show marks of a preserved palaeosurface, like e.g. glacial striae, one cannot be sure whether this relief is really representing total matrix erosion, or rather differential erosion of both parts of the rock. Rock coatings like desert varnish can form in a few thousand years and do not exclude prior detachment of material (Dorn & Phillips, 1991).

Measuring ^{26}Al along with ^{10}Be to determine the erosion rate (Lal, 1991) is also problematic. On the one hand, the implied ^{26}Al/^{10}Be ratio at production has a pronounced uncertainty, as it amounts to 7.1 in pure synthetic quartz (Reedy et al., 1994), but has been measured in rock quartz to fall between 5.7 (Masarik & Reedy, 1995) and 6.6 (Ivy-Ochs, 1996). On the other hand, the scatter in ^{26}Al/^{10}Be ratios measured in erratic boulders is

frequently observed to be higher than can be explained by the production-decay model. This may be due to analytical problems with ^{26}Al in quartz (Bierman & Caffee, 2002), or due to a source of inherited ^{10}Be in the rocks. Such a source could be selective production of ^{26}Al by muon reactions at depth (Heisinger & Nolte, 2000), but this assumption has not been confirmed yet. Anyhow, even if the $^{26}Al/^{10}Be$ ratio can be determined accurately, the difference between the decay constants of ^{10}Be and ^{26}Al is not large enough to measure both exposure ages and erosion rates in surfaces exposed for <100 ka (Gillespie & Bierman, 1995). Pairing of in-situ ^{10}Be with in-situ ^{36}Cl theoretically should yield more accurate results even for younger samples, because of the characteristic depth profile of ^{36}Cl production (Liu et al., 1994). However, as measured in-situ ^{36}Cl production rates from different sites up to now do not agree with each other (Phillips et al., 1996; Stone et al., 1996; Swanson & Caffee, 2001), large uncertainties have to be acknowledged in $^{36}Cl/^{10}Be$ ratio ages as well. The possibility of measuring in-situ ^{14}C along with ^{10}Be (Lifton et al., 2001) is promising, but has not been made commonly accessible yet.

Tab. 3.1. Published erosion rates of bare rock surfaces.

Paper	Site, petrology	Method	Erosion rate [mm ka^{-1}]
Zimmerman et al., 1994	Wyoming, granite	fire spalling extrapolation	0.3 - 5.9
Bierman & Turner, 1995	Australia, granite	$^{26}Al/^{10}Be$ equilibrium	0.6 - 2.9
Brown et al., 1995	Puerto Rico, quartz diorite	^{10}Be equilibrium	25
Brook et al., 1996	Norway, metamorphic rock	$^{26}Al/^{10}Be$ equilibrium	2.1-2.7
Phillips et al., 1997	Wyoming, gneiss	$^{36}Cl/^{10}Be$ pairing	< 0.2
Small et al., 1997	USA West, granite/gneiss	$^{26}Al/^{10}Be$ equilibrium	1.9 - 18.6
Small et al., 1997	various, granite, granodiorite	$^{26}Al/^{10}Be$ equilibrium	7 - 56
Bierman et al., 1999	Baffin Island, gneiss	$^{26}Al/^{10}Be$ pairing	0.5 - 1.1
Bierman et al., 1999	Baffin Island, quartzite, gneiss	$^{26}Al/^{10}Be$ equilibrium	4.6 - 10.7
Heimsath et al., 2001	SE-Australia, granite	^{10}Be equilibrium	3.8 - 30
Ivy-Ochs et al., 1999	New Zealand, gneiss	quartz vein relief	0.35
Barrows et al., 2001	Australia, granodiorite	^{10}Be equilibrium	3.35
Granger et al., 2001	California, granite	$^{26}Al/^{10}Be$ equilibrium	6 - 12

General estimates of erosion rates of rock surfaces, however, are available. They have been measured directly in a variety of locations using, e.g., the equilibrium cosmogenic radionuclide concentration approach. Rock surfaces exposed for several half-lives of the radionuclide are in equilibrium concerning its production and decay. The production rate and decay constant known, the erosion rate of such surfaces can be calculated from the ^{10}Be equilibrium concentration (Nishiizumi et al., 1993). Published measurements of erosion rates of bare rock surfaces in different parts of the world are summarized in Tab. 3.1.

Taking all values into account, a maximum erosion rate estimate of 5 ± 2 mm ka^{-1} is often used (e.g. Phillips et al., 1997, Owen et al, 2002).

Tectonic uplift has only been considered in a few SED studies up to now (Brown et al., 1991, Gosse & Stone, 2001, Kober et al., 2002). In tectonically active mountain regions like the Himalayas and the Central Asian mountain systems, however, uplift rates are comparatively high and should not be neglected. Kaufmann & Lambeck (1997) review published uplift rates of up to 5 mm a^{-1} for the Himalayas and up to 15 mm a^{-1} for Tibet. Burbank et al. (1996) measured incision rates of the Indus River in the northwestern Himalayas of 2-12 mm a^{-1} that should equal bedrock uplift rates. Other measurement approaches, e.g. using fission track dating or vertical terrace displacement along faults, yield more modest rates (Zeitler, 1985, Owen, 1989, Leland et al., 1998, Jain et al., 2000). An uplift rate of 3 ± 2 mm a^{-1} may be regarded as a conservative maximum estimate for High Asian sites.

Snow cover is another factor likely to increase uncertainties, as mean annual snow depth and density can only be estimated within large uncertainties for the time before the Holocene (Lifton et al., 2001). For mid- and high-latitude mountainous areas, a mean snow cover of between 50 cm lasting 2 months and 100 cm lasting 4 months may be a reasonable estimate. Assuming a mean snow density of 0.25 g cm^{-3}, these values translate into a mass cover of 5 ± 3 g cm^{-2}.

In order to re-examine uncertainties in surface exposure dates, including estimates of erosion and uplift rates as well as snow cover, we present a simple propagation of all larger associated errors, including erosion and uplift correction, which is included in our program for calculating cosmogenic exposure ages, TEBESEA (section 2).

3.1.2 Interpretative models to derive moraine ages from exposure ages

Exposure ages from a single moraine most often form a distribution with a more or less pronounced scatter. Several models of moraine development have been devised to account for this scatter. All these models assume boulders to be successively exhumed by linear removal of fine material from the deposit over time, and they provide some theoretical way to calculate the moraine age from the modal value of the boulder age distribution (Zreda et al., 1994; Hallet & Putkonen, 1994; Putkonen & Swanson, 2003), or from its scatter (Shanahan & Zreda, 2000). All these models, however, can only explain unimodal age distribu-

tions, as none of them does account for any discontinuity of matrix erosion. However, in several soil profiles adjacent to moraines, buried A horizons covered by thick colluvium indicate several phases of enhanced relief instability associated with climate change and glacial activity (Dahms, 1994; Zech et al., 1996, 2000a, b, 2003). During such phases, many more boulders will be freed from cover than at other times, and this exhumation will not proceed gradually, but up to tens of meters of sediment might be removed in a single landsliding, solifluction, or debris flow event. A comprehensive overview of such non-linear moraine degradation processes is given by Ballantyne (2002). Especially in the case of lateral moraines, degradation and modification processes are frequently recognized (Iturrizaga, 2003). In periglacial environments, other processes than cover removal may alter the exposure age of a boulder as well. One is the rotation of boulders partially sinking into thawed permafrost (Schaefer et al. 2002); another is the movement of boulders and matrix following the thawing out of dead ice enclosed inside the moraine body (Kjaer & Krueger, 2001; Balco et al., 2002, Everest & Bradwell, 2003). All these processes are likely to lead to more than one cluster of exposure ages younger than the moraine age.

Secondly, there is no way in which linear degradation models could detect inheritance in any boulder. The only ways proposed to account for inheritance are 1) to exclude older outliers, and to take the oldest age cluster as the best approximation of the moraine age (Phillips et al., 1996, Briner et al., 2001), or 2) to exclude the oldest ages following a scheme based on statistical experience (Putkonen & Swanson, 2003). Such concepts, however, are generalizations and are likely to fail locally.

We will show how the effects of all processes mentioned above can be recognized, if exposure age distributions of boulders from several local moraines of different stratigraphical ages are compared, and that clusters of younger ages can actually date phases of enhanced relief activity after the deposition of an older moraine.

3.2 Materials & Methods

Uncertainties of ^{10}Be exposure ages were calculated using the program TEBESEA (section 2), which employs a Gaussian propagation of the errors of all parameters of the simplified age eq. (11), with the decay constant of ^{10}Be $\lambda = (4.56 \pm 0.15) \cdot 10^{-7}$ a^{-1} (Holden, 1990), the physical erosion rate of the rock surface $\varepsilon = 0.0005 \pm 0.0002$ cm a^{-1}, the rock density $\rho = 2.7 \pm 0.1$ g cm^{-3}, the attenuation length for cosmic rays in rock $\Lambda_0 = 155 \pm 5$ g cm^{-2} for neu-

tron spallations and 1510 ± 500 g cm^{-2} for captures of negative muons (Heisinger et al., 2002), the measured ^{10}Be concentration in quartz $N = N' \pm 0.03\ N'$ atoms g^{-1}, the standard ^{10}Be production rate at sea level in high latitude $P_0 = 5.35 \pm 0.15$ atoms g^{-1} a^{-1}, multiplied by 0.988 for neutron spallations, and by 0.012 for captures of negative muons, respectively (Braucher et al., 2003), the scaling factor for local latitude and altitude calculated according to Stone (2000) $S = S' \pm 0.10\ S'$, calculated for neutron spallations and captures of negative muons separately, and the correction factor for shielding of the surface by any kind of cover $f_{SC} = 0.966 \pm 0.020$ for an assumed mean annual snow cover of 5 ± 3 g cm^{-2}). All other correction factors calculated for neutron spallations and captures of negative muons separately are associated with an assumed uncertainty of 10% of the term $(1 - f_C)$ each, except for $f_U(t)$, for which the uncertainty resulting from employing an uplift rate of 3 ± 2 mm a^{-1} has been calculated to be ~60% of the term $(1 - f_U(t))$.

Uncertainties calculated separately for neutron spallations and captures of negative muons were combined using the contributions of both fractions to total production as weights. The contributions of the considered parameters to the total uncertainty were estimated to be the same as the respective contributions to the total variance. The field data and measured concentration of boulder UK11, a single boulder from a degraded moraine in ~4400 m altitude in the eastern Pamir 38°N 74°E (section 5), have been used for illustration. In order to demonstrate age interpretation, surface exposure age distributions from Eastern Tibet (Schaefer et al., 2002, Tschudi et al., 2003, and Owen et al., 2003a, b) have been compared, all (re)calculated using TEBESEA (section 2).

3.3 Results & Discussion

3.3.1 Uncertainties of cosmogenic exposure ages

A general uncertainty of 11% is calculated to result from the present uncertainties of P_0, S, and N combined. The errors of the correction factors for sample geometry and geomagnetic variations do not contribute significantly to the total error, as is also true for the errors of the ^{10}Be decay constant, the rock density, and the attenuation lengths. In Fig. 3.1, the progressive accumulation of ^{10}Be in an exposed model rock surface (corresponding to sample UK11, section 5) is shown in the cases of no erosion and uplift, of slow erosion and uplift (1 mm ka^{-1} and 1 mm a^{-1}, respectively), and of fast erosion and uplift (5 mm ka^{-1} and 3 mm a^{-1}, respectively). Exposure ages corresponding to a measured concentration, including the

errors, can be read from the time axis, where the error interval of an accumulation function is equaled by the error interval of the measured concentration.

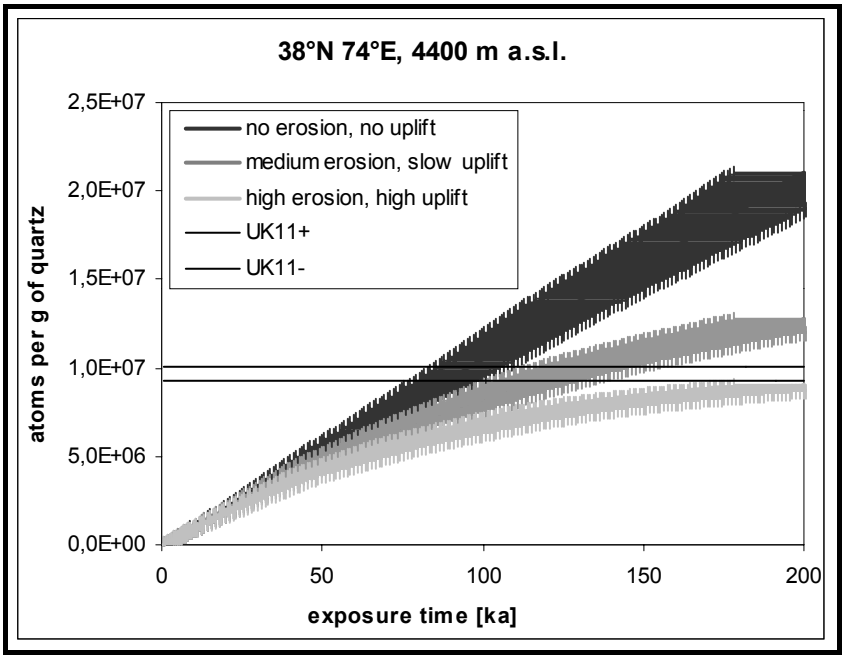

Fig. 3.1. Predicted accumulation of in-situ cosmogenic ^{10}Be in quartz as a function of exposure time at 38°N, 74°E, 4400 m a.s.l., for high erosion and fast uplift (5 mm ka^{-1}, 3 mm a^{-1}, respectively), medium erosion and slow uplift (3 mm ka^{-1}, 1 mm a^{-1}, respectively), and no erosion and uplift. Errors include an uncertainty of 10% due to the scaling factor. Measured maximum (UK11+) and minimum (UK11-) concentration of sample UK11 (section 5) shown by horizontal lines.

It is easily recognizable from Fig. 3.1 how age errors are increased by the presence of surface erosion and uplift. Erosion is effectively increasing the total decay, which may be considered in part 'real' radioactive decay and in part 'virtual' decay due to erosive loss of cosmogenic ^{10}Be (Lal, 1991). If 'virtual' decay is added to the 'real' decay, the accumulation function for an eroding surface approaches equilibrium more quickly than the one for a non-eroding surface, and its decreased slope leads to a broader overlap with the measured concentration interval. For sample UK11, the equilibrium is reached at a lower concentration than actually measured if erosion and uplift rates of 5 mm ka^{-1} and 3 mm a^{-1}, respectively, are applied. This shows that these erosion and uplift rates are in fact maximum estimates for the considered location, and that the real values of one or both of these parameters must be lower. Most likely, a better estimate of the erosion rate in this area would be 3 ± 2 mm ka^{-1}, including 5 mm ka^{-1} as its maximum rather than its mean. Other high concentration measurements in High Asia (Schaefer et al., 2002, Owen et al., 2003c, Zech et al., 2003) are in favour of this assumption.

The total propagated uncertainties resulting from our assumed erosion and uplift rates and their uncertainties are shown in Fig. 3.2. Fractions of uncertainty due to each of the main parameters, assumed to be the same as can be calculated for total variance, are also shown. Rates of surface erosion and tectonic uplift as they are estimated at present increase the total uncertainty of exposure ages to great extent, the former more than the latter. Given these estimates, exposure ages of ~50 ka, ~100 ka, ~150 ka and ~200 ka have uncertainties of ~20%, ~30%, ~50%, and ~90%, respectively. The influence of the uncertainty of the uplift rate decreases with altitude (Fig. 3.2A, B). If the erosion rate and the uplift rate are constrained to 5 ± 0.5 mm ka^{-1} and 3 ± 0.3 mm^{-1}, respectively, the total error is significantly reduced (Fig. 3.2C, D). In this case the uncertainty due to the uplift rate becomes insignificant, and the uncertainty due to the erosion rate becomes smaller than the uncertainty due to the scaling factor, which in case of erosion increases with exposure age due to the slope-lowering effect of approaching equilibrium. In case of high, but well-constrained erosion and uplift rates, the error of exposure ages would be ~20% for ages of ~100 ka and ~40% for ages of ~200 ka.

The estimated 60% uncertainty of snow cover correction does not increase total variance by more than 1%. Snow correction therefore can be considered to lead to a systematic uncertainty only.

The uncertainties given here are symmetrical as a result from the mathematics of Gauss' law. Approaching equilibrium, however, an asymmetry of error arises due to the decreasing slope of the accumulation function, and, strictly speaking, Gauss' law is no longer applicable. If it is applicated nonetheless, the lower boundary of the error interval of any erosion-corrected age at some point becomes lower than the respective one of the non-erosion-corrected age. Taking this into consideration, the lower boundary of the error interval of any exposure age should be calculated separately, inserting the lowest estimate of the erosion rate with a zero uncertainty. The mean age increased by its Gauss uncertainty can then be taken as an approximation of the upper boundary of the error interval, which is the better, the less the mean age reduced by its Gauss uncertainty underscores the separately calculated lower boundary.

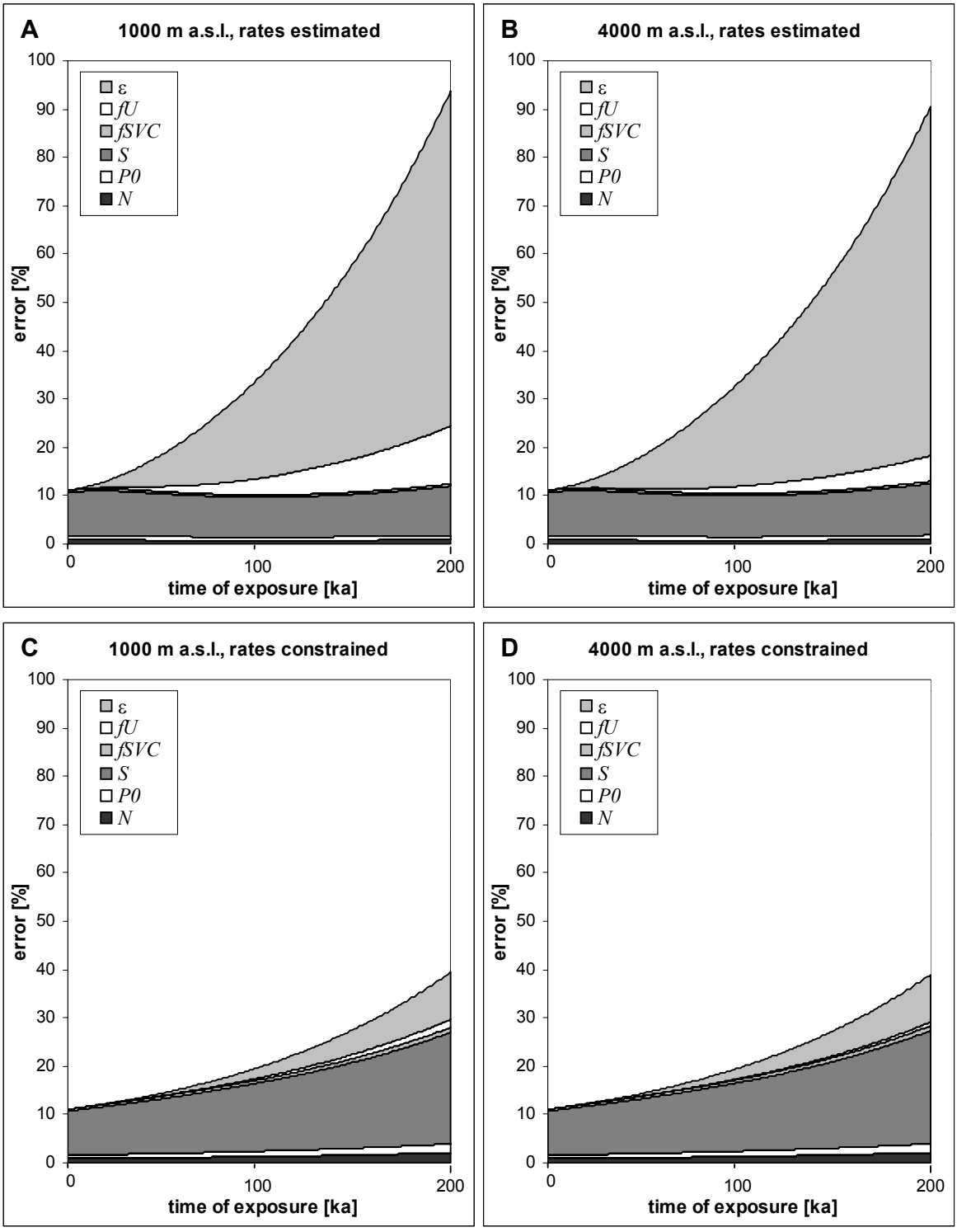

Fig. 3.2. Fully propagated total uncertainties of calculated ^{10}Be exposure ages as functions of the time of exposure in fractions as contributing to variance. Errors include estimated (A, B) or constricted (C, D) high erosion and uplift rates (5 mm ka^{-1} and 3 mm a^{-1}). Uncertainties of estimated erosion and uplift rates are ± 2 mm ka^{-1} and ± 2 mm a^{-1}, uncertainties of constrained rates are ± 0.5 mm ka^{-1} and ± 0.5 mm a^{-1}, respectively. In order to illustrate the influence of altitude, results are shown for 1000 m (A, C) and 4000 m a.s.l. (B, D).

3.3.2 Inheritance and moraine degradation

The distribution of exposure ages from several moraines sampled in Eastern Tibet is shown in Fig. 3.3. Most of them show a pronounced scatter of exposure ages. However, with the help of stratigraphical relationships of the sampled moraines, some boulders probably affected by inheritance are easily recognizable (moraines LJ11, LJ21). On other moraines, clusters of exposure ages can be recognized, which are clearly not equal to the deposition age of the moraine, but match exposure ages from other moraines of the same region (moraines QS11, LJ22). Distributions with both these features are difficult to explain with a linear moraine degradation model. More probably, they result from incorporation of older moraine material in younger moraine, followed by non-linear, climate-driven moraine degradation processes like mass movements and thermokarst activity. Even if these processes are generally thought to be active only for several hundreds of years after moraine deposition (Ballantyne, 2002, Everest & Bradwell, 2003), they may locally be in effect over much longer time periods, being at some time delayed by adverse and at some later time triggered by more favourable climate conditions. In addition, lateral moraines may have been active for different times at different locations, if a glacier has been melting back for a long time without losing thickness and width. This may be recognized, if samples taken along its course show an age progression.

Given all these effects, it is well possible that a distribution of boulder exposure ages does not include the principal deposition age of the moraine at all (e.g. moraine LJ13 in Fig. 3.3). In such a case, an approximate deposition age can nevertheless be inferred from an analogous distribution of exposure ages on other, stratigraphically related moraines.

In the interpretation of a set of exposure age distributions from stratigraphically related moraines, we suggest to proceed along the following lines:

1. The oldest exposure age found on each moraine may be interpreted as a first approximation of the actual deposition age.
2. If comparison with other dated moraines of the same age or older shows that the oldest age is unreasonably high, inheritance is probable.
3. An oldest age equaled by others on stratigraphically related moraines can be considered close to the deposition age of the moraine with increased confidence.

4. If comparison with other dated moraines of the same age or younger shows that the oldest age on a moraine is unreasonably low, the deposition age of the moraine is probably underestimated, i.e. all sampled boulders have likely been freed from cover or turned during moraine degradation.

5. Ages too low to indicate deposition ages, if matched by ages on other moraines in the same area, or by other pedological, sedimentological or climatological proxies, may be interpreted to indicate phases of pronounced landform surface instability.

6. Spatial trends of moraine ages can give information on depositional or degradational chronologies of a moraine.

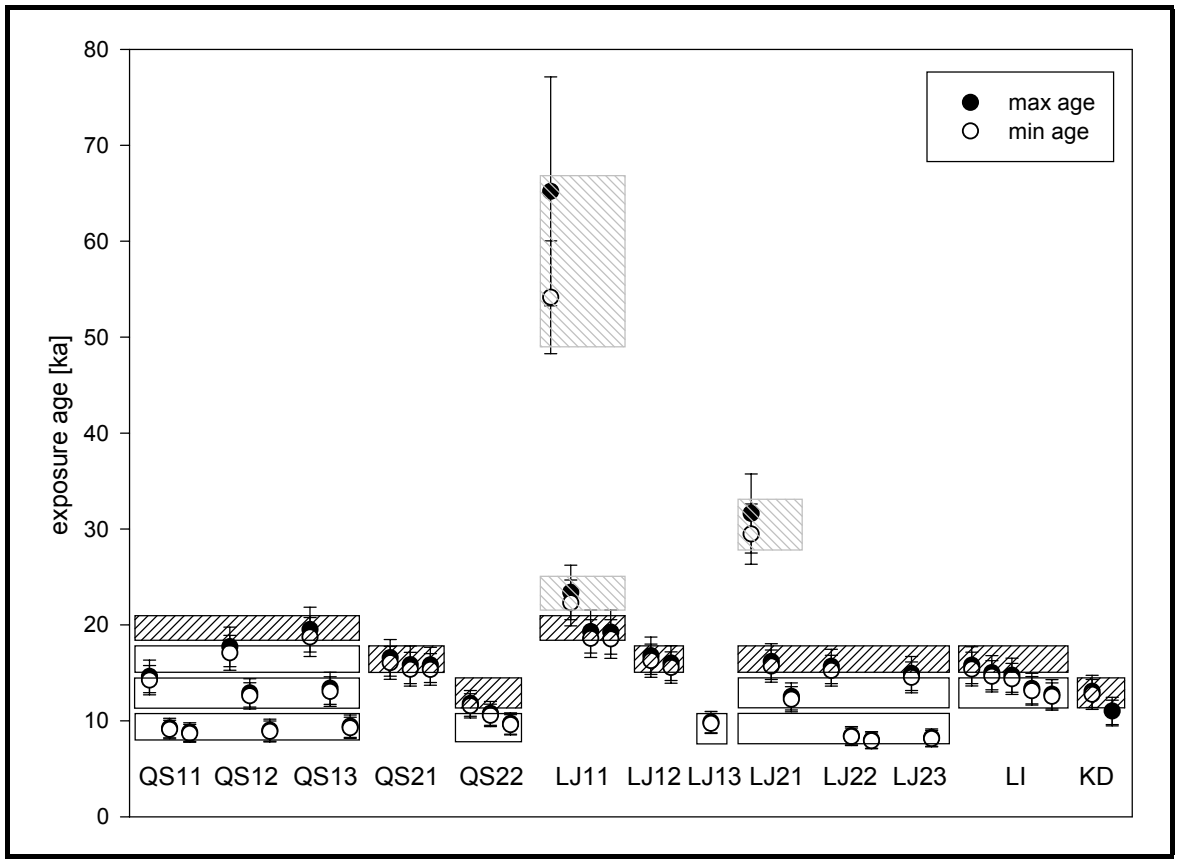

Fig. 3.3. Comparison of ^{10}Be-dated boulders from moraines in the Qilian Shan (QS, Owen et al., 2003b), the La Ji Mountains (LJ, Owen et al., 2003a), the Litang area (LI, Schaefer et al., 2002), and the Kanding area (KD, Tschudi et al., 2003). To allow comparison, all ages have been recalculated using TEBESEA (section 2). Minimum ages shown by white dots, conservative maximum ages by black dots. Different stratigraphical stages in one area are distinguished by a first arabic number, different deposits of any one stratigraphical stage are distinguished by a second arabic number. Boulder ages inferred to be affected by inheritance in boxes cross-hatched in grey, boulder ages inferred to be representing deposition ages in boxes cross-hatched in black, boulder ages inferred to be representing degradational stages in white boxes. Note the parallelism between stages in the different regions.

In this way, concise reconstructions of glaciation histories can be put forward, even if the dating results from any one sampled moraine are problematic. As a sampling strategy, it is therefore more promising to spread the number of possible samples over as many different, stratigraphically related moraines as possible, taking a minimum of three to five samples on each, than to concentrate on only one or two key moraines, taking ten or more samples from each moraine crest.

3.4 Conclusions

The uncertainties of ^{10}Be surface exposure ages are presently dominated by the errors of the scaling factor, the erosion rate, and, in mountainous areas, the tectonic uplift rate. The large uncertainty of snow cover correction does not significantly add to total variance.

As long as surface erosion and tectonic uplift cannot be reasonably constrained to within 10%, exposure ages older than 30-40 ka are no more than rough estimates and cannot be correlated with high resolution proxy events with any confidence. In order to increase the precision ^{10}Be exposure ages >40 ka, new methods are needed to put a better constraint on the surface erosion rates of any single exposed boulder.

At present, for High Asia, a surface erosion rate for granitic boulders of 3 ± 2 mm ka^{-1} seems to be a reasonable maximum estimate.

Not in accord with current models of linear moraine degradation, exposure age distributions from single moraines frequently contain ages older than the deposition age due to inherited ^{10}Be in some of the boulders, and they frequently are not unimodal, but show two or more age clusters. In some cases, age clusters younger than the deposition age of a moraine are synchronous on different moraines in the same region, possibly indicating phases of enhanced, climate-driven surface activity.

In order to obtain a concise glaciation history of a mountainous region, ^{10}Be exposure ages from several moraines within a region have to be interpreted in the light of the local stratigraphical and climatological context. Sampling of a minimum of 3-5 boulders from each of a maximum number of different moraines, which should be stratigraphically related and should cover all encountered relative ages, may be necessary to draw any climatological conclusions from SED.

3.5 Acknowledgements

This work was made possible by the German Research Foundation (DFG), grant ZE 154/51. We thank Dr. Peter W. Kubik for his cooperation in measuring the isotope concentration in our samples at the AMS facility of the Paul Scherrer Institute at the ETH Zurich.

3.6 References

BALCO, G., STONE, J. O. H., PORTER, S. C., CAFFEE, M. W. 2002. Cosmogenic-nuclide ages for New England coastal moraines, Martha's Vineyard and Cape Cod, Massachusetts, USA. Quaternary Science Reviews 21, 2127-2135.

BALLANTYNE, C. K. 2002. Paraglacial geomorphology. Quaternary Science Reviews 21, 1935-2017.

BARROWS, T. T., STONE, J. O., FIFIELD, L. K., CRESSWELL, R. G. 2001. Late Pleistocene glaciation of the Kosciuszko massif, Snowy Mountains, Australia. Quaternary Research 55, 179-189.

BIERMAN, P. R., CAFFEE, M. 2002. Cosmogenic exposure and erosion history of Australian bedrock landforms. Geological Society of America Bulletin 114, 787-803.

BIERMAN, P., TURNER, J. 1995. ^{10}Be and ^{26}Al evidence for exceptionally low rates of Australian bedrock erosion and the likely existence of pre-Pleistocene landscapes. Quaternary Research 44, 378-382.

BIERMAN, P., MARSELLA, K. A., PATTERSON, C., DAVIS, P. T., CAFFEE, M. 1999. Mid-Pleistocene cosmogenic minimum age limits for pre-Wisconsin glacial surfaces in southwestern Minnesota and southern Baffin Island: a multiple nuclide approach. Geomorphology 27, 25-40.

BRAUCHER, R., BROWN, E. T., BOURLÈS, D. L., COLIN, F. 2003. In situ produced ^{10}Be measurements at great depths: implications for production rates by fast muons. Earth and Planetary Science Letters 211, 251-258.

BRINER, J. P., SWANSON, T. W., CAFFEE, M. 2001. Late Pleistocene cosmogenic ^{36}Cl glacial chronology of the southwestern Ahklun Mountains, Alaska. Quaternary Research 56, 148-154.

BROOK, E. J., KURZ, M. D., ACKERT, R. P. JR., DENTON, G. H., BROWN, E. T., RAISBECK, G. M., YIOU, F. 1993. Chronology of Taylor Glacier advances in Arena Valley, Antarctica, using in-situ cosmogenic ^{3}He and ^{10}Be. Quaternary Research 39, 11-23.

BROOK, E. J., NESJE, A., LEHMAN, S. J., RAISBECK, G. M., YIOU, F. 1996. Cosmogenic nuclide exposure ages along a vertical transect in western Norway: Implications for the height of the Fennoscandian ice sheet. Geology 24, 207-210.

BROWN, E. T., EDMOND, J. M., RAISBECK, G. M., YIOU, F., KURZ, M. D., BROOK, E. J. 1991. Examination of surface exposure ages of Antarctic moraines using in-situ produced ^{10}Be and ^{26}Al. Geochimica et Cosmochimica Acta 55, 2269-2283.

BROWN, E. T., STALLARD, R. F., LARSEN, M. C., RAISBECK, G. M., YIOU, F. 1995. Denudation rates determined from the accumulation of in-situ produced ^{10}Be in the Luquillo experimental Forest, Puerto Rico. Earth and Planetary Science Letters 129, 193-202.

BURBANK, D. W., LELAND, J., FIELDING, E., ANDERSON, R. S., BROZOVIC, N., REID, M. R., DUNCAN, C. 1996. Bedrock incision, rock uplift and threshold hillslopes in the northwestern Himalayas. Nature 379, 505-510.

DAHMS, D. E. 1994. Mid-Holocene erosion of soil catenas on moraines near the type Pinedale Till, Wind River Range, Wyoming. Quaternary Research 42, 41-48.

DESILETS, D., ZREDA, M. 2003. Spatial and temporal distribution of secondary cosmic-ray nucleon intensities and applications to in situ cosmogenic dating. Earth and Planetary Science Letters 206, 21-42.

DORN, R. I., PHILLIPS, F. M. 1991. Surface exposure dating: review and critical evaluation. Physical Geography 12, 303-333.

DUNAI, T. J. 2000. Scaling factors for production rates of in situ produced cosmogenic nuclides: a critical reevaluation. Earth and Planetary Science Letters 176, 157-169.

DUNAI, T. J. 2001. Influence of secular variation of the geomagnetic field on production rates of in situ produced cosmogenic nuclides. Earth and Planetary Science Letters 193, 197-212.

EVEREST, J., BRADWELL, T. 2003. Buried glacier ice in southern Iceland and its wider significance. Geomorphology 52, 347-358.

GILLESPIE, A. R., BIERMAN, P. R. 1995. Precision of terrestrial exposure ages and erosion rates estimated from analysis of cosmogenic isotopes produced in situ. Journal of Geophysical Research 100, 24637-24649.

GOSSE, J. C., PHILLIPS, F. M. 2001. Terrestrial in situ cosmogenic nuclides: theory and application. Quaternary Science Reviews 20, 1475-1560.

GOSSE, J. C., STONE, J. O. 2001. Terrestrial cosmogenic nuclide methods passing milestones towards palaeoaltimetry. EOS Transactions of the American Geophysical Union 82, 82-89.

GOSSE, J. C., EVENSON, E. B., KLEIN, J., LAWN, B., MIDDLETON, R. 1995a. Precise cosmogenic ^{10}Be measurements in North America: support for a global Younger Dryas cooling event. Geology 23, 877-880.

GOSSE, J. C., KLEIN, J., EVENSON, E. B., LAWN, B., MIDDLETON, R. 1995b. Beryllium-10 dating of the duration and retreat of the last Pinedale Glacial Sequence. Science 268, 1329-1333.

GRANGER, D. E., RIEBE, C. S., KIRCHNER, J. W., FINKEL, R. C. 2001. Modulation of erosion on steep granitic slopes by boulder armouring as revealed by cosmogenic ^{26}Al and ^{10}Be. Earth and Planetary Science Letters 186, 269-281.

HALLET, B., PUTKONEN J. 1994. Surface dating of dynamic landforms: young boulders on aging moraines. Science 265, 937-940.

HEIMSATH, A. M., DIETRICH, W. E., NISHIIZUMI, K., FINKEL, R. C. 2001. Stochastic processes of soil production and transport: erosion rates, topographic variation and cosmogenic nuclides in the Oregon Coast Range. Earth Surface Processes and Landforms 26, 531-552.

HEISINGER, B., NOLTE, E. 2000. Cosmogenic in situ production of radionuclides: Exposure ages and erosion rates. Nuclear Instruments and Methods in Physics Research B 172, 790-795.

HEISINGER, B., LAL, D., JULL, A. J. T., KUBIK, P., IVY-OCHS, S., KNIE, K., NOLTE, E. 2002. Production of selected cosmogenic radionuclides by muons 2. Capture of negative muons. Earth and Planetary Science Letters 200, 357-369.

HOLDEN, N. E. 1990. Total half-lives for selected nuclides. Pure and Applied Chemistry 62, 941-958.

ITURRIZAGA, L. 2003. Distribution and genesis of lateroglacial valleys in the Karakoram Mountains (Pakistan). Zeitschrift fuer Geomorphologie N. F., Supplementband 130, 51-74.

IVY-OCHS, S. 1996. The dating of rock surface using in situ produced ^{10}Be, ^{26}Al and ^{36}Cl, with examples from Antarctica and the Swiss Alps. Diss. ETH No. 11763, Zurich, 197 pp.

IVY-OCHS, S., SCHLUECHTER, C., KUBIK, P. W., DENTON, G. H. 1999. Moraine exposure dates imply synchronous Younger Dryas glacier advances in the European Alps and in the Southern Alps of New Zealand. Geografiska Annaler A 81, 313-323.

JAIN, A. K., KUMAR, D., SINGH, S., KUMAR, A., LAL, N. 2000. Timing, quantification and tectonic modelling of Pliocene-Quaternary movements in the NW Himalaya: evidence from fission track dating. Earth and Planetary Science Letters 179, 437-451.

KAUFMANN, G., LAMBECK, K. 1997. Implications of late Pleistocene glaciation of the Tibetan Plateau for present-day uplift rates and gravity anomalies. Quaternary Research 48, 267-279.

KJAER, K. H., KRUEGER, J. 2001. The final phase of dead-ice moraine development: processes and sediment architecture, Koetlujoekull, Iceland. Sedimentology 48, 935-952.

KOBER, F., SCHLUNEGGER, F., IVY-OCHS, S., WIELER, R. 2002. The dependency of cosmogenic nuclides to climate and surface uplift in transient landscapes. Goldschmidt Conference Abstracts 2002, A 408.

LAL, D. 1991. Cosmic ray labelling of erosion surfaces: in situ nuclide production rates and erosion models. Earth and Planetary Science Letters 104, 424-439.

LELAND, J., REID, M. R., BURBANK, D. W., FINKEL, R., CAFFEE, M. 1998. Incision and differential bedrock uplift along the Indus River near Nanga Parbat, Pakistan Himalaya, from ^{10}Be and ^{26}Al exposure age dating of bedrock straths. Earth and Planetary Science Letters 154, 93-107.

LIFTON, N. A., JULL, A. J. T., QUADE, J. 2001. A new extraction technique and production rate estimate for in situ cosmogenic ^{14}C in quartz. Geochimica et Cosmochimica Acta 65, 1953-1969.

LIU, B., PHILLIPS, F. M., FABRYKA-MARTIN, J. T., FOWLER, M. M., STONE, W. D. 1994. Cosmogenic 36Cl accumulation in unstable landforms, 1. Effects of the thermal neutron distribution. Water Resources Research 30, 3115-3125.

MARSELLA, K. A., BIERMAN, P. R., DAVIS, P. T., CAFFEE, M. W. 2001. Cosmogenic ^{10}Be and ^{26}Al ages for the last glacial maximum, eastern Baffin Island, arctic Canada. Geological Society of America Bulletin 112, 1296-1312.

MASARIK, J., REEDY, R. C. 1995. Terrestrial cosmogenic-nuclide production systematics calculated from numerical simulations. Earth and Planetary Science Letters 136, 381-395.

NISHIIZUMI, K., KOHL, C. P., ARNOLD, J. R., KLEIN, J., FINK, D., MIDDLETON, R., LAL, D. 1993. Role of in situ cosmogenic nuclides ^{10}Be and ^{26}Al in the study of diverse geomorphic processes. Earth Surface Processes and Landforms 18, 407-425.

OWEN, L. A. 1989. Neotectonics and glacial deformation in the Karakoram Mountains and Nanga Parbat Himalaya. Tectonophysics 163, 227-265.

OWEN, L. A., FINKEL, R.C., CAFFEE, M. W., GUALTIERI, L. 2002. Timing of multiple glaciations during the Late Quaternary in the Hunza Valley, Karakoram Mountains, northern Pakistan: defined by cosmogenic radionuclide dating of moraines. Geological Society of America Bulletin 114, 593-604.

OWEN, L. A., MA, H., DERBYSHIRE, E., SPENCER, J. Q., BARNARD, P. L., ZENG, Y. N., FINKEL, R. C., CAFFEE, M. W. 2003a. The timing and style of Late Quaternary glaciation in the La Ji Mountains, NE Tibet: evidence for restricted glaciation during the latter part of the Last Glacial. Zeitschrift fuer Geomorphologie N. F., Supplementband 130, 263-276.

OWEN, L. A., SPENCER, J. Q., MA, H., BARNARD, P. L., DERBYSHIRE, E., FINKEL, R. C., CAFFEE, M. W., ZENG, Y. N. 2003b. Timing of Late Quaternary glaciation along the southwestern slopes of the Qilian Shan, Tibet. Boreas 32, 281-446.

OWEN, L. A., BARNARD, P., BENN, D., CAFFEE, M. W., DERBYSHIRE, E., FINKEL, R., GUALTIERI, L., MA, H., SHARMA, M., SPENCER, J. 2003c. Late Quaternary glaciation in the Himalaya and Tibet. XVI INQUA Congress Programs with Abstracts, DRI, Reno, Nv., p. 155.

PHILLIPS, F. M., ZREDA, M. G., FLINSCH, M. R., ELMORE, D., SHARMA, P. 1996. A reevaluation of cosmogenic ^{36}Cl production rates in terrestrial rocks. Geophysical Research Letters 23, 949-952.

PHILLIPS, F. M., ZREDA, M. G., GOSSE, J. C., KLEIN, J., EVENSON, E. B., HALL, R. D., CHADWICK, O. A., SHARMA, P. 1997. Cosmogenic ^{36}Cl and ^{10}Be ages of Quaternary glacial and fluvial deposits of the Wind River Range, Wyoming. Geological Society of America Bulletin 109, 1453-1463.

PUTKONEN, J., SWANSON, T. 2003. Accuracy of cosmogenic ages for moraines. Quaternary Research 59, 255-261.

REEDY, R. C., NISHIIZUMI, K., LAL, D., ARNOLD, J. R., ENGLERT, P. A. J., KLEIN, J., MIDDLETON, R., JULL, A. J. T., DONAHUE, D. J. 1994. Simulations of terrestrial in-situ cosmogenic-nuclide production. Nuclear Instruments and Methods in Physics Research B 92, 297-300.

SCHAEFER, J. M., TSCHUDI, S., ZHAO, Z., WU, X., IVY-OCHS, S., WIELER, R., BAUR, H., KUBIK, P. W., SCHLUECHTER, C. 2002. The limited influence of glaciations in Tibet on global climate over the past 170 000 yr. Earth and Planetary Science Letters 194, 287-297.

SHANAHAN, T. M., ZREDA, M. 2000. Chronology of Quaternary glaciations in East Africa. Earth and Planetary Science Letters 177, 23-42.

SMALL, E. E., ANDERSON, R. S., REPKA, J. L., FINKEL, R. 1997. Erosion rates of alpine bedrock surfaces deduced from in situ ^{10}Be and ^{26}Al. Earth and Planetary Science Letters 150, 413-425.

STONE, J. O. H. 2000. Air pressure and cosmogenic isotope production. Journal of Geophysical Research 105 B10, 23753-23759.

STONE, J. O., ALLAN, G. L., FIFIELD, L. K., CRESSWELL, R. G., 1996. Cosmogenic chlorine-36 from calcium spallation. Geochimica et Cosmochimica Acta 60, 679-692.

SWANSON, T. W., CAFFEE, M. L. 2001. Determination of ^{36}Cl production rates from the well-dated deglaciation surfaces of Whidbey and Fidalgo Islands, Washington. Quaternary Research 56, 366-382.

TSCHUDI, S., SCHAEFER, J. M., ZHAO, Z., WU, X., IVY-OCHS, S., KUBIK, P., SCHLUECHTER, C. 2003. Glacial advances in Tibet during the Younger Dryas? Evidence from cosmogenic ^{10}Be, ^{26}Al, and ^{21}Ne. Journal of Asian Earth Sciences 22, 301-306.

ZECH, W., BAEUMLER, R., SAVOSKUL, O., NI, A., PETROV, M. 1996. Bodengeographische Beobachtungen zur pleistozaenen und holozaenen Vergletscherung des Westlichen Tienshan (Usbekistan). Eiszeitalter und Gegenwart 46, 144-151.

ZECH, W., BAEUMLER, R., GUGGENBERGER, G., PETROV, M., NI, A., LEMZIN, I. 2000a. Pleistocene and Holocene landscape development in the Kichik Alay and Hissar Ranges (Kyrgyzstan and Uzbekistan) as deduced from soil morphology. Marburger Geographische Schriften 135, 53-68.

ZECH, W., GLASER, B., NI, A., PETROV, M., LEMZIN, I. 2000b. Soils as indicators of the Pleistocene and Holocene landscape evolution in the Alay Range (Kyrgyzstan). Quaternary International 65/66, 161-169.

ZECH, W., GLASER, B., ABRAMOWSKI, U., DITTMAR, C., KUBIK, P. W. 2003. Reconstruction of the Late Quaternary Glaciation of the Macha Khola Valley (Gorkha Himal, Nepal) using relative and absolute (^{14}C, ^{10}Be, dendrochronology) dating techniques. Quaternary Science Reviews 22, 2253-2265.

ZEITLER, P. K. 1985. Cooling history of the NW Himalaya, Pakistan. Tectonics 4, 127-151.

ZIMMERMAN, S. G., EVENSON, E. B., GOSSE, J. G., ERSKINE, C. P. 1994. Extensive boulder erosion resulting from a range fire on the type-Pinedale moraines, Fremont Lake, Wyoming. Quaternary Research 42, 255-265.

ZREDA, M. G., PHILLIPS, F. M., ELMORE, D. 1994. Cosmogenic ^{36}Cl accumulation in unstable landforms, 2. Simulations and measurements on eroding moraines. Water Resources Research 30, 3127-3136.

4. Late Pleistocene and Holocene palaeoglaciations of the Nepal Himalaya: relative chronologies based on soil development confirmed and complemented by ^{10}Be surface exposure dating

Uwe Abramowski[1], Bruno Glaser[1], Krishna Kharki[2], Peter W. Kubik[3], Wolfgang Zech[1]

[1] Institute of Soil Science and Soil Geography, University of Bayreuth, D-95440 Bayreuth, Germany

[2] Institute of Agricultural Research, Kathmandu, Nepal

[3] Paul Scherrer Institute, c/o Institute of Particle Physics, ETH Zurich, CH-8093 Zurich, Switzerland

Abstract

We applied ^{10}Be surface exposure dating (SED) of erratic boulders to confirm and complement the results of former soil geographic studies at two sites in the central Nepal Himalaya, the Macha Khola Valley, and the Langtang Valley. Results are compared with other SED and OSL dating studies in order to evaluate, to what extent glacial advances in different regions of central Nepal have been synchronous. ^{10}Be surface exposure ages have excellently confirmed and complemented former soil geographic work in the studied valleys. Late Pleistocene and Holocene glacier advances in the Macha Khola Valley have been dated 70-100, 20-23, 11-12 and around 3 cal. ka B.P. Lateglacial and Holocene glacier advances in the Langtang Valley have been dated 14-15, 8-9 and ~3.5 cal. ka B.P. Except for the Younger Dryas advance in the Macha Khola Valley, all ages excellently agree with the glacial chronology of the Khumbu area defined by Finkel et al. (2003). Glacial activity in the Nepal Himalaya seems to have been controlled by the Indian monsoon rather than the westerly circulation. In the MIS 2, the westerly jetstream appears to have shifted as far south as to have affected glaciation all over the Himalaya. During the Younger Dryas, the eastern limit of the influence of the westerly circulation on Himalaya glaciation may have been situated between the Manaslu and Langtang Himal.

4.1 Introduction

The late Pleistocene and Holocene glaciations of the Nepal Himalaya and their palaeo-climatic implications have been subject to investigation ever since the first scientific Himalaya expeditions at the beginning of the last century. But although a great number of Pleistocene and Holocene glacial stages has been identified in the Nepal Himalaya (Zheng, 1989a, Kuhle, 1998, Owen et al., 1998), numerical age information on these stages up to the end of the 1990s has been limited, and most of the existing dates have been confined to the Holocene (Roethlisberger, 1986, Zheng & Rutter, 1998, Baeumler, 2001a, b). The lack of older data has been caused by the poor preservation of carbon-containing Pleistocene deposits in the deeply dissected Himalaya valleys, where moraines are rapidly destroyed due to the large amount of relief energy available, and due to the high frequency of earthquakes (Richards et al., 2000). Given this situation, the application of soil development analyses has been a method of choice to provide a relative age frame for glacial advances in several parts of the Nepal Himalaya (Baeumler & Zech, 2000, Zech et al., 2001a, b, Baeumler, 2001a, b).

Things, however, have changed since the advent of optically stimulated luminescence (OSL) and in-situ cosmogenic nuclide dating techniques during the 1990s. Numerical ages can now be obtained for almost any remnant of glacial and glaciofluvial deposits, and a lot of effort is presently spent in defining new glacial chronologies for the Nepal Himalaya using these techniques (e.g. Richards et al., 2000, Tsukamoto et al., 2002, Asahi et al., 2003, Finkel et al., 2003). Studies like the above cited have already contradicted the notion of a plateau glaciation of Tibet during the late Pleistocene, the large outlet glaciers of which were supposed to have filled the valleys of the Nepal Himalaya (Kuhle, 1998, 1999). Instead, they have provided a new foundation for the discussion about past climatic conditions in the Himalaya as a whole, which is mainly about whether the past glaciations have been triggered during warm stages, in connection with an enhanced Indian monsoon, or during cold stages, in connection with a strengthening of the westerly circulation (Benn & Owen, 1998, Bush, 2000, Fort, 2000).

In this section, ^{10}Be surface exposure dating (SED) of erratic boulders is applied to confirm and complement the results of former soil geographic studies at two sites in the central Nepal Himalaya, the Macha Khola Valley (Zech et al., 2003), and the Langtang Valley (Baeumler et al., 1996, 1997, Baeumler, 2001a). Results are then compared with other

SED and OSL dating studies in order to evaluate, to which extent glacial advances in different regions of central Nepal have been synchronous.

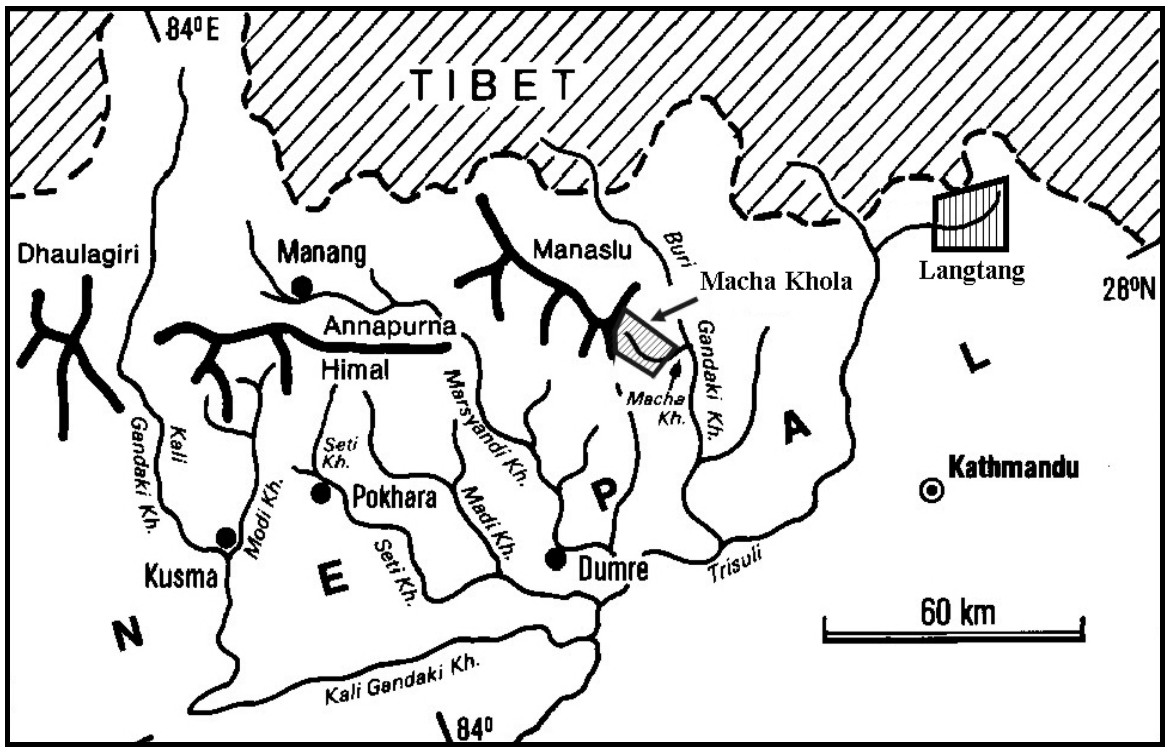

Fig. 4.1. Overview of the study area in central Nepal. Modified after Zech et al., 2003.

4.2 Materials & Methods

4.2.1 Study sites

4.2.1.1 Physical geography and climate of the Nepal Himalaya

The central Nepal Himalaya (28°N, 83-86°E) is the highest mountain chain of the Earth. It separates the Ganges plain in the south and the Tibetan plateau in the north. In the west, it is dominated by the Dhaulagiri and Annapurna, in the east by the Khumbu and Kangchenjunga massifs, all culminating above 8000 m a.s.l. The high Himalaya mainly consists of metamorphic rocks, in most cases gneisses and migmatites, of the so-called Higher Himalaya Crystalline (HHC) or Tibetan Slab formation (Barbey et al., 1996, Harrison et al., 1997). The relief gradient between the high Himalaya and the mountain foreland is extremely large, and valleys are deeply incised. Earthquake activity is high, and landslides and rockfalls are numerous (Fort, 1986, 2000).

Climate in the area is dominated by the Indian monsoon in summer, and cool, dry westerly winds in winter (Miehe, 1990, Denniston et al., 2000). West of the Annapurna and Dhaulagiri massifs, moisture advection with the winterly westerlies increases (Fort, 2000). Monsoon precipitation decreases from south to north and has two altitudinal maxima, in ~2000 m a.s.l. and in ~6000 m a.s.l., caused by the primary monsoon, and secondary condensation rain, respectively (Zheng et al., 1989b). The present equilibrium line altitude (ELA) of glaciation ranges from 5200 m a.s.l. in the south to 5800 m a.s.l. in the north (Williams, 1983, Heuberger et al., 1984, Miehe 1990). Glaciers in the Himalaya, however, are often avalanche-fed and heavily debris-covered, so that their tongues reach down to lower altitudes than it is implied by the ELA data (Roethlisberger, 1986, Fort, 2000, Benn & Owen, 2002). ELA depressions are therefore not always an adequate parameter for correlation of glacial stages in this region.

4.2.1.2 Macha Khola Valley, Gorkha Himal

The Macha Khola is a small first-order river originating at the southeastern end of the Manaslu massif and joining the Buri Gandaki Khola (Fig. 4.1). The present ELA in its valley is about 5100 m a.s.l. (Zech et al., 2003). This valley was selected for soil geographic investigation because of its well-preserved glacigenic deposits. The detailed results of the soil investigations are presented by Zech et al. (2003).

Moraine stages in the Macha Khola Valley are shown in Fig. 4.2. The recent glacier descends down to 4700 m a.s.l. The youngest set of moraines, probably deposited during the Little Ice Age (LIA) several hundred years ago, reaches down to 4270 m a.s.l. Three lateral moraines inferred to have been deposited during the Neoglacial are present down to 3600 m a.s.l. The most distinctive wall of these has been sampled in 3900 m a.s.l. for age confirmation (MK4). Further sampled moraines are two lateral moraines present in a bend in the middle part of the valley, the younger one situated in 3260 m a.s.l. (MK7), and inferred to be of lateglacial age, the older one situated in 3550 m a.s.l. (MK5), and inferred to have been deposited during the MIS 2 (Zech et al, 2003). Finally, boulders from a moraine reaching down to 2150 m a.s.l. have been sampled in 2364 m a.s.l. (MK2). This deposit is the oldest and most distal glacial remnant identified in the valley, and is correlated with the outermost lateral moraines in the above-mentioned valley bend. By analogy with the stratigraphy of the Khumbu Himal (Finkel et al., 2003), an MIS 5 age has been inferred for this stage. Between the MIS 5 and MIS 2 moraines, on the left valley side, lake Rukche Tal is situated, which has been drilled for palaeoclimatic investigation.

Radiocarbon dating of the base of this core (~18 cal. ka B.P., Schluetz & Zech, 2004) has confirmed the MIS 2 age of the inner moraine wall.

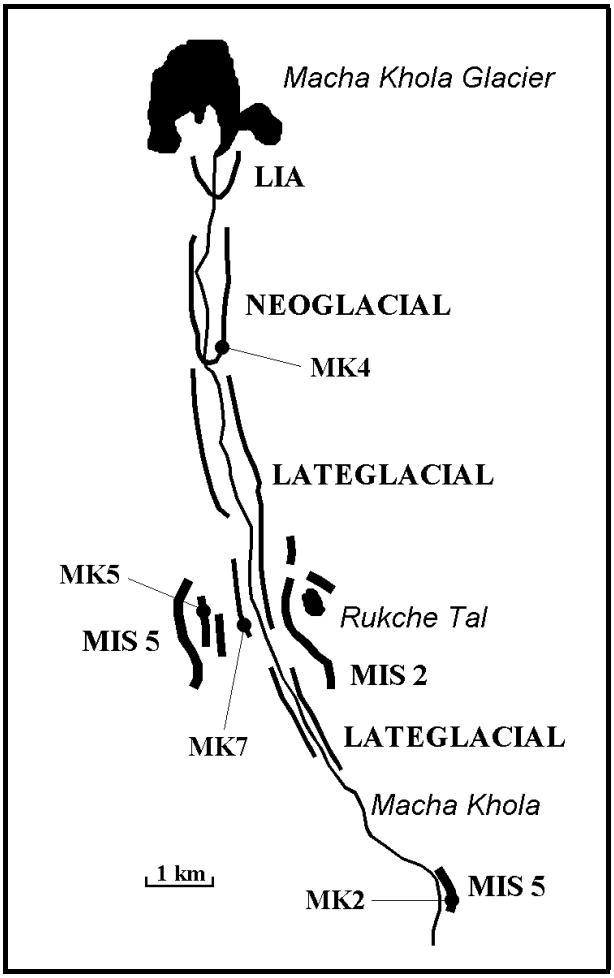

Fig. 4.2. Sketch of the Macha Khola catchment with glaciers (black), inferred moraine stages and sampling sites.

4.2.1.3 Langtang Valley, Langtang Himal

The Langtang Valley (Fig. 4.1, 4.3) is an east-west-trending valley between the massifs of the Langtang Lirung and the Xixabangma in the north and the massif of the Gosainkund in the south. It has a mean annual precipitation of 1200 mm, a mean annual temperature of 2.7°C and an ELA of 5300 m (Miehe, 1990). The investigation of the glacial deposits in this valley has a long tradition. Heuberger et al. (1984) recognized two moraine generations older than the (LIA), which they contribute to two lateglacial advances. The younger advance is thought to be represented by separate moraines from the Langtang Lirung south glacier at Langtang village (Fig. 4.3, LT6), from the Langtang Lirung north glacier west of Kyangchen Gomba, and from the main valley glacier east of Kyangchen Gomba (Fig. 4.3,

LT3). The older advance, on the other hand is thought to be represented by a high lateral moraine opposite of Kyangchen Gomba (Fig. 4.3, LT2). Ono (1986), staying with the late-glacial interpretation of the above-mentioned moraines, recognized additional remnants of an even older end moraine west of Ghora Tabela in 3200 m a.s.l. (Fig. 4.3, LT1).

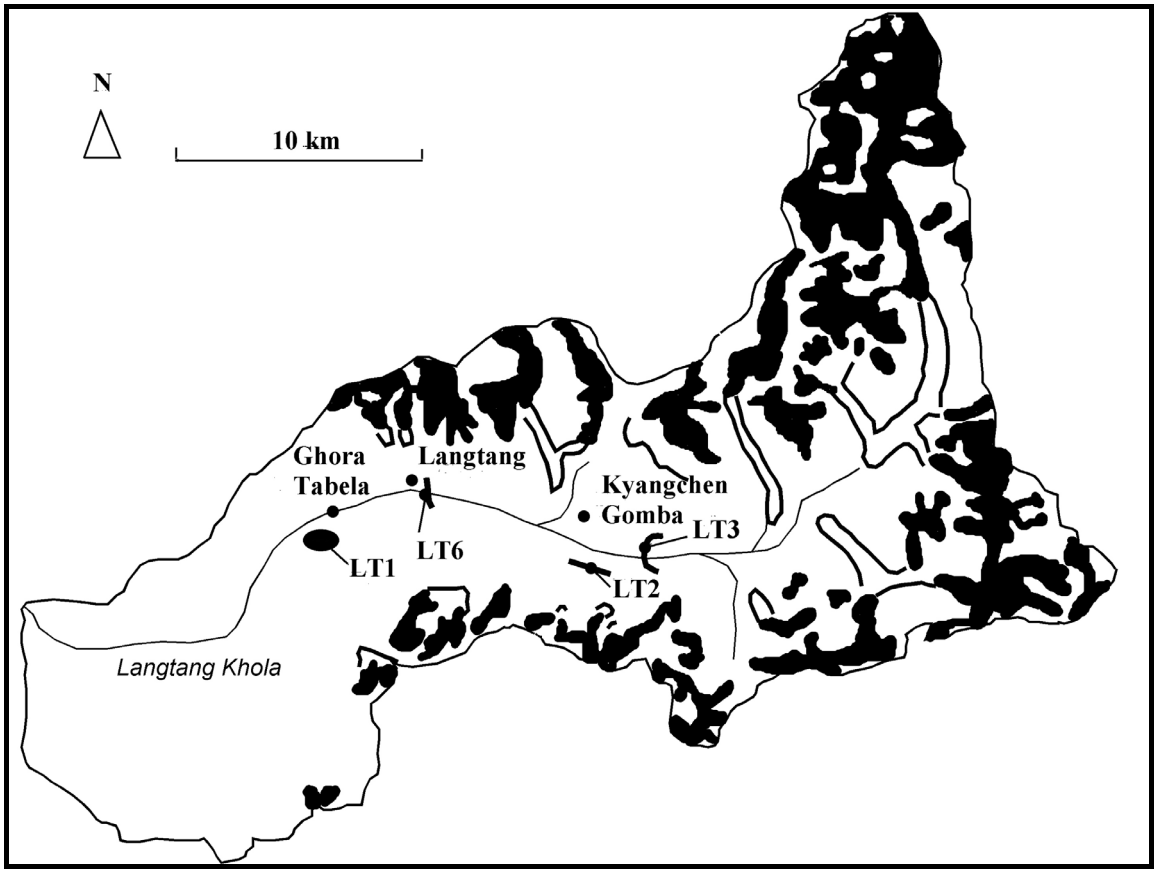

Fig. 4.3. Sketch of the Langtang catchment with glaciers (black), LIA moraines (continuous bold lines), and sampled deposits (LT1, 2, 3, 6).

Shiraiwa & Watanabe (1991) in turn proposed four glacial stages. The oldest *Lama* stage is thought to be represented by remnants of a trough profile reaching down to 2600 m a.s.l. The second stage is defined by the Ghora Tabela moraine. For the *Lama* and *Ghora Tabela* stages, no age estimates are given. All moraines upvalley, however, are interpreted to be neoglacial moraines by Shiraiwa & Watanabe (1991), based on radiocarbon dates of 3.0-3.6 ka B.P. for an advance of the Langtang Lirung south glacier reaching downvalley to Langtang village. The *Langtang* stage thus defined also comprises the main valley glacier moraine east of Kyangchen Gomba (LT3). Younger neoglacial moraines of the Langtang Lirung south glacier are placed into a separate *Lirung* stage with a radiocarbon age <2.8 ka.

Baeumler et al. (1996, 1997) and Baeumler (2001a) have used soil development and soil chemical analyses, as well as new radiocarbon ages, to reevaluate these chronologies. They show that the LT3 moraine is significantly older than the other moraines of the *Langtang* stage of Shiraiwa & Watanabe (1991), indirectly providing a radiocarbon age of >6 ka B.P., and that the LT2 moraine is even older than the LT3 moraine.

We sampled boulders on the moraines LT2, 3, and 6 to definitely determine the chronology of these lateglacial or Holocene glacier advances. In addition, samples were taken from a rockfall deposit on the moraine surface at Ghora Tabela (Fig. 4.3, LT1) in the hope of finding a constraint on the timing of the glacier advance which has left this oldest moraine deposit preserved in the valley.

4.2.2 ^{10}Be surface exposure dating

For ^{10}Be surface exposure dating (SED), chunks of up to 8 cm thickness have been loosened by hammer and chisel from the centre surfaces of the largest and tallest boulders positioned on the culminations of each sampled deposit. Boulders showing signs of spalling or recent dislocation were avoided. Position and altitude were read from a GPS and barometric altimeter combination. Topographic shielding and surface inclination were noted using a compass and inclinometer. Samples were analyzed for ^{10}Be following the procedure of Kohl & Nishiizumi (1992) as modified by Ivy-Ochs (1996). ^{10}Be/^{9}Be was measured at the AMS facility of the Paul Scherrer Institute at the ETH Zurich and corrected to conform to ICN standards.

Calculation of the exposure ages was done using TEBESEA (section 2), employing the scaling system of Lal (1991) as modified by Stone (2000) with a standard ^{10}Be production rate at sea level in high latitude (SLHL) of 5.35 ± 0.15 atoms g^{-1} a^{-1}, a negative muon capture contribution to SLHL production of 1.2%, as well as corrections for 1) geomagnetic variations, 2) sample thickness considering the depth profile of Heisinger et al. (2002a, b) as parametrized by Schaller et al. (2002), and 3) shielding by topography and surface inclination. The influence of surface erosion, tectonic uplift and snow cover has been estimated by calculating a minimum exposure age, assuming no erosion, uplift and cover, as well as a maximum exposure age, assuming a conservative maximum erosion rate of 3 ± 2 mm ka^{-1} (section 4), a tectonic uplift rate of 3 ± 2 mm a^{-1}, and a mean annual snow cover of 5 ± 3 g cm^{-2}. The tectonic uplift rate used is a good approximation of the published values for central Himalayan uplift, which range from 1-4 mm (Jain et al., 2000). Where stated, a

modified scaling system of Dunai (2001) has been used for comparison, employing a standard ^{10}Be production rate at sea level in high latitude (SLHL) of 5.47 ± 0.31 atoms g^{-1} a^{-1}, a negative muon capture contribution to SLHL production of 1.9%, and a fast muon reaction contribution of 1.7% (section 3). Muon contributions in this case were scaled as proposed by Schaller et al. (2002). All other corrections were applied as mentioned above. All surface exposure ages taken from the literature for comparison have been recalculated following the calculation scheme applied here and therefore may be slightly different from values given in the original studies. Interpretation of the exposure age distributions followed the scheme proposed in section 4.

4.3 Results & Discussion

4.3.1 Macha Khola Valley

Boulders from the oldest moraine in the Macha Khola Valley, MK2, yielded exposure ages between 34 and 97 ka (Tab. 4.1), allowing for possible deposition of the moraine during the MIS 3 through 5, or even earlier. A comparison with exposure ages from the Khumbu Himal (Finkel et al., 2003), however, shows a good agreement between the oldest exposure age of MK2 and the *Thyangboche* I stage, all pointing to 70-100 ka, which makes deposition during the MIS 5 most likely (Fig. 4.4). All younger ages on MK2 seem to reflect moraine degradation, as the like are found on the *Thyangboche* I moraine as well, where the respective boulders seem to have been exhumed during the younger *Thyangboche* II advance during the second half of the MIS 3 (Fig. 4.4, Finkel et al., 2003). The 70-100 ka age of the first, most extensive late Pleistocene glacier advance in the Nepal Himalaya is in agreement with an MIS 4-5 estimate of 70 ka for the *Ronbushi* I advance on the northern slope of the Himalaya given by Zheng and Rutter (1998). No remnants correlating to a *Thyangboche* II advance have been identified in the Macha Khola Valley.

The next younger advance dated in the Macha Khola Valley, MK5, yielded exposure ages between 11 and 26 ka (Tab. 4.1, Fig. 4.5). While the ages around 11 ka are clearly indicative of moraine degradation, the three oldest ages allow for glacial advance between 19 and 26 cal. ka B.P., which is in agreement with the 18 cal. ka basal age of lake Rukche Tal (Schluetz & Zech, 2004), and with other MIS 2 moraine ages determined in Nepal.

Tab. 4.1. Results of ^{10}Be surface exposure dating in the Nepal Himalaya.

Sample ID	Latitude [°N]	Longitude [°E]	Altitude [m]	f_{ST}, n[1]	f_{ST}, μ[2]	α[3] [°]	d[4] [cm]	^{10}Be [10^6 atoms g^{-1}]	Min. exposure age [ka]	Max. exposure age [ka]	Dunai / Lal[5]
MK22	28.3	84.5	2364	1.000	1.000	0	4	1.894 ± 0.137	71.7 ± 9.3	97 ± 26	1.00
MK23	28.3	84.5	2364	1.000	1.000	0	4	1.221 ± 0.094	45.3 ± 6.0	54 ± 10	1.00
MK24	28.3	84.5	2364	1.000	1.000	0	4	0.850 ± 0.054	33.5 ± 4.1	36.7 ± 5.6	1.00
MK25	28.3	84.5	2364	1.000	1.000	0	4	1.097 ± 0.079	41.2 ± 5.3	47.1 ± 8.1	1.00
MK41	28.3	84.5	3900	1.000	1.000	0	4	0.249 ± 0.022	4.78 ± 0.66	4.82 ± 0.67	0.95
MK42	28.3	84.5	3900	1.000	1.000	0	4	0.101 ± 0.015	2.00 ± 0.36	2.01 ± 0.37	0.94
MK43	28.3	84.5	3900	1.000	1.000	0	4	0.180 ± 0.014	3.51 ± 0.46	3.53 ± 0.47	0.96
MK44	28.3	84.5	3900	1.000	1.000	0	4	0.154 ± 0.024	3.07 ± 0.56	3.08 ± 0.57	0.95
MK45	28.3	84.5	3900	1.000	1.000	0	4	0.178 ± 0.034	3.48 ± 0.76	3.49 ± 0.77	0.96
MK51	28.3	84.5	3550	1.000	1.000	0	4	1.171 ± 0.097	24.0 ± 3.2	25.5 ± 3.8	0.97
MK52	28.3	84.5	3550	1.000	1.000	0	4	0.484 ± 0.035	10.5 ± 1.3	10.7 ± 1.4	0.97
MK53	28.3	84.5	3550	1.000	1.000	0	4	1.043 ± 0.080	21.7 ± 2.8	22.8 ± 3.3	0.97
MK54	28.3	84.5	3550	1.000	1.000	0	4	0.895 ± 0.078	18.9 ± 2.6	19.8 ± 2.9	0.97
MK55	28.3	84.5	3550	1.000	1.000	0	4	0.510 ± 0.055	11.1 ± 1.7	11.3 ± 1.8	0.97
MK71	28.3	84.5	3260	1.000	1.000	0	4	0.822 ± 0.062	20.3 ± 2.6	21.3 ± 3.0	0.98
MK73	28.3	84.5	3260	1.000	1.000	0	4	0.470 ± 0.056	12.0 ± 1.9	12.3 ± 2.0	0.98
MK74	28.3	84.5	3260	1.000	1.000	0	4	0.435 ± 0.044	11.1 ± 1.6	11.4 ± 1.7	0.98
MK75	28.3	84.5	3260	1.000	1.000	0	4	0.450 ± 0.039	11.5 ± 1.6	11.8 ± 1.7	0.98
LT12	28.2	85.5	2978	0.910	0.899	16	2	0.020 ± 0.006	0.72 ± 0.23	0.73 ± 0.23	1.00
LT13	28.2	85.5	2978	0.897	0.886	20	4	0.030 ± 0.011	1.06 ± 0.43	1.06 ± 0.44	1.00
LT14	28.2	85.5	2980	0.898	0.887	14	2	0.015 ± 0.006	0.55 ± 0.21	0.55 ± 0.21	1.00
LT15	28.2	85.5	2980	0.898	0.886	12	1	0.013 ± 0.004	0.49 ± 0.15	0.49 ± 0.15	1.00
LT16	28.2	85.5	3016	0.834	0.821	20	1.5	0.044 ± 0.007	1.71 ± 0.34	1.71 ± 0.34	0.99
LT17	28.2	85.5	3016	0.832	0.819	15	4	0.038 ± 0.011	1.44 ± 0.46	1.44 ± 0.46	0.99
LT18	28.2	85.5	3020	0.823	0.808	12	2	0.014 ± 0.004	0.56 ± 0.16	0.56 ± 0.16	1.00
LT22	28.2	85.6	4150	0.994	0.993	18	3	0.903 ± 0.045	14.3 ± 1.6	14.7 ± 1.8	0.94
LT23	28.2	85.6	4156	0.993	0.991	10	1	0.844 ± 0.032	13.3 ± 1.5	13.5 ± 1.6	0.94
LT24	28.2	85.6	4156	0.988	0.985	0	2	0.893 ± 0.047	14.1 ± 1.6	14.3 ± 1.8	0.94
LT26	28.2	85.6	4154	0.988	0.985	0	2	0.735 ± 0.036	11.6 ± 1.3	11.8 ± 1.4	0.93
LT32	28.2	85.6	3853	0.973	0.968	14	2.5	0.431 ± 0.017	8.11 ± 0.90	8.21 ± 0.94	0.95
LT33	28.2	85.6	3851	0.964	0.957	8	2.5	0.403 ± 0.016	7.68 ± 0.86	7.75 ± 0.89	0.95
LT35	28.2	85.6	3846	0.982	0.978	24	1	0.458 ± 0.021	8.66 ± 0.98	8.72 ± 1.03	0.95
LT36	28.2	85.6	3846	0.926	0.920	32	2	0.192 ± 0.008	4.25 ± 0.47	4.27 ± 0.48	0.96
LT61	28.2	85.5	3523	0.963	0.957	24	1.5	0.129 ± 0.008	3.25 ± 0.40	3.26 ± 0.40	0.97
LT63	28.2	85.5	3525	0.948	0.941	20	1	0.134 ± 0.007	3.40 ± 0.39	3.40 ± 0.40	0.97

[1] correction factor for topographic shielding of fast neutrons, corrected for the influence of surface inclination
[2] correction factor for topographic shielding of muons, corrected for the influence of surface inclination
[3] maximum slope angle of the sampled surface
[4] thickness of the sample
[5] ratio of ages calculated using the scaling systems of Lal (1991) as used in this study, and the scaling system of Dunai (2001) as modified by Schaller et al. (2002), for details see section 3.

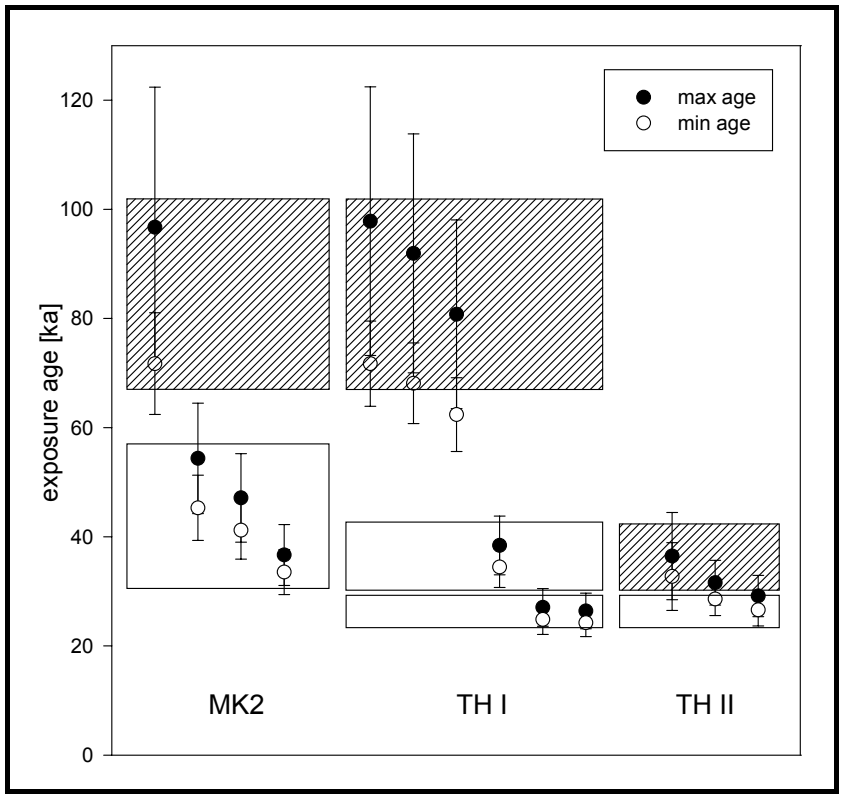

Fig. 4.4. Comparison of (recalculated) minimum (white dots) and conservative maximum (black dots) exposure ages from MIS 5-3 moraines in the Macha Khola Valley (MK2, this work), and the Khumbu Valley (Finkel et al., 2003, TH I, II: *Thyangboche* I, II stages). Glacial advances as interpreted from the data in crosshatched boxes, phases of moraine degradation in white boxes. See text for explanation.

A similar, but more narrowly constrained ^{10}Be age of 18-23 cal. ka B.P. has been found for the main MIS 2 advance in the Khumbu and Chhukung Valleys (*Phericheˆ* I stage, Finkel et al., 2003) (Fig. 4.5). In the Khumbu Valley, the *Phericheˆ* I moraine further yielded OSL ages of 18-25 ka (Richards et al., 2000) and another ^{10}Be age of ~20 cal. ka B.P. (Aoki & Imamura, 1997). These results are confirmed by OSL dates of 20-23 ka from the Kangchenjunga Himal (Asahi et al., 2000, Tsukamoto et al., 2002). An MIS 2 advance ~20 cal. ka B.P. is thus firmly established in the Nepal Himalaya by now. This, however, is not the case for any MIS 4 advance after 70 cal. ka B.P., and it is remarkable, that in the Nepal Himalaya, MIS 2 glacier advances seem to have occurred only after 23 cal. ka B.P., whereas farther northwest, MIS 2 advances occurred prior to 23 cal. ka B.P. as well (section 5). These two facts might indicate, that indeed only during the late MIS 2, the influence of the westerly circulation on glaciation extended over the whole Himalayan system. At that time, the jetstream was at the southernmost position it reached during the late Pleistocene (Benn & Owen, 1998, Ono et al., 2004). Before, and afterwards, glaciation in the southeastern part of the Himalaya as it seems was dominated by the influence of the

Indian monsoon, which was strong during the MIS 5, 3 and 1, but weak during the MIS 4 and 2 (Leuschner & Sirocko, 2000).

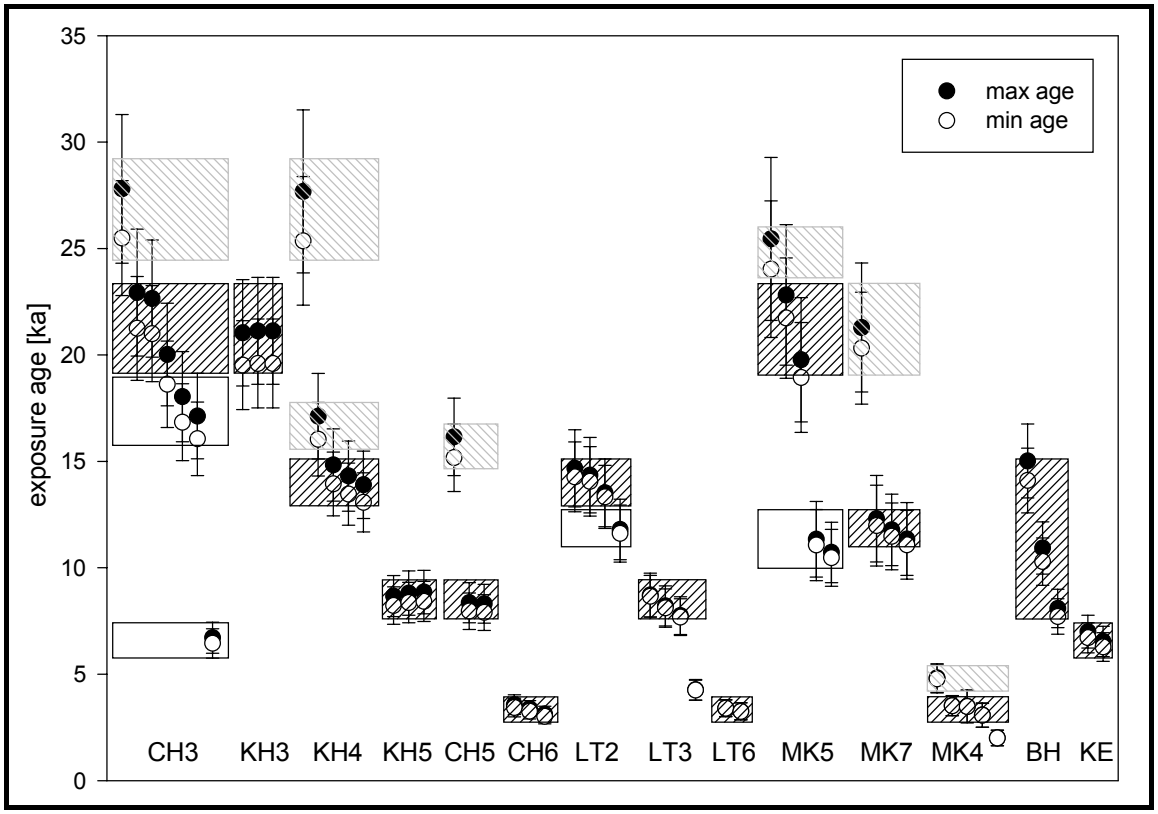

Fig. 4.5. Comparison of (recalculated) minimum (white dots) and conservative maximum (black dots) exposure ages of MIS 2-1 moraines from the Chhukung (CH) and Khumbu (KH) valleys (Finkel et al., 2003, 3: *Pheriche* I stage, 4: *Pheriche* II stage, 5: *Chhukung* stage, 6: *Thukhla* stage), the Langtang Valley (LT, this work), the Macha Khola Valley (MK, this work) and the Garhwal Himalaya (BH, KE; Barnard et al., 2004). BH = *Bhagirathi* stage, KE = *Kedar* stage. Boulders interpreted to be affected by inheritance in boxes crosshatched in grey, glacial advances as interpreted from the data in boxes crosshatched in black, phases of moraine degradation in white boxes. See text for explanation.

The lateglacial advance represented by MK7 is dated by our exposure ages to between 11.1 and 12.3 cal. ka B.P., covering the Younger Dryas event, excepting one age of 20-21 ka obviously affected by inheritance (Tab. 4.1, Fig. 4.5). Younger Dryas ages have not been reported from the Khumbu Valley (Finkel et al., 2003) and have not been found in the Langtang Valley as well. The like, however, have been reported from the Hunza Valley (*Batura* stage, Owen et al., 2002) as well as from the Lahul Himalaya (*Kulti* stage, Owen et al., 2001), and the Younger Dryas period is covered by the age range found on the *Bhagirathi* moraine in the Garhwal (BH in Fig. 4.5) by Barnard et al. (2004). All these regions are situated west of the Macha Khola Valley. In the Khumbu and Kangchenjunga regions east of the Macha Khola Valley, instead, the *Chhukung* stage is defined by surface

exposure ages of 8-10 ka (Finkel et al., 2003, KH5 and CH5 in Fig. 4.5) and OSL ages of around 9 ka (Asahi et al., 2000). It is thus definitely younger. Therefore, it may be that the influence of the westerly circulation during the time of the Younger Dryas just reached the Manaslu massif and did not extend farther to the east, while the monsoon influence on glaciation during the early Holocene just reached west of the Langtang Valley. Further dating however, is needed to confirm such a suggestion.

The neoglacial moraine MK4 finally is dated to around 3 cal. ka B.P. (Tab. 4.1, Fig. 4.5). Glacier advances during that time are already well documented by radiocarbon dating all over the Nepal Himalaya, e.g. in the Langtang Valley (Shiraiwa & Watanabe, 1991, Baeumler et al., 1996, Heuberger & Ibetsberger, 1998), or in the Annapurna Himal (Zech et al., 2001a, b), as well as from all over the Tibetan plateau (Zheng & Rutter, 1998). In the Khumbu area, glacial advances around 3 cal. ka B.P. have been defined as the *Thukhla* stage (Finkel et al., 2003, KH6 in Fig. 4.5). Our dating thus merely confirms the appropriateness of ^{10}Be SED of moraines in this area and the unlikeliness of inheritance in more than a single boulder out of a selection of five.

4.3.2 Langtang Valley

The rockfall covering the moraine at the end of the Ghora Tabela (LT1) surface has a very young exposure age of 1.0 ± 0.5 ka and is therefore unsuitable for constraining the age of the glacial advance. However, our dates shows that such a short time is sufficient for the formation of a well developed cambic horizon in fine material covering the deposit under the climatic conditions in an altitude of ~3000 m, which is not the case on a neoglacial moraine of roughly the same age in about 3700 m near Kyangchen Gomba (Baeumler et al, 1996).

The high lateral moraine opposite Kyangchen Gomba, LT2, yielded older exposure ages than the other moraines studied in the Langtang Valley, as was already suggested by the soil parameters studied by Baeumler (2001a). With ages of 11.6-14.7 ka (Tab. 4.1, Fig. 4.5), it is clearly correlative with the *Pheriche* II stage in the Khumbu area (Finkel et al., 2003, KH 4 in Fig. 4.5).

The end moraine of the main valley glacier east of Kyangchen Gomba, LT3, dated by Baeumler (2001a) to be older than 6 ka is in fact 7.7-8.7 ka old (Tab. 4.1, Fig. 4.5). A single younger exposure age of ~4.8 ka can be explained by later exhumation of this

particular boulder. This deposit excellently correlates with the *Chhukung* stage in the Khumbu area (Finkel et al., 2003, KH5, CH5 in Fig. 4.5), which is also documented in the Kangchenjunga Himal by an OSL age of 9 ka (Asahi et al., 2000). This stage occurred during the Holocene maximum of monsoon strength (Leuschner & Sirocko, 2000) and is clearly indicative of monsoon influence on glaciation in the Himalaya. It has also been recognized in the Nanga Parbat massif at the present-day margin of the Indian monsoon (Phillips et al., 2000).

Finally, the moraine at Langtang village, LT6, has an exposure age of 3.3-3.5 ka (Tab. 4.1), again confirming earlier radiocarbon dating (Shiraiwa & Watanabe, 1991), and correlating with the *Thukhla* stage of the Khumbu area (Finkel et al., 2003, KH6 in Fig. 4.5) and a similar advance in the Macha Khola Valley (this work, MK4 in Fig. 4.5).

Barnard et al. (2003) in parallel, dating all sorts of landforms in the Langtang Valley, found ^{10}Be surface exposure dates of Holocene moraines of 3.5 ka, and 8.5 ka, confirming our dating of moraines LT3 and LT6. They also found moraine ages of 19-23 ka, proving the existence of a glacier advance in the Langtang Valley correlated to the *Pheriche* I stage of the Khumbu area.

4.4 Conclusions

Late Pleistocene and Holocene glacier advances in the Macha Khola Valley have been dated at 70-100, 20-23, 11-12 and around 3 cal. ka B.P. In the Langtang Valley, lateglacial and Holocene glacier advances have been dated at 14-15, 8-9 and ~3.5 cal. ka B.P.

Except for the Younger Dryas advance in the Macha Khola Valley, all ages excellently agree with the glacial chronology of the Khumbu area defined by Finkel et al. (2003).

The new glacial chronology of the Nepal Himalaya shows that, except for the MIS 2, the Indian monsoon rather than the westerly circulation has controlled the glacial activity in the region. During the coldest phase of the MIS 2, the westerly jetstream appears to have shifted far enough south to affect glaciation all over the Himalaya. During the Younger Dryas, the eastern limit of the influence of the westerly circulation on Himalaya glaciation may have been situated between the Manaslu and Langtang Himal.

^{10}Be surface exposure ages have excellently confirmed and complemented former soil geographic work in the studied valleys.

4.5 Acknowledgements

This work was made possible by the German Research Foundation (DFG), grant ZE 154-51, and was supported by the Volkswagen Foundation (Az. I/71665). We gratefully acknowledge all support.

4.6 References

AOKI, T., IMAMURA, M. 1997. Reconstructing the glacial chronology based on the ^{10}Be exposure age. In: Nihon Daigaku Bunrigakubu Shizen Kagaku Kenkyousho: Kasokuki Shitsuryo Bunseki Shinpojumu, Tokyo, 159-166. (in Japanese)

ASAHI, K., TSUKAMOTO, S., AOKI, T., WATANABE, T. 2000. Late Quaternary glaciations in the Kangchenjunga Himal, eastern Nepal: based on absolute and relative dating. In: Abstract volume for the symposium on Quaternary glaciation in Monsoonal Asia, Academica Sinica, Chengdu, June 5-18, p. 1.

ASAHI, K., WATANABE, T., TSUKAMOTO, S. 2003. History of glaciations in the Nepal Himalayas and reconstruction of palaeoclimate since the last glacial. XVI INQUA Congress Programs with Abstracts, DRI, Reno, Nv., p. 156.

BAEUMLER, R. 2001a. Vergleichende bodenkundliche Untersuchungen in Hochasien und Kamtschatka. Relief Boden Palaeoklima 16, Gebrueder Borntraeger, Berlin, 125 p.

BAEUMLER, R. 2001b Pedogenic studies in aeolian deposits in the high mountain area of eastern Nepal. Quaternary International 76/77, 93-102.

BAEUMLER, R., ZECH, W. 2000. Soil development as an indicator of the Pleistocene and Holocene landscape history in Western Tian Shan and Nepal. Marburger Geographische Schriften 135, 69-82.

BAEUMLER, R., KEMP-OBERHETTINGER, M., ZECH, W., HEUBERGER, H., SIEBERT, A., MADHIKARMI, D. P., POUDEL, K. P. 1996. Soil weathering on glacial and glaciofluvial deposits in the Langtang Valley (central Nepal) and its relation to the glacial history. Zeitschrift fuer Geomorphologie N. F., Supplement-Band 103, 373-387.

BAEUMLER, R., MADHIKARMI, D. P., ZECH, W. 1997. Fine silt and and clay mineralogical changes of a soil chronosequence in the Langtang Valley (central Nepal). Zeitschrift fuer Pflanzenernaehrung und Bodenkunde 160, 413-421.

BARBEY, P., BROUAND, M., LE FORT, P., PECHER, A. 1996. Granite-migmatite genetic link: the example of the Manaslu granite and Tibetan Slab migmatites in central Nepal. Lithos 38, 63-79.

BARNARD, P. L., OWEN, L. A., FINKEL, R. C. 2003. The role of paraglacial processes in the evolution of high mountain landscapes, the high Himalaya of India and Nepal. XVI INQUA Congress Programs with Abstracts, p. 65.

BARNARD, P. L., OWEN, L. A., FINKEL, R. C. 2004. Style and timing of glacial and paraglacial sedimentation in a monsoon-influenced high Himalayan environment, the upper Bhagirathi Valley, Garhwal Himalaya. Sedimentary Geology 165, 199-221.

BENN, D. I., OWEN, L. A. 1998. The role of Indian summer monsoon and the mid-latitude westerlies in Himalayan glaciations: review and speculative discussion. Journal of the Geological Society of London 155, 353-363.

BENN, D. I., OWEN, L. A. 2002. Himalayan glacial sedimentary environments: a framework for reconstructing and dating the former extent of glaciers in high mountains. Quaternary International 97-98, 3-25.

BUSH, A. B. G. 2000. A positive climatic feedback mechanism for Himalayan glaciation. Quaternary International 65/66, 3-13.

DENNISTON, R. F., GONZÁLEZ, L. A., ASMEROM, Y., SHARMA, R. H., REAGAN, M. K. 2000. Evidence for changes in Indian summer monsoon precipitation over the last ~2300 years. Quaternary Research 53, 196-202.

DUNAI, T. J. 2001. Influence of secular variation of the geomagnetic field on production rates of in situ produced cosmogenic nuclides. Earth and Planetary Science Letters 193, 197-212.

FINKEL, R. C., OWEN, L. A., BARNARD, P. L., CAFFEE, M. W. 2003. Beryllium-10 dating of Mount Everest moraines indicates a strong monsoon influence and glacial synchroneity throughout the Himalaya. Geology 31, 561-564.

FORT, M. 1986. Glacial extension and catastrophic dynamics along the Annapurna front, Nepal Himalaya. Goettinger Geographische Abhandlungen 81, 105-121.

FORT, M. 2000. Glaciers and mass wasting processes: their influence on the shaping of the Kali Gandaki Valley (higher Himalaya of Nepal). Quaternary International 65/66, 101-119.

HARRISON, T. M., RYERSON, F. J., LE FORT, P., YIN, A., LOVERA, O. M., CATLOS, E. J. 1997. A Late Miocene-Pliocene origin for the central Himalayan inverted metamorphism. Earth and Planetary Science Letters 146, E1-E7.

HEISINGER, B., LAL, D., JULL, A. J. T., KUBIK, P., IVY-OCHS, S., NEUMAIER, S., KNIE, K., LAZAREV, V., NOLTE, E. 2002a. Production of selected cosmogenic radionuclides by muons 1. Fast muons. Earth and Planetary Science Letters 200, 345-355.

HEISINGER, B., LAL, D., JULL, A. J. T., KUBIK, P., IVY-OCHS, S., KNIE, K., NOLTE, E. 2002b. Production of selected cosmogenic radionuclides by muons 2. Capture of negative muons. Earth and Planetary Science Letters 200, 357-369.

HEUBERGER, H., IBETSBERGER, H. 1998. Problems of Holocene glacier advances in Langtang, central Nepal. In: Chalise, S. R. (ed.): Ecohydrology of high mountain areas. JCIMOD, Kathmandu, 459-465.

HEUBERGER, H, MASCH, E., PREUSS, E., SCHROECKER, A. 1984. Quaternary landslides and rock fusion in central Nepal and the Tyrolian Alps. Mountain Research and Development 4, 345-362.

IVY-OCHS, S. 1996. The dating of rock surface using in situ produced ^{10}Be, ^{26}Al and ^{36}Cl, with examples from Antarctica and the Swiss Alps. Diss. ETH No. 11763, Zuerich, 197 p.

JAIN, A. K., KUMAR, D., SINGH, S., KUMAR, A., LAL, N. 2000. Timing, quantification and tectonic modelling of Pliocene-Quaternary movements in the NW Himalaya: evidence from fission track dating. Earth and Planetary Science Letters 179, 437-451.

KOHL, C. P., NISHIIZUMI, K. 1992. Chemical isolation of quartz for measurement of in-situ produced cosmogenic nuclides. Geochimica et Cosmochimica Acta 56, 3583-3587.

KUHLE, M. 1998. Reconstruction of the 2.4 million km² Late Pleistocene ice sheet on the Tibetan Plateau and its impact on the global climate. Quaternary International 45/46, 71-108.

KUHLE, M. 1999. Reconstruction of an approximately complete Quaternary Tibetan inland glaciation between the Mt. Everest- and Cho Oyu Massifs and the Aksai Chin. A new glaciogeomorphological SE-NW diagonal profile through Tibet and its consequences for the glacial isostasy and Ice Age cycle. GeoJournal 47, 3-276.

LAL, D. 1991. Cosmic ray labelling of erosion surfaces: in situ nuclide production rates and erosion models. Earth and Planetary Science Letters 104, 424-439.

LEUSCHNER, D. C., SIROCKO, F. 2000. The low latitude monsoon climate during Dansgaard-Oeschger cycles and Heinrich events. Quaternary Science Reviews 19, 243-254.

MIEHE, G. 1990. Langtang Himal. Flora und Vegetation als Klimazeiger und -zeugen im Himalaya. Dissertationes Botanicae 158, 559 p.

ONO, Y. 1986. Glacial fluctuations in the Langtang Valley, Nepal Himalaya. Goettinger Geographische Abhandlungen 81, 31-38.

ONO, Y., SHULMEISTER, J., LEHMKUHL, F., ASAHI, K., AOKI, T. 2004. Timings and causes of glacial advances across the PEP-II transect (East-Asia to Antarctica) during the last glaciation cycle. Quaternary International 118-119, 55-68.

OWEN, L. A., DERBYSHIRE, E., FORT, M. 1998. The Quaternary glacial history of the Himalaya. Quaternary Proceedings 6, 91-120.

OWEN, L. A., GUALTIERI, L., FINKEL, R. C., CAFFEE, M. W., BENN, D. I., SHARMA, M. C. 2001. Cosmogenic radionuclide dating of glacial landforms in the Lahul Himalaya, northern India: defining the timing of Late Quaternary glaciation. Journal of Quaternary Science 16, 555-563.

OWEN, L. A., FINKEL, R. C., CAFFEE, M. W., GUALTIERI, L. 2002. Timing of multiple glaciations during the Late Quaternary in the Hunza Valley, Karakoram Mountains, northern Pakistan: defined by cosmogenic radionuclide dating of moraines. Geological Society of America Bulletin 28, 431-434.

PHILLIPS, W. M., SLOAN, V. F., SHRODER, J. F. JR., SHARMA, P., CLARKE, M. L., RENDELL, H. M. 2000. Asynchronous glaciation at Nanga Parbat, northwestern Himalaya Mountains, Pakistan. Geology 28, 431-434.

RICHARDS, B. W. M., BENN, I. D., OWEN, L. A., RHODES, E. J., SPENCER, J. Q. 2000. Timing of Late Quaternary glaciations south of Mount Everest in the Khumbu Himal, Nepal. Geological Society of America Bulletin 112, 1621-1632.

ROETHLISBERGER, F. 1986. Himalaya & Karakorum. In: 10000 Jahre Gletschergeschichte der Erde. Verlag Sauerlaender, Aarau, 79-153.

SCHALLER, M., BLANCKENBURG, F. V., VELDKAMP, A., TEBBENS, L. A., HOVIUS, N., KUBIK, P. W. 2002. A 30 000 yr record of erosion rates from cosmogenic ^{10}Be in Middle European river terraces. Earth and Planetary Science Letters 204, 307-320.

SCHLUETZ, F., ZECH, W. 2004. Palynological investigations on vegetation and climate change in the Late Quaternary of Lake Rukche area, Gorkha Himal, central Nepal. Vegetation History and Archaeobotany 13, 81-90.

SHIRAIWA, T., WATANABE, T. 1991. Late Quaternary glacial fluctuations in the Langtang Valley, Nepal Himalaya, reconstructed by relative dating methods. Arctic and Alpine Research 23, 404-416 .

STONE, J. O. H. 2000. Air pressure and cosmogenic isotope production. Journal of Geophysical Research 105 B10, 23753-23759.

TSUKAMOTO, S., ASAHI, K., WATANABE, T., RINK, W. J. 2002. Timing of past glaciations in Kangchenjunga Himal, Nepal by optically stimulated luminescence dating of tills. Quaternary International 97-98, 57-67.

WILLIAMS, V. S. 1983. Present and former equilibrium line altitudes near Mount Everest, Nepal, and Tibet. Arctic and Alpine Research 15, 201-211.

ZECH, W., MADHIKARMI, D., GERL, T., BECK, E. 2001a Rekonstruktion der spaetglazialen und holozaenen Vergletscherung des Annapurna III-Nordgletschers unter besonderer Beruecksichtigung der Boeden als Indikatoren für Klimaschwankungen. Zeitschrift fuer Gletscherkunde und Glazialgeologie 37, 141-158.

ZECH, W., BAEUMLER, R., MADHIKARMI, D., GERL, T., BECK, E. 2001b. Zur pleistozaenen und holozaenen Landschaftsgeschichte des Modi-Khola-Tales (Annapurna, Nepal). Zeitschrift fuer Gletscherkunde und Glazialgeologie 37, 159-190.

ZECH, W., GLASER, B., ABRAMOWSKI, U., DITTMAR, C., KUBIK, P. W. 2003. Reconstruction of the Late Quaternary Glaciation of the Macha Khola Valley (Gorkha Himal, Nepal) using relative and absolute (14C, 10Be, dendrochronology) dating techniques. Quaternary Science Reviews 22, 2253-2265. .

ZHENG, B. 1989a. Controversy regarding the existence of a large ice sheet on the Qinghai-Xizang (Tibet) Plateau during the Quaternary period. Quaternary Research 32, 121-123.

ZHENG, B. 1989b. The influence of Himalayan uplift on the development of Quaternary glaciers. Zeitschrift fuer Geomorphologie N. F. Supplementband 76, 89-115.

ZHENG, B., RUTTER, N. 1998. On the problem of quaternary glaciations, and the extent and patterns of Pleistocene ice cover in the Qinghai-Xizang (Tibet) Plateau. Quaternary International 45/46, 109-122.

5. Late Pleistocene palaeoglaciations of Central Asia: a new chronology based on ^{10}Be surface exposure ages of erratic boulders from the Pamir (Tajikistan), and the Alay and Turkestan Ranges (Kyrgyzstan)

Abramowski, U.[1], Bergau, A.[1], Seebach, D.[1], Zech, R.[1], Glaser, B.[1], Sosin, P.[2], Kubik, P. W.[3], Zech, W.[1]

[1] Institute of Soil Science and Soil Geography, University of Bayreuth, D-95440 Bayreuth, Germany

[2] Institute of Soil Science, Tajik Academy of Agriculture, Dushanbe, Tajikistan

[3] Paul Scherrer Institute, c/o Institute of Particle Physics, ETH Zurich, CH-8093 Zurich, Switzerland

Abstract

We have determined the timing of palaeoglaciations in the Pamir (Tajikistan) and the Alay and Turkestan Ranges (Kyrgyzstan) using ^{10}Be surface exposure dating of erratic boulders. Glacial advances in the area have occurred >93->136, ~60-80, (40-55), ~27-25, ~22-20, ~18, ~15.5, ~14.3, and 10.5 cal. ka B.P. All late Pleistocene glaciers in the Pamir, Alay and Turkestan Ranges have been valley glaciers except for the most extended glaciers on the plateau, which have formed local piedmont glaciations. In the eastern Pamir, these are characterized by ELA depressions of ~370-380 m (THAR 0.5). In the Turkestan and Alay Ranges, ELA depressions at the same time were >750 m, and 600 m, respectively. Late Pleistocene glacier advances all over western High Asia were contemporaneous with climatic cold phases rather than monsoonal maxima. Their maximum extent and that of the western hemisphere ice sheets were asynchronous, due to increasing aridity in the region over the course of the last glacial. Late Pleistocene climate in Central Asia seems to have been influenced by the interplay of the westerly circulation and the Siberian anticyclone. Some indirect monsoonal influence in the eastern Pamir may be responsible for the existence of some of the lateglacial moraine stages in this area. High altitude glaciers seem to have reached their maximum extent earlier (MIS 5-4) than low altitude glaciers (first half of MIS 3), possibly due to prolonged glacial aridity imparting with moisture advection onto high altitude sites, inducing glacial retreat, but prolonged cold during the same time imparting with glacier ablation at lower altitude sites, inducing glacial advance.

5.1 Introduction

5.1.1 Rationale

Understanding Earth's climate is one of the most important and urgent tasks science is facing today. An accurate prediction of future climate shifts due to anthropogenic and natural impacts on atmospheric temperature and circulation is paramount for long-term planning of political and economic measures to secure and promote man's welfare in a changing environment. Physical circulation models could ultimately be able to simulate the non-linear effects of changes in climate forcing in a way precise enough for these purposes (Intergovernmental Panel on Climate Change, 1997). Such models, however, integrally depend on palaeoclimate datasets to serve as either boundary conditions or evaluation benchmarks. These datasets have to be improved continually by increased spatial coverage and dating control (Kohfeld & Harrison, 2000).

One important palaeo-dataset for the evaluation of climate system models is the record of past mountain glaciations. Magnitude and timing of these glaciations depend on local temperature and precipitation history (Gillespie & Molnar, 1995), parameters that can be predicted by climate system models. Studies in the tropics, for instance, have shown that there are still discrepancies between past mountain glacier advances and sea surface temperatures, which are not explained by the current models (e.g. Porter, 2001). On the other hand, transect studies along the American Cordilleras (Clapperton, 1995) and between eastern Asia and New Zealand (Ono et al., 2004) have documented late Pleistocene shifts of mid-latitude climate system boundaries as predicted by the models (e.g. COHMAP members, 1988).

For the High Asian mountain ranges and plateaus, little information on the timing of palaeoglaciations has been available up to the end of the 1990s (Derbyshire, 1996, Lehmkuhl, 1997, Derbyshire & Owen, 1997, Owen et al., 1998), even though this region was extensively glaciated in the past and is considered a key locality for the understanding of the world's climate (Prell & Kutzbach, 1992, Kuhle, 1998, Benn & Owen, 1998). This lack of data has mainly been caused by insufficient organic material for radiocarbon dating present in cold and dry environments like these.

This situation has changed with the advent of in-situ cosmogenic nuclide dating techniques during the 1990s, and a lot of effort is presently spent in defining absolute glacial chro-

nologies all over High Asia (e.g. Owen et al., 2002a, Owen et al., 2003c, Gillespie et al., 2003). However, there still is no consensus about the timing of glaciations in the different parts of the region. Some authors argue for synchroneity (Zheng et al., 2002), while most of the others argue for asynchroneity (Benn & Owen, 1998, Ono et al., 2004, He et al., 2004) of subregional glacier advances.

This study is a contribution to the general reconstruction effort of glacial history in High Asia, covering its northwestern part, namely the Central Asian mountains between the Turkestan and Alay Ranges of southwestern Kyrgyzstan, and the south-central Pamir plateau of eastern Tajikistan.

5.1.2 Former glacial chronologies of Central Asia

The scientific description of past glaciations in Central Asia set in at the beginning of the last century with the reports of several western expeditions. These resulted in a long-standing dispute about a possible former plateau glaciation of the Pamir and Tibet plateaus (see Derbyshire et al., 1991, for a review). In the 1930s, detailed descriptions of prominent glacial deposits in the western Pamir and the Alay Range have been given by German and Austrian expedition participants (Noeth, 1931, Ficker, 1933, Klebelsberg, 1934). Their chronological interpretation of Central Asian glacial landforms, however, relies on the contemporaneous Alpine stratigraphy, and is not supported by physical dating. Trough shoulders and polished bedrock high above the valley floor are supposed to be remnants of the last (Ficker, 1933), or the penultimate glaciation (Noeth, 1931, Klebelsberg, 1934). Younger glaciations are represented by moraines, which are assumed to be of late-glacial (Ficker, 1933) or global last glacial maximum (LGM) age (Noeth, 1931, Klebelsberg, 1934).

Zabirov (1955) has mapped the equilibrium line altitudes (ELAs) of the present and maximum Pleistocene glaciation all over the Pamir, using preserved end moraines as indicators of the maximum advance of the local glaciers. These moraines give no evidence for a plateau glaciation. Instead, Zabirov (1955) shows that the present ELA rises from ~4600 m a.s.l. at the margins of the Plateau to ~5400 m a.s.l. at its centre, and that the maximum Pleistocene ELA depression decreased from ~950 m to ~260 m in the same direction. Wissmann (1959) has reviewed and complemented Zabirov's (1955) data in his standard work on ELAs in High Asia. Sidorov (1960, 1979) reports moraine evidence for a twofold Pleistocene glaciation, the former having been more extensive than the latter, but does not give any age estimates.

Later Russian workers recognize four moraine generations (Bondarev et al., 1997, Dodonov, 2002):

The oldest moraine generation (Q_1) is represented by troughs up to ~1000 m above the valley floor in the western Pamir (*Tupchak* or *Kokbai complex*), and sediment remnants 500 - 800 m above the valley floor in the eastern Pamir (*East-Pamir complex*). It is inferred to have been deposited in the early Pleistocene, arguably between 1.5 and 1.0 Ma B.P.

The next younger generation (Q_2), is represented by moraines and troughs 300-400 m above the valley floor in the western Pamir (*Bartang complex*), and by moraines of a local piedmont glaciation reaching up to 200-300 m above the valley floors in the eastern Pamir (*Murgab complex*). The deposition of these moraines is inferred to have occurred during the middle Pleistocene between 300 and 120 ka B.P. In the eastern Pamir, the moraines of the Q_2 glaciation are often distinguished by their typical hummocky surfaces, locally called "chukur" (Dodonov, 2002).

The third moraine generation (Q_3), called *Badakhshan complex* in the western Pamir, and *Alichur complex* in the eastern Pamir, is represented by valley moraines that do not rise more than 200 m above the valley floor. It is inferred to have been deposited during the late Pleistocene with a main phase 44-30 ka B.P. In narrow, shielded valleys of the eastern Pamir and Tian Shan, the *Alichur complex* often consists of up to eight or even nine end moraine crests with gradually decreasing distance from the recent glaciers or valley fins.

Finally, all Holocene moraines are put together into a fourth complex (Q_4).

This standard Russian glacial chronology, however, is based on only a few numerical dates. The age of Q_3 rests on two radiocarbon and thermoluminescence ages of lake terraces of the Karakul region (Bondarev et al., 1997, Dodonov, 2002), while the age of Q_2 is based on a single thermoluminescence age of a moraine from the Muksu catchment (Dodonov, 2002). Apart from these ages, a broad correlation with the Russian continental stratigraphy is assumed, which is not able to detect any asynchroneity in glaciation. In spite of this standard chronology, the theory of a late Pleistocene plateau glaciation in Central Asia, resulting from a regionally uniform ELA depression of ~1000 m, has received further support as well (Grosswald & Orlyankin, 1979, Grosswald et al., 1994, Kuhle, 1997, 1998).

Soil analyses on moraines in the Tian Shan (Zech et al., 1996), the Hissar Range and Kichik Alay (Zech et al., 2000a, Baeumler, 2001), as well as the Alay Range (Zech et al., 2000b), have shown that late Pleistocene ELA depressions in northern Central Asia have been in the range of 600-750 m, while Heuberger & Sgibnev (1998) and Baume (2002) have reconstructed maximum late Pleistocene ELA depressions of 800-900 m in the Kirgiz Tian Shan. Still, numerical dates of the studied moraines are scarce. Baume (2002) assumes his inferred maximum late Pleistocene glacier advance to be synchronous with the global LGM (18-21 ^{14}C ka B.P.). Zech et al. (2000b) report a radiocarbon age of 24 ka B.P. from the total soil organic matter of a buried soil on top of a lateral moraine correlated to their maximum late Pleistocene advance. On the base of this interstadial soil age, they interpret the moraine to have been deposited during the marine isotope stage (MIS) 4. Karabanov et al. (1998), finally, inferred a most extensive MIS 5d glaciation of the Pamir from dated properties of Tajik loess. For such an advance there has been additional evidence from ^{10}Be surface exposure dates from the Kirgiz Tian Shan (Koppes et al., 2003).

In order to define a more consistent glacial chronology for south-western Kyrgyzstan and Tajikistan, we applied ^{10}Be surface exposure dating to determine the ages of moraines stratigraphically ascribed to the period between the middle Pleistocene and the early Holocene from six selected areas in the region. Results are compared to each other and to other recently published glacial chronologies from neighbouring regions. Finally, we discuss how our findings fit into the current theories of Pleistocene climate change in High Asia.

5.2 Materials & Methods

5.2.1 Study sites

5.2.1.1 Physical geography and climate of the Pamir-Alay region

The Pamir (37-39°N, 71-75°E) is one of the highest mountain regions of the world with several peaks rising above 7000 m a.s.l. (Fig. 5.1). The western Pamir consists of rugged mountain chains with deeply incised valleys and large valley glaciers. The eastern Pamir, in contrast, is a high plateau of ~4000 m a.s.l., topped by more subdued and often heavily debris-covered mountain ranges, most of which at present are not or only scarcely glaciated. The contrast in relief between the western and the eastern Pamir is paralleled by a contrast in climate. The western Pamir receives medium to low annual precipitation with its maximum in early spring, and supports mountain forests and steppe. The eastern Pamir

receives very low annual precipitation with its maximum in summer, and supports only very scarce semi-desert and desert vegetation (Succow, 1989, UNEP, 2002).

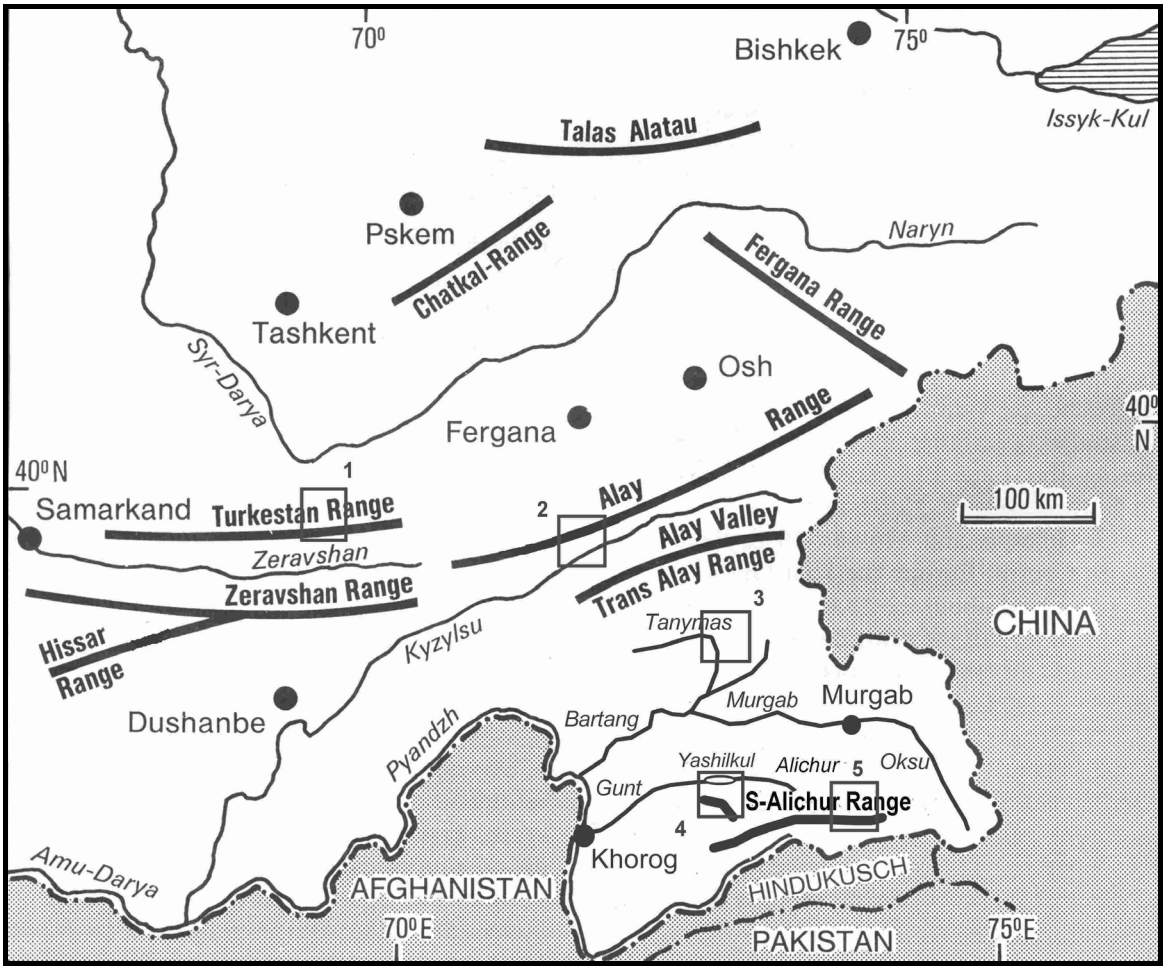

Fig. 5.1. Overview of Central Asian study sites (modified after Zech et al., 2000a). 1: Aksu Valley, 2: Koksu Valley, 3: Ailuitek Pass, 4: Lake Yashilkul, 5: Kol-Uchkol and Gurumdy Valleys.

The culminations of the Pamir mostly consist of granodioritoid plutons, surrounded by Palaeozoic schists (Brookfield, 2000). To the north, the Pamir block is tectonically converging on the east-west-trending Turkestan-Alay Range, both separated by the broad Alay Valley. The Alay-Turkestan Range consists of a Palaeozoic carbonate platform, intruded by Permian granitoid plutons (Brookfield, 2000). Like the western Pamir, it has a semihumid mountain climate with a winter-spring maximum in precipitation, and is characterized by deeply incised valleys (Succow, 1989).

The climate in Central Asia is determined by the position of the westerly jetstream (Weiers, 1995). In winter (November-January), when a strongly negative radiation balance causes a cold cell to develop over the mountains of High Asia, the jetstream is split into a

northern, polar branch situated over the Tian Shan, and a southern, subtropical branch which runs southeast along the Himalaya Front Range. In summer, when a strongly positive radiation balance leads to high-level troughs above the Pamir and Tibet plateaus, the southern branch moves north into Siberia after some oscillations during spring (January - April).

Along the westerly jetstream, cyclones from the west and southwest can enter the region, which advect moisture from the Mediterranean, the Caspian Sea and the Gulf of Persia. These cyclones are responsible for most of the precipitation in Central Asia. However, winter and spring cyclones are mostly shallow and seldom reach altitudes above ~2000 m, leaving the eastern Pamir in the rain shadow of the western and southwestern ranges (Lydolph, 1977). As the westerly jetstream moves north, the spring precipitation maximum shifts from the southwest to the northeast, occurring earliest in the western Badakhshan ranges, and latest in the Kirgiz Tian Shan, where early cyclones are deflected by the strong influence of the winterly Siberian Anticyclone (Dodonov & Baiguzina, 1995, Ricketts et al., 2001, Aizen et al., 2001). In summer, stable high-pressure conditions prevail all over the region. Low altitude sites experience few rainstorms during this time. However, local heat convection cells can carry moisture to high altitudes, leading to low summer precipitation maxima in the eastern Pamir and at elevations above ~2500 m a.s.l. in the other Central Asian mountain chains. In these high altitudes, the circulation is zonal all year round (Lydolph, 1977, Aizen et al., 2001).

Precipitation in the easternmost Pamir is to some degree indirectly influenced by the summer monsoon, as sometimes moisture advected by strong monsoon rains into Northern Pakistan can be carried across the Karakoram to the north-east on the leeside of a high level trough above the central Pamir (Weiers, 1995, 1998). This phenomenon is responsible for the extensive glaciation of the Muztag Ata and Kongur Shan in the Chinese eastern Pamir (Kuhle, 1997). Some indirect influence of monsoon precipitation has also been noted by lower ELAs in the Oksu Valley of southeastern Tajikistan (Sidorov, 1960). The Indian summer monsoon itself, however, presently ends south of the NW-Himalaya and only infrequently moves up the larger valleys of the Hindu Kush and Karakoram (Weiers, 1995). It is unclear, however, whether the area of summer monsoon influence was larger in the past during periods of higher mid-latitude insolation (Prell & Kutzbach, 1987, Sirocko et al., 1996, Schulz et al., 1998).

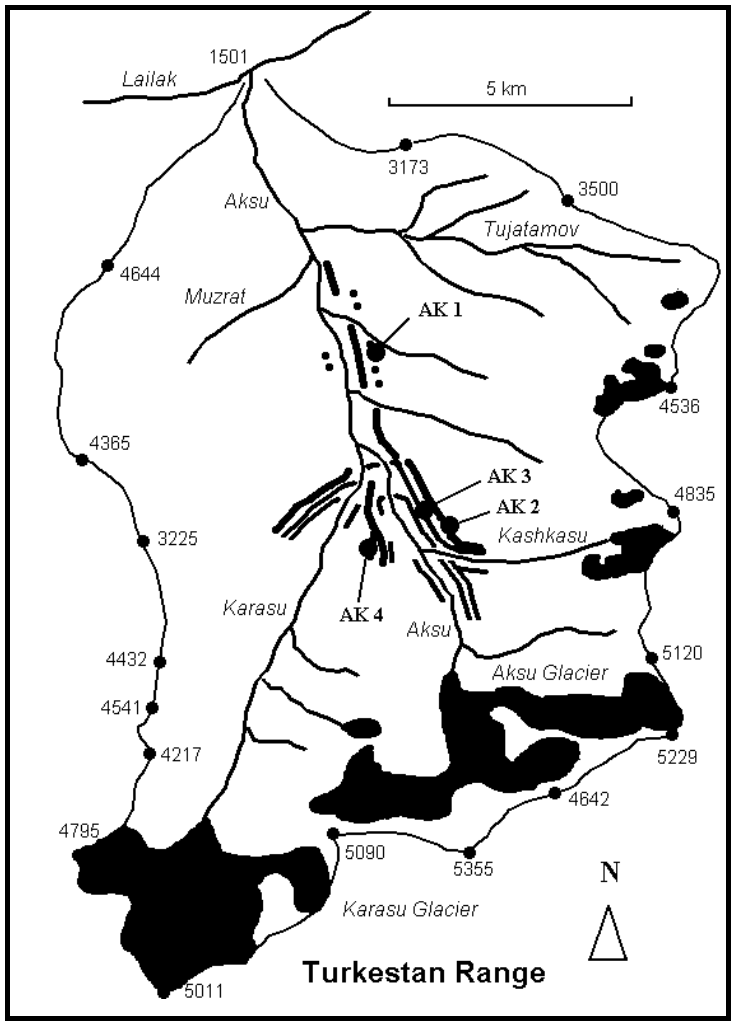

Fig. 5.2. Sketch of the Aksu catchment, Turkestan Range, Kyrgyzstan, with altitudes along the rim in m a.s.l. Recent glaciers are shown in black. Moraines from the lateglacial (narrow line), the last glacial maximum (bold line) and an older glaciation (dots) are illustrated as mapped in the field.

5.2.1.2 Aksu Valley, central Turkestan Range, Kyrgyzstan

The valley of the river Aksu (39.6°N, 69.5°E) is a south-north trending valley in the east-west-trending Turkestan Range (Fig. 5.1, 5.2). It has a semi-humid Central Asian climate with spring rains and dry summers. The recent Aksu and Karasu glaciers reach down to ~3350 m. The present local equilibrium line altitude (ELA), using a toe-to-headwall altitude ratio (THAR) of 0.5, is ~4110 m a.s.l. Huge lateral moraine walls of the local LGM glacier reach down to at least 1950 m a.s.l., implying an ELA depression of >750 m. Remnants of an older, more extensive glaciation are present above the LGM moraines in the form of isolated erratic granodiorite boulders along the valley sides. Based on soil development and weathering, these boulders have been interpreted to be remnants of a middle Pleistocene glacial advance (Glaser et al., 1999). Inside the LGM moraines, several younger

moraines have been identified, the most extensive one reaching down to 2600 m a.s.l., corresponding to an ELA depression of ~420 m.

For sampling, three of the isolated erratic boulders in 2440 m a.s.l. (AK1), boulders from the LGM lateral moraine 1) in 2900 m a.s.l. on the right valley side (AK2), and 2) in 2930 m a.s.l. on the left valley side (AK4), as well as boulders form the oldest late-glacial lateral moraine in 2860 m a.s.l. on the right valley side (AK3) were chosen.

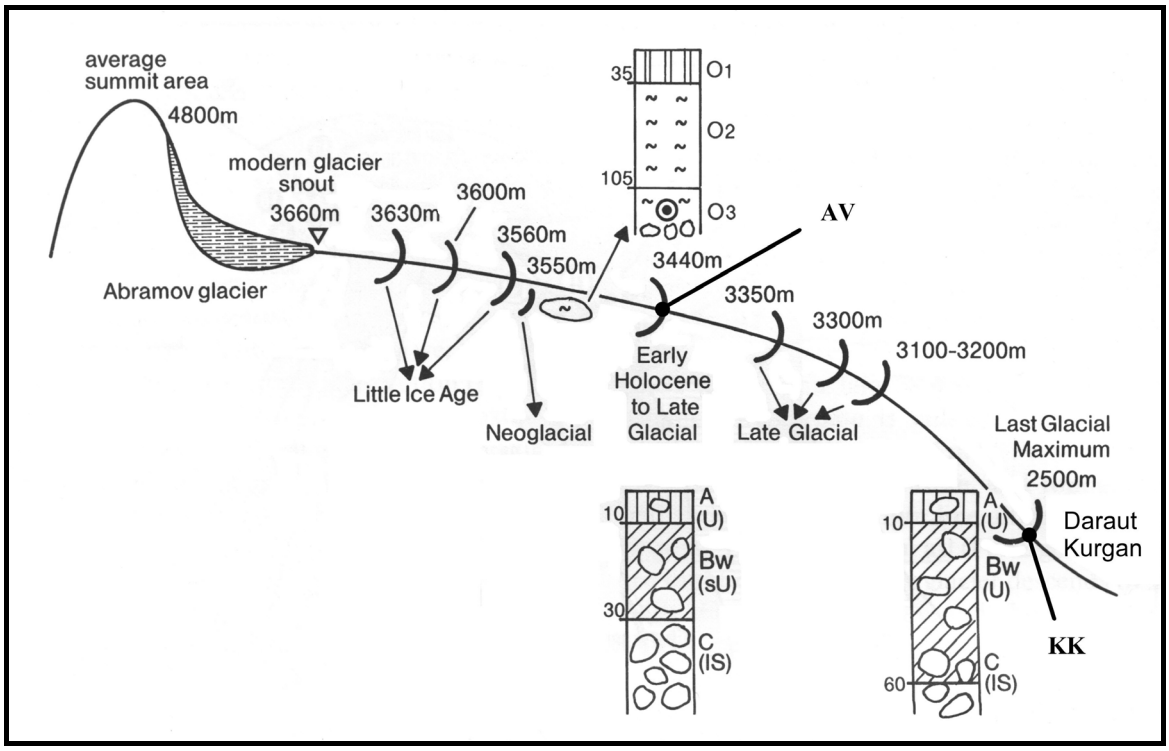

Fig. 5.3. Catena sketch of moraines in the Koksu Valley, Alay Range, Kyrgyzstan, with their tentative chronology. Sampled sites are indicated (AV, KK). Soil horizons are shown with depth in cm and horizon symbols (texture symbols). Modified from Zech et al., 2000b.

5.2.1.3 Koksu Valley, western Alay Range, Kyrgyzstan

The Koksu Valley (39.6°N, 72.0°E) originates at the Abramov glacier in the Alay Range, Kyrgyzstan (Fig. 5.1). Initially, it runs in south-north direction, but in its course describes a wide eastward loop of 180° until it enters the Alay Valley in north-direction and joins the westward-flowing Kyzylsu. It has a semiarid climate with a precipitation maximum in spring. Zech et al. (2000b) distinguish several moraine stages, which have been brought into a relative chronology using soil development and radiocarbon dating (Fig. 5.3). The present Abramov glacier has an ELA (THAR 0.5) of ~4230 m a.s.l.

The late-glacial or early Holocene moraine (AV) in 3440 m a.s.l. (ELA depression ~110 m) was sampled in order to determine whether or not it represents the Younger Dryas event, and the lowermost moraine at Daraut Kurgan (KK, 2500 m a.s.l., ELA depression ~600 m), was sampled in order to clear the timing and extent of the maximum last Pleistocene glaciation in this area.

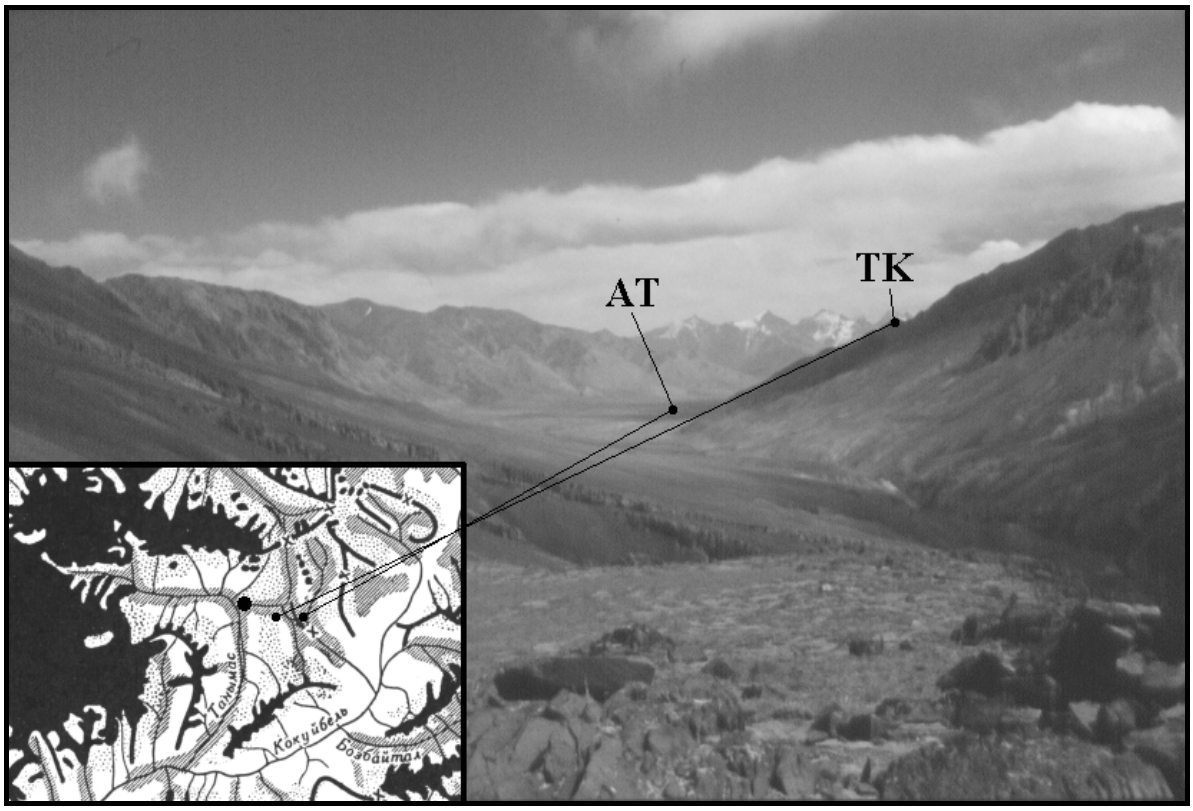

Fig. 5.4. View from the Kokjar transfluence pass eastward towards the Ailuitek Pass and the Muzkol Range. The inset map shows the maximum Pleistocene glaciation as reconstructed by Zabirov (1955). The point the photograph was taken from is shown in the map by a big dot. Sampling sites at Ailuitek Pass (AT) and on the high lateral moraine opposite the Takhtakorum valley entrance (TK) are depicted on both map and photo by small dots. *Танымас* = Tanymas, *Кокуйбель* = Kokuibel, *Бозбайтал* = Bozbaital. Crosses in the map depict passes.

5.2.1.4 Ailuitek Pass area, north-central Pamir, Tajikistan

Ailuitek Pass (38.6°N, 72.9°E) in the arid north-central Pamir is situated east of the Kokjar transfluence pass, at which the large Pleistocene Tanymas glacier, originating at the eastern margin of the Fedshenko glacier, split into a main trunk turning southward, and a secondary trunk continuing eastward. The eastward trunk at its maximum extent passed the Ailuitek and continued towards the Kokuibel River (Fig. 5.1, 5.4; Zabirov, 1955). This phase, which is associated with the *Bartang complex*, is marked by granite erratics originating from the upper Tanymas Valley. They are dominant on a large lateral moraine in

~4100 m a.s.l. at the south slope of the main valley opposite the entry of the Takhtakorum river (TK).

Still a few erratic granite boulders are present on a set of younger moraines on the valley bottom just west of the Ailuitek in ~3850 m a.s.l. These moraines are associated with the late Pleistocene *Badakhshan complex*. They were already described by Noeth (1931), and were obviously deposited by the local Takhtakorum and Shuralisu glaciers after the retreat of the secondary trunk of the Tanymas glacier. The granite boulders obviously were incorporated from older morainal deposits. After this retreat, the flow direction west of the Ailuitek has reversed itself, and the Kokjar river has incised ~300 m into the transfluence pass to join the Tanymas river (Noeth, 1931, Klebelsberg, 1934).

We sampled the granite boulders from the lateral moraine representing the last maximum glaciation of the Pamir (TK), as well as a remnant granite boulder and three quartz veins of schist boulders situated on the younger moraines at Ailuitek (AT), in order to determine 1) the timing of the *Bartang complex* of the Tanymas glacier and its retreat, which is constrained by the granite boulders deposited on the *Badakhshan complex* moraines, as well as 2) the age of the *Badakhshan complex* itself.

5.2.1.5 Lake Yashilkul area, Bogchigir Range, south-central Pamir, Tajikistan

Lake Yashilkul (37.8°N 72.8°E, Fig. 5.1, 5.5) is situated in the climatic transition zone between the semiarid western and the arid eastern Pamir, in the east-west-trending valley of the river Alichur. The geologic history of the lake has been discussed by Maximov (1992). At the western end of the lake, a big blocky landslide covers the valley floor. From the granodiorite Bogchigir Range in the south several small rivers enter the lake, the catchments of which have been fully glaciated in the Pleistocene.

In the Yashilkul basin, east of the lake, Sidorov & Sapov (1965) distinguish two typical late Pleistocene moraine generations, the younger one situated at the entrance or some way upstream in the second order valleys, the older one advancing 2-3 km into the main Alichur valley. At some places in the main valley, they recognize a third moraine generation as well, which is still older, subdued, and is assigned a middle Pleistocene age. At the deposition time of the oldest moraine, the glaciers formed a local piedmont glaciation in the broad, sediment-filled Alichur Valley.

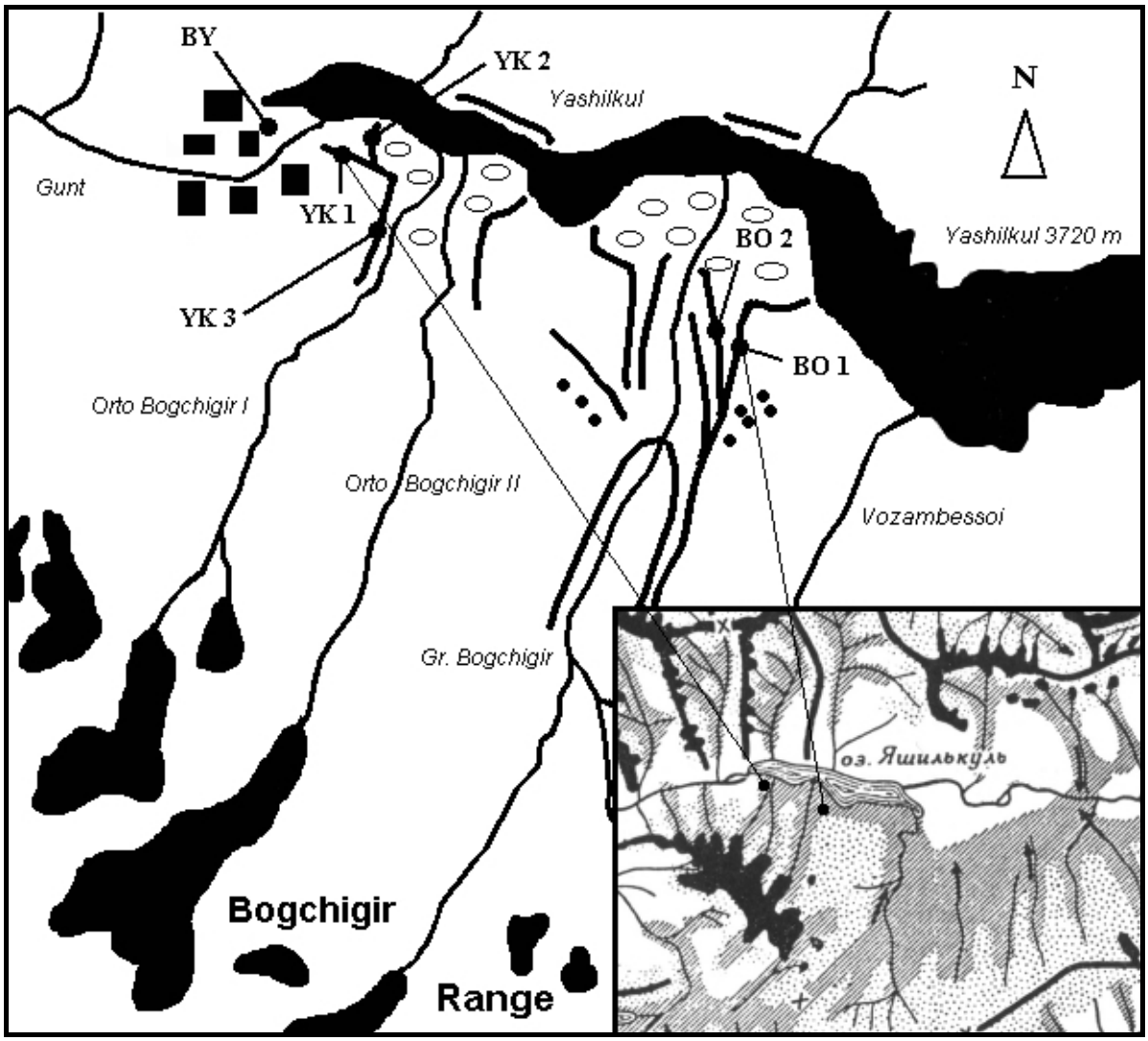

Fig 5.5. Sketch of lake Yashilkul area. The lake and recent glaciers are drawn in black, the landslide is shown by black rectangles, moraine walls by bold lines, hummocky relief by white ellipses; isolated erratics are depicted by small black dots, sampled sites by large black dots. The inset map shows maximum Pleistocene glaciation of the area as reconstructed by Zabirov (1955). *Оз. Яшилькуль* = lake Yashilkul.

At lake Yashilkul, the oldest moraine generation is represented by an east-west-trending latero-frontal moraine on the left shore of the westernmost lake (Fig. 5.5, YK1). It is characterized by a subdued surface morphology with unclear outer slopes, some intensely tafonized boulders, a relatively dense vegetation and a relatively dark surface colour. At its western end, the wall is covered by the above-mentioned landslide. Zabirov (1955) has taken this oldest stage as indicative of the maximum Pleistocene glaciation. Dodonov (2002) correlates moraines of this kind in the Alichur Valley with the early Pleistocene *East-Pamir complex*.

High lateral moraines are present on the side-slopes of the tributary valleys, e.g. the Orto Bogchigir I Valley (Fig. 5.5, YK3), or the Gr. Bogchigir Valley (Fig. 5.5, BO 1), which

also feature the dark surface colour of the oldest moraine YK1. They may belong to the deposits of the oldest glacial advance documented in the region. They may however, belong to the deposits of the next younger glacial advance as well: inside these lateral moraines, the valley floors are covered by light-coloured, streamlined ground moraine, which enters the main valley in lobes of equally light-coloured latero-frontal moraine. The latter are characterized by a hummocky, barely vegetated surface and terminate in clearcut walls with steep slopes (Fig. 5.5). These "chukur" lobes cover the lower ends of the lateral moraines as well, but they do not reach the extent of the older moraine YK1, and do not merge into a complete piedmont cover. Moraines like these have been correlated with the first late Pleistocene advance by Sidorov & Sapov (1965). Dodonov (2002) associates them with the middle Pleistocene *Murgab complex*. This moraine stage was sampled both at the Orto Bogchigir I (on the outer wall, YK2), and at the Gr. Bogchigir (on a recession wall some way inside the lobe, BO2), as shown in Fig. 5.5.

All moraines described reach down to ~3800 m a.s.l. The recent ELA (THAR 0.5) in this area is 4970 m a.s.l. (Wissmann, 1959), implying an ELA depression for both glacial advances of ~370 m, which has also been noted by Dodonov (2002). All mentioned walls as well as the landslide covering YK1 (BY) have been sampled to provide a chronology of the maximum glaciation, and the typical "chukur" lobes of the next younger generation.

5.2.1.6 Kol-Uchkol and Gurumdy Valleys, southern Alichur Range, southeast-central Pamir, Tajikistan

The valleys of the rivers Kol-Uchkol (37.7°N, 73.7°E) and Gurumdy (37.6°N, 73.9°E) both are south-north trending valleys in the eastern part of the southern Alichur Range, in the cold, arid eastern Pamir (Fig. 5.1, 5.6). Recent glaciation in the area is sparse. The local ELA (THAR 0.5) is ~5050 m a.s.l. Several moraine ridges can be distinguished in the area, which is one of the type localities for the late Pleistocene *Alichur complex* (Vasilev, 1966).

The oldest deposits attributable to past glaciations in the Kol-Uchkol-Gurumdy area are single granodiorite boulders lying on broad valley shoulders above about 4400 m a.s.l. in a matrix of weathered local schists. According to their characteristics and altitude, they belong to the early Pleistocene *East-Pamir complex* (Dodonov, 2002). On the other hand, boulders of this kind are considered to be typical remnants of a late Pleistocene ice sheet covering the whole eastern Pamir plateau (Kuhle, 1997). Boulders from these deposits have been sampled in both catchments (Fig. 5.6, UK1, GU1).

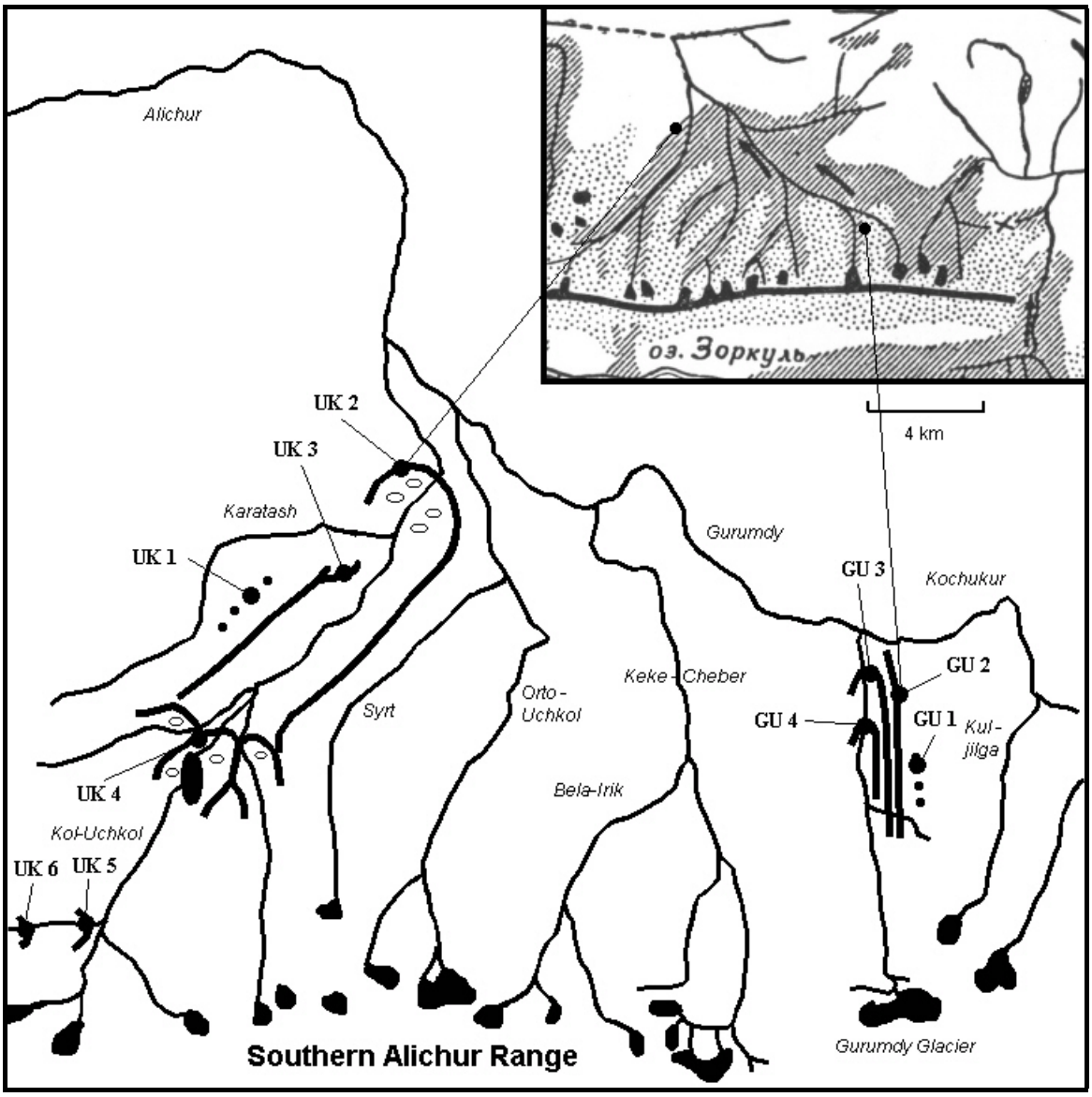

Fig 5.6. Sketch of Kol-Uchkol-Gurumdy area. Lakes and recent glaciers are drawn in black, moraine walls shown by bold lines, hummocky surface by white ellipses; single erratics are depicted by small black dots, sampled sites by large black dots. Inset map shows maximum Pleistocene glaciation of the area as reconstructed by Zabirov (1955). *Оз. Зоркуль* = lake Zorkul.

The next younger moraine generation is a large set of latero-frontal moraines, which are remnants of a local piedmont glaciation with an ELA depression of ~380 m and have been mapped as the maximum Pleistocene glaciation by Zabirov (1955). Because of their typical "chukur" morphology and altitude, they are associated with the middle Pleistocene *Murgab complex* (Dodonov, 2002). The frontal lobe was sampled at the lower Kol-Uchkol (Fig. 5.6, UK2) and the corresponding lateral moraine in the upper Gurumdy catchment (Fig. 5.6, GU2). In the Kol-Uchkol catchment, the latero-frontal moraine of a recessional stage (Fig. 5.6, UK3) of the UK 2 moraine was also sampled. This deposit is situated at the foot

of an kolluvial fan, which has eroded the older lateral moraine(s) above, but is separated from the fan surface by a natural ditch.

At the border between the upper part of the Kol-Uchkol catchment, framed by high mountains, and the lower part, surrounded by the shoulders of the oldest glaciation, a large moraine deposit is situated in the valley bottom, which is clearly a composite of glacial deposits from the main and two tributary valleys meeting at this location (Fig. 5.6, UK4). The corresponding glacier advance was characterized by an ELA depression of ~290 m. In the Gurumdy Valley, two correlative moraines (Fig. 5.6, GU3, GU4) are present, implying ELA depressions of ~320 m and ~280 m, respectively. In a small tributary of the Kol-Uchkol Valley, two further recessional moraines (Fig. 5.6, UK5, 6), characterized by ELA depressions of ~210 m and ~170 m, respectively, can be found. All these moraines belong to the *Alichur complex* (Dodonov, 2002).

All mentioned moraines were sampled in order to develop a concise glacial chronology for the southeast-central Pamir.

5.2.2 ^{10}Be surface exposure dating

For ^{10}Be surface exposure dating (SED), chunks of up to 8 cm thickness have been loosened by hammer and chisel from the centre surfaces of the largest and tallest boulders positioned on the culminations of each sampled deposit. Boulders showing signs of spalling or recent dislocation were avoided. Position and altitude were read from a global positioning system (GPS) receiver and barometric altimeter combination. Topographic shielding and surface inclination of the boulders were noted using a compass and inclinometer. Samples were analyzed for ^{10}Be following the procedure of Kohl & Nishiizumi (1992) as modified by Ivy-Ochs (1996). ^{10}Be/^{9}Be was measured at the AMS facility of the Paul Scherrer Institute at the ETH Zurich and corrected to conform with ICN standards (Nishiizumi et al., 1989).

Calculation of the exposure ages was done using TEBESEA (section 2), employing the scaling system of Lal (1991) as modified by Stone (2000) with a standard ^{10}Be production rate at sea level in high latitude (SLHL) of 5.35 ± 0.15 atoms g^{-1} a^{-1}, a negative muon capture contribution to SLHL production of 1.2%. The influence of surface erosion, tectonic uplift and snow cover has been estimated by calculating a minimum exposure age, assuming no erosion, uplift and cover, as well as a maximum exposure age, assuming a conser-

vative maximum surface erosion rate of 3 ± 2 mm ka^{-1} (section 3), a tectonic uplift rate of 3 ± 2 mm a^{-1}, and a mean annual snow cover of 5 ± 3 g cm^{-2}. The tectonic uplift rate used is a good approximation of published values for Pamir uplift, which range from 1-4 mm (Dodonov, 2002). Where stated, a modified scaling system of Dunai (2001) has been used for comparison, employing a standard ^{10}Be production rate at sea level in high latitude (SLHL) of 5.47 ± 0.31 atoms g^{-1} a^{-1}, a negative muon capture contribution to SLHL production of 1.9%, and a fast muon reaction contribution of 1.7% (section 2). Muon contributions in this case were scaled as proposed by Schaller et al., (2002).

All surface exposure ages taken from the literature for comparison have been recalculated following the calculation scheme applied here and therefore may be slightly different from values given in the original papers. Interpretation of the exposure age distributions followed the scheme proposed in section 3.

5.3 Results & Discussion

5.3.1 Aksu Valley (Turkestan Range)

All moraines in the Aksu Valley, notwithstanding their different stratigraphical ages, yield similar distributions of erratic boulder exposure ages, which range from 9 to 25 ka (Tab. 5.1, Fig. 5.7A). A radiocarbon date of 21,226 ± 146 a B.P. (~24 cal. ka B.P.), however, has been found by analyzing humic substances from a buried A horizon in a depression on the youngest of the proposed lateglacial moraines (W. Zech, unpubl.). Thus, the exposure age of 25 ka on the oldest of the proposed lateglacial moraines (AK3) may be considered closest to the deposition age of the respective moraine. All other studied moraine surfaces in the valley must have experienced heavy degradation during the end of the last glacial, so that no boulder exposed ever since deposition was selected even by careful sampling.

Comparison with the Koksu chronology reported below suggests that the maximum late Pleistocene glacier advance with an ELA depression of >750 m, having left moraines AK2 and 4, probably occurred during MIS 4-3. The older remnants (AK1), accordingly, may still be considered to be of middle Pleistocene age (Glaser et al., 1999). The distribution of the exposure ages (Fig. 5.7A) suggests phases of accelerated moraine degradation around 22 ka, 20-16 ka, and 12-10 ka, which affected all older moraines in the valley, indicating a harsh climate with sparse vegetation during the last high and late glacial phases, as well as during the Pleistocene-Holocene transition. In the early MIS 2, instead, there may have

been phases relatively humid and warm, shown by the buried soil on the third moraine of the youngest Pleistocene generation.

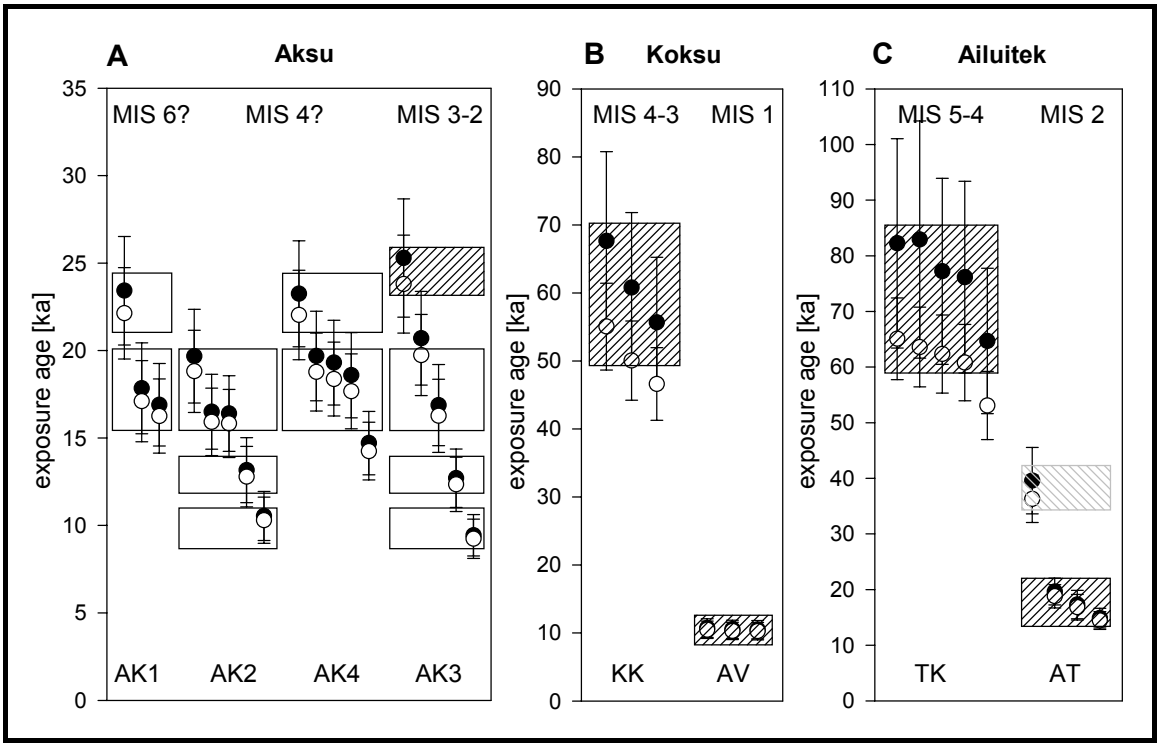

Fig. 5.7. Interpretation of exposure ages from the A) Aksu, B) Koksu, and C) Ailuitek areas. Minimum ages are depicted by white dots, conservative maximum ages by black dots. Samples interpreted to be affected by inheritance in boxes cross-hatched in grey, phases of glacier advance in boxes cross-hatched in black, phases of moraine degradation in white boxes. Note different timescales. See text for explanation.

5.3.2 Koksu Valley (Alay Range)

Exposure ages of 47-68 ka from the moraine at the entrance of the Koksu Valley (Tab. 5.1, Fig. 5.7B) indicate deposition during the MIS 4 or early MIS 3, which shows that the maximum late Pleistocene advance in this area with an ELA depression of ~600 m occurred early during the last glacial. This is supported by the radiocarbon date of 24,300 ± 1160 ^{14}C a B.P. (~28 cal. ka B.P.) from a buried soil on top of a correlated lateral moraine in the upper catchment (Zech et al., 2000b), as well as by TL ages of 16.4 ± 1.5 and 13.2 ± 1.4 ka (W. Zech, unpubl.) from loess covering a younger wall in the Koksu Valley in 2700 m a.s.l. This second wall has probably been deposited during the late MIS 3 or early MIS 2, as the dated loess cover is separated from the till by a buried cambic horizon. By analogy of ELA depression, the maximum late Pleistocene advances reported from the Hissar Range (ELA depression 750 m), from the Kichik Alay (ELA depression 600 m, Zech et al., 2000a, Baeumler, 2001), and perhaps even from the Pskem Range (ELA depression 700-

800 m, Zech et al., 1996) and the northwestern Tian Shan (ELA depression ~800 m, Heuberger & Sgibnev, 1998, Baume, 2002), probably have occurred early in the late Pleistocene as well. As in the Aksu Valley (section 5.3.1), the proposed late-glacial advances in all these areas probably have occurred already during the early and high last glacial. This chronology is supported by other recently published ^{10}Be exposure ages from western Central Asia (Gillespie et al., 2003).

The proposed Younger Dryas moraine in 3440 m a.s.l. unambiguously yields exposure ages of ~10.5 ka (Tab. 5.1, Fig. 5.7B), which are in agreement with the radiocarbon date of 7290 ± 80 ^{14}C a B.P. (~9 cal. ka B. P.) of a buried A horizon on top of a similar moraine in 3490 m a.s.l. in the Kichik Alay (Zech et al., 2000a, Baeumler, 2001). It apparently postdates the Younger Dryas event (YD, 11.5-12.9 cal. ka B.P.) by about 1500 years. Probably, the increasing moisture supply at the beginning of the Holocene had a larger effect on the advancing Abramov glacier than the temperature decrease during the YD. The moisture sensitivity of this glacier may also explain the maximum advance during the late MIS 4-early MIS 3.

5.3.3 Ailuitek Pass area (north-central Pamir)

Four of five exposure ages from the high lateral moraine TK opposite the Takhtakorum valley lie between 61 and 83 ka, covering the late MIS 5 and the MIS 4, the fifth is slightly younger (Tab. 5.1, Fig. 5.7C). Thus, the last maximum advance in this region documented by moraines probably has not occurred during the middle Pleistocene, as suggested by most Russian researchers (Dodonov, 2002), but during the early late Pleistocene. As the dated boulders are from a lateral moraine well behind the end moraines of the respective advance, its maximum may even have occurred somewhat earlier, but still after the last interglacial.

The isolated granite boulder left on the younger moraines, AT11, has an exposure age of 36-40 ka (Tab. 5.1, Fig. 5.7C). Because it is indeed affected by inheritance, the ages of the other AT boulders being significantly younger, it provides a minimum time for the recession of the Tanymas glacier behind the Kokjar. This recession probably has occurred earlier than implied by the exposure age, because the boulder most likely has been rotated during its incorporation into the younger moraine. If glacier recession behind the Kokjar pass is assumed to have occurred at the beginning of the last interglacial ~50 ka B.P., the 300 m fluvial incision of the Kokjar (Noeth, 1931) would have proceeded at a maximum

rate of ~6 mm a^{-1}. This value compares well with studies in the Karakoram and western Himalaya (Burbank et al., 1996, Leland et al., 1998), which have yielded fluvial incision rates of 1-12 mm a^{-1}.

The other three exposure ages from the younger moraines at the Ailuitek lie between 14 and 20 ka (Tab. 5.1, Fig. 5.7C), documenting the associated glacier advance to have occurred during the MIS 2, in accord with their stratigraphic interpretation in the Russian literature, where they belong to the typical Q_3 deposits (Dodonov, 2002).

5.3.4 Lake Yashilkul area (Bogchigir Range)

At lake Yashilkul, the boulders from the oldest moraine, YK1, yield exposure ages ranging between 58 and 84 ka, covering the MIS 4 and late MIS 5 (Tab. 5.1, Fig. 5.8). These ages are in excellent agreement with the ages found on the TK moraine (section 5.3.3). Therefore, YK1 most probably was deposited early in the last glacial, at a time of maximum ice extent in the Pamir as mapped by Zabirov (1955). The only interpretation of the exposure ages in agreement with an early or middle Pleistocene age of this moraine (Dodonov, 2002, Sidorov & Sapov, 1965, respectively) would be that all boulders from YK1 are affected by intensive desquamation and have ^{10}Be concentrations in equilibrium between production and surface erosion. This appears to be unlikely given the properties of the sampled boulder surfaces and given the good agreement of all 7 boulder ages. The landslide BY covering YK1 is shown to be a middle Holocene feature by all exposure ages closely clustering around 5.0 ka.

The age of the second moraine generation, however, is problematic. The ages obtained from the outer wall of the Orto Bogchigir lobe (YK2) scatter between 18 ka and 61 ka, while the ages of the recessional wall inside the Gr. Bogchigir lobe (BO2) closely group around 18 ka (Tab. 5.1, Fig. 5.8). The latter wall is situated well outside the second late Pleistocene stage as described by Sidorov & Sapov (1965), which is well expressed upstream in the Gr. Bogchigir Valley (Fig. 5.5). Unfortunately, this wall has not yet been dated. The ages of the high lateral moraines YK3 and BO1, in turn, scatter between 12 and 65 ka, clustering around 41, 30, 22, and 12 ka (Tab. 5.1, Fig. 5.8). While the ages below 40 ka on the lateral moraines YK3 and BO1 can easily be explained by moraine degradation, the older ages of these moraines taken together with the exposure ages of the Orto Bogchigir lobe (YK2) allow two ways of interpretation (Fig. 5.8A, B):

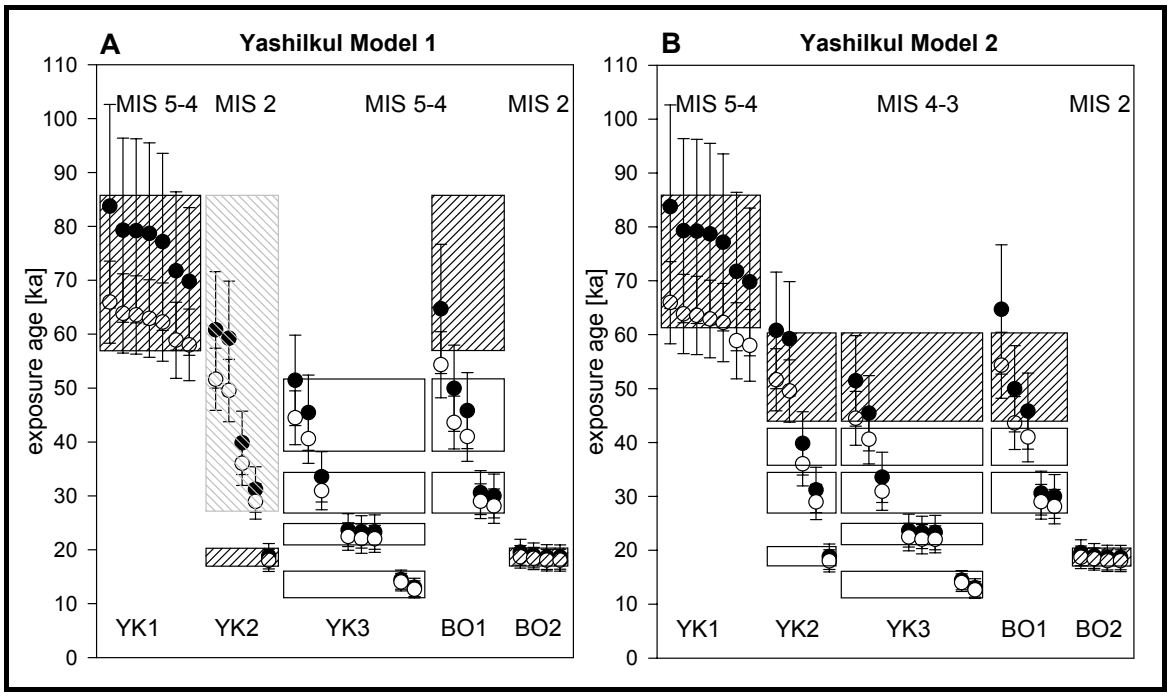

Fig. 5.8. Competing interpretations A, B of exposure ages from lake Yashilkul area. Minimum ages are depicted by white dots, conservative maximum ages by black dots. Samples interpreted to be affected by inheritance in boxes cross-hatched in grey, phases of glacier advance in boxes cross-hatched in black, phases of moraine degradation in white boxes. See text for explanation.

1) The lateral moraines belong to the older moraine generation (like YK1) deposited during the MIS 5-4, and have been degraded in later times, leaving only one exposure age on BO1 close to the deposition age (Fig. 5.8A). The younger lobes were deposited later, at some time before 18 cal. ka B.P. The older ^{10}Be ages on the Orto Bogchigir lobe (YK2) then have to be explained by inheritance. Preexposure of the YK2 boulders is possible, because the younger advance may have incorporated some of the till of the older moraine, which in fact has been taken to be a prerequisite for the generation of hummocky moraines (Hambrey et al., 1997, Eyles et al., 1999). However, it does not altogether seem likely, given the measured age distribution. The probability of getting two boulders with close maximum ages by a selection of five out of a distribution of randomly incorporated preexposed boulders is rather low, even if such boulders may be concentrated on the outer wall by upthrust, or may have unintentionally been picked out in preference because of their surface properties. Another problematic point in this hypothesis is the similarity of ELA depressions of both advances. Such a similarity is not found for the early and late glacier advances of the last glacial cycle in the Kol-Uchkol and Gurumdy valleys (section 5.3.5).

2) The lateral moraines (YK3, BO1) have been deposited along with of the younger lobes (YK2) during the early MIS 3, 60-40 cal. ka B.P. (Fig. 5.8B). The period 52-45 cal. ka B.P. has been a cold phase in western High Asia as shown by the δ^{18}O record from the Guliya

ice core (Thompson et al., 1997). This hypothesis is supported by the similarity of ELA depression between YK1 and YK2 (both ~370 m). However, it makes it difficult to explain the different surface characteristics of the younger and older moraines, and the obviously much younger age of the recessional stage represented by BO2. Zech et al. (2004) have explained the distribution of exposure ages on YK2 with long lasting ice-decay, which, in their opinion, is also responsible for the generation of the hummocky relief. However, the typical boulder distribution in pockets and stripes expected to be present on moraines affected by ice-decay (Kjaer & Krueger, 2001) has not been observed on the lobes.

At present, there is no way of deciding between the two hypotheses. Future ^{10}Be SED in the area may help to solve the problem. However, it remains clear that the interpretation of Dodonov (2002), placing the older moraines into the early and the younger hummocky lobes into the middle Pleistocene, needs revision. The interpretation of Sidorov & Sapov (1965) may be right concerning the younger lobes, but not concerning the older moraines.

Remnants of a middle Pleistocene advance in the lake Yashilkul area may be present in the form of isolated boulders above the clear-shaped moraines (Fig.5.5), which have not been sampled for this study.

5.3.5 Kol-Uchkol & Gurumdy area (Southern Alichur Range)

The oldest glacial deposit in the southern Alichur Range area, isolated erratic boulders on a shoulder in above 4400 m a.s.l. in the Kol-Uchkol Valley (UK1), yielded exposure ages of 66-86, and 93-136 ka (Tab. 5.1, Fig. 5.9A). If the highest age is considered to be the one closest to the deposition age of these boulders, they were left by an MIS 5 or MIS 6 advance. If, as Kuhle (1997) believes, they have been left by a plateau glacier covering the whole plateau with a height of more than 1000 m, this glaciation must have ended within the MIS 5. If, as we think is more likely, these boulders are remnants of a moraine the matrix of which has been completely washed away, the moraine most probably was left by a middle Pleistocene or even earlier advance. The same deposit in the Gurumdy Valley (GU1, Tab. 5.1, Fig. 5.9B) has yielded exposure ages only below 70 ka, which show that the deposit has been degrading all through the late Pleistocene. Phases of accelerated moraine degradation may be recognized at 40-50, around 25, and around 20 cal. ka B.P., close to dated or inferred glacial advances in the region (see below). Moraine degradation may have occurred in association with solifluction activity, which has been high in this area all over the Pleistocene (Gorbunov & Seversky, 1999). Even if we cannot decide,

whether the deposit represented by UK1 and GU1 is of middle Pleistocene or earlier age, it is certainly older than the last Pleistocene maximum as mapped by Zabirov (1955).

The maximum glaciation of Zabirov (1955) in the Kol-Uchkol-Gurumdy area is represented by the deposits UK2 and GU2 (Tab. 5.1, Fig. 5.9B) with an ELA depression of 380 m. The oldest boulders of UK2 yield exposure ages of 57-75 ka, covering the MIS 4. These ages most likely represent the end of the respective glacial advance, as boulder UK28 is situated several 100 m behind the end moraine wall. They show that the typical "chukur" moraine of this maximum advance was deposited early in the last glacial cycle and does not belong to the middle Pleistocene, as assumed by some Russian researchers (Pakhomov & Nikonov, 1977, Dodonov, 2002). The correlative lateral moraine in the Gurumdy catchment GU2 yields exposure ages below 60 ka only (Tab. 5.1, Fig. 5.9B). As they parallel the ages from the older GU1 deposit, these ages are obviously all degradation ages.

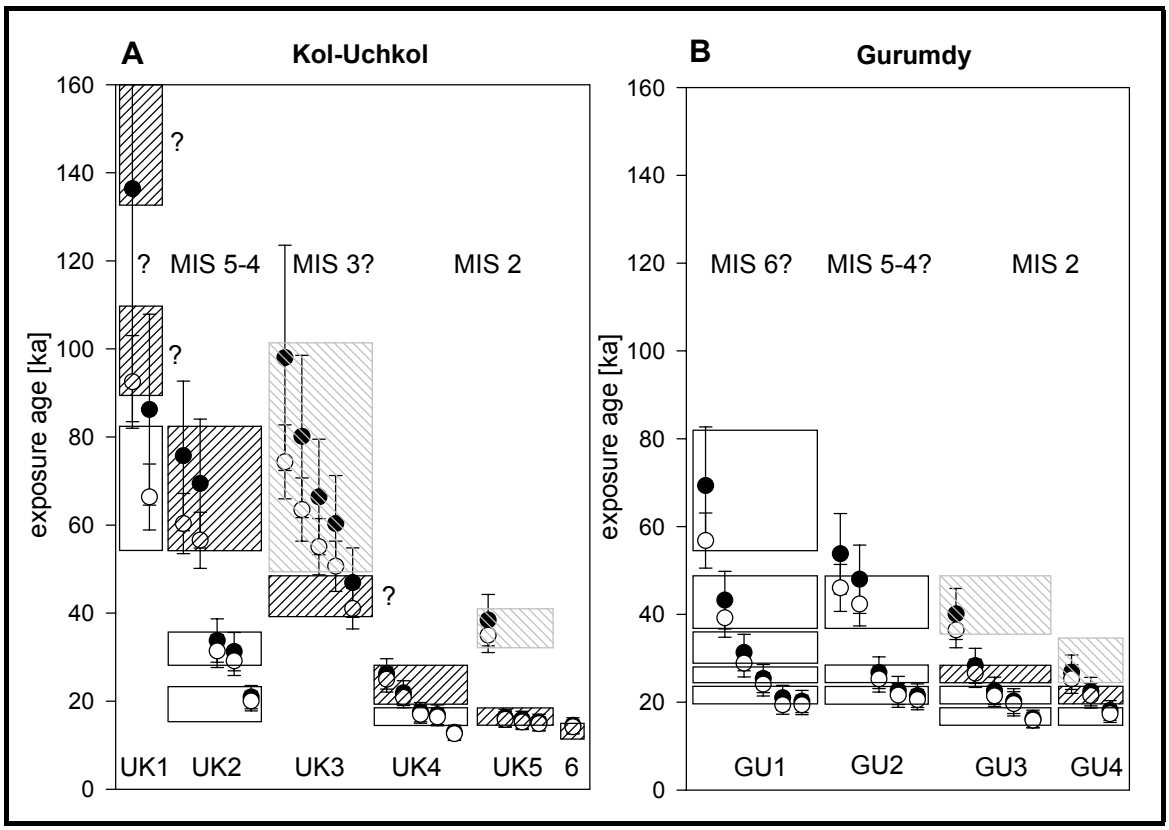

Fig. 5.9. Interpretation of exposure ages from the A) Kol-Uchkol and B) Gurumdy catchments. Minimum ages are depicted by white dots, conservative maximum ages by black dots. Samples interpreted to be affected by inheritance in boxes cross-hatched in grey, phases of glacier advance in boxes cross-hatched in black, phases of moraine degradation in white boxes. See text for explanation.

Tab. 5.1. Results of ^{10}Be surface exposure dating in Central Asia.

Sample ID	Latitude [°N]	Longitude [°E]	Altitude [m]	f_{ST}, n[1]	f_{ST}, μ[2]	α[3] [°]	d[4] [cm]	^{10}Be [10^6 atoms g^{-1}]	Min. exposure age [ka]	Max. exposure age [ka]	Dunai / Lal[4]
AK11	39.6	69.5	2240	0.978	0.974	0	4	0.462 ± 0.036	16.3 ± 2.1	16.9 ± 2.4	0.99
AK12	39.6	69.5	2240	0.978	0.974	0	4	0.638 ± 0.035	22.1 ± 2.6	23.4 ± 3.1	0.99
AK13	39.6	69.5	2240	0.978	0.974	0	4	0.487 ± 0.042	17.1 ± 2.3	17.8 ± 2.6	0.99
AK21	39.6	69.5	2900	0.980	0.977	0	4	0.821 ± 0.056	18.8 ± 2.4	19.7 ± 2.7	0.95
AK22	39.6	69.5	2900	0.980	0.977	0	4	0.447 ± 0.033	10.3 ± 1.3	10.5 ± 1.4	0.95
AK23	39.6	69.5	2900	0.980	0.977	0	4	0.551 ± 0.047	12.8 ± 1.7	13.2 ± 1.9	0.95
AK24	39.6	69.5	2900	0.980	0.977	0	4	0.686 ± 0.045	15.8 ± 2.0	16.4 ± 2.2	0.95
AK25	39.6	69.5	2900	0.980	0.977	0	4	0.690 ± 0.042	15.9 ± 1.9	16.5 ± 2.1	0.95
AK31	39.6	69.5	2860	0.983	0.981	0	4	0.391 ± 0.024	9.2 ± 1.1	9.4 ± 1.2	0.95
AK32	39.6	69.5	2860	0.983	0.981	0	4	1.032 ± 0.055	23.8 ± 2.8	25.3 ± 3.4	0.95
AK33	39.6	69.5	2860	0.983	0.981	0	4	0.845 ± 0.045	19.7 ± 2.3	20.7 ± 2.7	0.95
AK34	39.6	69.5	2860	0.983	0.981	0	4	0.691 ± 0.052	16.3 ± 2.1	16.9 ± 2.3	0.95
AK35	39.6	69.5	2860	0.983	0.981	0	4	0.522 ± 0.036	12.4 ± 1.6	12.7 ± 1.7	0.95
AK41	39.6	69.5	2930	0.987	0.989	0	4	0.995 ± 0.051	22.0 ± 2.6	23.3 ± 3.0	0.94
AK42	39.6	69.5	2930	0.987	0.989	0	6	0.815 ± 0.038	18.4 ± 2.1	19.3 ± 2.4	0.94
AK43	39.6	69.5	2930	0.987	0.989	0	8	0.774 ± 0.047	17.7 ± 2.1	18.6 ± 2.4	0.94
AK44	39.6	69.5	2930	0.987	0.989	0	5	0.837 ± 0.047	18.8 ± 2.2	19.7 ± 2.6	0.94
AK45	39.6	69.5	2930	0.987	0.989	0	4	0.631 ± 0.031	14.3 ± 1.7	14.7 ± 1.8	0.94
AV1	39.6	72.0	3440	1.000	1.000	0	4	0.623 ± 0.041	10.3 ± 1.3	10.5 ± 1.4	0.91
AV2	39.6	72.0	3440	1.000	1.000	0	4	0.627 ± 0.039	10.3 ± 1.3	10.6 ± 1.3	0.91
AV3	39.6	72.0	3440	1.000	1.000	0	4	0.637 ± 0.040	10.5 ± 1.3	10.7 ± 1.4	0.91
KK1	39.6	72.0	2500	1.000	1.000	0	4	1.850 ± 0.087	50.1 ± 5.8	61 ± 11	0.97
KK2	39.6	72.0	2500	1.000	1.000	0	4	2.019 ± 0.094	55.1 ± 6.4	68 ± 13	0.97
KK3	39.6	72.0	2500	1.000	1.000	0	4	1.727 ± 0.076	46.6 ± 5.3	56 ± 10	0.97
AT11	38.6	72.9	3857	0.997	0.996	0	2	2.892 ± 0.151	36.3 ± 4.3	39.6 ± 6.0	0.89
AT13	38.6	72.9	3856	0.994	0.992	0	2	1.254 ± 0.111	16.8 ± 2.3	17.3 ± 2.5	0.89
AT21	38.6	72.9	3836	0.997	0.996	5	4	1.391 ± 0.052	18.8 ± 2.1	19.7 ± 2.4	0.89
AT22	38.6	72.9	3836	0.996	0.994	0	4	1.055 ± 0.040	14.4 ± 1.6	14.9 ± 1.8	0.89
TK11	38.7	72.9	4088	0.988	0.985	15	2	5.575 ± 0.210	62.3 ± 7.0	77 ± 17	0.84
TK12	38.7	72.9	4090	0.997	0.996	25	2	4.796 ± 0.216	53.1 ± 6.1	65 ± 13	0.84
TK13	38.7	72.9	4094	0.998	0.997	25	2	5.458 ± 0.205	60.8 ± 6.9	76 ± 17	0.84
TK14	38.7	72.9	4131	0.997	0.995	15	2	6.016 ± 0.226	65.1 ± 7.3	82 ± 19	0.84
TK15	38.7	72.9	4134	1.000	1.000	33	2	5.739 ± 0.215	63.6 ± 7.2	83 ± 21	0.83
BY1	37.8	72.7	3770	0.996	0.995	0	3	0.315 ± 0.022	4.7 ± 0.6	4.8 ± 0.6	0.91
BY4	37.8	72.7	3770	0.995	0.993	0	3	0.336 ± 0.036	5.1 ± 0.8	5.1 ± 0.8	0.91
BY6	37.8	72.7	3770	0.994	0.993	0	5	0.295 ± 0.029	4.4 ± 0.6	4.5 ± 0.7	0.91
BY8	37.8	72.7	3760	0.995	0.993	0	3	0.310 ± 0.029	4.7 ± 0.7	4.7 ± 0.8	0.91
BY10	37.8	72.7	3760	0.995	0.993	0	4	0.345 ± 0.029	5.2 ± 0.7	5.3 ± 0.7	0.91
YK11	37.8	72.8	3815	0.997	0.996	0	2	4.480 ± 0.191	58.0 ± 6.6	70 ± 14	0.86
YK12	37.8	72.8	3815	0.997	0.996	0	5	4.823 ± 0.201	62.9 ± 7.2	79 ± 17	0.86
YK14	37.8	72.8	3820	0.997	0.996	0	3	4.814 ± 0.230	62.3 ± 7.3	77 ± 16	0.86
YK15	37.8	72.8	3815	0.997	0.996	0	3	4.541 ± 0.250	58.9 ± 7.1	72 ± 15	0.86
YK16	37.8	72.8	3815	0.997	0.996	0	3	5.099 ± 0.230	65.9 ± 7.6	84 ± 19	0.86

Tab. 5.1 continued.

Sample ID	Latitude [°N]	Longitude [°E]	Altitude [m]	f_{ST}, n[1]	f_{ST}, μ[2]	α[3] [°]	d[4] [cm]	^{10}Be [10^6 atoms g^{-1}]	Min. exposure age [ka]	Max. exposure age [ka]	Dunai / Lal[5]
YK17	37.8	72.8	3830	0.997	0.996	0	2	4.972 ± 0.220	63.9 ± 7.4	79 ± 17	0.86
YK18	37.8	72.8	3830	0.997	0.996	0	2	4.950 ± 0.206	63.6 ± 7.3	79 ± 17	0.86
YK20	37.8	72.8	3770	0.998	0.998	0	1	3.934 ± 0.138	51.6 ± 5.8	61 ± 11	0.87
YK21	37.8	72.8	3755	0.997	0.996	0	3	3.759 ± 0.180	49.6 ± 5.8	59 + 11	0.87
YK23	37.8	72.8	3755	0.997	0.996	0	4	1.251 ± 0.059	18.0 ± 2.1	18.8 ± 2.4	0.89
YK25	37.8	72.8	3755	0.998	0.998	0	4	2.091 ± 0.086	29.0 ± 3.3	31.2 ± 4.2	0.89
YK29	37.8	72.8	3770	0.998	0.998	0	5	2.676 ± 0.117	36.0 ± 4.1	39.8 ± 5.9	0.89
YK30	37.8	72.8	3945	0.999	0.998	0	5	1.059 ± 0.054	14.0 ± 1.6	14.5 ± 1.8	0.88
YK31	37.8	72.8	4040	0.997	0.996	0	6	1.781 ± 0.082	22.0 ± 2.5	23.3 ± 3.0	0.88
YK32	37.8	72.8	4040	0.997	0.996	0	5	1.792 ± 0.115	22.1 ± 2.7	23.3 ± 3.2	0.88
YK33	37.8	72.8	4040	0.997	0.996	0	4	1.834 ± 0.082	22.5 ± 2.6	23.7 ± 3.0	0.88
YK34	37.8	72.8	4035	0.998	0.997	0	3	3.926 ± 0.147	44.5 ± 5.0	51.4 ± 8.4	0.86
YK35	37.8	72.8	4020	0.998	0.997	0	3	3.520 ± 0.132	40.6 ± 4.6	45.4 ± 7.0	0.87
YK36	37.8	72.8	4006	0.998	0.997	0	4	2.567 ± 0.112	30.9 ± 3.5	33.5 ± 4.7	0.88
YK37	37.8	72.8	3960	0.999	0.998	0	5	0.963 ± 0.063	12.7 ± 1.6	13.0 ± 1.7	0.88
BO11	37.7	72.8	4250	0.994	0.992	0	1	2.698 ± 0.102	29.0 ± 3.2	30.6 ± 4.1	0.86
BO12	37.7	72.8	4225	0.994	0.992	0	3	2.576 ± 0.116	28.1 ± 3.2	30.0 ± 4.1	0.86
BO13	37.7	72.8	4240	0.994	0.992	0	3	4.253 ± 0.160	43.6 ± 4.9	50.0 ± 8.0	0.85
BO14	37.7	72.8	4240	0.996	0.995	0	2	5.260 ± 0.197	54.3 ± 6.1	65 ± 12	0.83
BO17	37.7	72.8	4230	0.995	0.993	0	2.5	3.958 ± 0.149	41.0 ± 4.6	45.8 ± 7.1	0.86
BO21	37.7	72.8	4180	0.997	0.995	0	1.5	1.595 ± 0.062	18.4 ± 2.1	18.9 ± 2.3	0.87
BO24	37.7	72.8	4170	0.997	0.996	0	2	1.560 ± 0.059	18.1 ± 2.0	18.7 ± 2.3	0.87
BO28	37.7	72.8	4130	0.998	0.997	0	4.5	1.577 ± 0.064	18.7 ± 2.1	19.5 ± 2.4	0.87
BO29	37.7	72.8	4120	0.998	0.997	0	2	1.522 ± 0.064	18.1 ± 2.0	18.7 ± 2.3	0.87
UK11	37.7	73.7	4416	1.000	1.000	20	2	9.662 ± 0.369	93 ± 11	136 ± 53	0.80
UK12	37.7	73.7	4416	0.999	0.998	25	2	6.909 ± 0.261	66.4 ± 7.5	86 ± 22	0.81
UK21	37.7	73.7	4060	1.000	1.000	25	2	5.240 ± 0.204	60.3 ± 6.8	75 ± 17	0.84
UK24	37.7	73.7	4038	1.000	1.000	10	2	2.655 ± 0.147	31.4 ± 3.7	33.8 ± 4.9	0.88
UK25	37.7	73.7	4055	1.000	1.000	25	2	1.622 ± 0.066	20.0 ± 2.2	20.9 ± 2.7	0.88
UK26	37.7	73.7	4055	1.000	1.000	20	2	2.457 ± 0.105	29.1 ± 3.3	31.3 ± 4.3	0.88
UK28	37.7	73.7	4085	0.999	0.999	25	2	4.986 ± 0.190	56.5 ± 6.4	69 ± 15	0.84
UK31	37.7	73.7	4139	0.999	0.999	10	2	4.691 ± 0.178	50.6 ± 5.7	60 ± 11	0.83
UK32	37.7	73.7	4146	0.999	0.999	20	2	5.801 ± 0.225	63.5 ± 7.2	80 ± 18	0.83
UK33	37.7	73.7	4147	1.000	1.000	15	2	5.075 ± 0.234	55.1 ± 6.4	66 ± 13	0.83
UK34	37.7	73.7	4149	1.000	1.000	30	2	3.735 ± 0.144	41.1 ± 4.6	46.9 ± 7.9	0.86
UK35	37.7	73.7	4154	1.000	1.000	10	2	6.868 ± 0.260	74.4 ± 8.4	98 ± 26	0.83
UK41	37.6	73.7	4225	1.000	1.000	20	2	1.442 ± 0.089	16.4 ± 2.0	16.9 ± 2.2	0.87
UK42	37.6	73.7	4230	0.999	0.999	0	2	1.508 ± 0.079	17.0 ± 2.0	17.5 ± 2.2	0.87
UK43	37.6	73.7	4226	1.000	1.000	30	2	1.823 ± 0.071	20.8 ± 2.3	21.8 ± 2.8	0.87
UK44	37.6	73.7	4223	1.000	0.999	25	2	1.089 ± 0.067	12.6 ± 1.5	12.9 ± 1.7	0.86
UK45	37.6	73.7	4232	0.998	0.997	0	2	2.270 ± 0.105	24.9 ± 2.9	26.2 ± 3.5	0.87
UK51	37.6	73.6	4376	0.982	0.978	40	2	1.342 ± 0.053	15.3 ± 1.7	15.8 ± 1.9	0.86
UK52	37.6	73.6	4377	0.969	0.962	0	2	1.461 ± 0.057	15.9 ± 1.7	16.2 ± 1.9	0.86
UK53	37.6	73.6	4400	0.990	0.989	30	2	3.481 ± 0.135	35.0 ± 3.9	38.4 ± 5.8	0.85

Tab. 5.1 continued.

Sample ID	Latitude [°N]	Longitude [°E]	Altitude [m]	f_{ST}, n[1]	f_{ST}, μ[2]	α[3] [°]	d[4] [cm]	^{10}Be [10^6 atoms g^{-1}]	Min. exposure age [ka]	Max. exposure age [ka]	Dunai / Lal[5]
UK54	37.6	73.6	4396	0.973	0.967	0	2	1.385 ± 0.054	14.9 ± 1.7	15.2 ± 1.8	0.86
UK61	37.6	73.6	4465	0.944	0.937	25	2	1.303 ± 0.051	14.1 ± 1.6	14.5 ± 1.7	0.85
GU11	37.6	73.9	4600	1.000	0.999	0	2.5	4.522 ± 0.189	39.2 ± 4.4	43.2 ± 6.6	0.84
GU12	37.6	73.9	4600	1.000	1.000	10	6	3.163 ± 0.093	28.9 ± 3.2	31.3 ± 4.2	0.84
GU13	37.6	73.9	4600	0.998	0.997	60	5	1.656 ± 0.059	19.4 ± 2.1	21.0 ± 2.8	0.84
GU15	37.6	73.9	4590	0.999	0.999	0	3	2.607 ± 0.090	24.1 ± 2.7	25.4 ± 3.2	0.84
GU16	37.6	73.9	4600	0.994	0.992	0	3	2.061 ± 0.094	19.4 ± 2.2	20.2 ± 2.5	0.84
GU19	37.6	73.9	4585	0.999	0.999	0	6	6.418 ± 0.192	56.8 ± 6.3	69 ± 13	0.80
GU21	37.6	73.9	4240	1.000	1.000	0	3	2.316 ± 0.123	25.3 ± 3.0	26.7 ± 3.6	0.87
GU22	37.6	73.9	4250	1.000	1.000	0	4	1.954 ± 0.140	21.6 ± 2.7	22.7 ± 3.2	0.86
GU24	37.6	73.9	4270	1.000	0.999	0	3	4.196 ± 0.209	42.3 ± 5.0	48.0 ± 7.8	0.85
GU25	37.6	73.9	4270	0.999	0.999	0	3	4.528 ± 0.219	46.0 ± 5.4	53.8 ± 6.9	0.84
GU26	37.6	73.9	4275	0.999	0.999	0	3	1.884 ± 0.083	20.6 ± 2.3	21.5 ± 2.7	0.86
GU31	37.6	73.9	4140	1.000	0.999	0	1	1.342 ± 0.056	15.9 ± 1.8	16.2 ± 2.0	0.88
GU32	37.6	73.9	4140	1.000	0.999	0	4	3.297 ± 0.116	36.4 ± 4.0	40.1 ± 5.8	0.87
GU34	37.6	73.9	4150	0.999	0.999	0	6	1.825 ± 0.069	21.4 ± 2.4	22.6 ± 2.8	0.87
GU36	37.6	73.9	4160	1.000	0.999	0	3.5	2.348 ± 0.143	26.6 ± 3.2	28.3 ± 4.0	0.87
GU38	37.6	73.9	4170	0.999	0.999	0	1.5	1.697 ± 0.160	19.6 ± 2.8	20.3 ± 3.1	0.87
GU42	37.6	73.9	4230	0.993	0.991	0	2.5	1.918 ± 0.153	21.5 ± 2.8	22.4 ± 3.3	0.87
GU44	37.6	73.9	4235	0.995	0.994	0	6	1.519 ± 0.068	17.3 ± 2.0	18.1 ± 2.2	0.87
GU47	37.6	73.9	4235	0.994	0.993	0	4	2.290 ± 0.170	25.3 ± 3.2	26.8 ± 4.0	0.87

[1] correction factor for topographic shielding of fast neutrons, corrected for the influence of surface inclination
[2] correction factor for topographic shielding of muons, corrected for the influence of surface inclination
[3] maximum slope angle of the sampled surface
[4] thickness of the sample
[5] ratio of ages calculated using the scaling systems of Lal (1991) as used in this study, and the scaling system of Dunai (2001) as modified by Schaller et al. (2002), for details see section 2.

The recessional deposit UK3 clearly yields exposure ages that are too old in comparison with the ages of the stratigraphically lower UK2 moraine (Tab. 5.1, Fig. 5.9A). Most likely, UK3 contains some preexposed material carried down from above-slope by the adjacent kolluvial fan. The ditch separating both deposits may have been formed at a later time. Processes allowing for such coverage of parts of lateral moraines have been described as common from the neighbouring Karakoram (Iturrizaga, 2003). No unambiguous deposition age can therefore be inferred from the UK3 data. Most likely, the moraine has been laid down between 40 and 60 cal. ka B.P., in possible analogy to the Yashilkul area.

The deposits UK4, GU3 and GU4 yield similar exposure ages between 13 and 28 ka, if one boulder (GU32) is excluded as obviously preexposed (Tab. 5.1, Fig. 5.9). Therefore, UK4 can be correlated to GU3 or GU4, or even both, as its horizontal dimensions exceed those

of the latter, and its ELA depression lies in between. As GU3 is stratigraphically lower than GU4, it probably dates to around 27 cal. ka B.P., while GU4 probably dates to around 22 cal. ka B.P. UK4 most likely has been deposited 27-20 cal. ka B.P.

The recessional stages represented by UK5 and UK6 have occurred in the lateglacial period, around ~15.5 cal. ka B.P., and ~14.3 cal. ka B.P. It may be noteworthy that calculation applying the scaling system of Dunai (2001) results in ages of UK5 and UK6 that correspond with the beginning and end of the Younger Dryas period (13.0 ka, 11.5 ka, respectively). However, the two moraines are too different in their dimensions and too far separated from each other to be an example of a typical double Younger Dryas advance (Easterbrook, 2003), hence this implication is rather doubtful at present.

All these dating results show, that the up to nine moraine walls constituting the *Alichur complex* (Dodonov, 2002) have been deposited during the second half of the late Pleistocene, while the most prominent advance among them has been synchronous with or slightly earlier than the global LGM, 21-25 cal. ka B.P., but has been much more constrained than the maximum late Pleistocene glaciation, which in this region occurred early in the last glacial cycle.

5.3.6 Comparison with neighbouring regions

5.3.6.1 Western Central Asian plains

The western foreland of the Central Asian mountains features one of the most complete Quaternary loess-palaeosol records of the world (Bronger et al., 1998, Dodonov, 2002). In this record, warm, moist climate phases are indicated by pedocomplexes (PC), while cold, dry phases are indicated by unweathered loess. The record of the last glacial cycle begins with the first pedocomplex (PC1), which is associated with the MIS 5. The luminescence age of PC1 at Darai Kalon, western Tajikistan, has been measured to between >117 ka at the base and 60-80 ka at the top (Frechen & Dodonov, 1998). Mestdagh et al. (1999), using soil micromorphology, have shown that during this time precipitation in the region has dropped from ~700-800 mm at the beginning of soil development to below 400 mm at its end. During the rest of the last glacial, conditions have been adverse for soil formation, as loess deposited during the MIS 3 is only slightly weathered and does not contain a fully developed palaeosol (Frechen & Dodonov, 1998). Mestdagh et al. (1999) attribute this increasing drought to a successive strengthening of the Siberian anticyclone. The same has been inferred from the successively more constrained glaciation in the Siberian Arctic in

the course of the last glacial cycle (Velichko et al., 1997, Svendsen, 2003), and has also been described by a climate model (Krinner et al., 2003). The successive drying-out of the Central Asian mountain foreland seems to be reflected by the decreasing extent of glaciation which is documented in the Pamir.

5.3.6.2 Kunlun Shan & Tibetan Plateau

In the Kunlun Shan, southeast of the Pamir, the most extensive glacier advances date from the early and middle Pleistocene. One of these advances may correlate with the advance having deposited the isolated boulders left today above 4400 m in the Pamir (e.g. UK1, GU1) or above the highest intact lateral moraine in the Aksu Valley (AK1). In the Kunlun Shan, thermoluminescence (TL) ages of 700-500 ka (Wu et al., 2001), as well as TL and ESR ages around 330 ka, and around 206 ka have been reported from early and middle Pleistocene deposits (Zheng & Rutter, 1998). Late Pleistocene advances in the Kunlun were dated to 67 cal. ka B.P. (TL from correlated sandy loess, Zheng & Rutter, 1998), between 23 and 21 ^{14}C ka B.P. (27-24 cal. ka B.P.), and between 18 and 16 ^{14}C ka B.P. (ca. 21-19 cal. ka B.P., Derbyshire et al., 1991). The last dates have been confirmed by other workers dating a correlative advance between 16 and 18 ^{14}C ka B.P. as well (Li & Shi 1992, cited in Gillespie & Molnar, 1995). These late Pleistocene ages are in excellent agreement with the glacier advances from the Pamir dated in this work.

Thompson et al. (1997) have provided an ice core δ^{18}O record from the Guliya ice cap in the Kunlun Shan, which can serve as a temperature indicator for the northwestern part of High Asia. It has recently been shown to have been influenced mostly by the westerly circulation during the Holocene, in contrast to the Dunde ice core record from the Qilian Shan in northeastern Tibet (Thompson et al., 1989), which has been influenced mostly by the Asian monsoon (He et al., 2004). In the late Pleistocene, a rough correlation with 30°N insolation (Berger & Loutre, 1991) is noticeable (Fig. 5.12). The Guliya record shows pronounced cold phases at 75-62 cal. ka B.P., 52-45 cal. ka B.P. and 32-15 cal. ka B.P., with which glacial activity in the Pamir most probably is contemporaneous (Fig. 5.12).

In the Tanggula Shan in east-central Tibet, ^{10}Be exposure ages of >125-130 ka and 58-70 ka have been determined for two successively less extensive moraines (Schaefer et al., 2002, recalculated data). The younger ages are synchronous with the oldest late Pleistocene Pamir ages found in this study (Fig. 5.10). In northeastern Tibet, Owen et al. (2003a, b)

have found exposure ages on late Pleistocene moraines of 22-23 ka, 18-20 ka, and 15-16 ka, again in excellent agreement with dated advances in the Pamir (Fig. 5.11).

5.3.6.3 Hindu Kush, Karakoram & northwestern Himalaya

In the Hindu Kush, southwest of the Pamir, the most extensive *Drosh* glaciation, with an ELA depression of 1200 m, has been dated by Kamp (1999) to have occurred during the MIS 6 (ages >200-149 ka), using optically stimulated luminescence (OSL). Another advance with an ELA depression of 1000 m, the *Pret* stage, has been OSL-dated to 54-43 ka. A third, not very well defined stage called *Sonoghar* has been assumed to have occurred during the MIS 2. Kamp's (1999) OSL data, however, have been corrected by Owen et al. (2002b), placing the *Drosh* advance into the MIS 3 (55-31 cal. ka B.P.), the *Pret* stage into the MIS 2 (>7.7 cal ka B.P.) and the *Sonoghar* stage into the Lateglacial (Kamp et al., 2003). If these recalculated ages are correct, the early late Pleistocene glacier advance in the Hindu Kush is antiphased with respect to that in the Pamir. Owen et al. (2002b) and Kamp et al. (2003) accordingly argue for a strong monsoonal influence on glaciation in the Hindu Kush. A comparison of OSL and ^{10}Be surface exposure ages in the neighbouring Karakoram by Spencer & Owen (2004), however, has shown that OSL ages as calculated by L. A. Owen's group may be significantly lower than ^{10}Be ages of the same deposits. The revised chronology of the Hindu Kush therefore remains in doubt, and should be tested by an SED study.

The glacial chronology of the Karakoram, south-southeast of the Pamir, has been defined in the Hunza Valley. The recalculated ^{10}Be ages of Owen et al. (2002c) show that the *Borit Jheel* stage has occurred prior to 47-57 ka (Fig. 5.10), which is corroborated by an earlier TL age of >50-65 ka (Derbyshire et al., 1984). The MIS 2 stages *Ghulkin* I, II and *Batura* at the Pasu glacier accordingly occurred 27-20, 18, and ~14.5 cal. ka B.P. (Fig. 5.11, 5.12). These ages agree well with our results from the Pamir.

In the Swat Himalaya, Richards et al. (2000) have measured an OSL age of ~77 ka for the maximum glacier advance (*Gabral*), and an OSL age of >38 ka for the next younger one (*Kalam I*). In the upper Indus Valley, the maximum stage (*Shatial*) yielded an OSL age of ~60 ka, while three younger and smaller advances yielded OSL ages of 27 ka, 21-23 ka, and 15 ka (Richards et al., 2000). Phillips et al (2000), using ^{10}Be SED, have dated the maximum late Pleistocene advance at the Nanga Parbat to 52-65 cal. ka B.P. (ages recalculated), while one boulder from a younger moraine gave an age of ~20 ka. This 20 ka age

indicates an MIS 2 advance, as suggested by Richards et al. (2001), if the other Holocene ages from this deposit are interpreted as degradation ages. Again, the agreement with the Pamir data is good, especially for the MIS 2 ages. Even in the Zanskar Range and the Garhwal Himalaya, both still further southeast, the maximum late Pleistocene stages have OSL ages of 40-78 cal. ka (*Batal* stage, Taylor & Mitchell (2000), and around 63 ka (*Bhagirathi* stage, Sharma & Owen, 1996), respectively.

5.3.7 Climatic interpretation

As the previously discussed data show, late Pleistocene glaciation in the northwestern part of High Asia has been regionally synchronous, but globally asynchronous. The maximum late Pleistocene advance in this region most probably occurred during the MIS 4, 75-60 cal. ka B.P., or during the early MIS 3 (52-45 cal. ka B.P.). MIS 2 moraines are ubiquitous, but they significantly smaller in extent than those of the earlier late Pleistocene advances. Glaciation in western High Asia thus seems to be coupled to cold phases associated with insolation minima (Fig. 5.12), but also to be clearly sensitive to moisture advection, which in the region has been successively decreasing over the course of the last glacial cycle. The reason for this aridification most likely is to be found in the growing strength of the Siberian Anticyclone, leading to a deflection of precipitation in winter and spring (Krinner et al., 2003).

As shown in Fig. 5.10A, ^{10}Be SED data suggest, that the maximum late Pleistocene advance has occurred earlier on high altitude plateaus (Pamir, Tibet) than in lower altitude valleys (Koksu, Hunza, Nanga Parbat), where it seems to have occurred during or lasted until the early MIS 3. This observation may point to a systematic error in the altitude scaling of ^{10}Be production rate used here. Following any of the more recently developed scaling systems, e.g. the one of Dunai (2001), the ages from the high altitude sites would be diminished, and the maximum advance all over Central Asia would have occurred during the early MIS 3 (Fig. 5.10B). Given, however, that calibration studies as yet do not support the more recently developed scaling systems (section 2), this explanation remains doubtful. More likely, a climatic effect is responsible for the maximum advance being earlier at high altitude. Moisture advection to high altitude requires high amounts of latent heat. Latent heat production, however, decreases with insolation and moisture advection to the foreland during the course of a cold stadial. Thus, for the growth of a high altitude glacier, conditions are more favourable at the beginning of the stadial. Glacier growth at lower altitudes instead may be favoured by reduced ablation under the prolonged cold conditions that have

prevailed at the end of a stadial. In fact, the possible early recessional stages of the early maximum glaciations in the Pamir (UK3, YK2?) may be synchronous with later maximum advances in lower altitudes (KK, BJ).

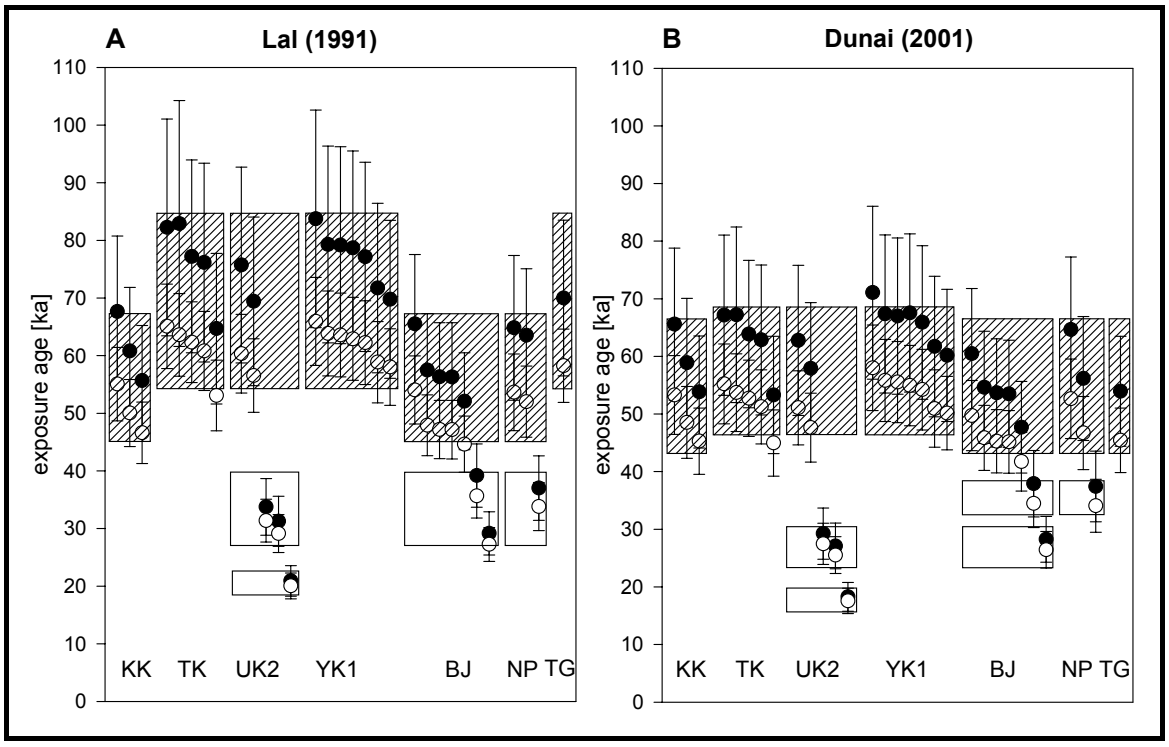

Fig. 5.10. Comparison of exposure ages from moraines deposited around the MIS 4 from this study and other ^{10}Be dating-studies from High Asia. All ages calculated from published concentrations according to A) Lal (1991) as used in this study, and B) Dunai (2001) as modified by Schaller et al. (2002). All calculations were done using TEBESEA (section 2). Minimum ages are depicted by white dots, conservative maximum ages by black dots. Phases of glacier advance in crosshatched boxes, phases of moraine degradation in white boxes. BJ = *Borit Jheel* glaciation from the Karakorum (Owen et al., 2002c), NP = maximum late Pleistocene glaciation of Nanga Parbat (Phillips et al., 2000), TG = second moraine stage from Tanggula Shan, central Tibet (Schaefer et al., 2002). See text for explanation.

Comparison of the dated MIS 2 advances (Fig. 5.11) shows a wide regional synchroneity, including even northeastern Tibet. Advances are documented at 25-27, 22-20, ~18, and ~15 cal. ka B.P. The 25-27 and 22-20 cal. ka B.P. advances are high-glacial advances, the excellent synchroneity of which supports a southward shift of the subtropical jet stream during that time (Ono et al., 2004). This shift would leave all considered areas in the same climatic zone of westerly circulation. The ~15 cal. ka B.P. advance in turn may be an indicator of beginning monsoonal influence, as it is most pronounced in eastern Tibet (Fig. 5.11, QSII, LJII), but also occurred in the eastern Pamir (UK5) and in the Indus Valley (Richards et al., 2000a). Indeed, the 8-9 late Pleistocene stages in the eastern Pamir (the *Alichur complex* c.f. Dodonov, 2002) might be indicative of an interplay between westerly

and indirect monsoon influence on a background of continuing aridification and slow glacier recession.

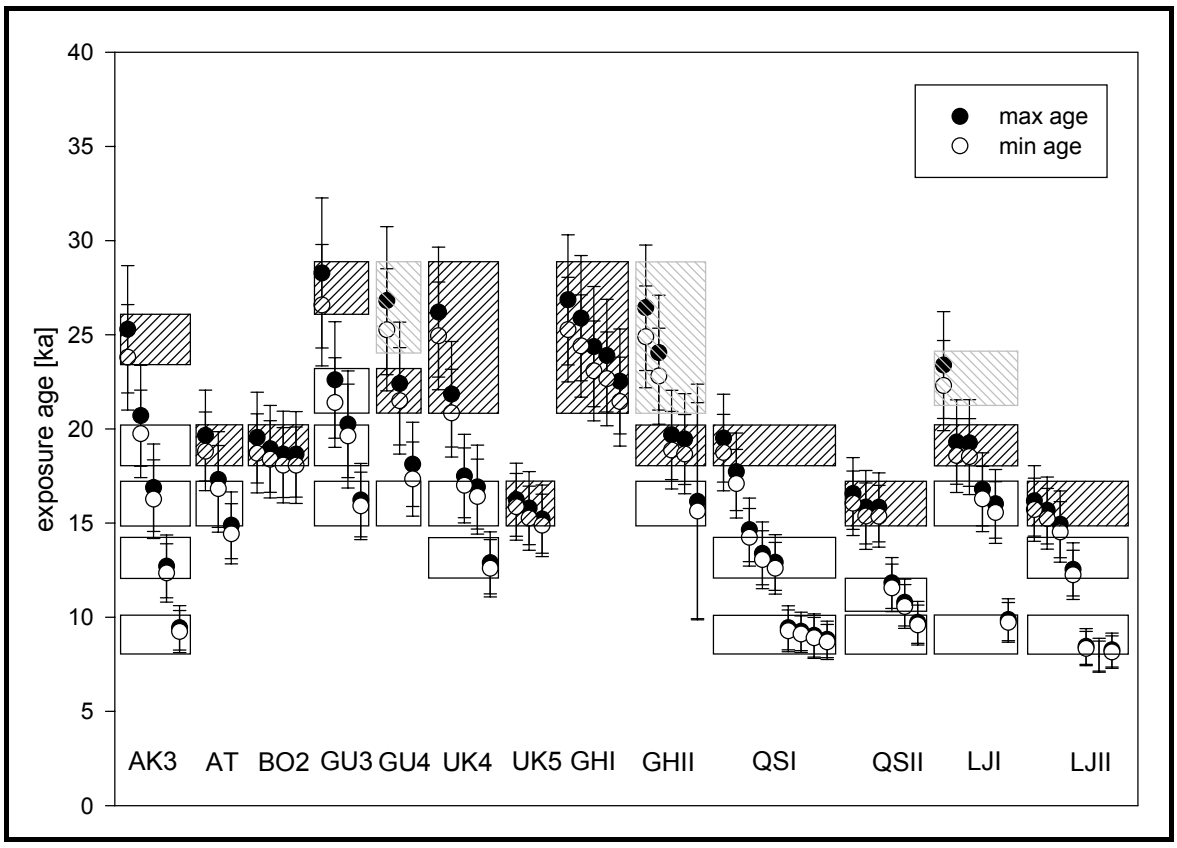

Fig. 5.11. Comparison of exposure ages from moraines deposited around the MIS 2 from this study and other ^{10}Be dating-studies from northern High Asia. All ages calculated from published concentrations using TEBESEA (section 2). Minimum ages are depicted by white dots, conservative maximum ages by black dots. Samples interpreted to be affected by inheritance in boxes cross-hatched in grey, phases of glacier advance in boxes cross-hatched in black, phases of moraine degradation in white boxes. GHI, GHII = *Ghulkin* I, II glaciations from the Karakoram (Owen et al., 2002c), QSI, QSII = older and younger dated glaciation in the Qilian Shan (Owen et al., 2003b), LJI, LJII = older and younger dated glaciation in the La Ji Mountains (Owen et al., 2003a). See text for explanation.

On the Pamir plateau, no neoglacial moraines are present (Patzelt, 1978). Apparently, moisture advection onto the plateau has been insufficient for glacial advance during this time of global cooling, moraines of which are well identified all over the Central Asian mountain ranges to the north (Zech et al, 2000a, b, Baeumler, 2001, Baume, 2002), as well as all over the Himalaya to the south (Roethlisberger, 1986, Owen et al., 1998). Even today, glacier recession in the Pamir is continuing slowly, showing less impact of recent climate warming than the neighbouring regions (Konovalov & Shchetinnicov, 1992).

The theory of a late Pleistocene plateau glaciation of the Pamir c.f. Kuhle (1997, 1998) along with its climatic implications is contradicted by our data. A possible remnant of such a glaciation with an exposure age of >93-136 ka has been deposited during the MIS 5d at the latest, but much more probably during the middle Pleistocene or even earlier.

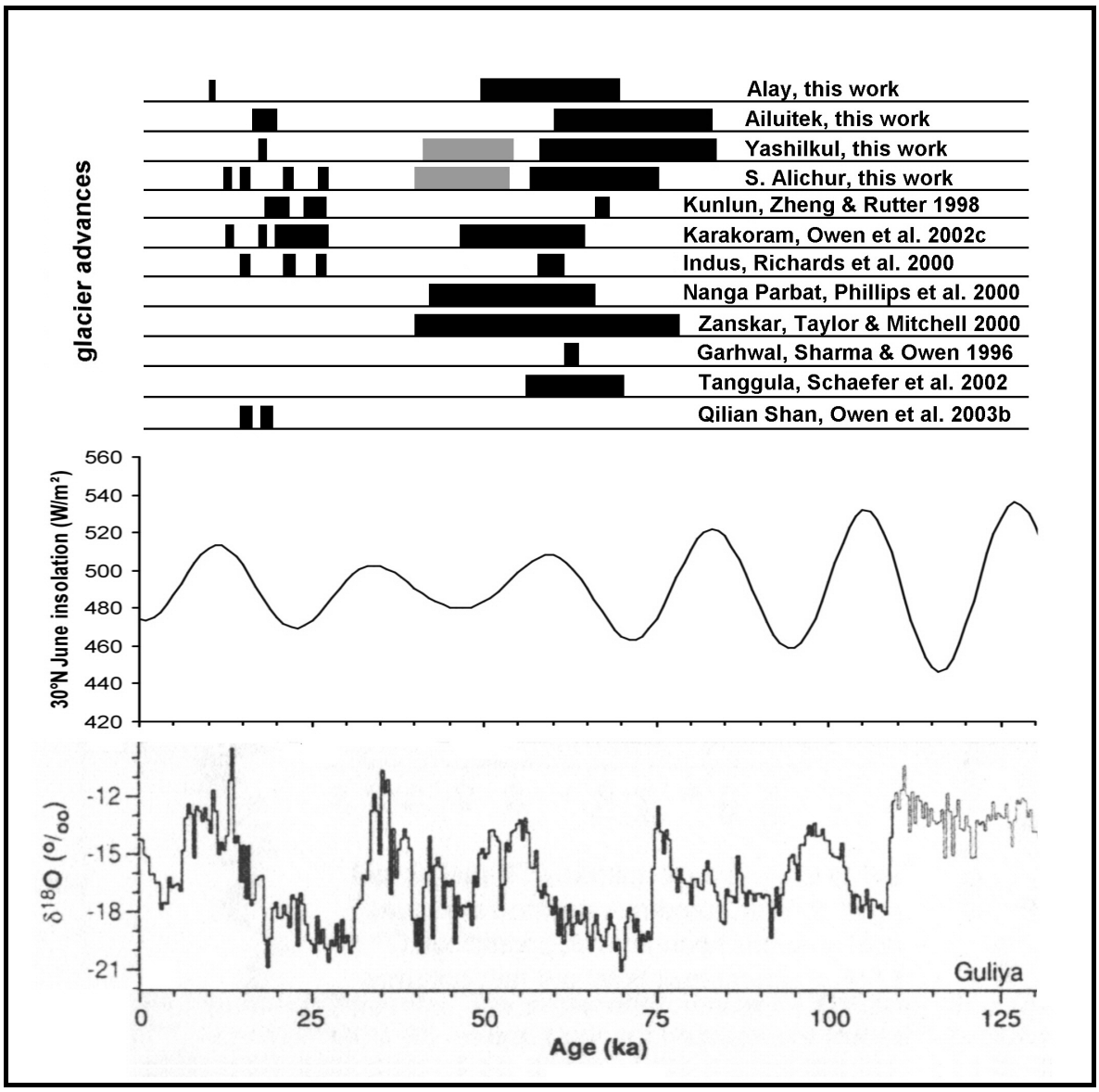

Fig. 5.12. Dated glacier advances in High Asia compared with 30°N June insolation (Berger & Loutre, 1991) and $\delta^{18}O$ of the Guliya ice core (Thompson et al., 1997). Age scale in 1000 calendar years. Uncertain advances depicted in grey.

5.4 Conclusions

The oldest erratic boulders in the Pamir and Alay-Turkestan Range have exposure ages of >93-136 ka. Most probably they have been deposited during the middle Pleistocene. Previously, they were associated with an early Pleistocene glacial stage.

Late Pleistocene glacial stages of successively reduced extent in the Pamir and the Alay Range are characterized by exposure ages of ~60-80 ka, (40-55 ka), ~27-25 ka, ~22-20 ka, ~18 ka, ~15.5 and ~14.3 ka, and 10.5 ka. The first two stages, of which the second is uncertain yet, have previously been associated with early or middle Pleistocene advances.

All late Pleistocene glaciers in the Pamir have been valley glaciers, forming only local piedmont glaciations on the plateau. The most extensive late Pleistocene glaciation occurred during the MIS 5-3 and is characterized by ELA depressions (THAR 0.5) of ~370-380 m in the eastern Pamir, as well as 600 m and >750 m, in the Alay and Turkestan Ranges, respectively.

Late Pleistocene glacier advances in the Pamir and all over western High Asia were contemporaneous with climatic cold phases. The maximal extent of glaciation occurred regionally synchronous but globally asynchronous, due to increasing aridity in Central Asia over the course of the last glacial cycle. Climate in this region seems to have been influenced mostly by the westerly circulation and the Siberian Anticyclone. During the global LGM, the westerly jetstream was shifted southward of its present location. Some indirect monsoonal influence in the eastern Pamir may be responsible for the existence of some of the lateglacial moraine stages in this area.

High altitude glaciers seem to have reached their maximum extent earlier (MIS 4) than low altitude glaciers (first half of MIS 3), possibly due to prolonged glacial aridity imparting with moisture advection into high altitudes, inducing glacial retreat, but prolonged cold during the same time imparting with glacier ablation in lower altitudes, inducing glacial advance.

5.5 Acknowledgements

This work was made possible by the German Research Foundation (DFG), grant ZE 154-51, and was supported by the Workgroup for Alpine Research of the German Academy of Sciences (ARGE), and by the German Academic Exchange Agency (DAAD). We gratefully acknowledge all support.

5.6 References

AIZEN, E. M., AIZEN, V. B., MELACK, J. M., NAKAMURA, T., OHTA, T. 2001. Precipitation and atmospheric circulation patterns at mid-latitudes of Asia. International Journal of Climatology 21, 535-556.

BAUME, O. 2002. Spaetpleistozaene bis holozaene Gletscherschwankungen ausgewaehlter Gebiete im Kaukasus, Tienschan und Altai. Muenchener Geographische Abhandlungen A52, 45-79.

BAEUMLER, R. 2001. Vergleichende bodenkundliche Untersuchungen in Hochasien und Kamtschatka. Relief Boden Palaeoklima 16, Gebrueder Borntraeger, Berlin, 125 pp.

BENN, D. I., OWEN, L. A. 1998. The role of Indian summer monsoon and the mid-latitude westerlies in Himalayan glaciations: review and speculative discussion. Journal of the Geological Society of London 155, 353-363.

BERGER, A. L., LOUTRE, M. F. 1991. Insolation values for the climate of the last 10 million years. Quaternary Science Reviews 10, 297-317.

BONDAREV, L. G., GOBEDZHISVILI, R. G., SOLOMINA, O. N. 1997. Fluctuations of local glaciers in the southern ranges of the former USSR: 18,000-8000 BP. Quaternary International 38/39, 103-108.

BRONGER, A., WINTER, R., HEINKELE, T. 1998. Pleistocene climatic history of East and Central Asia based on paleopedological indicators in loess-paleosol sequences. Catena 34, 1-17.

BROOKFIELD, M. E. 2000. Geological development and Phanerozoic crustal accretion in the western segment of the southern Tian Shan (Kyrgyzstan, Uzbekistan and Tajikistan). Tectonophysics 328, 1-14.

BURBANK, D. W., LELAND, J., FIELDING, E., ANDERSON, R. S., BROZOVIC, N., REID, M. R., DUNCAN, C. 1996. Bedrock incision, rock uplift and threshold hillslopes in the northwestern Himalayas. Nature 379, 505-510.

CLAPPERTON, C. M. 1995. Fluctuations of local glaciers at the termination of the Pleistocene. Quaternary International 28, 41-50.

COHMAP MEMBERS 1988. Climatic changes of the last 18000 years: observations and model simulations. Science 241, 1043-1052

DERBYSHIRE, E. 1996. Quaternary glacial sediments, glaciation style, climate and uplift in the Karakoram and northwest Himalaya: review and speculations. Palaeogeography, Palaeoclimatology, Palaeoecology 120, 147-157.

DERBYSHIRE, E., OWEN, L. 1997. Quaternary glacial history of the Karakoram mountains and northwest Himalayas: a review. Quaternary International 38/39, 85-102.

DERBYSHIRE, E., LI, J., PERROTT, F. A., XU, S., WATERS, R. S. 1984. Quaternary glacial history of the Hunza Valley, Karakoram Mountains, Pakistan. In: Miller, K. J.: The International Karakoram Projekt, Vol. 2. Cambridge University Press, Cambridge, 456-495.

DERBYSHIRE, E., SHI, Y., LI, J., ZHENG, B., LI, S., WANG, J. 1991. Quaternary glaciation of Tibet: the geological evidence. Quaternary Science Reviews 10, 485-510.

DODONOV, A. E. 2002. The Quaternary of Middle Asia. Transactions of the Russian Academy of Sciences, Geological Institute 546, 250 pp (in Russian).

DODONOV, A. E., BAIGUZINA, L. L. 1995. Loess stratigraphy of Central Asia: palaeoclimatic and palaeoenvironmental aspects. Quaternary Science Reviews 14, 707-720.

DUNAI, T. J. 2001. Influence of secular variation of the geomagnetic field on production rates of in situ produced cosmogenic nuclides. Earth and Planetary Science Letters 193, 197-212.

EASTERBROOK, D. 2003. Global double Younger Dryas glacial fluctuations in ice sheets and alpine glaciers. XVI INQUA Congress Programs with Abstracts, p. 73.

EYLES, N., BOYCE, J. I., BARENDREGT, R. W. 1999. Hummocky moraine: sedimentary record of stagnant Laurentide Ice Sheet lobes resting on soft beds. Sedimentary Geology 123, 163-174.

FICKER, H. V. 1933. Die eiszeitliche Vergletscherung der nordwestlichen Pamirgebiete. Sitzungsberichte der Preussischen Akademie der Wissenschaften, Physikalisch-Mathematische Klasse 1, 61-86.

FRECHEN, M., DODONOV, A. E. 1998. Loess chronology of the Middle and Upper Pleistocene in Tajikistan. Geologische Rundschau 87, 2-20.

GILLESPIE, A., MOLNAR, P. 1995. Asynchronous maximum advances of mountain and continental glaciers. Reviews of Geophysics 33, 311-364.

GILLESPIE, A., RUPPER, S., ROE, G. 2003. Climatic interpretation from mountain glaciations in Central Asia. XVI INQUA Congress Programs with Abstracts, DRI, Reno, Nv., p. 170.

GLASER, B., NI, A., ZECH, W. 1999. Bodengeographische Untersuchungen zur Rekonstruktion spaetquartaerer Klima- und Gletscherschwankungen: Alai- und Turkestangebirge, Kirgistan. Proceedings of the IGCP 415 meeting, Potsdam.

GORBUNOV, A. P., SEVERSKY, E. V. 1999. Solifluction in the mountains of Central Asia: distribution, morphology, processes. Permafrost and Periglacial Processes 10, 81-89.

GROSSWALD, M. G., ORLYANKIN, V. N. 1979. The late Quaternary ice cap of the Pamir. Materials of Glaciological Research 35, 85-97 (in Russian).

GROSSWALD, M. G., KUHLE, M., FASTOOK, J. L. 1994. Wuerm glaciation of Lake Issyk-Kul Area, Tian Shan Mts.: a case study in glacial history of Central Asia. GeoJournal 33, 273-310.

HAMBREY, M. J., HUDDART, D., BENNETT, M. R., GLASSER, N. F. 1997. Genesis of 'hummocky moraines' by thrusting in glacier ice: evidence from Svalbard and Britain. Journal of the Geological Society, London 154, 623-632.

HE, Y., THEAKSTONE, W. H., ZHANG, Z., ZHANG, D., YAO, T., CHEN, T., SHEN, Y., PANG, H. 2004. Asynchronous Holocene climatic change across China. Quaternary Research 61, 52-63.

HEUBERGER, H., SGIBNEV, V. V. 1998. Paleoglaciological studies in the Ala-Archa National Park, Kyrgyzstan, NW Tian-Shan mountains, and using multitextural analysis as a sedimentological tool for solving stratigraphical problems. Zeitschrift fuer Gletscherkunde und Glazialgeologie 34, 95-123.

INTERGOVERNMENTAL PANEL ON CLIMATE CHANGE, Working Group I 1997. An introduction to simple climate models used in the IPCC second assessment report. Technical Paper II. World Meteorological Organization, Geneva, Switzerland.

ITURRIZAGA, L. 2003. Distribution and genesis of lateroglacial valleys in the Karakoram Mountains (Pakistan). Zeitschrift fuer Geomorphologie N. F., Supplementband 130, 51-74.

IVY-OCHS, S. 1996. The dating of rock surface using in situ produced ^{10}Be, ^{26}Al and ^{36}Cl, with examples from Antarctica and the Swiss Alps. Diss. ETH No. 11763, Zuerich, 197 p.

KAMP, U. 1999. Jungquartaere Geomorphologie und Vergletscherung im oestlichen Hindukusch, Chitral, Nordpakistan. Berliner Geographische Studien, vol. 50. Technische Universitaet Berlin, Berlin, 254 p.

KAMP, U. JR., HASERODT, K., SHRODER, J. F. JR. 2003. Quaternary landscape evolution in the eastern Hindu Kush, Pakistan. Geomorphology 57, 1-27.

KARABANOV, E. B., PROKOPENKO, A. A., WILLIAMS, D. F., COLMAN, S. M. 1998. Evidence from Lake Baikal for Siberian Glaciation during oxygen-isotope substage 5d. Quaternary Research 50, 46-55.

KJAER, K. H., KRUEGER, J. 2001. The final phase of dead-ice moraine development: processes and sediment architecture, Koetlujoekull, Iceland. Sedimentology 48, 935-952.

KLEBELSBERG, R. V. 1934. Die gletscherkundlichen und glazialgeologischen Ergebnisse der Alai-Pamir-Expedition 1928. Zeitschrift fuer Gletscherkunde 21, 205-212.

KOHFELD, K. E., HARRISON, S. P. 2000. How well can we simulate past climates? Evaluating the models using global palaeoenvironmental datasets. Quaternary Science Reviews 19, 321-346.

KOHL, C. P., NISHIIZUMI, K. 1992. Chemical isolation of quartz for measurement of in-situ produced cosmogenic nuclides. Geochimica et Cosmochimica Acta 56, 3583-3587.

KONOVALOV, V. G., SHCHETINNICOV, A. S. 1994. Evolution of glaciation in the Pamiro-Alai Mountains and its effect on river run-off. Journal of Glaciology 40, 149-157.

KOPPES, M. N., GILLESPIE, A. R., BURKE, R. M., THOMPSON, S. C., CLARK, D. H. 2003. Late Quaternary glaciation in western Central Asia. XVI INQUA Congress Programs with Abstracts, DRI, Reno, Nv., p.156.

KRINNER, G., MANGERUD, J., JAKOBSSON, M., CRUCIFIX, M., RITZ, C., SVENDSEN, J. I., GENTHON, C. 2003. Impact of ice-dammed lakes on the early Weichselian climate of northern Eurasia. XVI INQUA Congress Programs with Abstracts, DRI, Reno, Nv., p. 207.

KUHLE, M. 1997. New findings concerning the ice age (Last Glacial Maximum) glacier cover of the East Pamir, of the Nanga Parbat up to the Central Himalaya and of Tibet, as well as the age of the Tibetan inland ice. GeoJournal 42, 87-257.

KUHLE, M. 1998. Reconstruction of the 2.4 million km² Late Pleistocene ice sheet on the Tibetan Plateau and its impact on the global climate. Quaternary International 45/46, 71-108.

LAL, D. 1991. Cosmic ray labelling of erosion surfaces: in situ nuclide production rates and erosion models. Earth and Planetary Science Letters 104, 424-439.

LEHMKUHL, F. 1997. Late Pleistocene, late Glacial and late Holocene glacier advances on the Tibetan Plateau. Quaternary International 38/39, 77-83.

LELAND, J., REID, M. R., BURBANK, D. W., FINKEL, R., CAFFEE, M. 1998. Incision and differential bedrock uplift along the Indus River near Nanga Parbat, Pakistan Himalaya, from ^{10}Be and ^{26}Al exposure age dating of bedrock straths. Earth and Planetary Science Letters 154, 93-107.

LI, S., SHI, Y. 1992. Glacial and lake fluctuations in the area of West Kunlun Mountains during the last 45,000 years. Annals of Glaciology 16, 79-84.

LYDOLPH, E. 1977. Climates in the Soviet Union. World Survey of Climatology 7, 151-189.

MAXIMOV, E. W. 1992. Historical geology of the mountain lakes of Middle Asia. University of St. Petersburg, St. Petersburg, 302 p. (in Russian).

MESTDAGH, H., HAESAERTS, P., DODONOV, A., HUS, J. 1999. Pedosedimentary and climatic reconstructions of the last interglacial and early glacial loess-paleosol sequence in South Tajikistan. Catena 35, 197-218.

NISHIIZUMI, K., WINTERER, E. L., KOHL, C. P., KLEIN, J., MIDDLETON, R., LAL, D., ARNOLD, J. R. 1989. Cosmic ray production rates of ^{10}Be and ^{26}Al in quartz from glacially polished rocks. Journal of Geophysical Research B 94, 17907-17915.

NOETH, L. 1931. Glazialgeologische und morphologische Untersuchungen im Nordwest-Pamir. Mitteilungen der geographischen Gesellschaft in Muenchen 24, 154-192.

ONO, Y., SHULMEISTER, J., LEHMKUHL, F., ASAHI, K., AOKI, T. 2004. Timings and causes of glacial advances across the PEP-II transect (East-Asia to Antarctica) during the last glaciation cycle. Quaternary International 118-119, 55-68.

OWEN, L. A., DERBYSHIRE, E., FORT, M. 1998. The Quaternary glacial history of the Himalaya. Quaternary Proceedings 6, 91-120.

OWEN, L. A., FINKEL, R. C., CAFFEE, M. W. 2002a. A note on the extent of glaciation throughout the Himalayas during the Last Glacial Maximum. Quaternary Science Reviews 21, 147-157.

OWEN, L. A., KAMP, U., SPENCER, J. Q., HASERODT, K. 2002b. Timing and style of Late Quaternary glaciation in the eastern Hindu Kush, Chitral, northern Pakistan: a review and revision of the glacial chronology based on new optically stimulated luminescence dating. Quaternary International 97-98, 41-55.

OWEN, L. A., FINKEL, R. C., CAFFEE, M. W., GUALTIERI, L. 2002c. Timing of multiple glaciations during the Late Quaternary in the Hunza Valley, Karakoram Mountains, northern Pakistan: defined by cosmogenic radionuclide dating of moraines. Geological Society of America Bulletin 28, 431-434.

OWEN, L. A., BARNARD, P., BENN, D., CAFFEE, M. W., DERBYSHIRE, E., FINKEL, R., GUALTIERI, L., MA, H., SHARMA, M., SPENCER, J. 2003a. Late Quaternary glaciation in the Himalaya and Tibet. XVI INQUA Congress Programs with Abstracts, DRI, Reno, Nv., p. 155.

OWEN, L. A., SPENCER, J. Q., MA, H., BARNARD, P. L., DERBYSHIRE, E., FINKEL, R. C., CAFFEE, M. W., ZENG, Y. N. 2003b. Timing of Late Quaternary glaciation along the southwestern slopes of the Qilian Shan, Tibet. Boreas 32, 281-446.

OWEN, L. A., MA, H., DERBYSHIRE, E., SPENCER, J. Q., BARNARD, P. L., ZENG, Y. N., FINKEL, R. C., CAFFEE, M. W. 2003c. The timing and style of Late Quaternary glaciation in the La Ji Mountains, NE Tibet: evidence for restricted glaciation during the latter part of the Last Glacial. Zeitschrift fuer Geomorphologie N. F., Supplementband 130, 263-276.

PAKHOMOV, M. M., NIKONOV, A. A. 1977. On the Pliocene glaciation and on the Kokbay interglacial in the Pamir. Communications of the Academy of Sciences of the USSR, Geological Series 8, 126-134 (in Russian).

PATZELT, G. 1978. Gletscherkundliche Untersuchungen im "Grossen Pamir". In: Senarclens de Grancy, R., Kostka, R.: Grosser Pamir. Akademische Druck- und Verlagsanstalt, Graz, 131-149.

PHILLIPS, W. M., SLOAN, V. F., SHRODER, J. F. JR., SHARMA, P., CLARKE, M. L., RENDELL, H. M. 2000. Asynchronous glaciation at Nanga Parbat, northwestern Himalaya Mountains, Pakistan. Geology 28, 431-434.

PORTER, S. C. 2001. Snowline depression in the tropics during the last glaciation. Quaternary Science Reviews 20, 1067-1091.

PRELL, W. L., KUTZBACH, J. E. 1987. Monsoon variability over the past 150,000 years. Journal of Geophysical Research 92, 8411-8425.

PRELL, W. L., KUTZBACH, J. E. 1992. Sensitivity of the Indian monsoon to forcing parameters and implications for its evolution. Nature 360, 647-652.

RICHARDS, B. W. M., OWEN, L. A., RHODES, E. J. 2000. Timing of Late Quaternary glaciations in the Himalayas of northern Pakistan. Journal of Quaternary Science 15, 283-297.

RICHARDS, B. W. M., OWEN, L. A., RHODES, E. J. 2001. Comment on: Asynchronous glaciation at Nanga Parbat, northwestern Himalaya Mountains, Pakistan by Phillips et al. Geology 29, 287.

RICKETTS, R. D., JOHNSON, T. C., BROWN, E. T., RASMUSSEN, K. A., ROMANOVSKY, V. V. 2001. Holocene palaeolimnology of Lake Issyk-Kul, Kyrgyzstan: trace element and stable isotope composition of ostracodes. Palaeogeography, Palaeoclimatology, Palaeoecology 176, 207-227.

ROETHLISBERGER, F. 1986. 10000 Jahre Gletschergeschichte der Erde. Verlag Sauerlaender, Aarau, 79-153.

SCHAEFER, J. M., TSCHUDI, S., ZHAO, Z., WU, X., IVY-OCHS, S., WIELER, R., BAUR, H., KUBIK, P. W., SCHLUECHTER, C. 2002. The limited influence of glaciations in Tibet on global climate over the past 170 000 yr. Earth and Planetary Science Letters 194, 287-297.

SCHALLER, M.; BLANCKENBURG, F. V.; VELDKAMP, A.; TEBBENS, L. A.; HOVIUS, N.; KUBIK, P. W. 2002. A 30 000 yr record of erosion rates from cosmogenic 10Be in Middle European river terraces. Earth and Planetary Science Letters 204, 307-320.

SCHULZ, H., RAD, U. V., ERLENKEUSER, H. 1998. Correlation between Arabian Sea and Greenland climate oscillations of the past 110,000 years. Nature 393, 54-57.

SHARMA, M. C., OWEN, L. A. 1996. Quaternary glacial history of NW Garhwal, Central Himalayas. Quaternary Science Reviews 15, 335-365.

SIDOROV, L. F. 1960. Early glaciation of the Pamirs. In: Doklady of the Academy of Science of the U.S.S.R., Earth Science Sections 127, 732-733.

SIDOROV, L. F. 1979. Nature of the Pamir during the Quaternary. Nauka Press, Moscow, 145 p. (in Russian).

SIDOROV, L. F., SAPOV, O. P. 1965. On the Quaternary landscape history of the lake Yashilkul basin in the Pamir. Izvestija Vsesojuznovo Geograficheskovo Obshchestvo 6, 518-526 (in Russian).

SIROCKO, F., GARBE-SCHOENBERG, D., MCINTYRE, A., MOLFINO, B. 1996. Teleconnections between the subtropical monsoon and high latitude climates during the last deglaciation. Science 272, 526-529.

SPENCER, J. Q., OWEN, L. A. 2004. Optically stimulated luminescence dating of Late Quaternary glaciogenic sediments in the upper Hunza Valley: validating the timing of glaciation and assessing dating methods. Quaternary Science Reviews 23, 175-191.

STONE, J. O. H. 2000. Air pressure and cosmogenic isotope production. Journal of Geophysical Research 105, B10, 23753-23759.

SUCCOW, M. 1989. Die Mittelasiatischen Hochgebirge. In: Klotz, G.: Hochgebirge der Erde. Urania-Verlag, Leipzig, 187-204.

SVENDSEN, J. I. 2003. Late Quaternary ice sheet history of northern Eurasia. XVI INQUA Congress Programs with Abstracts, DRI, Reno, Nv., p. 195.

TAYLOR, P. J., MITCHELL, W. A. 2000. Late Quaternary glacial history of the Zanskar Range, northwest Indian Himalaya. Quaternary International 65/66, 81-99.

THOMPSON, L. G., MOSLEY-THOMPSON, E., DAVIS, M. E., BOLZAN, J. F., DAI, J., YAO, T., GUNDESTRUP, N., WU, X., KLEIN, L., XIE, Z. 1989. Holocene-late Pleistocene climatic ice core records from the Qinghai-Tibetan Plateau. Science 246, 474-477.

THOMPSON, L. G., YAO, T., DAVIS, M. G., HENDERSON, K. A., MOSLEY-THOMPSON, E., LIN, P. N., BEER, J., SYNAL, H. A., COLE-DAI, J., BOLZAN, J. F. 1997. Tropical climate instability: the last glacial cycle from a Qinghai-Tibetan ice core. Science 276, 1821-1825.

UNEP 2002. Vital maps and graphics on climate change, Tajikistan. www.grida.no/enrin/htmls/tadjik/vitalgraphics/eng/html/climate.htm.

VASILEV, Y. M. 1966. The Cenozoic of the Pamir. Donish, Dushanbe, 221 pp. (in Russian).

VELICHKO, A. A., KONONOV, Y. M., FAUSTOVA, M. A. 1997. The last glaciation of Earth: size and volume of ice sheets. Quaternary International 41/42, 43-51.

WEIERS, S. 1995. Zur Klimatologie des NW-Karakorum und angrenzender Gebiete. Bonner Geographische Abhandlungen 92, 156 p.

WEIERS, S. 1998. Wechselwirkungen zwischen sommerlicher Monsunaktivitaet und außertropischer Westzirkulation in den Hochgebirgsregionen Nordpakistans. Petermanns Geographische Mitteilungen 142, 85-104.

WISSMANN, H. V. 1959. Die heutige Vergletscherung und Schneegrenze in Hochasien, mit Hinweisen auf die Vergletscherung der letzten Eiszeit Akademie der Wissenschaften und der Literatur, Abhandlungen der mathematisch-naturwissenschaftlichen Klasse 14, 1105-1407.

WU, Y., CUI, Z., LIU, G., GE, D., YIN, J., XU, Q., PANG, Q. 2001. Quaternary geomorphological evolution of the Kunlun pass area and uplift of the Qinghai-Xizang (Tibet) plateau. Geomorphology 36, 203-216.

ZABIROV, R. D. 1955. Oledenenie Pamira. GeografGIZ, Moskva, 371 p. (in Russian).

ZECH, W., BAEUMLER, R., SAVOSKUL, O., NI, A., PETROV, M. 1996. Bodengeographische Beobachtungen zur pleistozaenen und holozaenen Vergletscherung des Westlichen Tienschan (Usbekistan). Eiszeitalter und Gegenwart 46, 144-151.

ZECH, W., BAEUMLER, R., GUGGENBERGER, G., PETROV, M., NI, A., LEMZIN, I. 2000a. Pleistocene and Holocene landscape development in the Kichik Alay and Hissar Ranges (Kyrgyzstan and Uzbekistan) as deduced from soil morphology. Marburger Geographische Schriften 135, 53-68.

ZECH, W., GLASER, B., NI, A., PETROV, M., LEMZIN, I. 2000b. Soils as indicators of the Pleistocene and Holocene landscape evolution in the Alay Range (Kyrgyzstan). Quaternary International 65/66, 161-169.

ZECH, R., ABRAMOWSKI, U., GLASER, B., SOSIN, P., KUBIK, P. W., ZECH, W. 2004. Late Quaternary glacial and climate history of the lake Yashilkul area, Pamir, derived from cosmogenic ^{10}Be exposure ages. Quaternary Research, accepted.

ZHENG, B., RUTTER, N. 1998. On the problem of quaternary glaciations, and the extent and patterns of Pleistocene ice cover in the Qinghai-Xizang (Tibet) Plateau. Quaternary International 45/46, 109-122.

ZHENG, B., XU, Q., SHEN, Y. 2002. The relationship between climate change and Quaternary glacial cycles on the Qinghai-Tibetan plateau: review and speculation. Quaternary International 97-98, 93-101.

Dank

Allen, die mir im Laufe dieser Arbeit mit Rat und Tat zur Seite gestanden haben, möchte ich ganz herzlich danken. Im Einzelnen bedanke ich mich bei

Herrn Prof. Dr. Wolfgang Zech für die Stellung dieses interessanten Themas, für die Organisation der Exkursionen, sowie für die engagierte Betreuung der Arbeit;

Herrn Dr. Peter W. Kubik für die freundliche Kooperation bezüglich der Messung der $^{10}Be/^{9}Be$-Verhältnisse in den Proben, ohne die diese Arbeit nicht möglich gewesen wäre;

der Deutschen Forschungsgemeinschaft für die großzügige Finanzierung des Projektes (Az. ZE 154-51), der Volkswagen-Stiftung für die Unterstützung der Nepal-Exkursionen, sowie dem Deutschen Akademischen Austauschdienst (Go-East-Programm) und der Arbeitsgemeinschaft für Vergleichende Hochgebirgsforschung für die Unterstützung der Exkursionen nach Zentralasien;

Herrn Dr. Bruno Glaser für die Vorbereitung des Projektes, die Begründung der Kooperation mit dem Paul-Scherrer-Institut, die Probenahme im Aksu-Tal und Macha-Khola Tal, sowie das Korrekturlesen der Manuskripte;

Herrn Dr. Ludwig Haumaier für die verlässliche Betreuung im Labor sowie die geduldige Hilfe bei vielen organisatorischen Dingen;

Herrn Roland Zech für die Mitarbeit im Projekt im Rahmen seiner Diplomarbeit, das Korrekturlesen der Manuskripte, sowie für viele fruchtbare Diskussionen, sowie ebenso Herrn Arne Bergau und Herrn Dominik Seebach für ihre Mitarbeit im Projekt im Rahmen ihrer Diplomarbeiten;

Herrn Dr. Pjotr Sosin für die kompetente Führung im Pamir, sowie für den ausgezeichneten selbstgemachten Wein, sowie den beteiligten tadjikischen Studenten und Fahrern für ihren Beitrag zum Gelingen der Exkursion 2002;

Herrn Dr. Krishna Kharki, Herrn Rajendra Uprety sowie allen beteiligten nepalischen Sherpas und Trägern für ihre Unterstützung der Nepal-Exkursion 2003;

Herrn Prof. Dr. Hanns Kerschner für die freundliche und fachkundige Führung am Bergsturz Köfels;

Frau Anne Reuther für die Unterstützung bei der Literaturbeschaffung, das Korrekturlesen der Manuskripte, sowie für viele fruchtbare Diskussionen und hilfreiche Informationen;

Frau Alexandra Oberthür für ungezählte kleine Tipps und Hilfestellungen bei der Büroarbeit, sowie für ein angenehmes Arbeitsklima, ebenso Frau Dr. Silke Marczinek und Herrn Markus Bauer für ihren Beitrag dazu;

Frau Karin Jeschke für ihre Hilfe beim Einarbeiten des Analysenganges;

Herrn André Wetzel, Frau Tanja Gonter, Frau Marcela Weiß und allen anderen Mitarbeiterinnen, Mitarbeitern, Studentinnen und Studenten im Labor des Lehrstuhls für Bodenkunde für die gute Zusammenarbeit und das angenehme Betriebsklima;

Frau Cornelia Schreiber und Frau Gabriele Wittke für ihre freundliche Unterstützung in allen Sekretariatsangelegenheiten;

Herrn Rainer Goller und Frau Sonja Brodowski für viele wichtige Tipps zum Erstellen und Abgeben der Dissertation;

sowie - last not least - meinen Eltern und Freunden für ihren Rückhalt und ihren Beitrag zu meiner auch persönlichen Weiterentwicklung im Zuge meiner Arbeit.

Appendix 1. Extended database

Tab. A1.1. Sample documentation I: General description, slope angle and azimuth.

Sample ID	Height [cm]	Rock type	Vegetation	Snow cover [g/cm²]	Slope angle [°]	Sl. azimuth [°]
AK11	n.d.	granodiorite	n.d.	n.d.	n.d.	n.d.
AK12	n.d.	granodiorite	n.d.	n.d.	n.d.	n.d.
AK13	n.d.	granodiorite	n.d.	n.d.	n.d.	n.d.
AK21	n.d.	granodiorite	n.d.	n.d.	n.d.	n.d.
AK22	n.d.	granodiorite	n.d.	n.d.	n.d.	n.d.
AK23	n.d.	granodiorite	n.d.	n.d.	n.d.	n.d.
AK24	n.d.	granodiorite	n.d.	n.d.	n.d.	n.d.
AK25	n.d.	granodiorite	n.d.	n.d.	n.d.	n.d.
AK31	n.d.	granodiorite	n.d.	n.d.	n.d.	n.d.
AK32	n.d.	granodiorite	n.d.	n.d.	n.d.	n.d.
AK33	n.d.	granodiorite	n.d.	n.d.	n.d.	n.d.
AK34	n.d.	granodiorite	n.d.	n.d.	n.d.	n.d.
AK35	n.d.	granodiorite	n.d.	n.d.	n.d.	n.d.
AK41	n.d.	granodiorite	n.d.	n.d.	n.d.	n.d.
AK42	n.d.	granodiorite	n.d.	n.d.	n.d.	n.d.
AK43	n.d.	granodiorite	n.d.	n.d.	n.d.	n.d.
AK44	n.d.	granodiorite	n.d.	n.d.	n.d.	n.d.
AK45	n.d.	granodiorite	n.d.	n.d.	n.d.	n.d.
AV1	n.d.	granodiorite	alpine meadow	n.d.	n.d.	n.d.
AV2	n.d.	granodiorite	alpine meadow	n.d.	n.d.	n.d.
AV3	n.d.	granodiorite	alpine meadow	n.d.	n.d.	n.d.
KK1	n.d.	granodiorite	semi-desert	n.d.	n.d.	n.d.
KK2	n.d.	granodiorite	semi-desert	n.d.	n.d.	n.d.
KK3	n.d.	granodiorite	semi-desert	n.d.	n.d.	n.d.
MK22	n.d.	gneiss	deciduous forest	6	n.d.	n.d.
MK23	n.d.	gneiss	deciduous forest	6	n.d.	n.d.
MK24	n.d.	gneiss	deciduous forest	6	n.d.	n.d.
MK25	n.d.	gneiss	deciduous forest	6	n.d.	n.d.
MK41	n.d.	gneiss	alpine meadow	4	n.d.	n.d.
MK42	n.d.	gneiss	alpine meadow	4	n.d.	n.d.
MK43	n.d.	gneiss	alpine meadow	4	n.d.	n.d.
MK44	n.d.	gneiss	alpine meadow	4	n.d.	n.d.
MK45	n.d.	gneiss	alpine meadow	4	n.d.	n.d.
MK51	n.d.	gneiss	deciduous forest	6	n.d.	n.d.
MK52	n.d.	gneiss	deciduous forest	6	n.d.	n.d.
MK53	n.d.	gneiss	deciduous forest	6	n.d.	n.d.
MK54	n.d.	gneiss	deciduous forest	6	n.d.	n.d.
MK55	n.d.	gneiss	deciduous forest	6	n.d.	n.d.
MK71	n.d.	gneiss	deciduous forest	6	n.d.	n.d.
MK73	n.d.	gneiss	deciduous forest	6	n.d.	n.d.
MK74	n.d.	gneiss	deciduous forest	6	n.d.	n.d.
MK75	n.d.	gneiss	deciduous forest	6	n.d.	n.d.
BK1	>100	gneiss	pine forest	5	0	n.d.
BK4	>100	quartz vein	pine forest	5	20	n.d.
BK5	>100	gneiss	pine forest	5	12	n.d.
GU11	90	granodiorite	semi-desert	n.d.	0	n.d.
GU12	80	granodiorite	semi-desert	n.d.	10	n.d.
GU13	130	granodiorite	semi-desert	n.d.	60	n.d.
GU15	80	granodiorite	semi-desert	n.d.	0	n.d.
GU16	80	granodiorite	semi-desert	n.d.	0	n.d.
GU19	70	granodiorite	semi-desert	n.d.	0	n.d.
GU21	160	granodiorite	semi-desert	n.d.	0	n.d.

Tab. A1.1 continued.

Sample ID	Height [cm]	Rock type	Vegetation	Snow cover [g/cm²]	Slope angle [°]	Sl. azimuth [°]
GU22	100	granodiorite	semi-desert	n.d.	0	n.d.
GU24	80	granodiorite	semi-desert	n.d.	0	n.d.
GU25	60	granodiorite	semi-desert	n.d.	0	n.d.
GU26	70	granodiorite	semi-desert	n.d.	0	n.d.
GU31	95	granodiorite	semi-desert	n.d.	0	n.d.
GU32	70	granodiorite	semi-desert	n.d.	0	n.d.
GU34	50	granodiorite	semi-desert	n.d.	0	n.d.
GU36	130	granodiorite	semi-desert	n.d.	0	n.d.
GU38	60	granodiorite	semi-desert	n.d.	0	n.d.
GU42	80	granodiorite	semi-desert	n.d.	0	n.d.
GU44	60	granodiorite	semi-desert	n.d.	0	n.d.
GU47	100	granodiorite	semi-desert	n.d.	0	n.d.
BY1	n.d.	granodiorite	semi-desert	n.d.	n.d.	n.d.
BY4	n.d.	granodiorite	semi-desert	n.d.	n.d.	n.d.
BY6	n.d.	granodiorite	semi-desert	n.d.	n.d.	n.d.
BY8	n.d.	granodiorite	semi-desert	n.d.	n.d.	n.d.
BY10	n.d.	granodiorite	semi-desert	n.d.	n.d.	n.d.
YK11	n.d.	granodiorite	semi-desert	n.d.	n.d.	n.d.
YK12	n.d.	granodiorite	semi-desert	n.d.	n.d.	n.d.
YK14	n.d.	granodiorite	semi-desert	n.d.	n.d.	n.d.
YK15	n.d.	granodiorite	semi-desert	n.d.	n.d.	n.d.
YK16	n.d.	granodiorite	semi-desert	n.d.	n.d.	n.d.
YK17	n.d.	granodiorite	semi-desert	n.d.	n.d.	n.d.
YK18	n.d.	granodiorite	semi-desert	n.d.	n.d.	n.d.
YK20	n.d.	granodiorite	semi-desert	n.d.	n.d.	n.d.
YK21	n.d.	granodiorite	semi-desert	n.d.	n.d.	n.d.
YK23	n.d.	granodiorite	semi-desert	n.d.	n.d.	n.d.
YK25	n.d.	granodiorite	semi-desert	n.d.	n.d.	n.d.
YK29	n.d.	granodiorite	semi-desert	n.d.	n.d.	n.d.
YK30	n.d.	granodiorite	semi-desert	n.d.	n.d.	n.d.
YK31	n.d.	granodiorite	semi-desert	n.d.	n.d.	n.d.
YK32	n.d.	granodiorite	semi-desert	n.d.	n.d.	n.d.
YK33	n.d.	granodiorite	semi-desert	n.d.	n.d.	n.d.
YK34	n.d.	granodiorite	semi-desert	n.d.	n.d.	n.d.
YK35	n.d.	granodiorite	semi-desert	n.d.	n.d.	n.d.
YK36	n.d.	granodiorite	semi-desert	n.d.	n.d.	n.d.
YK37	n.d.	granodiorite	semi-desert	n.d.	n.d.	n.d.
UK11	50	granodiorite	semi-desert	n.d.	20	0
UK12	100	granodiorite	semi-desert	n.d.	25	130
UK21	90	granodiorite	semi-desert	n.d.	25	250
UK24	40	granodiorite	semi-desert	n.d.	10	70
UK25	45	granodiorite	semi-desert	n.d.	25	110
UK26	55	granodiorite	semi-desert	n.d.	20	230
UK28	500	granodiorite	semi-desert	n.d.	25	50
UK31	70	granodiorite	semi-desert	n.d.	10	90
UK32	30	granodiorite	semi-desert	n.d.	20	140
UK33	50	granodiorite	semi-desert	n.d.	15	340
UK34	50	granodiorite	semi-desert	n.d.	30	270
UK35	30	granodiorite	semi-desert	n.d.	10	210
UK41	45	granodiorite	semi-desert	n.d.	20	220
UK42	40	granodiorite	semi-desert	n.d.	0	0
UK43	50	granodiorite	semi-desert	n.d.	30	210
UK44	50	granodiorite	semi-desert	n.d.	25	290
UK45	50	granodiorite	semi-desert	n.d.	0	0
UK51	50	granodiorite	semi-desert	n.d.	40	130
UK52	40	granodiorite	semi-desert	n.d.	0	0

Tab. A1.1 continued.

Sample ID	Height [cm]	Rock type	Vegetation	Snow cover [g/cm²]	Slope angle [°]	Sl. azimuth [°]
UK53	30	granodiorite	semi-desert	n.d.	30	220
UK54	40	granodiorite	semi-desert	n.d.	0	0
UK61	60	granodiorite	semi-desert	n.d.	25	100
AT11	30	granite	semi-desert	n.d.	0	0
AT13	50	quartz vein	semi-desert	n.d.	0	0
AT21	30	quartz vein	semi-desert	n.d.	5	180
AT22	30	quartz vein	semi-desert	n.d.	0	0
TK11	30	granite	semi-desert	n.d.	15	70
TK12	30	granite	semi-desert	n.d.	25	180
TK13	150	granite	semi-desert	n.d.	25	250
TK14	60	granite	semi-desert	n.d.	15	180
TK15	75	granite	semi-desert	n.d.	33	180
BO11	n.d.	granodiorite	semi-desert	n.d.	n.d.	n.d.
BO12	n.d.	granodiorite	semi-desert	n.d.	n.d.	n.d.
BO13	n.d.	granodiorite	semi-desert	n.d.	n.d.	n.d.
BO14	n.d.	granodiorite	semi-desert	n.d.	n.d.	n.d.
BO17	n.d.	granodiorite	semi-desert	n.d.	n.d.	n.d.
BO21	n.d.	granodiorite	semi-desert	n.d.	n.d.	n.d.
BO24	n.d.	granodiorite	semi-desert	n.d.	n.d.	n.d.
BO28	n.d.	granodiorite	semi-desert	n.d.	n.d.	n.d.
BO29	n.d.	granodiorite	semi-desert	n.d.	n.d.	n.d.
LT12	50	gneiss	deciduous forest	11	16	140
LT13	70	gneiss	deciduous forest	10	20	310
LT14	200	gneiss	deciduous forest	9	14	220
LT15	70	gneiss	deciduous forest	9	12	30
LT16	150	gneiss	deciduous forest	6	20	210
LT17	70	gneiss	deciduous forest	6	15	190
LT18	50	gneiss	deciduous forest	6	12	330
LT22	200	gneiss	deciduous forest	4	18	180
LT23	50	gneiss	deciduous forest	4	10	180
LT24	50	gneiss	deciduous forest	4	0	0
LT26	250	gneiss	deciduous forest	4	0	0
LT32	80	gneiss	deciduous forest	4	14	230
LT33	60	gneiss	deciduous forest	4	8	40
LT35	60	gneiss	deciduous forest	4	24	120
LT36	50	gneiss	deciduous forest	4	32	165
LT61	170	gneiss	deciduous forest	4	24	70
LT63	300	gneiss	deciduous forest	4	20	230

Tab. A1.2. Sample documentation II: Horizon shielding (A = azimuth, H = horizon angle).

Sample ID	A1 [°]	A2	H1 [°]	A3	H2	A4	H3	A5	H4	A6	H5	A7	H6	A8	H7	A9	H8	A10	H9	A11	H10
AK11	0	81	12	120	0	158	23	202	18	221	8	242	16	292	11	321	30	360	20		
AK12	0	81	12	120	0	158	23	202	18	221	8	242	16	292	11	321	30	360	20		
AK13	0	81	12	120	0	158	23	202	18	221	8	242	16	292	11	321	30	360	20		
AK21	0	37	4	68	0	167	12	184	9	201	21	220	17	244	14	281	30	318	22	0	16
AK22	0	37	4	68	0	167	12	184	9	201	21	220	17	244	14	281	30	318	22	0	16
AK23	0	37	4	68	0	167	12	184	9	201	21	220	17	244	14	281	30	318	22	0	16
AK24	0	37	4	68	0	167	12	184	9	201	21	220	17	244	14	281	30	318	22	0	16
AK25	0	37	4	68	0	167	12	184	9	201	21	220	17	244	14	281	30	318	22	0	16
AK31	0	37	5	68	0	167	13	184	9	201	22	220	17	244	14	281	26	318	22	0	16
AK32	0	37	5	68	0	167	13	184	9	201	22	220	17	244	14	281	26	318	22	0	16
AK33	0	37	5	68	0	167	13	184	9	201	22	220	17	244	14	281	26	318	22	0	16
AK34	0	37	5	68	0	167	13	184	9	201	22	220	17	244	14	281	26	318	22	0	16
AK35	0	37	5	68	0	167	13	184	9	201	22	220	17	244	14	281	26	318	22	0	16

Tab. A1.2 continued.

Sample ID	A1 [°]	A2	H1 [°]	A3	H2	A4	H3	A5	H4	A6	H5	A7	H6	A8	H7	A9	H8	A10	H9	A11	H10
AK41	0	39	10	56	25	106	16	133	20	160	17	192	12	255	2	315	12	341	22	0	16
AK42	0	39	10	56	25	106	16	133	20	160	17	192	12	255	2	315	12	341	22	0	16
AK43	0	39	10	56	25	106	16	133	20	160	17	192	12	255	2	315	12	341	22	0	16
AK44	0	39	10	56	25	106	16	133	20	160	17	192	12	255	2	315	12	341	22	0	16
AK45	0	39	10	56	25	106	16	133	20	160	17	192	12	255	2	315	12	341	22	0	16
AV1	n.d.																				
AV2	n.d.																				
AV3	n.d.																				
KK1	n.d.																				
KK2	n.d.																				
KK3	n.d.																				
MK22	n.d.																				
MK23	n.d.																				
MK24	n.d.																				
MK25	n.d.																				
MK41	n.d.																				
MK42	n.d.																				
MK43	n.d.																				
MK44	n.d.																				
MK45	n.d.																				
MK51	n.d.																				
MK52	n.d.																				
MK53	n.d.																				
MK54	n.d.																				
MK55	n.d.																				
MK71	n.d.																				
MK73	n.d.																				
MK74	n.d.																				
MK75	n.d.																				
BK1	185	260	10	320	5	340	0	10	10	40	15	65	10	100	15	125	18	185	5		
BK4	200	250	10	310	20	350	0	10	8	40	14	60	6	140	16	200	0				
BK5	180	250	10	320	8	340	0	360	6	50	14	70	6	150	14	180	2				
GU11	270	40	0	120	1	210	8	270	4												
GU12	270	40	2	120	2	210	10	270	4												
GU13	280	40	7	110	2	210	9	280	3												
GU15	250	60	1	120	3	220	9	250	2												
GU16	220	60	5	110	5	150	10	220	20												
GU19	260	50	1	145	5	260	8														
GU21	130	240	6	130	3																
GU22	130	240	6	130	3																
GU24	120	280	7	120	3																
GU25	120	280	8	120	3																
GU26	190	240	10	260	6	110	2	190	7												
GU31	130	190	6	230	8	130	5														
GU32	240	110	3	190	8	240	6														
GU34	140	240	8	140	5																
GU36	260	110	4	260	7																
GU38	320	120	3	200	8	320	8														
GU42	0	50	2	180	10	0	15														
GU44	0	40	2	130	7	200	8	0	14												
GU47	0	40	2	130	6	200	8	0	15												
BY1	50	140	4	180	7	230	15	280	6	50	12										
BY4	50	140	4	180	7	230	15	280	6	310	10	10	17	50	10						
BY6	50	140	4	180	7	230	15	280	10	310	10	10	17	50	10						
BY8	50	140	4	180	7	230	15	280	7	310	10	10	17	50	10						
BY10	50	140	4	180	7	230	15	280	6	310	10	10	17	50	10						
YK11	10	110	5	180	7	250	15	300	4	10	10										
YK12	10	110	5	180	7	250	15	300	4	10	10										
YK14	10	110	5	180	7	250	15	300	4	10	10										
YK15	10	110	5	180	7	250	15	300	4	10	10										
YK16	10	110	5	180	7	250	15	300	4	10	10										
YK17	10	110	5	180	7	250	15	300	4	10	10										
YK18	10	110	5	180	7	250	15	300	4	10	10										
YK20	20	140	5	180	7	230	13	280	5	20	8										
YK21	20	80	6	110	2	180	7	230	10	310	5	20	15								
YK23	20	80	6	110	2	180	7	230	10	310	5	20	15								
YK25	20	140	5	180	7	230	13	280	5	20	8										
YK29	20	140	5	180	7	230	13	280	5	20	8										
YK30	60	110	1	200	7	250	12	310	3	350	7	60	4								
YK31	60	110	1	210	8	230	23	270	10	60	4										

Tab. A1.2 continued.

Sample ID	A1 [°]	A2	H1 [°]	A3	H2	A4	H3	A5	H4	A6	H5	A7	H6	A8	H7	A9	H8	A10	H9	A11	H10
YK32	60	110	1	210	8	230	23	270	10	60	4										
YK33	60	110	1	210	8	230	21	270	10	60	4										
YK34	60	110	1	210	8	230	20	270	10	60	4										
YK35	60	110	1	210	8	230	20	270	10	60	4										
YK36	60	110	1	210	8	230	18	270	10	60	4										
YK37	60	110	1	200	7	250	13	310	3	350	7	60	4								
UK11	90	220	3	260	5	330	3	45	1	90	3										
UK12	90	220	3	260	5	330	3	45	1	90	3										
UK21	130	230	3	270	6	340	4	355	2	100	4	130	1								
UK24	130	170	3	220	4	270	6	340	4	0	2	110	4	130	1						
UK25	5	110	4	125	1	140	3	225	4	315	7	330	3	5	2						
UK26	110	120	1	170	3	240	4	270	6	340	4	355	2	111	5						
UK28	0	110	4	120	1	140	3	230	3	280	7	330	4	0	1						
UK31	130	250	5	5	6	80	3	130	2												
UK32	140	250	4	300	10	5	5	80	3	140	2										
UK33	130	250	4	300	10	5	5	80	3	130	2										
UK34	130	250	4	300	10	10	5	80	3	130	2										
UK35	130	250	4	300	10	10	5	80	3	130	2										
UK41	20	70	1	130	3	160	7	185	10	230	6	280	9	330	6	20	3				
UK42	20	70	1	130	3	160	7	185	10	230	6	280	9	330	6	20	3				
UK43	30	60	2	120	3	150	7	185	9	220	6	275	9	340	6	30	3				
UK44	10	60	2	130	3	170	7	200	11	240	5	300	9	350	5	10	4				
UK45	0	70	1	120	3	140	8	170	12	220	5	280	13	0	5						
UK51	10	40	12	80	2	140	14	210	27	240	15	300	17	10	27						
UK52	10	50	8	80	1	140	18	210	25	240	15	270	11	295	22	10	25				
UK53	40	80	0	120	5	220	22	260	12	310	18	340	29	40	14						
UK54	40	80	0	120	4	220	20	260	14	310	18	0	30	40	14						
UK61	20	50	7	75	1	120	15	205	27	240	19	285	13	20	24						
AT11	220	270	8	300	2	320	6	10	12	60	14	90	8	160	3	220	10				
AT13	230	270	12	310	4	340	7	20	10	100	15	140	4	200	11	230	17				
AT21	40	130	10	160	2	200	9	260	15	270	5	290	2	330	8	30	12	40	4		
AT22	40	130	10	160	2	200	9	260	15	270	5	290	2	330	8	30	12	40	4		
TK11	230	270	15	350	8	10	5	50	7	90	4	120	2	150	8	230	22				
TK12	230	310	18	10	4	70	5	110	9	130	5	150	2	210	10	230	24				
TK13	260	350	9	10	4	50	7	90	4	120	2	150	7	210	22	260	19				
TK14	260	350	7	10	3	50	7	90	4	120	2	150	6	210	16	260	20				
TK15	260	310	4	350	7	10	3	50	7	90	4	120	2	150	7	220	20	260	14		
BO11	270	40	4	120	10	180	20	220	5	270	10										
BO12	270	0	4	90	10	180	18	220	5	270	10										
BO13	270	40	4	90	10	180	18	220	5	270	10										
BO14	270	70	4	130	8	180	18	220	5	270	10										
BO17	270	90	4	120	7	180	20	270	7												
BO21	270	90	4	140	10	180	18	200	12	270	8										
BO24	270	90	4	140	10	180	17	200	13	270	8										
BO28	270	90	4	150	8	200	15	270	7												
BO29	270	90	4	150	8	200	15	270	7												
LT12	200	240	6	280	24	0	42	60	24	90	10	110	26	180	38	200	16				
LT13	200	240	6	280	24	0	42	60	24	90	10	110	26	180	38	200	16				
LT14	200	240	6	280	24	0	42	60	24	90	10	110	26	180	38	200	16				
LT15	200	240	6	280	24	0	42	60	24	90	10	110	26	180	38	200	16				
LT16	210	230	2	280	20	60	48	80	14	120	28	190	36	210	16						
LT17	210	230	2	280	20	60	48	80	14	120	28	190	36	210	16						
LT18	210	230	2	280	20	60	48	80	14	120	28	190	36	210	16						
LT22	0	30	4	80	12	170	18	220	12	240	4	0	16								
LT23	0	30	4	80	12	170	18	220	12	240	4	0	16								
LT24	0	30	4	80	12	170	18	220	12	240	4	0	16								
LT26	0	30	4	80	12	170	18	220	12	240	4	0	16								
LT32	270	290	6	310	10	0	14	80	30	110	9	270	20								
LT33	270	290	5	310	10	0	14	80	30	110	10	270	20								
LT35	270	290	5	310	10	0	14	80	30	110	10	270	20								
LT36	270	290	5	310	10	0	14	80	30	110	10	270	20								
LT61	270	320	18	330	28	50	38	80	16	100	6	140	16	180	20	220	30	250	12	270	4
LT63	270	320	18	330	28	50	38	80	16	100	6	140	16	180	20	220	30	250	12	270	4

Tab. A1.3. Measurement data.

Zurich Label	Sample ID	Blank	Current [nA]	$^{10}Be/^{9}Be$ [10^{-12}]	Error [%]	Mass carrier [mg]	Mass sample [g]
ZB1475	AK blank 1	-	393	0.058	46.4	0.401	-
ZB1476	AK11	AK blank 2, 3	408	0.453	6.7	0.408	25.054
ZB1477	AK12a	AK blank 2, 3	123	0.983	7.3	0.408	29.699
ZB1478	AK13	AK blank 2, 3	199	0.554	7.7	0.407	29.301
ZB1480	AK blank 2	-	296	0.036	30.2	0.401	-
ZB1481	AK21	AK blank 2, 3	224	0.791	6.0	0.410	25.460
ZB1482	AK22	AK blank 2, 3	192	0.741	6.5	0.400	42.600
ZB1483	AK23	AK blank 2, 3	148	0.723	7.7	0.400	33.640
ZB1484	AK24	AK blank 2, 3	220	0.881	5.7	0.400	33.190
ZB1485	AK blank 3	-	587	0.022	24.9	0.401	-
ZB1486	AK31	AK blank 2, 3	396	0.625	5.2	0.425	43.400
ZB1487	AK32	AK blank 2, 3	542	1.379	4.7	0.435	38.100
ZB1488	AK33	AK blank 2, 3	431	1.118	4.6	0.435	37.580
ZB1489	AK34	AK blank 2, 3	134	1.017	6.8	0.415	39.700
ZB1570	AV1	KK blank	492	0.680	5.7	0.413	28.881
ZB1571	AV2	KK blank	502	0.723	5.5	0.413	30.643
ZB1572	AV3	KK blank	454	0.895	5.5	0.413	37.599
ZB1573	KK1	KK blank	306	2.874	4.0	0.413	42.472
ZB1574	KK2	KK blank	366	2.686	3.9	0.413	36.336
ZB1575	KK3	KK blank	473	2.437	3.6	0.413	38.492
ZB1576	KK blank	-	650	0.027	21.1	0.413	-
ZB1577	AK12b	AK blank 4	622	1.078	4.6	0.397	43.635
ZB1578	AK25	AK blank 4	830	1.046	5.4	0.399	39.554
ZB1579	AK35	AK blank 4	677	0.373	5.6	0.394	17.703
ZB1580	AK41	AK blank 4	865	0.698	4.9	0.998	46.239
ZB1581	AK42	AK blank 4	649	1.286	3.8	0.395	40.967
ZB1582	AK43	AK blank 4	601	1.541	5.4	0.399	52.346
ZB1583	AK44	AK blank 4	746	0.836	4.8	0.394	25.632
ZB1584	AK45	AK blank 4	778	1.071	4.1	0.398	44.214
ZB1585	AK blank 4	-	852	0.022	33.4	0.400	-
ZB1763	MK22	MK blank 1	143	2.438	7.0	0.603	51.574
ZB1764	MK23	MK blank 1	265	1.406	7.4	0.603	45.925
ZB1765	MK24	MK blank 1	385	1.224	6.0	0.602	57.215
ZB1766	MK25	MK blank 1	306	0.933	6.9	0.602	33.672
ZB1768	MK42	MK blank 1	432	0.192	13.0	0.595	70.039
ZB1769	MK43	MK blank 1	286	0.578	7.5	0.598	124.938
ZB1770	MK44	MK blank 1	107	0.356	14.6	0.595	87.812
ZB1771	MK45	MK blank 1	118	0.218	17.7	0.596	45.554
ZB1772	MK blank 1	-	632	0.019	38.7	0.450	-
ZB1774	MK52	MK blank 2	151	1.430	6.8	0.441	86.006
ZB1777	MK55	MK blank 2	118	1.101	10.4	0.447	63.366
ZB1780	MK blank 2	-	628	0.018	39.9	0.447	-
ZB1784	MK71	MK blank 3	71	2.382	7.4	0.598	114.778
ZB1787	MK74	MK blank 3	115	0.540	9.4	0.591	47.188
ZB1789	MK blank 3	-	501	0.027	32.4	0.442	-
ZB1949	MK41	MK blank 1	172	0.408	8.3	0.594	62.641
ZB1950	MK51	MK blank 2	91	1.482	7.9	0.450	37.593
ZB1951	MK53	MK blank 2	83	2.014	7.3	0.450	57.567
ZB1952	MK54	MK blank 2	41	2.136	8.3	0.448	70.853
ZB1957	MK73	MK blank 3	62	0.957	11.5	0.596	79.428
ZB1958	MK75	MK blank 3	151	0.558	8.2	0.591	47.188
ZB1959	BK1	BK blank	430	0.818	5.6	0.443	112.035
ZB1960	BK2	BK blank	865	0.554	4.9	0.447	110.843
ZB1961	BK3	BK blank	911	0.466	5.3	0.449	85.839
ZB1962	BK4	BK blank	817	0.688	3.8	0.452	101.692

Tab. A1.3 continued.

Zurich Label	Sample ID	Blank	Current [nA]	$^{10}Be/^{9}Be$ [10^{-12}]	Error [%]	Mass carrier [mg]	Mass sample [g]
ZB1963	BK5	BK blank	570	0.927	6.4	0.449	128.942
ZB1964	BK blank	-	820	0.020	29.1	0.452	-
ZB1969	BY 10a	YK blank 1	242	0.433	8.1	0.452	34.365
ZB1970	YK20	YK blank 1	515	4.418	2.7	0.451	33.617
ZB1971	YK 23	YK blank 1	463	1.945	4.1	0.452	46.251
ZB1972	YK 25	YK blank 1	592	2.215	3.4	0.453	31.648
ZB1973	YK 29	YK blank 1	441	2.659	3.7	0.453	29.750
ZB1974	YK blank 1	-	1288	0.029	16.5	0.452	-
ZB1975	GU11	GU blank 1	435	3.072	3.4	0.425	19.086
ZB1976	GU12	GU blank 1	723	3.743	1.9	0.451	35.371
ZB1977	GU13	GU blank 1	702	2.127	2.7	0.445	37.648
ZB1978	GU15	GU blank 1	615	2.491	2.6	0.453	28.576
ZB1979	GU19	GU blank 1	444	6.253	2.0	0.455	29.480
ZB1980	GU31	GU blank 1	680	1.641	3.4	0.449	36.009
ZB1981	GU32	GU blank 1	572	3.743	2.7	0.450	33.853
ZB1982	GU34	GU blank 1	821	2.064	3.0	0.448	33.362
ZB1983	GU36	GU blank 1	592	2.516	5.6	0.452	31.983
ZB1984	GU blank 1	-	1047	0.031	11.2	0.447	-
ZB2057	YK11	YK blank 2	765	6.867	3.6	0.452	45.893
ZB2058	YK12	YK blank 2	1422	10.162	3.5	0.451	63.130
ZB2059	YK14	YK blank 2	1514	9.776	4.2	0.451	60.827
ZB2060	YK16	YK blank 2	1186	10.498	3.9	0.450	61.557
ZB2061	YK17	YK blank 2	1566	9.847	3.8	0.449	59.060
ZB2062	YK18	YK blank 2	978	13.940	3.5	0.450	84.323
ZB2063	YK30	YK blank 2	1228	1.212	4.3	0.452	32.891
ZB2064	YK33	YK blank 2	1635	3.827	3.8	0.451	61.902
ZB2065	YK36	YK blank 2	1507	2.187	3.6	0.447	24.756
ZB2066	YK blank 2	-	988	0.060	8.5	0.450	-
ZB2067	YK15	YK blank 3	837	7.001	5.0	0.449	46.087
ZB2068	YK21	YK blank 3	812	3.875	4.2	0.449	30.712
ZB2069	YK31	YK blank 3	1238	4.696	4.0	0.448	78.501
ZB2070	YK32	YK blank 3	525	1.444	5.9	0.450	23.771
ZB2071	YK37	YK blank 3	933	1.439	6.0	0.450	44.055
ZB2072	GU16	YK blank 3	1063	1.609	3.9	0.449	23.027
ZB2074	GU47	YK blank 3	772	2.117	7.0	0.450	27.441
ZB2075	YK blank 3	-	1045	0.027	22.3	0.450	-
ZB2076	BY1	YK blank 4	849	0.498	5.9	0.452	43.536
ZB2077	BY4	YK blank 4	1187	0.192	7.2	0.451	13.324
ZB2078	BY6	YK blank 4	985	0.231	7.1	0.453	19.316
ZB2079	BY 8	YK blank 4	1005	0.255	6.9	0.451	20.546
ZB2080	BY10b	YK blank 4	1035	0.598	7.4	0.451	48.477
ZB2081	YK blank 4	-	883	0.043	16.0	0.452	-
ZB2082	GU blank 2	-	769	0.049	17.4	0.450	-
ZB2083	GU21	GU blank 2	966	2.490	4.7	0.449	31.619
ZB2084	GU22	GU blank 2	605	1.930	6.6	0.450	28.946
ZB2085	GU24	GU blank 2	253	4.572	4.4	0.454	32.700
ZB2086	GU25	GU blank 2	571	5.837	4.2	0.453	38.234
ZB2087	GU26	GU blank 2	511	2.687	3.7	0.451	42.195
ZB2089	GU38	GU blank 2	88	1.176	8.7	0.452	20.045
ZB2090	GU42	GU blank 2	80	2.375	7.5	0.452	36.633
ZB2091	GU44	GU blank 2	948	1.898	3.7	0.451	36.675
ZB2371	UK11	UK blank 1	1257	6.718	3.0	0.442	20.254
ZB2372	UK12	UK blank 1	882	10.427	3.0	0.445	44.482
ZB2373	UK21	UK blank 1	913	6.621	3.1	0.441	36.718
ZB2374	UK24	UK blank 1	1108	1.062	4.4	0.444	10.824

Tab. A1.3 continued.

Zurich Label	Sample ID	Blank	Current [nA]	$^{10}Be/^{9}Be$ [10^{-12}]	Error [%]	Mass carrier [mg]	Mass sample [g]
ZB2375	UK26	UK blank 1	976	1.747	3.3	0.445	20.015
ZB2376	UK blank 1	-	802	0.095	11.6	0.438	-
ZB2377	UK28	UK blank 1	488	7.198	3.0	0.441	41.996
ZB2378	UK31	UK blank 1	852	6.208	3.0	0.447	38.943
ZB2379	UK33	UK blank 1	893	4.221	3.9	0.445	24.206
ZB2380	UK35	UK blank 1	1181	8.243	3.0	0.448	35.522
ZB2381	UK34	UK blank 2	1021	8.752	3.0	0.419	65.260
ZB2382	UK41	UK blank 2	258	1.392	5.4	0.416	25.823
ZB2383	UK42	UK blank 2	892	1.645	4.5	0.423	29.849
ZB2384	UK43	UK blank 2	878	4.007	3.0	0.415	60.189
ZB2385	UK44	UK blank 2	529	0.782	5.1	0.416	18.617
ZB2386	UK blank 2	-	663	0.053	10.9	0.421	0.000
ZB2387	UK51	UK blank 2	1300	3.476	3.0	0.414	70.449
ZB2388	UK53	UK blank 2	782	4.891	3.0	0.417	38.764
ZB2389	UK54	UK blank 2	1035	2.438	3.0	0.427	49.183
ZB2390	UK61	UK blank 2	1101	2.941	3.0	0.417	61.833
ZB2391	UK25	UK blank 3	979	1.801	3.1	0.411	29.873
ZB2392	UK32	UK blank 3	929	5.316	3.0	0.415	25.245
ZB2393	UK45	UK blank 3	228	5.119	3.9	0.408	61.081
ZB2394	UK52	UK blank 3	882	3.670	3.0	0.412	68.524
ZB2395	AT11	UK blank 3	378	1.407	4.5	0.426	13.489
ZB2396	UK blank 3	-	879	0.036	19.3	0.420	-
ZB2397	AT 13	UK blank 3	1309	2.863	8.4	0.422	63.544
ZB2449	TK blank	-	1505	0.027	14.3	0.449	-
ZB2450	TK11	TK blank	1107	3.418	3.0	0.449	18.240
ZB2451	TK12	TK blank	1029	8.599	3.9	0.449	53.591
ZB2452	TK13	TK blank	1451	6.470	3.0	0.449	35.398
ZB2453	TK14	TK blank	1390	4.590	3.0	0.449	22.740
ZB2454	TK15	TK blank	715	7.101	3.0	0.449	36.958
ZB2455	AT21	TK blank	1440	3.010	3.0	0.449	64.323
ZB2456	AT22	TK blank	1506	1.780	3.0	0.449	49.620
ZB2457	YK34	TK blank	988	7.281	3.0	0.449	55.408
ZB2458	YK35	TK blank	1422	4.622	3.0	0.449	39.139
ZB2541	BO blank	-	1363	0.030	10.4	0.452	-
ZB2542	BO11	BO blank	850	3.966	3.0	0.449	43.758
ZB2543	BO12	BO blank	1411	4.480	3.9	0.449	51.831
ZB2544	BO13	BO blank	1180	4.891	3.0	0.450	34.367
ZB2545	BO14	BO blank	1013	6.623	3.0	0.450	37.685
ZB2546	BO17	BO blank	1142	4.573	3.0	0.449	34.442
ZB2547	BO21	BO blank	757	2.227	3.1	0.450	41.408
ZB2548	BO24	BO blank	1026	3.004	3.0	0.450	57.325
ZB2549	BO28	BO blank	924	1.527	3.3	0.450	28.538
ZB2550	BO29	BO blank	924	1.052	3.4	0.451	20.248
ZB2643	LT12	LT blank 1	791	0.059	12.9	0.449	39.851
ZB2644	LT13	LT blank 1	785	0.071	19.9	0.449	38.845
ZB2645	LT14	LT blank 1	1098	0.053	14.6	0.449	43.908
ZB2646	LT15	LT blank 1	752	0.062	12.2	0.449	69.229
ZB2647	LT16	LT blank 1	736	0.099	10.4	0.449	45.707
ZB2648	LT22	LT blank 1	353	1.610	4.3	0.449	52.408
ZB2649	LT23	LT blank 1	863	1.228	3.0	0.449	42.472
ZB2650	LT24	LT blank 1	296	1.397	4.6	0.449	45.855
ZB2651	LT26	LT blank 1	484	1.528	4.2	0.449	61.077
ZB2652	LT blank 1	-	1014	0.032	9.5	0.449	-
ZB2653	LT17	LT blank 2	759	0.058	19.5	0.449	31.695
ZB2654	LT18	LT blank 2	902	0.040	13.1	0.448	47.711

Tab. A1.3 continued.

Zurich Label	Sample ID	Blank	Current [nA]	$^{10}Be/^{9}Be$ [10^{-12}]	Error [%]	Mass carrier [mg]	Mass sample [g]
ZB2655	LT32	LT blank 2	971	0.776	3.1	0.450	52.902
ZB2656	LT33	LT blank 2	885	0.524	3.2	0.449	37.676
ZB2657	LT35	LT blank 2	633	0.611	3.7	0.447	38.720
ZB2658	LT36	LT blank 2	1034	0.445	3.0	0.448	66.762
ZB2659	LT61	LT blank 2	1216	0.162	4.8	0.450	33.852
ZB2660	LT63	LT blank 2	937	0.265	3.9	0.449	55.384
ZB2661	LT blank 2	-	905	0.017	21.5	0.448	-
ZB2662	LT22b	LT blank 1	1117	1.524	3.1	0.449	52.408

Appendix 2. Recalculated exposure ages

Tab. A2.1. Recalculated exposure ages used in the figures.

Figure	Stage	Source	Original label	Minimum age [ka]	Maximum age [ka]
Fig. 3.3	KD	Tschudi et al. 2003	KAN1	12.7 ± 1.5	13.0 ± 1.6
Fig. 3.3	KD	Tschudi et al. 2003	KAN2	10.8 ± 1.3	11.0 ± 1.4
Fig. 3.3	LI	Schaefer et al., 2002	Lit 3	13.1 ± 1.4	13.3 ± 1.5
Fig. 3.3	LI	Schaefer et al., 2002	Lit 4a	16.6 ± 1.9	17.1 ± 2.1
Fig. 3.3	LI	Schaefer et al., 2002	Lit 4bc	14.1 ± 1.6	14.4 ± 1.7
Fig. 3.3	LI	Schaefer et al., 2002	Lit 5a	14.3 ± 1.6	14.7 ± 1.7
Fig. 3.3	LI	Schaefer et al., 2002	Lit 5b	14.3 ± 1.6	14.7 ± 1.7
Fig. 3.3	LI	Schaefer et al., 2002	Lit 6	14.6 ± 1.6	15.0 ± 1.7
Fig. 3.3	LI	Schaefer et al., 2002	Lit 7	12.5 ± 1.4	12.7 ± 1.5
Fig. 3.3	LJ11	Owen et al., 2003a	LJ7	18.5 ± 2.0	19.2 ± 2.3
Fig. 3.3	LJ11	Owen et al., 2003a	LJ8	22.3 ± 2.3	23.3 ± 2.8
Fig. 3.3	LJ11	Owen et al., 2003a	LJ9	54.1 ± 5.8	65 ± 12
Fig. 3.3	LJ11	Owen et al., 2003a	LJ10	18.5 ± 1.9	19.3 ± 2.2
Fig. 3.3	LJ12	Owen et al., 2003a	LJ13	16.2 ± 1.7	16.7 ± 1.9
Fig. 3.3	LJ12	Owen et al., 2003a	LJ14	15.5 ± 1.6	16.0 ± 1.8
Fig. 3.3	LJ13	Owen et al., 2003a	LJ4	9.7 ± 1.0	9.8 ± 1.1
Fig. 3.3	LJ21	Owen et al., 2003a	LJ1	15.7 ± 1.6	16.1 ± 1.8
Fig. 3.3	LJ21	Owen et al., 2003a	LJ2	12.2 ± 1.3	12.5 ± 1.4
Fig. 3.3	LJ21	Owen et al., 2003a	LJ3	29.4 ± 3.1	31.6 ± 4.1
Fig. 3.3	LJ22	Owen et al., 2003a	LJ15	8.3 ± 0.9	8.4 ± 0.9
Fig. 3.3	LJ22	Owen et al., 2003a	LJ16	7.9 ± 0.8	8.0 ± 0.8
Fig. 3.3	LJ22	Owen et al., 2003a	LJ17	15.2 ± 1.6	15.6 ± 1.7
Fig. 3.3	LJ23	Owen et al., 2003a	LJ11	8.1 ± 0.8	8.2 ± 0.9
Fig. 3.3	LJ23	Owen et al., 2003a	LJ12	14.5 ± 1.6	14.9 ± 1.7
Fig. 3.3	QS11	Owen et al. 2003b	Q1	14.2 ± 1.5	14.6 ± 1.6
Fig. 3.3	QS11	Owen et al. 2003b	Q2	8.6 ± 0.9	8.8 ± 0.9
Fig. 3.3	QS11	Owen et al. 2003b	Q3	9.1 ± 0.9	9.2 ± 1.0
Fig. 3.3	QS12	Owen et al. 2003b	Q18	17.0 ± 1.8	17.7 ± 2.0
Fig. 3.3	QS12	Owen et al. 2003b	Q19	8.9 ± 1.0	9.0 ± 1.1
Fig. 3.3	QS12	Owen et al. 2003b	Q20	12.6 ± 1.3	12.9 ± 1.4
Fig. 3.3	QS13	Owen et al. 2003b	Q12	9.2 ± 1.1	9.4 ± 1.1
Fig. 3.3	QS13	Owen et al. 2003b	Q13	18.7 ± 2.0	19.5 ± 2.3
Fig. 3.3	QS13	Owen et al. 2003b	Q14	13.0 ± 1.5	13.3 ± 1.6
Fig. 3.3	QS21	Owen et al. 2003b	Q15	16.0 ± 1.7	16.5 ± 1.9

Tab. A2.1 continued.

Figure	Stage	Source	Original label	Minimum age [ka]	Maximum age [ka]
Fig. 3.3	QS21	Owen et al. 2003b	Q16	15.4 ± 1.8	15.8 ± 2.0
Fig. 3.3	QS21	Owen et al. 2003b	Q17	15.4 ± 1.6	15.8 ± 1.8
Fig. 3.3	QS22	Owen et al. 2003b	Q9	9.6 ± 1.1	9.7 ± 1.1
Fig. 3.3	QS22	Owen et al. 2003b	Q10	11.6 ± 1.3	11.8 ± 1.4
Fig. 3.3	QS22	Owen et al. 2003b	Q11	10.6 ± 1.2	10.8 ± 1.2
Fig. 4.4	TH I	Finkel et al., 2003	E84	71 ± 8	98 ± 24
Fig. 4.4	TH I	Finkel et al., 2003	E85	68 ± 7	92 ± 22
Fig. 4.4	TH I	Finkel et al., 2003	E86	62 ± 7	81 ± 17
Fig. 4.4	TH I	Finkel et al., 2003	E87	34 ± 4	38 ± 5
Fig. 4.4	TH I	Finkel et al., 2003	E88	24.3 ± 2.6	26.4 ± 3.3
Fig. 4.4	TH I	Finkel et al., 2003	E89	24.8 ± 2.7	27.1 ± 3.5
Fig. 4.4	TH II	Finkel et al., 2003	E75	28.6 ± 3.0	32 ± 4
Fig. 4.4	TH II	Finkel et al., 2003	E76	33 ± 6	36 ± 8
Fig. 4.4	TH II	Finkel et al., 2003	E77	26.6 ± 2.9	29.1 ± 3.8
Fig. 4.5	BH	Barnard et al., 2003	BH35B	14.1 ± 1.5	15.0 ± 1.7
Fig. 4.5	BH	Barnard et al., 2003	BH36	10.3 ± 1.1	10.9 ± 1.2
Fig. 4.5	BH	Barnard et al., 2003	BH37	7.7 ± 0.8	8.1 ± 0.9
Fig. 4.5	CH3	Finkel et al., 2003	E39	16.8 ± 1.8	18.0 ± 2.1
Fig. 4.5	CH3	Finkel et al., 2003	E40	21.0 ± 2.3	22.7 ± 2.8
Fig. 4.5	CH3	Finkel et al., 2003	E45	25.5 ± 2.7	27.8 ± 3.5
Fig. 4.5	CH3	Finkel et al., 2003	E46	16.1 ± 1.7	17.1 ± 2.0
Fig. 4.5	CH3	Finkel et al., 2003	E57	18.6 ± 2.0	20.0 ± 2.4
Fig. 4.5	CH3	Finkel et al., 2003	E58	21.3 ± 2.4	22.9 ± 3.0
Fig. 4.5	CH3	Finkel et al., 2003	E59	6.5 ± 0.7	6.7 ± 0.7
Fig. 4.5	CH5	Finkel et al., 2003	E29	15.2 ± 1.6	16.1 ± 1.8
Fig. 4.5	CH5	Finkel et al., 2003	E30	8.0 ± 0.9	8.4 ± 0.9
Fig. 4.5	CH5	Finkel et al., 2003	E31	7.9 ± 0.8	8.3 ± 0.9
Fig. 4.5	CH6	Finkel et al., 2003	E61	3.4 ± 0.4	3.6 ± 0.5
Fig. 4.5	CH6	Finkel et al., 2003	E62	3.3 ± 0.4	3.4 ± 0.4
Fig. 4.5	CH6	Finkel et al., 2003	E63	3.0 ± 0.4	3.1 ± 0.4
Fig. 4.5	KE	Barnard et al., 2003	BH19	6.7 ± 0.7	7.0 ± 0.8
Fig. 4.5	KE	Barnard et al., 2003	BH20	6.3 ± 0.7	6.5 ± 0.7
Fig. 4.5	KH3	Finkel et al., 2003	E9	19.5 ± 2.1	21.0 ± 2.5
Fig. 4.5	KH3	Finkel et al., 2003	E10	19.6 ± 2.1	21.1 ± 2.5
Fig. 4.5	KH3	Finkel et al., 2003	E11	19.6 ± 2.1	21.1 ± 2.5
Fig. 4.5	KH4	Finkel et al., 2003	E5	16.0 ± 1.7	17.1 ± 2.0
Fig. 4.5	KH4	Finkel et al., 2003	E6	13.1 ± 1.4	13.9 ± 1.6
Fig. 4.5	KH4	Finkel et al., 2003	E7	13.9 ± 1.5	14.8 ± 1.7
Fig. 4.5	KH4	Finkel et al., 2003	E71	25.4 ± 3.0	27.7 ± 3.8
Fig. 4.5	KH4	Finkel et al., 2003	E73	13.5 ± 1.5	14.3 ± 1.7
Fig. 4.5	KH5	Finkel et al., 2003	E79	8.2 ± 0.9	8.7 ± 1.0
Fig. 4.5	KH5	Finkel et al., 2003	E80	8.4 ± 0.9	8.8 ± 1.0
Fig. 4.5	KH5	Finkel et al., 2003	E81	8.4 ± 0.9	8.9 ± 1.0
Fig. 4.5	KH6	Finkel et al., 2003	E82	1.3 ± 0.2	1.4 ± 0.2
Fig. 5.10	BJ	Owen et al., 2002c	KK98-47	45 ± 5	52 ± 8
Fig. 5.10	BJ	Owen et al., 2002c	KK98-50	54 ± 6	66 ± 12
Fig. 5.10	BJ	Owen et al., 2002c	KK98-55	48 ± 5	57 ± 10
Fig. 5.10	BJ	Owen et al., 2002c	KK98-56	47 ± 5	56 ± 9
Fig. 5.10	BJ	Owen et al., 2002c	KK98-57	47 ± 5	56 ± 9
Fig. 5.10	BJ	Owen et al., 2002c	KK98-64	27.3 ± 2.9	29.2 ± 3.7
Fig. 5.10	BJ	Owen et al., 2002c	KK98-65	35 ± 4	39 ± 5
Fig. 5.10	NP	Phillips et al., 2000	R97-0187	54 ± 7	65 ± 13
Fig. 5.10	NP	Phillips et al., 2000	R97-0859	34 ± 4	37 ± 6
Fig. 5.10	NP	Phillips et al., 2000	R97-0183	52 ± 6	64 ± 12
Fig. 5.10	TG	Schaefer et al., 2002	TAN 7	58 ± 6	70 ± 14

Tab. A2.1 continued.

Figure	Stage	Source	Original label	Minimum age [ka]	Maximum age [ka]
Fig. 5.11	GHI	Owen et al., 2002c	KK98-6	23.1 ± 2.7	24.4 ± 3.2
Fig. 5.11	GHI	Owen et al., 2002c	KK98-7	22.7 ± 2.5	23.9 ± 3.0
Fig. 5.11	GHI	Owen et al., 2002c	KK98-8	25.3 ± 2.8	26.9 ± 3.5
Fig. 5.11	GHI	Owen et al., 2002c	KK98-9	24.4 ± 2.7	25.9 ± 3.3
Fig. 5.11	GHI	Owen et al., 2002c	KK98-10	21.5 ± 2.4	22.5 ± 2.8
Fig. 5.11	GHII	Owen et al., 2002c	KK98-11	15.6 ± 5.8	16.2 ± 6.2
Fig. 5.11	GHII	Owen et al., 2002c	KK98-12	24.9 ± 2.7	26.4 ± 3.3
Fig. 5.11	GHII	Owen et al., 2002c	KK98-13	18.9 ± 2.1	19.7 ± 2.4
Fig. 5.11	GHII	Owen et al., 2002c	KK98-14	22.8 ± 2.6	24.1 ± 3.1
Fig. 5.11	GHII	Owen et al., 2002c	KK98-15	18.7 ± 2.1	19.5 ± 2.4
Fig. 5.11	LJI	Owen et al., 2003a	LJ4	9.7 ± 1.1	9.9 ± 1.1
Fig. 5.11	LJI	Owen et al., 2003a	LJ13	16.3 ± 1.7	16.8 ± 1.9
Fig. 5.11	LJI	Owen et al., 2003a	LJ14	15.6 ± 1.6	16.0 ± 1.8
Fig. 5.11	LJI	Owen et al., 2003a	LJ7	18.5 ± 2.0	19.3 ± 2.3
Fig. 5.11	LJI	Owen et al., 2003a	LJ8	22.3 ± 2.4	23.4 ± 2.8
Fig. 5.11	LJI	Owen et al., 2003a	LJ9	54 ± 6	65 ± 12
Fig. 5.11	LJI	Owen et al., 2003a	LJ10	18.6 ± 2.0	19.3 ± 2.2
Fig. 5.11	LJII	Owen et al., 2003a	LJ1	15.7 ± 1.7	16.2 ± 1.9
Fig. 5.11	LJII	Owen et al., 2003a	LJ2	12.3 ± 1.3	12.5 ± 1.4
Fig. 5.11	LJII	Owen et al., 2003a	LJ3	29.5 ± 3.2	32 ± 4
Fig. 5.11	LJII	Owen et al., 2003a	LJ15	8.3 ± 0.9	8.5 ± 1.0
Fig. 5.11	LJII	Owen et al., 2003a	LJ16	7.9 ± 0.8	8.0 ± 0.9
Fig. 5.11	LJII	Owen et al., 2003a	LJ17	15.2 ± 1.6	15.7 ± 1.8
Fig. 5.11	LJII	Owen et al., 2003a	LJ11	8.2 ± 0.9	8.3 ± 0.9
Fig. 5.11	LJII	Owen et al., 2003a	LJ12	14.5 ± 1.6	14.9 ± 1.8
Fig. 5.11	QSI	Owen et al. 2003b	Q1	14.2 ± 1.5	14.6 ± 1.7
Fig. 5.11	QSI	Owen et al. 2003b	Q2	8.7 ± 0.9	8.8 ± 1.0
Fig. 5.11	QSI	Owen et al. 2003b	Q3	9.1 ± 1.0	9.3 ± 1.0
Fig. 5.11	QSI	Owen et al. 2003b	Q18	17.1 ± 1.8	17.7 ± 2.1
Fig. 5.11	QSI	Owen et al. 2003b	Q19	8.9 ± 1.1	9.0 ± 1.2
Fig. 5.11	QSI	Owen et al. 2003b	Q20	12.6 ± 1.4	12.9 ± 1.5
Fig. 5.11	QSI	Owen et al. 2003b	Q12	9.3 ± 1.1	9.4 ± 1.2
Fig. 5.11	QSI	Owen et al. 2003b	Q13	18.7 ± 2.0	19.5 ± 2.3
Fig. 5.11	QSI	Owen et al. 2003b	Q14	13.1 ± 1.5	13.4 ± 1.7
Fig. 5.11	QSII	Owen et al. 2003b	Q15	16.1 ± 1.7	16.6 ± 1.9
Fig. 5.11	QSII	Owen et al. 2003b	Q16	15.4 ± 1.8	15.8 ± 2.0
Fig. 5.11	QSII	Owen et al. 2003b	Q17	15.4 ± 1.6	15.8 ± 1.8
Fig. 5.11	QSII	Owen et al. 2003b	Q9	9.6 ± 1.1	9.7 ± 1.1
Fig. 5.11	QSII	Owen et al. 2003b	Q10	11.6 ± 1.3	11.8 ± 1.4
Fig. 5.11	QSII	Owen et al. 2003b	Q11	10.6 ± 1.2	10.8 ± 1.2

Appendix 3. TEBESEA User Guide

The program TEBESEA.xls can be found on the included CD-ROM. To calculate exposure ages, the following steps have to be performed:

1. Open the file TEBESEA.xls in MS Excel™.
2. Open the worksheet "Data Entry".
3. For each sample, enter sample data, each sample in a separate row. Start with the uppermost row (row 3). Do not leave free rows between samples.
4. For each sample, enter sample name (column A), geographic coordinates (c. B, C) and altitude (c. D).
5. a) For each sample enter topographic shielding factors for fast neutrons and muons, concerning the production rate (c. E, F) and the attenuation length (c. G, H); if any of the topographic shielding factors is not known, enter "1" in the respective cell to neglect this factor; make sure all topographic shielding cells in each sample row are filled, but leave open columns I-BP;

   or

   b) Leave open all topographic shielding cells and for each sample enter shielding data in columns I-BP to calculate topographic shielding factors with the subroutine "Horizon Shielding". Enter azimuth data (N = 0° = 360°) in clockwise fashion. To each pair of azimuth angles, enter the mean horizon angle measured in between. Enter azimuth sections (the first azimuth angle of any section is equal to the second azimuth angle of the previous section) starting in c. I until the full circle is described (sum of sections = 360°), and the second azimuth of the last section is equal to the first azimuth of the first section. Leave free all other horizon angle cells. For each sample enter maximum slope angle (c. BQ) and its azimuth (c. BR); If not known, enter "0" in both cells. Then press the "Horizon Shielding" button (BS1-2) to calculate shielding factors. Factors will be filled in into columns E-H automatically.
6. For each sample, if not already done in step 5b, enter maximum slope angle (c. BQ) and its azimuth (c. BR). If not known, enter "0" in both cells. Do not leave these cells free in any sample row.

7. For each sample, enter sample thickness [cm] (c. BT) and snow/vegetation cover [g cm^{-2}] (c. BU). Do not leave these cells free in any sample row.

8. a) For each sample, enter measured ^{10}Be concentration and its error [atoms g^{-1}] in c. BV and BW, respectively, and leave open c. BX-CH;

   or

   b) leave open c. BV-BW and for each sample enter measurement data into cells BX-CH to calculate the measured concentration with its error using the subroutine "10Be data". Enter the measured $^{10}Be/^{9}Be$ ratio of the sample [10^{-12}] (c. BX) with its error [%] (c. BY), the measured $^{10}Be/^{9}Be$ ratio of the respective blank [10^{-12}] (c. BZ) with its error [%] (c. CA), the mass of ^{9}Be carrier [mg] added to the sample (c. CB) and the respective blank (c. CC), the error of these carrier masses [mg] (c. CD), the concentration of the carrier [ppm] (c. CE) with its error [ppm] (c. CF), as well as the sample mass [g] (c. CG) with its error [g] (c. CH). Then press the "10Be data" button (CI1-2). The measured ^{10}Be concentration and its error will be entered into c. BV and BW automatically.

9. For each sample, enter the erosion rate of the sampled surface and its error [cm a^{-1}] (c. CJ, CK), the tectonic uplift rate [m a^{-1}] (c. CL), the rock density with its error [g cm^{-3}] (c. CM, CN), as well as the sediment cover [g cm^{-2}] (c. CO). Do not leave free these cells in any sample row.

10. Press the "TEBESEA" button (CP1-2). Calculation of exposure ages will procede. Wait until the button returns into its normal position. This may take about 10 seconds per sample.

11. To see results, open worksheet "Results". Exposure ages with fully propagated errors are shown calculated following the scaling systems of Lal (1991) modification 1 without geomagnetic and uplift correction ("classic") (c. B, C), Lal (1991) modification 1 with all corrections (c. D, E), Lal (1991) modification 2 (c. F, G), Dunai (2001) (c. H, I), Dunai (2001) modification (c. J, K), and Desilets & Zreda (2003) (c. L, M). For explanation of the modifications see section 2.

Erklärung

Hiermit erkläre ich, den Eigenanteil der vorliegenden Dissertation eigenständig und unter Zuhilfenahme nur der im Text erwähnten Quellen und Hilfsmittel angefertigt zu haben.

Der Eigenanteil der kumulativen Arbeit beträgt bei der Einarbeitung des Analysenganges (Abschnitt 1) sowie bei der Auswertung und Interpretation der Daten und der Literatur einschließlich der Schriftfassung der Arbeit durchweg 100%. Bei der Erstellung und Nutzung des Programms TEBESEA (Abschnitte 2 und 3) beträgt der Eigenanteil ebenfalls 100%. Bei der Erhebung der ^{10}Be-Daten entfallen auf den Eigenanteil bei der Probenahme 100% (Abschnitt 2), 49% (Abschnitt 4) bzw. 34% (Abschnitt 5), bei der Probenaufarbeitung 100% (Abschnitte 2 & 4) bzw. 41% (Abschnitt 5). Die nicht als Eigenanteil deklarierte Probenaufarbeitung in Abschnitt 5 wurde von Diplomanden unter meiner Anleitung ausgeführt. Die Messung der aufgearbeiteten Proben am AMS musste in allen Fällen Herrn Dr. Peter Kubik, Zürich, überlassen bleiben.

Ich erkläre ferner, weder diese Arbeit noch Teile davon andernorts zum Zwecke der Promotion eingereicht zu haben, noch vormals eine andere Dissertation verfasst oder eine diesbezügliche Prüfung endgültig nicht bestanden zu haben.

Bayreuth, den 16. 08. 2004.